# Crustal History Indicators on Mercury

## Thesis

# Crustal history indicators on Mercury

Emma Rosalind Fegan

MESci MSc

9th August 2017

*A thesis submitted to The Open University in the subject of Planetary Geology for the degree of Doctor of Philosophy.*

**School of Physical Sciences**
**The Open University**

## Abstract

In this thesis, I investigated curvilinear features on the surface of Mercury and the impact of illumination bias upon observations of those features. I also demonstrated their utility with regard to photostratigraphy and suggest areas where BepiColombo will provide beneficial additional data.

Basin-edge scarps occur within volcanically-filled impact basins in all areas of the surface of Mercury. Many large impact basins are filled with Smooth Plains (volcanic) units. I hypothesise that fault nucleation occurs on the mechanically weak interface between the base of the volcanic fill units and the original floor of the impact basin. Using crater size-frequency distribution analysis I have established that resolvable deformation of basin-edge scarps ceased between 1.1 and 0.6 Ga.

Based upon location and morphology, I concluded that catenae are likely to be formed by secondary impact ejecta. They are of use when establishing stratigraphic relationships between impact basins, since they extend further away from the primary basin than the ejecta blanket, and tend to remain observable for longer. The stratigraphic map of impact basins Aneirin, Sanai and the immediately surrounding areas demonstrated this, as – despite the basins being the same morphological class (C2) – catenae related to Aneirin were formed after the formation of Sanai. Aneirin is therefore the younger basin.

Mercury's near-zero obliquity means that curvilinear features aligned parallel with the illumination azimuth (east-west at low-mid latitudes) would be likely to be under-represented in the global population. Using shaded-relief models with alternative artificial illumination to complete resurveys, I found that my global survey of basin-edge scarps has been affected. Consequently, I advise the use of shaded-relief models in addition to imagery when mapping curvilinear features.

I anticipate that the improved instrumentation of BepiColombo MPO will be invaluable when carrying out stratigraphic mapping and global surveys of specific features such as basin-edge scarps and catenae.

## Acknowledgements

This thesis was funded by by a Science and Technology Facilities Council (SFTC) studentship. All work presented in this thesis is my own, except for the contributions (amounting to 20%) made by my coauthors in the paper from which chapter 2 is derived. Many thanks to my supervisors Dave Rothery, Susan Conway and Mahesh Anand for all the assistance they provided. Particular thanks also to Becca Thomas, Jack Wright and Tom Barrett (among many others) for their invaluable help and moral support.

# List of Contents

## List of Figures

# List of Tables

# 1 Introduction

## 1.1 Observations and exploration

Prior to the NASA Mariner 10 mission to Mercury, observations of the planet were limited to those using ground-based telescopes (such as the work of Italian astronomer Giovanni Virginio Schiaparelli, who made the first map of Hermean surface features (Galluzzi, 2015) ). Ground-based observations of Mercury are problematic due to the proximity of Mercury and the Sun, and for the same reason telescopes in Earth orbit (including the Hubble Space Telescope) do not observe Mercury. Mariner 10 carried out two fly-bys in 1974 that produced images of 45% of the surface (Murray *et al*., 1975; Solomon, 2003). From these initial images, the surface of Mercury was interpreted to be comparable to that of the Moon (Davies *et al.*, 1978).

The next mission occurred when NASA launched the MESSENGER (Mercury Surface, Space ENvironment, GEochemistry, and Ranging) mission (Gold *et al.*, 2001; Santo *et al.*, 2001; Solomon *et al.*, 2001) in 2004, whichcarried out two flybys in 2008 and a third in 2009 before entering its orbit in 2011, becoming the first - and at time of writing, only - spacecraft to orbit Mercury (Galluzzi, 2015). MESSENGER carried 7 instruments including the Mercury Dual Imaging System (MDIS). I have used MDIS data for the majority of this project, and it is discussed further below. In addition, MESSENGER carried the Mercury Laser Altimeter (MLA), Gamma-Ray and Neutron Spectrometer (GRNS), Magnetometer (MAG), Mercury Atmospheric and Surface Composition Spectrometer (MASCS), Energetic Particle and Plasma Spectrometer (EPPS) and Radio Science (RS) (www3).

The MESSENGER mission improved the understanding of the geology and evolution of Mercury in many ways. For example, the existence of volcanic units on Mercury and their place in the geological history of the planet was uncertain (Solomon, 2003) prior to the mission. The first flyby MESSENGER undertook of Mercury allowed workers to confirm the existence of volcanic plains emplaced by effusive volcanism (Head *et al.*, 2009).

First flyby imaged tectonic features (confirming the finding of Mariner 10 that the

majority of tectonic features on Mercury are contractional) the only graben complex currently named on Mercury, Pantheon Fossae within Caloris Plainitia (Watters *et al.*, 2009). First flyby also allowed Strom *et al.* (2008) to ascertain that the plains surrounding Caloris Plainitia are unlikely to be ejecta or impact melt from the Caloris impact, based upon the lower crater density of the external plains, and allowed the identification of young craters with large ray systems that were not imaged by the Mariner 10 mission. The orbital observations allowed additional investigations, for example allowing the identification of large (~ 4 km diameter) regions of permanent shadow in the south polar regions (Chabot *et al.*, 2012) confirming the global distribution of smooth plains, covering ~27% of the surface of the planet (Denevi *et al.*, 2013) and allowed Byrne *et al.* (2014) to confirm the total contraction of Mercury to date as 7 km along its radius.

The next Mercury mission, BepiColombo, is now expected to arrive in orbit around Mercury in 2025, according to the ESA webpage (www1) and its payload of instrumentation will have capabilities greater than those of MESSENGER – for example, the High-resolution imaging channel of the Spectrometer and Imagers for MPO BepiColombo- Integrated Observatory SYStem (SIMBIO-SYS) package will provide colour images of the surface with resolutions up to 5 m/pixel (Flamini *et al.*, 2016).

### 1.2 Physical properties and geology

Mercury is the innermost planet of the solar system, and the smallest of the terrestrial planets (with a radius of 2440 km), though it has the highest uncompressed bulk density (5.3 g/cm$^3$, compared with 4.4 g/cm$^3$ for the Earth) due to a disproportionately large iron core (Siegfried and Solomon, 1974) – approximately 60% of the planet, by mass with a radius of 2030 km (Solomon, 2003). One Mercury 'day' is nearly 59 terrestrial days, and is longer than the planet's orbital period (1 day is equal to 2 years) (Solomon, 2011). Mercury's rotation rate was faster early in the planet's history and has slowed over time, a process called "despinning", as discussed further below.

Mercury has no atmosphere, meaning that there has been a lack of surface modification (what has occurred has been due to subsequent impacts) and the

surface diurnal temperature range is ~600 K, reaching as high as ~695 K and dropping to ~100 K.

### 1.3 Chronostratigraphy

The stratigraphic system of Mercury is shown in Table 1, alongside terrestrial epochs. The system was based upon the lunar one, where large impact events define the base of each epoch (which are then named after the relevant impact basin (Van Gasselt and Neukum, 2011).

Approximate dates for the bases of each epoch are shown on the left hand side of Table 1, and are based upon crater size-frequency distributions (which provide relative ages of surfaces) – these are calibrated to lunar size-frequency distributions where the absolute surface age is known from dating of lunar samples (Neukum *et al*., 2001; Van Gasselt and Neukum, 2011).

**Table 1.1**: Comparison of epochs for Mercury and Earth, dates as Van Gasselt and Neukum (2011) and Neukum *et al.* (2001).

| Time before present (Ga) | EARTH | MERCURY |
|---|---|---|
| 0.5 | Phanerozoic | Kuiperian |
| **1** | | |
| 1.5 | Proterozoic | Mansurian |
| **2** | | |
| 2.5 | | |
| **3** | Archean | |
| 3.5 | | Calorian |
| 3.8 | | |
| **4** | | Tolstojan |
| 4.1 | Hadean | |
| 4.5 | | Pre-Tolstojan |

The method described above (and the dates in Table 1) are from the Neukum Production Function (NPF) method (e.g.Neukum, Ivanov and Hartmann (2001)) More recently, a new method – the Marchi Production Function has been created by (Marchi *et al.*, 2009) and brought into use (e.g. (Massironi *et al.*, 2009; Marchi *et al.*, 2011)**.** I discuss this further in Chapters 2 and 3, but briefly, this method employs data from models of solar system impactor fluxes – which are assumed to be variable throughout solar system history (Strom *et al.*, 2011) – to calculate crater size-frequency isochrons for a given body. As with NPF, the size-frequency data are calibrated using lunar sample ages (Massironi *et al.*, 2009)**.**

## 1.4 Photogeology

Photogeological units on Mercury, units that are identified using imaging only, are as follows:

- Intercrater Plains: “level to gently rolling ground between and around large craters and basins” (Trask and Guest, 1975).

- Intermediate Plains: “planar to undulating surfaces that have higher crater density than smooth plains material, but are less heavily cratered than intercrater plains material” (Spudis and Prosser, 1984).

- Smooth Plains: “relatively flat, sparsely cratered material” (Strom, Trask and Guest, 1975; Trask and Guest, 1975; Spudis and Guest, 1988) “that displays sharp boundaries with adjacent regions and is level to gently sloped over a baseline of ~100–200 km” (Denevi *et al.*, 2013).

The order of the list above reflects the chronology of the formation of these provinces, with the oldest type listed first (the Intercrater Plains) and the youngest listed last (Smooth Plains). Each type of plains is thought to be degraded volcanic units (that would have appeared similar to Smooth Plains when first emplaced) by most workers (Murray, Strom and Trask, 1975; Trask and Guest, 1975; Kiefer and Murray, 1987; Spudis and Guest, 1988; Whitten *et*

*al.*, 2014) though some suggest that the Intercrater Plains might be fluidized impact ejecta instead (Wilhelms, 1976; Oberbeck *et al.*, 1977).

Additional variation in surface properties results from fresh craters and their rays and ejecta blankets, which are brighter than the mature, weathered surfaces (Blewett *et al.*, 2014). This is helpful when categorising craters (for example crisp craters with bright rays and/or ejecta are likely geologically young).

### 1.5 Tectonic Landforms

MESSENGER flyby and orbital imaging has established that tectonic landforms are common on the surface of Mercury, and the majority take the form of shortening features (Strom, Trask and Guest, 1975; Byrne *et al.*, 2014; Klimczak, 2015). The only area on Mercury's surface where extension features have been identified is within the Caloris Plains that fill the largest impact basin on the planet (Caloris), where radial and concentric graben can be observed (Strom, Trask and Guest, 1975; Dzurisin, 1978; Murchie *et al.*, 2008; Watters *et al.*, 2009).

Byrne *et al.* (2014) carried out global mapping of lobate scarps, wrinkle ridges and high relief ridges on Mercury and identified ~6000 of these features, all of which are interpreted to be shortening structures in the literature. The most widely accepted formation theory for the many Hermean shortening structures is as follows: global cooling and contraction resulted in wrinkling and thrust faulting in the lithosphere (Watters *et al.*, 2004). Most commonly observed features are lobate scarps: curvilinear surface expressions of thrust faults, with a steeply front scarp and lower gradient back scarp, and topographic reliefs of a few 100 m to a couple of kilometres (Watters *et al.*, 2002; Solomon, 2011; Ruiz, López and Egea-González, 2013). They are widespread, but most commonly found in pre-Tolstojan intercrater plains and Tolstojan and Calorian smooth plains and rarely overprinted by large craters, implying ages younger than the most recent widespread effusive activity on the planet (Watters *et al.*, 2004; Rothery and Massironi, 2010).

Lobate scarps are found in many geological settings and one of these was identified shortly prior to the start of my PhD but not yet thoroughly investigated: at the edges of volcanically filled impact structures (Rothery and Massironi, 2010).

The global contraction theory would produce thrust features with no preferential alignment (Watters *et al.*, 2004; Dombard and Hauck, 2008; Byrne *et al.*, 2014), but whether or not this is the case has remained contentious throughout analysis of MESSENGER data. Mariner 10 data indicated no preferential orientation - and based upon measurements of the shortening involved in the observed features produced an estimated global contraction of 1-2 km along the planet's radius. However, work carried out using Mariner 10 images indicates that most scarps are oriented between NNW and NNE (north, plus or minus 45 degrees) (Watters *et al.*, 2004) did also note that the data could be biased as a result of the incidence angle in the images; only 20% of the lobate scarps they identified were spotted on an image with incidence angle <50 degrees.

It is possible that despinning of the planet to its current ~59 day axial rotation period may have contributed to the tectonic regime on the developing planet, by putting the lithosphere under tensile stress at the poles (resulting in east-west normal faults) and compression (thrust faulting) at lower latitudes through the collapse of a tidal bulge originally supported by the planet's rotation. In fact, Mariner 10 data supported greater numbers of scarps in high southern latitudes than at the equator, which is not consistent with the despinning theory (Dombard and Hauck, 2008). A recent study by Byrne *et al*. (2014) catalogued all of the wrinkle ridges and lobate scarps on Mercury's surface with the aim of calculating the level of contraction of the planet from a global dataset, and concluded that the planet had contracted by 7 km along its radius. The timing of when this contraction occurred is important when attempting to understand the evolution of the planet. Contraction can have an influence on volcanism - since a multitude of horizontal shortening structures ought to inhibit volcanism by suppressing magma upwelling through the lithosphere (Denevi *et al.*, 2009).

One subset of lobate scarps has been observed at the edge of volcanic plains that have filled impact basins and craters (Rothery and Massironi, 2013). These

are the subject of Chapters 2 and 3 of this thesis, and I refer to them as basin-edge scarps.

## 1.6 Catenae

Features such as the one shown in Figure 1.2 (referred to as catenae in this report, in accordance with the USGS definition: “chains of craters” can be seen in various locations on the surface of Mercury. There are three Hermean features formally named Catenae, for example Goldstone Catena (see Figure 2.1), but there is very little currently in the literature discussing catenae, named or otherwise, although they are frequently occurring across the entire surface of the planet and so will have been observed by any worker spending time examining images of the surface. References to them in the literature that do exist state that they are secondary crater chains (e.g. Gault *et al.* (1975)) although there have not been any studies examining them in detail to support this statement.

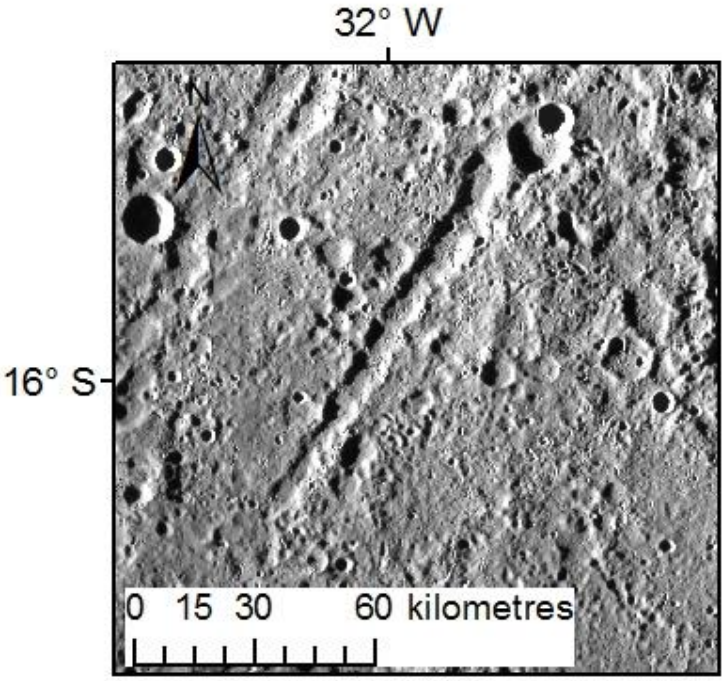


*Figure 1.2: Goldstone Catena, Mercury. MDIS global mosaic, equirectangular projection.*

However, global mapping brings to light examples of catenae on Mercury that cannot straightforwardly be related back to a primary impact feature. One

explanation for this might be that the primary basin being buried beneath later volcanic units. Alternatively, the primary impact basin having such a large diameter that its secondary ejecta material travelled so far as to be no longer easily linked back to it.  However, examining the wider planetary geology literature, there are some alternative explanations for the formation of crater chains on other bodies in the solar system.

For example, there are morphologically similar features on Mars' moon Phobos (Murray and Iliffe, 2011). These families of parallel grooves on the leading hemisphere of Phobos have been hypothesised to be secondary chains or rolling boulder tracks from the largest impact structure on the moon (Stickney), or possibly fractures from that impact or from tidal forces (Murray and Iliffe, 2011). However, ejecta from Stickney wouldn't attain sufficient velocity to form crater chains, no boulders are found at the end of the chains and the grooves are morphologically different from fractures (Murray and Iliffe, 2011). The authors propose that the grooves are secondary chains, where the primary impacts were on Mars. I discuss the possible formation mechanisms for catenae on Mercury in greater detail in Chapter 4.

## 1.7 Illumination bias

Mercury's near-zero obliquity (Yseboodt and Margot, 2006; P.K. Byrne *et al.*, 2014) means that for a given point on the surface the solar azimuth will be either east or west (depending on the time in the Hermean day the image was taken), but with no other notable variation in illumination geometry. Features trending parallel to the illumination direction are at greater risk of being overlooked (Melosh and McKinnon, 1988; Watters *et al.*, 2004) particularly with solar incidence angles of <75° (as measured from the zenith) (Klimczak, 2015). For this reason, illumination bias is more likely to have a significant impact on observations of topographic features on Mercury than on Mars or The Moon or other planetary bodies with a degree of obliquity.

## 1.8 The formation of impact craters

Impact craters are the dominant surface feature on Mercury (and the Moon), and are formed by hypervelocity impacts (Melosh, 2011). Craters on Mercury

are either simple or complex (Melosh, 2011) and the transition between the two categories is dependent on 1/g, and target rock strength. (Collins *et al.*, 2012).

Simple craters are approximately hemispherical cavities, with sharp rims, no terracing on their interior walls and a depth-to-diameter ratio of approximately 1:5. Beneath simple craters, a lens of brecciated material (with a depth of 1/3 – ½ the rim-to-floor depth). Continuous ejecta blankets surround simple craters to a distance of one crater diameter from the rim, and secondary craters (formed by the impact of larger ejecta material) can extend to distances of multiple crater diameters. In contrast, complex craters have terracing on their internal walls, flat floors with either a central peak or a peak-ring (a ring of mountains surrounding the centre of the crater).

Complex craters have flat floors, terraced walls and a depth-to-diameter radio of <1:5. Their floors are composed of melted and impact-shocked material. Complex craters also have continuous ejecta blankets extending to approximately one crater diameter. They also have fields of secondary craters, frequently forming clusters and herringbone patterns, and young complex craters often exhibit bright ray systems (Melosh, 2011; Collins *et al.*, 2012).

### *1.8.1 Stages of an impact*

Impact crater creation occurs in three phases: contact and compression, excavation and ejecta emplacement, and collapse (Melosh, 2011; Collins *et al.*, 2012).

- **Contact and compression:** In the contact and compression stage (the shortest of the three stages) the impactor makes contact with, and transfers its energy to, the target body. This results in sudden compression and increase in temperature of both the impactor and the target body beneath the impact site as shock waves travel through both. When the waves of compression reach free surfaces, rarefaction waves propagate back in the direction of the centre of the impact site, allowing both pressure and temperature to drop adiabatially (Collins *et al.*, 2012). At the same time, ejecta jets form where compression waves intersect a

free surface – in the case of impact cratering these jets occur in a circle around the centre of the impact site.

- **Excavation and ejecta emplacement:** The second stage is excavation and ejecta emplacement, as the shock waves propagate beneath and around the impact site and attenuate, an approximately hemispherical cavity known as a “transient crater” is formed. In the case of highly oblique impacts, the transient crater may be elongated along the direction of initial impact rather than hemispherical (Collins *et al.*, 2012). The jets of ejecta are emplaced upon the surrounding area of the target body, in a continuous blanket within ~1 crater diameter, which is thickest near the rim of the transient crater and thins with increasing distance from it (Collins *et al*., 2012). Secondaries close to primary crater are created by the lower velocity impacts, and occur in clusters and herringbone patterns (clusters separated by v-shaped dunes). At greater distances (multiple crater diameters) from the crater rim, fine dust and larger items of ejecta impact the surface, forming secondaries that can be harder to distinguish from primary craters due to their distance from the primary (Collins *et al*., 2012).

  In the case of complex craters, the downward excavation of the transient crater stops before the outward excavation does, resulting in craters that are shallower relative to simple craters of the same diameter (Collins *et al.*, 2012).

- **Collapse:** Driven by gravity, the transient crater collapses. In the smaller-diameter craters the steep rims collapse to create the breccia lens referred to above, forming simple craters. Transient craters with larger diameters collapse in a more complicated manner, involving uplift of the crater floor particularly the area that becomes the central peak (or peak-ring), and the slumping of the transient crater walls to create terraces (Collins *et al.*, 2012)

## 1.9 Overview of methods

The images used in my work come from the MDIS instrument on MESSENGER, which has two cameras – Narrow Angle and Wide Angle (NAC and WAC). The former is higher resolution (500 m/pixel up to 12 m/pixel), but monochrome and covers smaller areas, while the latter is lower resolution (1-2 km/pixel) but covers greater areas and has 12 colour filters (Hawkins et al., 2007). WAC and NAC images have been combined and used to create global and polar mosaics with a resolution of 250 m/pixel which can be downloaded from online sources (for example www2). A digital elevation model (DEM) of the northern hemisphere has been constructed from MLA (Mercury Laser Altimeter) tracks, but until the global DEM was released in 2016, topographic information for the southern hemisphere was available only from stereo image pairs.

With regard to obtaining absolute model ages, the majority of the Mercury literature (that makes use of crater statistics for modelling surface ages) now chooses to avoid the NPF method in favour of more modern alternative Model Production Functions such as the Marchi Production Function, and I have done the same (for example in Chapters 2 and 3) in order that my work be comparable.

For the reasons discussed in section 1.7, illumination bias is likely to have a significant impact on observations of topographic features on Mercury, and this will be particularly relevant to linear features, for reasons that I discuss in Chapter 5. The two types of features that are the topic of Chapters 2 through 5 (basin-edge lobate scarps and catenae) are both linear features. Therefore, the problem of illumination bias, and the impact of it upon my global surveys, is one that was important for me to understand. I have therefore attempted to take this into account, and investigate the extent to which this bias might have impacted on my results. I have done this by using digital elevation models to create shaded relief models, for which it is possible to artificially set illumination azimuth and elevation. I have used these to resurvey areas with different illumination conditions and investigate the impact of this upon the orientations of the population of linear features observed.

## 1.10 Aims

The aims of this project are as follows:

- Investigate the occurrence of basin-edge scarps on Mercury, and when they were forming relative to associated features.

- Identify the likely formation mechanism for basin-edge scarps.

- To map the global occurrence of catenae on Mercury.

- To determine a likely mechanism of formation for catenae on Mercury.

- Investigate the impact of the Hermean illumination bias on my basin-edge scarps and catenae datasets.

- Create a photostratigaphic map of an area of interest, and investigate the application of catenae and basin-edge scarps to interpreting the geological history of that area.

- Identify opportunities for additional study by joint European Space Agency (ESA) and Japan Aerospace Exploration Agency (JAXA) mission, BepiColombo.

# 2 Basin-edge scarps

## 2.1 Statement of originality

The paper below was published in Icarus in 2017 (Fegan *et al.*, 2017) and documents the work of me and my co-authors on features on the surface of Mercury called basin-edge scarps. The work in this chapter was 80% mine, 20% that of my co-authors: D.A. Rothery, S.J. Conway, M. Anand, S. Marchi, M. Massironi.

I presented a talk on my initial work on the identification of basin-edge scarps and their absolute ages (some of which is in Chapter 3 of this thesis, as well as material from the paper in Chapter 2) at the Lunar and Planetary Science Congress (LPSC) in 2015. I also presented a poster on further absolute age dating using the Marchi *et al.* (2009) production function, and my initial findings on the orientations of basin-edge scarps at LPSC in 2016.

## 2.2 Late movement of basin-edge lobate scarps on Mercury

### *2.2.1 Introduction*

Data from the MESSENGER (MErcury Surface, Space ENvironment, GEochemistry, and Ranging) mission flybys and orbital operations have confirmed that tectonic landforms, and shortening structures in particular, are widespread on Mercury's surface (Byrne et al., 2014). Among the most frequently observed features are lobate scarps: curvilinear surface deformations associated with thrust faults, with a steep front scarp and gently dipping back scarp, and topographic relief of hundreds of metres to 1-3 km (Strom et al., 1975; Watters et al., 2002; Solomon, 2011). The generally accepted formation mechanism for the many shortening structures on Mercury, including lobate scarps, is that secular interior cooling and attendant global contraction resulted in thrust faulting in the lithosphere (Strom et al., 1975; Watters et al., 2004; Byrne et al., 2014).

The distribution and orientation of Mercury's population of shortening structures were detailed by Byrne *et al.* (2014). In this work we focus on a subset of lobate scarps found at the edges of numerous impact basins (defined here as an impact crater >100 km in diameter), and which can be hundreds of kilometres in

length (Rothery and Massironi, 2013). The interiors of these basins are occupied by smooth plains deposits, which are interpreted to be formed due to volcanic infilling; these plains have similar morphological and spectral properties to those of the northern volcanic plains (Denevi *et al.*, 2013; Byrne *et al.*, 2016). The majority of these basin-specific scarps (Byrne *et al.,* 2014) are spatially collocated with the edge of their corresponding basin. Four examples of this feature —which we refer to in this study as “basin-edge scarps” —are illustrated in 2.1 and 2.2; an additional example associated with the impact basin Aneirin is shown in Figure 2.3. They share the morphological features of lobate scarps described above, but follow the edge of the volcanic infill. The vergence of the basin-edge scarps (the facing direction of the steep front scarp, interpreted as the shorter of two limbs of an asymmetric anticline) is always away from the centre of the basin.

Although these features bear a morphological similarity to the steep sides of thick, lobate lava flows within these basins, we interpret these basin-edge scarps as tectonic in nature. We take this view because basin-filling lavas generally onlap basin walls without discernible relief, and because there are examples of impact craters in the basin fill that have been cut by these scarps (shown in Section 5.2). Moreover, crater areal density measurements at some sites show a resolvable difference in age between the basin fill and a corresponding basin-edge scarp (see section 5.1).

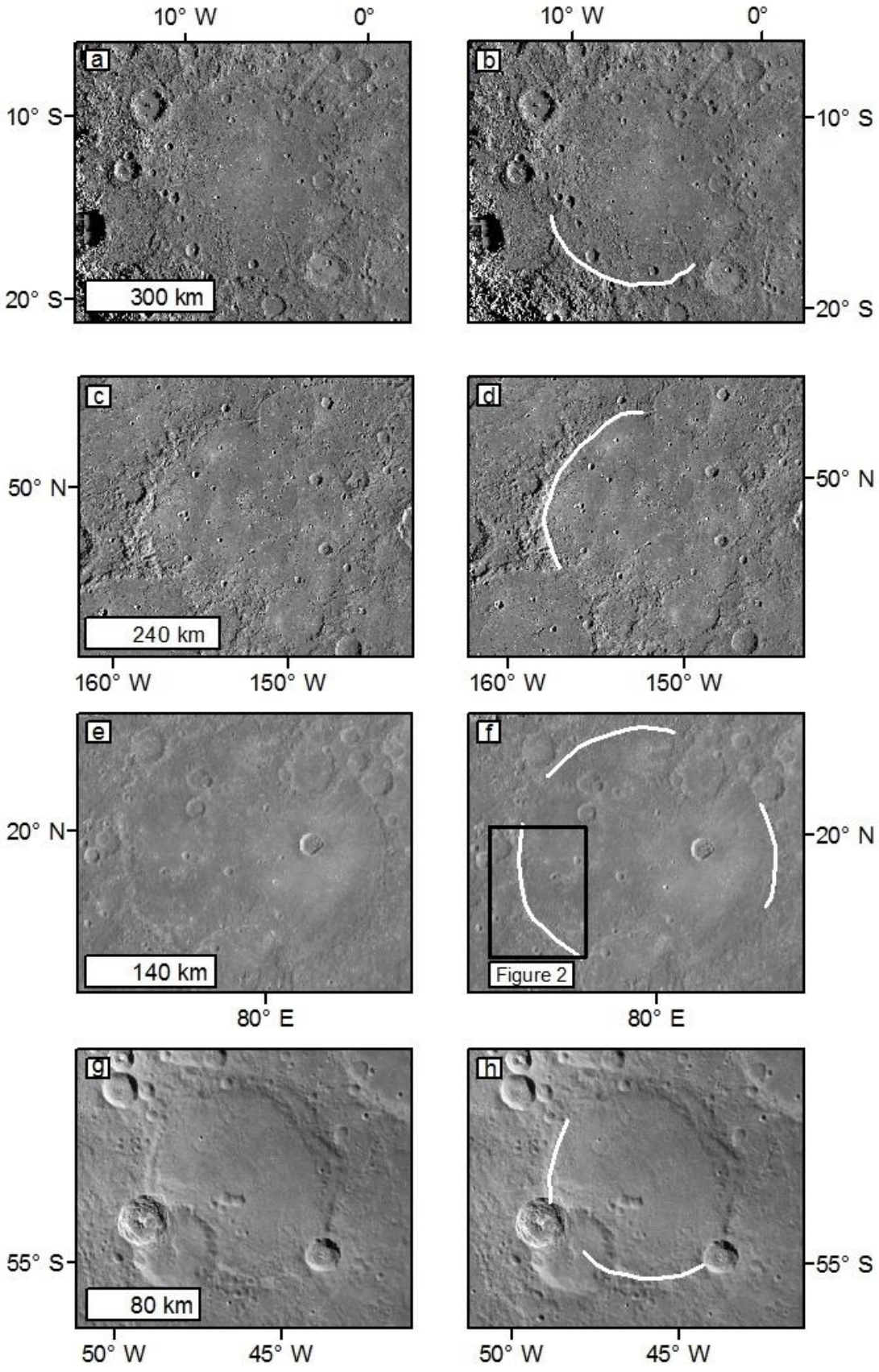
10° W
0°
a
b
10° S
20° S
300 km
c
d
50° N
240 km
160° W
150° W
e
f
20° N
140 km
Figure 2
80° E
g
h
55° S
80 km
50° W
45° W

*Figure 2.1 (above): Examples of four basins in which the volcanic infill is part-bounded by one or more lobate scarps. Figure 2.1 (a) and (b): Sanai (490 km diameter); (c) and (d): Shakespeare (399 km diameter); (e) and (f): Hafiz (280 km diameter); (g) and (h): Shevchenko (143 km diameter).*
*White lines on (b), (d), (f) and (h) delineate resolvable lobate scarps where basin-fill is thrust towards or over the basin rim. The black rectangle on (f) denotes the area shown in greater detail in Figure 2.2. Images are from the MESSENGER MDIS global monochrome base map, which has a resolution of 250 m/px (available: http://messenger.jhuapl.edu/the_mission/mosaics.html).*

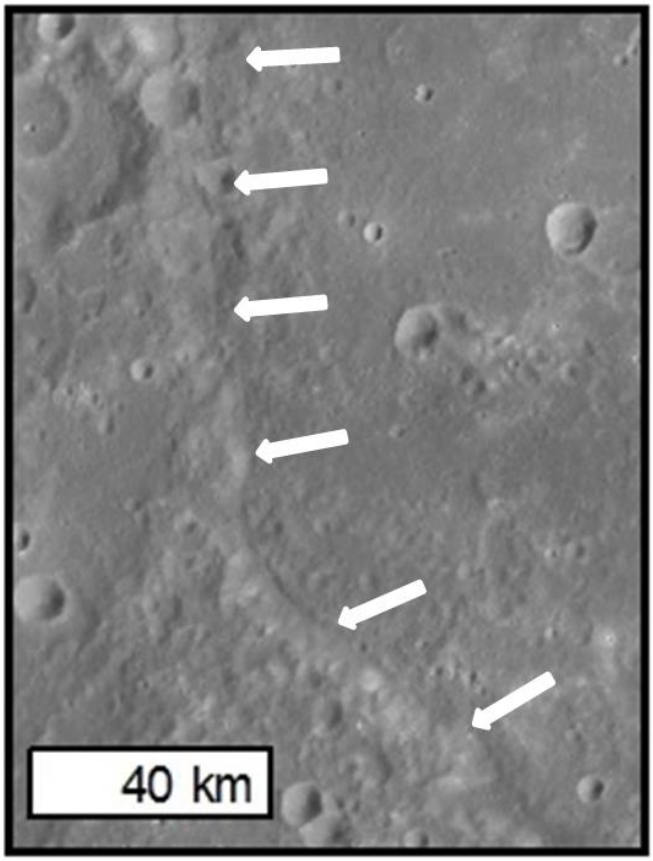


*Figure 2.2: A closer view of a section of the basin-edge scarp of Hafiz basin (as outlined by the back rectangle in Figure 2.1(f)). The white arrows indicate the basin-edge lobate scarp, and the approximate vergence (i.e. direction of tectonic displacement of the hanging wall).*

We conducted a global survey to document the occurrence of scarps at the edges of basin fills. We investigated the distribution of this type of scarp with photogeological mapping, and of both the relative and absolute timing of volcanic infill and scarp formation, using crater size–frequency distribution measurements.

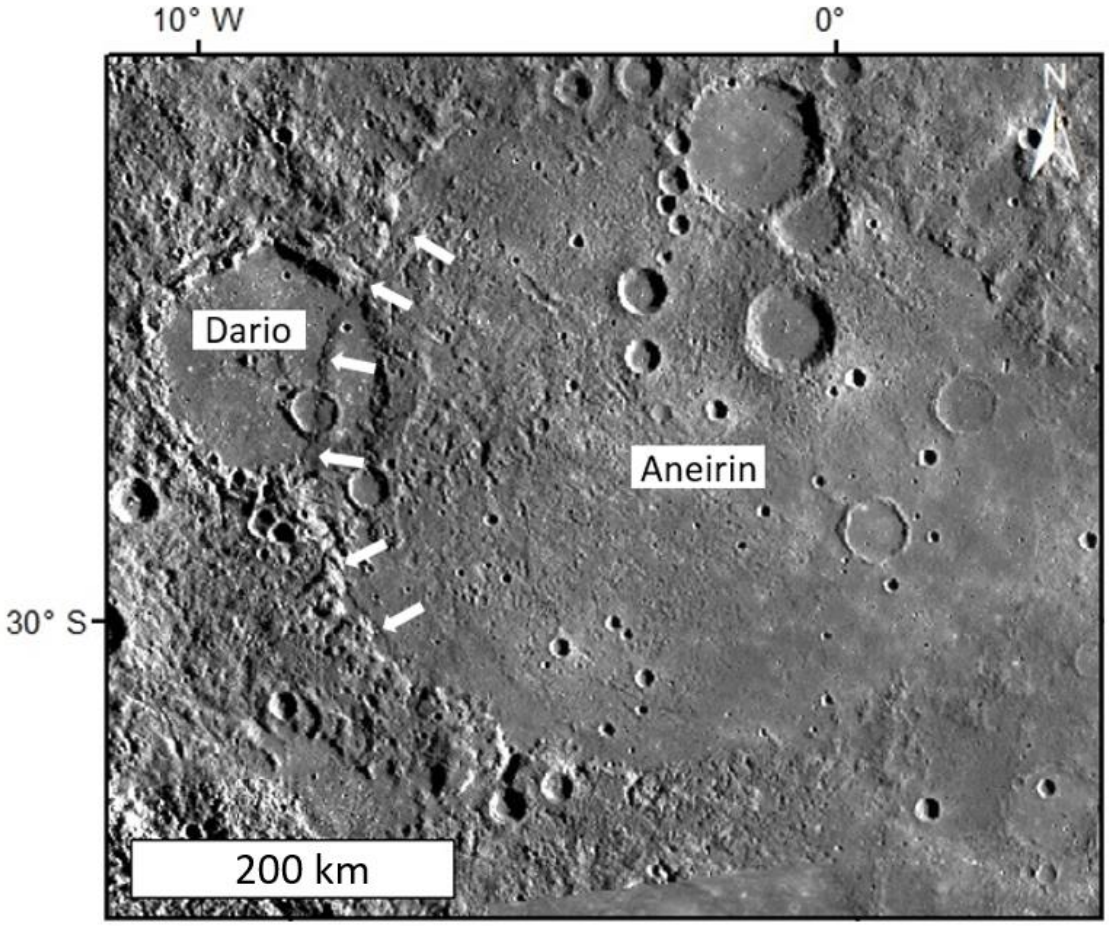


*Figure 2.3: Aneirin basin, and associated basin-edge scarp (indicated by white arrows, which also indicate approximate vergence). The basin-edge scarp of Aneirin cuts through the rim and volcanic infill of the neighbouring younger basin Dario as well as through a still later, unnamed crater inside Dario. Two "ghost craters" can be seen in the east of the smooth plains unit of Aneirin.*

### *2.2.2. Global occurrence of basin-edge lobate scarps*

To investigate how common basin-edge scarps are on Mercury, we carried out a global survey with the MESSENGER Dual Imaging Systems (MDIS) (Hawkins *et al.*, 2007) global mosaic (average resolution 250m/pixel). We used the Fassett *et al.* 2012 database of basins >100 km in diameter, adding basins not included in that study. We then identified all discernible basin-edge lobate scarps within that aggregate population of >100 km diameter basins. Visual examination of each basin in a global database of basins based upon the database of Figure 2.4 shows the global database of basins examined in this study, all of which have been volcanically filled, and distinguishes those that show evidence for lobate scarps along at least part of the margin of their fill

from those that do not. Our survey indicates that basins without basin-edge lobate scarps, have comparable diameters to, and are found in proximity with, those where such scarps are present, indicating that factors other than basin-location and basin-size are involved.

Regarding the uncertainty involved in creating this global distribution map of basin-edge scarps, using a method I set out in Chapter 5 (particularly section 5.2.4) I estimate that the global population of basin-edge scarps could be greater than set out above, when the surface is examined at greater resolution than I have employed here and when measures are put in place to limit the impact of illumination bias (discussed below).It is possible that the global population of basin-edge scarps on Mercury might be up to 5 times greater than set out above.

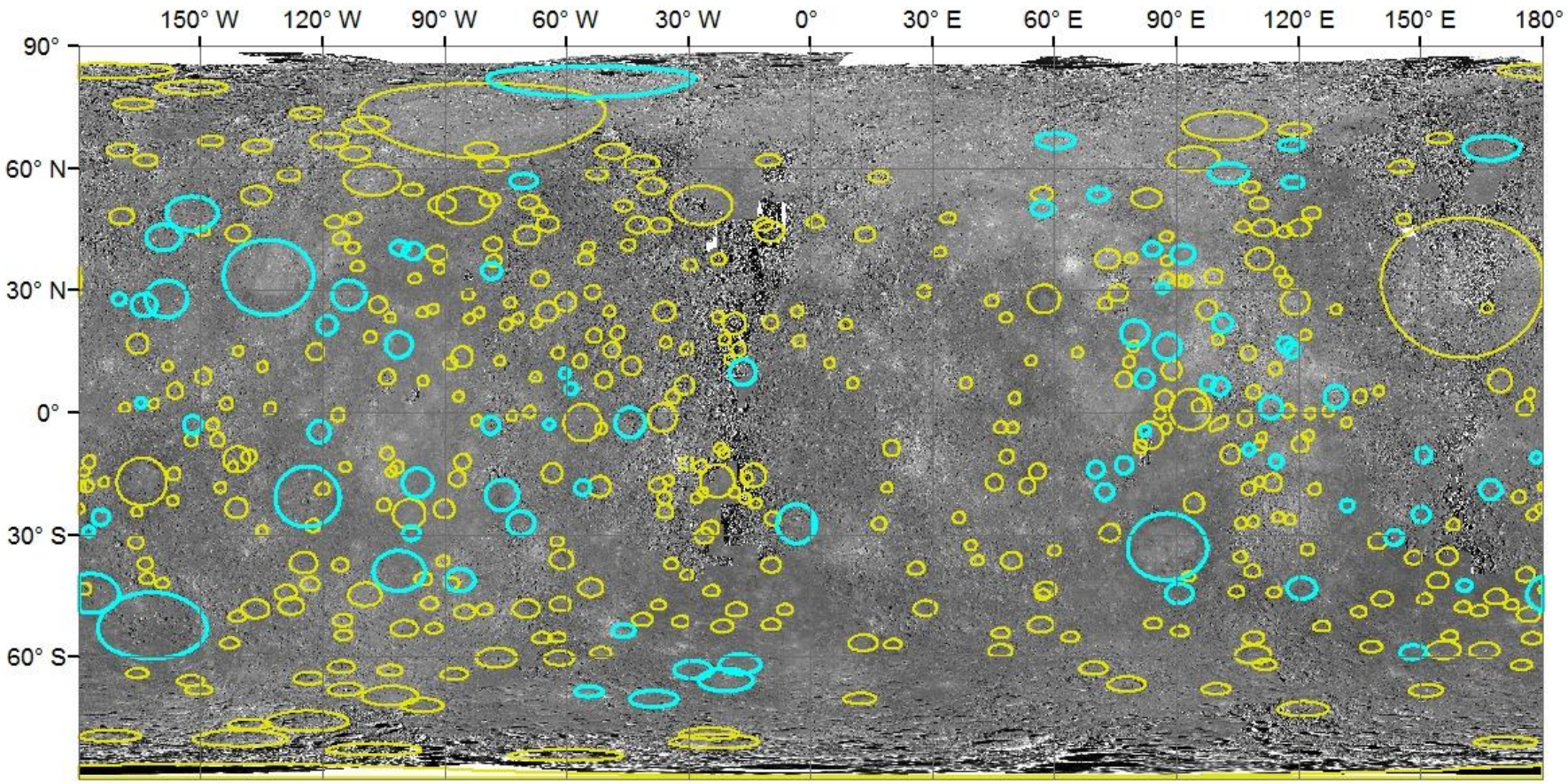


*Figure 2.4: Our photogeological survey results. Basins outlined in yellow have no identifiable lobate scarps at the periphery of their volcanic fills, whereas those outlined in blue have a lobate scarp on some part of the margins of their fill.*

### *2.2.3 Orientation and facing directions*

Analysis of shortening structures on Mercury can provide and insight into the global processes responsible for their formation (e.g. Strom et al. 1975, Melosh and McKinnon, 1988, Watters et al., 2009, Byrne et al., 2014). One process proposed to have influenced the tectonic evolution of Mercury is tidal despinning; under this scenario, the decrease in rotationional period, leads to the relaxation of an equatorial tidal bulge (Melosh & Dzurisin 1978; Melosh & McKinnon 1988; Dombard & Hauck 2008; Watters et al. 2015). Despinning has been predicted to form a diagnostic pattern of tectonic features: preferential north–south alignments of shortening structures at low latitudes, and east–west orientations of normal faults at high latitudes (Melosh & McKinnon 1988; Dombard & Hauck 2008; Beuthe 2010).

However, should despinning have operated in combination with global contraction due to secular cooling, which is known to have been extensive on Mercury (Byrne et al., 2014), models have suggested either that north–south aligned thrust faults would be the dominant tectonic structure present (Pechmann and Melosh, 1979; Beuthe, 2010). Alternatively, models that employ a more realistic value for rock strength indicate that north–south-aligned thrust faults would dominantly form at low latitudes with thrust faults with no preferred orientation would preferentially form at higher latitudes (Klimczak *et al.*, 2015).

Previous efforts to investigate whether Mercury's lobate scarps display any preferential trend in orientation (e.g., Watters *et al*., 2009; Di Achille *et al*., 2012; Byrne *et al.*, 2014) yielded inconclusive results on account of unvarying illumination geometry on the surface resulting in observational bias (Cordell and Strom, 1977). However, Watters *et al.* (2015) claimed to have identified a definitive orientation preference of structures independent of illumination conditions, with ~north–south orientations (either west- or east-facing) for shortening structures at low latitudes, and ~east–west orientations (either north- or south-facing) at higher latitudes. These results imply that a combination of despinning and global contraction continued until well after the end of the late heavy bombardment (Watters *et al.*, 2015), which is thought to have ended by around 3.6–3.9 Ga (Marchi *et al.,* 2013).

Both the orientations and facing direction of the basin-edge lobate scarps we surveyed in this work are shown in Figures 2.5–2.7. The data plotted are the frequency of occurrence of lobate scarps per 1° segment of basin circumference (where 0°, i.e., due north, is indicated by a black arrow). For example, Figure 2.5 indicates a preference for ~east- and ~west-facing directions, and thus a preponderance of ~north–south strikes, for the lobate scarps in our global survey, and in particular a preference for west-facing over east-facing scarps. Note that although this method allows both scarp orientation and facing direction to be displayed, it does not indicate the length of each constituent scarp; for example, scarps that subtend 45° of arc along the circumference of a 100 km-diameter basin and of a 500 km-diameter basin would have necessarily different lengths, but would contribute equally to a plot of this nature.

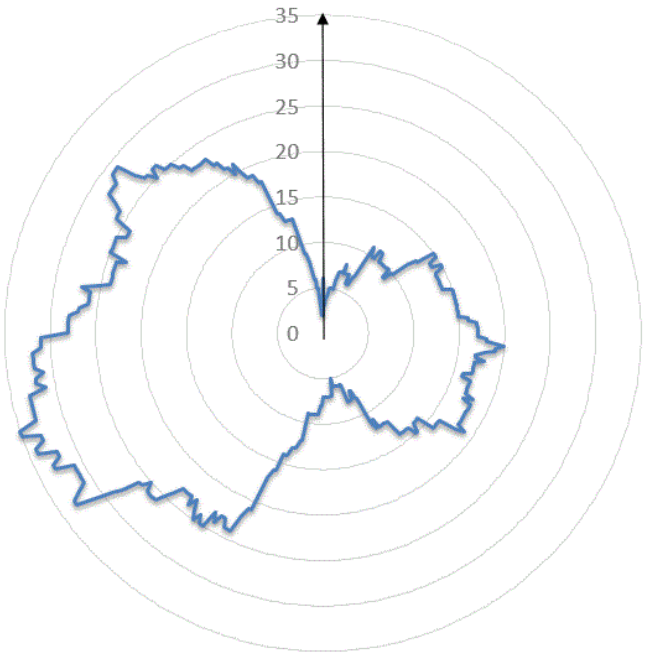


*Figure 2.5: A radial plot displaying the facing directions of the global population of basin-edge scarps (n = 142). The black arrow denotes north; the radial axis indicates frequency of lobate scarp facing direction occurrence (per degree of bearing). This plot indicates a north–south alignment of scarps, which are more commonly west-facing than east-facing.*

To test whether or not our results are subject to the same illumination bias suspected in earlier studies, we resurveyed those basin-edge scarps present on shaded-relief models of selected portions of Mercury's surface created from digital terrain models (DTMs). Preusker *et al.* (2011) produced these DTMs with stereo images from MESSENGER's flybys of Mercury, and we created shaded-relief models with artificial lighting directions (method as referred to in the

supplementary material of Watters *et al*. (2015)**.** Briefly, we used the Hillshade tool in the Spatial Analyst Toolbox of ArcGIS 10.1 to create two hillshade models with illumination azimuths of 090° and 000°, respectively. The hillshade model with the illumination azimuth of 090° is approximately similar to that of the global monochrome mosaic we carried out our survey on (Section 2), while the illumination azimuth of 000° is perpendicular to the natural illumination in that mosaic (and in all low-Sun images except at polar latitudes).

We found that the preferential orientation results from the radial plots with artificial illumination differed from the results shown in Figure 2.5. Two examples are shown in Figures 2.6 and 2.7 which also show that changing the illumination azimuth resulted in a change of observed preference for facing direction of our surveyed scarps (the number of scarps included in each survey are indicated by "n" in the captions). Because of this apparent dependence of scarp facing direction (and thus strike) on solar illumination angle, we are unable to discount the influence of illumination geometry on our global survey and scarp orientation results (Figure 2.5), despite the features involved being several hundred km in length and being relatively easy to identify (as they are, by definition, on the edge of impact basins). Thus, we cannot be certain that basin-edge lobate scarps are preferentially oriented north–south on Mercury.

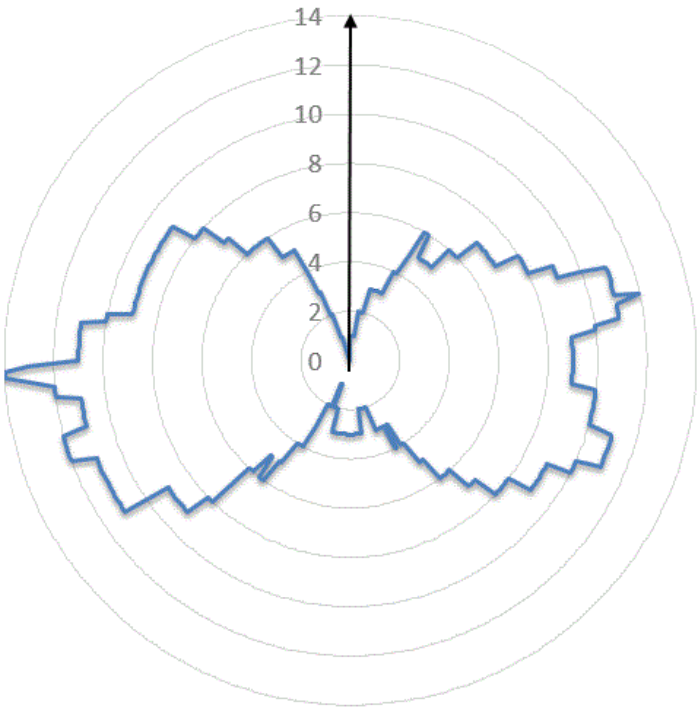


*Figure 2.6: Radial plot of facing directions produced from hillshade models artificially illuminated from the east (n = 40). The scarps show strong preferences for east- or west-facing directions. Note that the total frequency is lower than the global plot (Figure 2.5) as the DTM we used covers only a portion of the surface.*

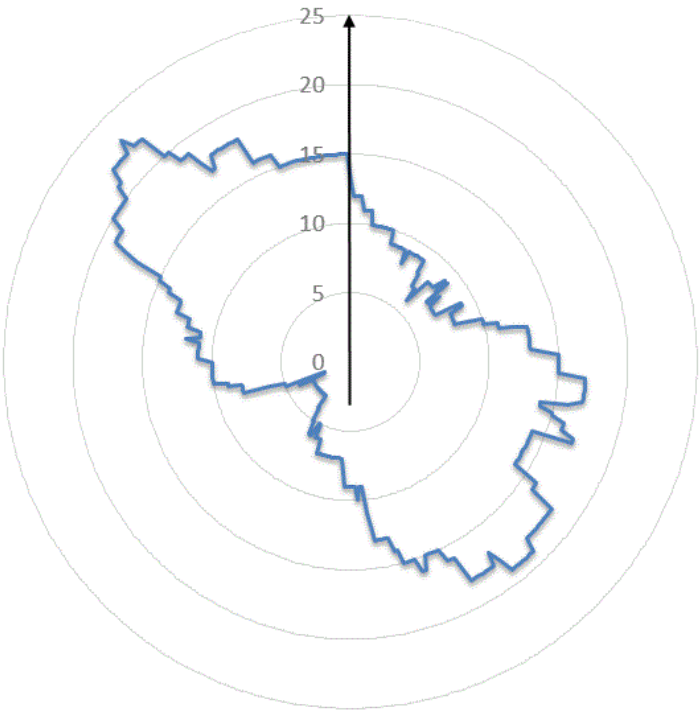


*Figure 2.7: Radial plot of facing directions produced when hillshade model (as used for Figure 2.6) was artificially illuminated from the north (n = 56), yielding preferential scarp facing directions to the northwest and southeast.*

That caveat aside, like Byrne *et al*. (2014) and Watters *et al*. (2015), we observe a preference globally for ~north–south orientations of basin-edge lobate scarps (Figure 2.5), and specifically ~north–south orientations at low latitudes and ~east–west orientations at high latitudes. Byrne *et al*. (2014) examined the orientation of the global population of shortening structures on Mercury and found them to have ~north–south orientations at low latitudes, and a northeast–southwest trend at higher northern latitudes, but no preferred orientations at high southern latitudes. Our observations agree with this first finding, but not the third (we have not examined the variation of apparent trends with latitude in this study so are unable to comment on the second finding). Klimczak *et al.* (2015) tested end-member scenarios under which despinning ended prior to the onset of global contraction, or where despinning was still operating when contraction began, and compared their model predictions against the observations of Byrne *et al*. (2014). Klimczak *et al*. (2015) concluded, as did Watters *et al*. (2015), that observational evidence supports a scenario under which despinning was still underway when global contraction began.

## 2.3 Relative and absolute ages

### *2.3.1 N numbers and model crater retention ages*

To investigate the timing of smooth plains emplacement within basins, and the timing of subsequent basin-edge lobate scarp formation, we conducted a size-frequency distribution (SFD) analysis of a number of smooth plains surfaces both for basins with and without a basin-edge lobate scarp. When identifying craters to produce SFDs for the surface of our selected volcanic fills, we used the highest available resolution MDIS images (which have an average resolution of 50 m/pixel) that cover the count areas. We processed the images with USGS ISIS3 software before importing them into the ArcGIS environment. We determined crater SFDs for these units with CraterTools (Kneissl *et al*., 2011) within ArcGIS, digitising primary craters >1 km in diameter. Secondary craters (as identified by clustering, chains and herringbone patterns) were excluded from the counts, although their corresponding areas (accounting for between 0 and 1% of the count areas) were left in. We do not believe removing these areas would have had any impact on our model ages, particularly since we quote them to only two significant figures. The inclusion of craters as small as 1 km in diameter makes it highly likely that secondary craters have been included, despite our efforts to avoid them. However, without including craters down to 1 km in diameter the SFD statistics would have been too unreliable (due to too few craters being included in the counts) to draw any conclusions from.

We selected a subset of eight impact basins >100 km in diameter that have basin-edge lobate scarps for our model age analysis. Note that these eight samples represent approximately 10% of the total population of basin-edge scarps (n = 78), as identified in our survey (see section 2). For comparison, we also determined SFDs for the volcanic fill of eight basins >100 km in diameter that do not have basin-edge scarps. We did so to investigate whether the smooth plains within basins with basin-edge scarps are, in general, older, younger, or comparable in absolute age with the smooth plains within those basins that lack such scarps.

To enable direct comparison between the relative ages of the smooth plains units in Table 2.2, we calculated the cumulative number of craters equal to or

greater than 10 km and 20 km in diameter (N(10) and N(20) respectively) (Arvidson *et al*., 1979). The smaller the number of superposed craters, the younger the surface is likely to be.

**Table 2.1**: Count areas and N(10) and N(20) numbers for a subset of basins with and without basin-edge scarps . Confidence intervals (conf. int.) are ± one standard deviation, derived as the square root of the number of craters counted, divided by the area over which the count was made, per million square km. Basins where the crater SFD did not include any craters of diameter greater than 10 km or 20 km are indicated by N/A. Columns titled 'Fill (conf. int.)' and 'Scarp (conf. int.)' list our model ages, produced using the Marchi production function (Marchi et al. 2009). Italics indicate poor fits to the data, in which cases the cratering age is highly uncertain as the crater production function does not represent the shape of the cumulative SFD. The unnamed basins are distinguished by the coordinates of their centre points in decimal degrees.

| With basin-edge scarps | | | | | | Without basin-edge scarps | | | | |
|---|---|---|---|---|---|---|---|---|---|---|
| **Name** | **Count Area km$^2$** | **N(10) (conf. int.)** | **N(20) (conf. int.)** | **Fill (conf. int.) Ga** | **Scarp (conf. int.) Ga** | **Name** | **Count Area km$^2$** | **N(10) (conf. int.)** | **N(20) (conf. int.)** | **Fill (conf. int.) Ga** |
| Aneirin | $7.5x10^4$ | 93 (±35) | 27 (±19) | 2.2 (±0.3) | 0.6 (±0.1) | Mendelson | $4.4x10^4$ | 45 (±32) | 23 (±23) | 1.8 (±0.2) |
| Beethoven | $1.6x10^4$ | 88 (±23) | 31 (±14) | 3.5 (±0.1) | 1.0 (±0.1) | Hugo | $1.3x10^3$ | 155 (±109) | N/A | 3.7 (±0.1) |
| Hafiz | $2.1x10^5$ | 242 (±108) | 97 (±69) | 2.9 (±0.5) | *1.0 (±0.1)* | Khansa | $4.6x10^3$ | N/A | N/A | 0.9 (±0.1) |
| Shakespeare | $7.0x10^4$ | 72 (±32) | 29 (±20) | 2.9 (±0.1) | 1.0 (±0.1) | Copland | $2.4x10^3$ | N/A | N/A | 1.7 (±0.4) |
| Shevchenko | $6.1x10^3$ | N/A | N/A | 1.5 (±0.2) | 1.1 (±0.1) | Unnamed[166°S, 25°W] | $4.0x10^3$ | N/A | N/A | 3.4 (±0.1) |
| Unnamed[40°S, 70°W] | $7.5x10^4$ | 239 (±57) | 76 (±32) | 3.9 (±0.1) | 1.1 (±0.1) | Unnamed[154°N, 67°E] | $3.8x10^3$ | 261 (±261) | N/A | 2.7 (±0.2) |
| Unnamed[91°N, 38°E] | $1.8x10^4$ | N/A | N/A | 3.9 (±0.1) | 1.1 (±0.1) | Unnamed[69°S, 0°E] | $8.0x10^3$ | 126 (±126) | N/A | 2.4 (±0.3) |
| Unnamed[150°N, 10°W] | $1.4x10^4$ | 138 (±97) | N/A | 3.0 (±0.3) | 1.1 (±0.1) | Unnamed[13°S, 22°W] | $4.2x10^3$ | 416 (±315) | N/A | 2.6 (±0.4) |

Denevi *et al.* (2013) published N(10) and N(20) values for the smooth plains within Beethoven basin, one of the basins we examine in this work. They obtained an N(10) value of 82 ±19 and an N(20) value of 32 ±12 for this unit; we obtained N(10) and N(20) values of 88 ±23 and 31 ±14, respectively, for these smooth plains units, in good agreement with the Denevi *et al.* (2013) values.

**Table 2.2**: N(10) and N(20) values published by previous authors. References: [1]Denevi et al. (2013), [2]Ostrach et al. (2015).

| Area | N(10) (error) | N(20) (error) |
|---|---|---|
| **Intercrater plains [1]** | 217 (±14) | 94 (±9) |
| **Caloris interior plains [1]** | 80 (±7) | 26 (±4) |
| **Smooth plains south of Rachmaninoff [1]** | 58 (±13) | 17 (±7) |
| **Northern smooth plains (NSP) [2]** | 51 (±8) – 81 (±9) | 16 (±5) – 30 (±5) |
| **Northern Heavily Catered Terrain (NHCT) [2]** | 184 (±14) – 256 (±14) | 74 (±9) – 122 (±14) |

N(10) and N(20) values cannot be used to estimate the last tectonic activity of basin-edge scarps, because N values correspond to the aerial density of impact craters, and provide no absolute age data. To compare the approximate timing of emplacement of the smooth plains units with the age of cessation of resolvable activity on their associated basin-edge scarp, we applied the model production function of Marchi *et al.* (2009), Massironi *et al*. (2009), and Marchi *et al*. (2013) to the crater SFD and buffered SFD data.

To derive relative and absolute model ages on the lobate scarps, which are linear features rather than surface units, we applied the buffered count method (Fassett and Head, 2008), following the example of Giacomini *et al.* (2015) in applying it to tectonic features.

In this approach, craters that superpose the lobate scarp are counted, except those cut by a clear trace of the scarp —for example, the ~20 km diameter unnamed crater inside Dario in Figure 2.3 would not be included because the

basin-edge scarp of Aneirin cuts straight across it. For a subset of eight of the basin-edge lobate scarps we identified in the survey, we then calculated the feature width (W) by measuring the distance between the base of the front scarp and the base of the back slope (as identified by the break in slope, manifested in image data as a change in shading). Since the lobate scarps also vary in width along their length we took 20–30 measurements at regular intervals and used the mean of these as the value for W for each scarp. For each crater, we measured the diameter (D) and created a buffer around the scarp at a distance $S_{Buffer}$ (using ArcGIS 10.1). The areas of these buffers were then used in the crater statistics calculations, and were calculated as follows:

$$S_{Buffer} = 1.5\,D + 0.5\,W \quad (1)$$

Since the buffered method was not initially designed to be used on tectonic features, the following points should be borne in mind:

- The method includes craters that are not directly superposed onto the structure of interest (although their ejecta is superposed onto the structure).
- Faults are frequently composed of segments on which discrete slip events can occur, and so obtaining a single model age for the cessation of activity along the aggregate structure is an oversimplification.
- The count areas involved in linear features (as described above) are necessarily small, which can result in large errors from small-number statistics.

It is important to note that this buffered method provides an estimate for the age of cessation of resolvable activity on the scarp. Due to likely fault reactivation, it is not possible to use this method to determine the time at which faulting began.

Marchi *et al*. (2013) defined the terms “hard rock” and “cohesive soil” to characterise two end-member target properties, the choice of which changes the applicable production function. Here, we followed the example of Giacomini *et al*. (2015) in regarding the former term to mean unfractured rock and the latter to denote rock with reduced strength due to fracturing. The Marchi *et al*.

(2009) MPF also accommodated rheological layering of the target material, if observations of the surface or crater SFD data support the possibility of crustal layering (Marchi *et al.*, 2011; Ferrari *et al.*, 2015). To facilitate comparison between data obtained for the basins in Table 2.1, we consistently applied the following parameters: hard rock scaling (tensile strength: $2 \times 10^8$ dyne $cm^{-2}$) with no rheological layering and with predominantly Near-Earth Object population of impactors.

Along with our areal crater density values, we present our model age results in Table 2.1; plots for the volcanic infill of Shakespeare basin, and associated basin-edge scarp, using the Marchi *et al*. (2009) MPF are shown in Figure 2.8. Plots for the other results in Table 2.1 can be found in Appendix 1 (p. 175 – 189). The errors in Table 2.1 result from the process of fitting a production function to the cumulative SFD data only and do not include methodological errors involved in crater SFD analysis (such as those set out above).

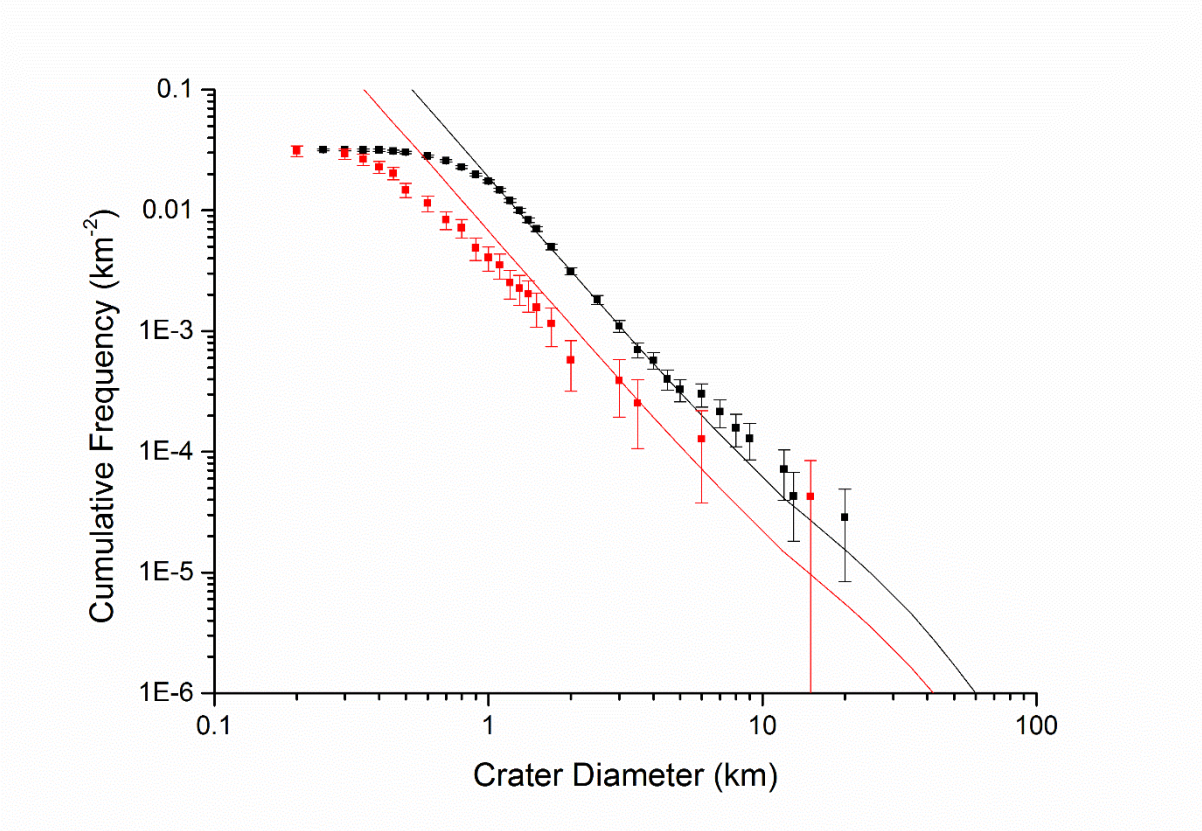


*Figure 2.8: Marchi production function model age plots for the volcanic fill (black) and basin-edge scarp (red) of Shakespeare.*

The absolute model ages derived by consistent application of the Marchi *et al*. (2009) MPF (Table 2.1) for the volcanic infills in the basins of this study with basin-edge scarps suggest a range of model ages for this last volcanic activity between 1.5 and 3.9 Ga. For the basins without basin-edge scarps, we obtained absolute model ages ranging from 0.9 Ga to 3.7 Ga. The sample size is small —eight basins with basin-edge scarps and eight basins without such structures— but our data indicate a range of ages for smooth plains units, whether or not they have basin-edge scarps. Our N(10) and N(20) values for Aneirin and Beethoven are the same, within error, to values recently found by Byrne *et al*. (2016). Byrne *et al*. (2016) derived an N(10) value for Aneirin of 72 ± 20 (our value: 93 ± 35), an N(20) value of 22 ± 11 (our value: 27 ± 19), and for Beethoven an N(10) value of 92 ± 22 (our value: 88 ± 23) and an N(20) value of 31 ± 13 (our value: 31 ± 14). Our absolute model ages for the smooth plains units of these two basins differ, however, from those of Byrne *et al*. (2016), who applied a different MPF (that of Le Feuvre & Wieczorek (2011)) and obtained absolute model ages of ~3.7/3.8 Ga for both smooth plains units using porous

scaling. When they used non-porous scaling, Byrne *et al*. (2016) obtained ages of ~2.2 Ga (Aneirin) and 2.7 Ga (Beethoven) which are comparable to our absolute ages but the errors for the non-porous scaling fits were of the order of several billion years.

Comparison between the model ages for the tectonic landforms and the smooth plains indicates that the application of the buffered method to linear tectonic features, as opposed to the Martian valley floors for which it was designed, produces results consistent with the stratigraphic observation that the last tectonic activity on the basin-edge scarps post-dates the emplacement of the most recent volcanic infill. This comparison is also consistent with new evidence of recent tectonic activity in the form of detection of small scale and necessarily young thrust scarps during MESSENGER's end-of-mission low altitude campaign (Watters *et al*., 2016).

Our results also indicate that the interval between the smooth plains emplacement and the last discernible movement on the associated basin-edge lobate scarp usually exceeds 1 Ga. The absolute model ages for the last resolvable slip on the basin-edge lobate scarps are clustered around approximately 1 Ga (with a range of 0.6 to 1.1 Ga). Giacomini *et al*. (2015) suggested that activity on small scarp segments or small individual scarps continued, perhaps even to the present, having found that buffer-derived model ages for a ~2000 km-long thrust system (composed of multiple lobate scarps 100 – 350 km in length), the "Blossom thrust system", indicated that these structures were most active prior to 3.5 Ga (Model ages in this case were produced under the assumption of a layered target with cohesive soil on top of hard rock, which we note is likely to produce generally older results than the uniform hard rock composition of the target body in the model ages we present). Our results suggest that activity continued on the subset of lobate scarps that we investigate here until considerably more recently than 3.5 Ga.

### *2.3.2 Verification of the Mansurian age of basin-edge scarps*

Because the MPF model ages for the basin-edge scarps in Table 2.1 extend well into the Mansurian, we examined these structures in more detail with high-resolution MDIS images. Our aim was to determine whether any craters cross-cut by the lobate scarps appear themselves to be Mansurian in age, in order to

provide additional evidence to support our inference that the formation of basin-edge scarps was indeed still occurring during the Mansurian (Table 2.1). The Mansurian epoch is now considered to extend from 1.9–0.3 Ga (Banks et al. 2016). Using the established method for estimating age of Hermean craters on the basis of their degradation state (Spudis and Guest, 1988), we searched for the presence of morphologically crisp rims, visible terracing within a given crater, a visible central peak, and a visible ejecta blanket (with or without rays) . Using the global MDIS mosaic basemap we identified three craters that match the above morphological requirements and that are crosscut by basin-edge scarps. We then examined these craters with higher resolution (average 50 m/pixel) MDIS images (Figures 2.9a–c).

In the case of Figure 2.9a, the unnamed crater centred at 04°S, 123°W, there are subtle morphological indications that the scarp affects at least the northern rim, but the evidence for tectonic deformation here is equivocal. However, the craters in Figures 2.9b and c are definitely cut by their proximal basin-edge lobate scarps, as the trace of the scarp can be seen on both the crater floor and in the crater wall.

Our observations of craters we assess as Mansurian on the basis of their morphology that are cross-cut by basin-edge lobate scarps supports our model ages results (Table 2.1), since they also indicate tectonic activity was occurring along these structures after the emplacement of the volcanic infill (in the Mansurian or possibly Kuiperian epoch).

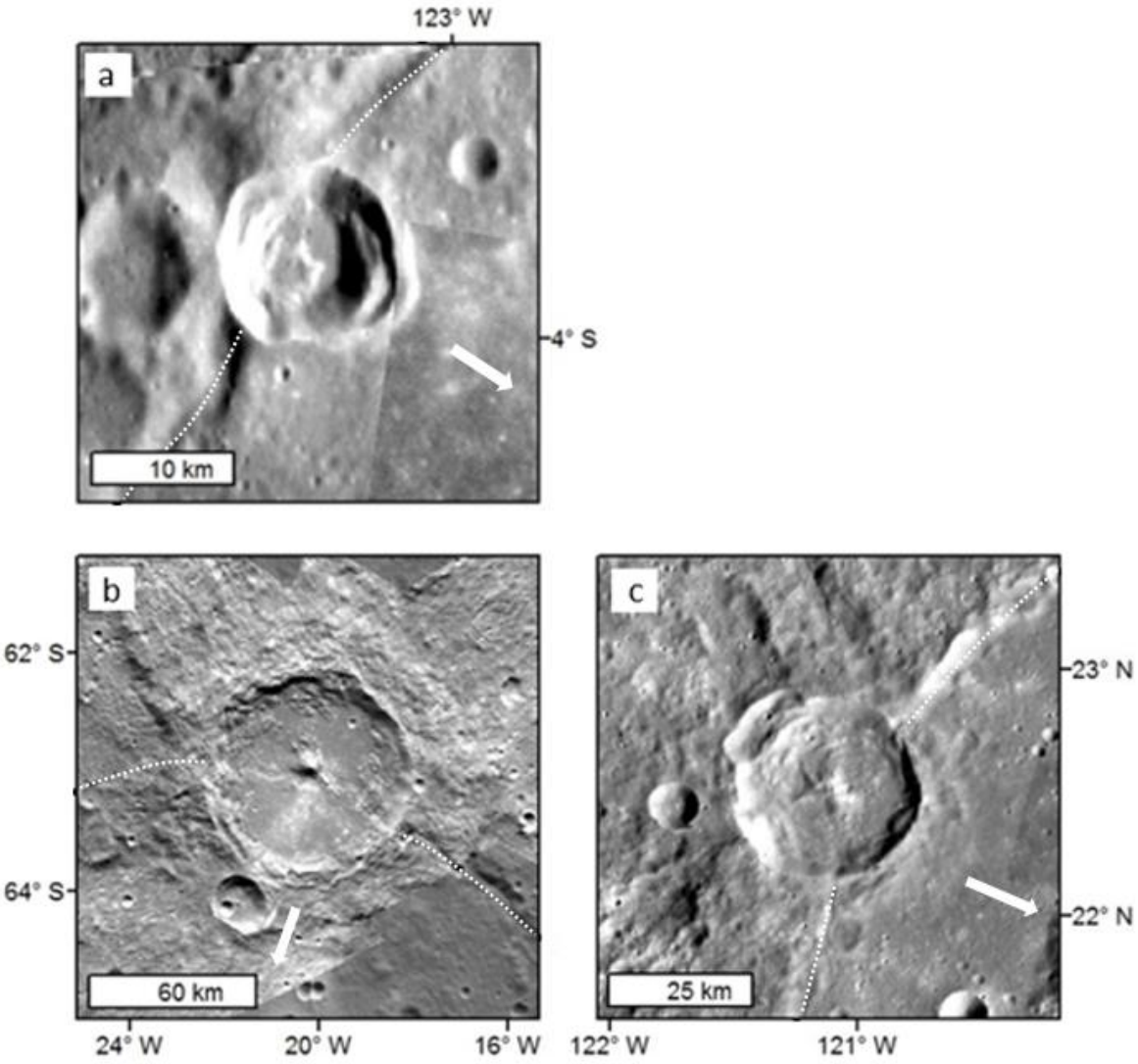


*Figure 2.9 (a–c): Three examples of craters, assessed to have formed during the Mansurian on the basis of degradation state, which are cut and deformed by basin-edge scarps. The white dotted lines indicate the basin-edge scarp (delineated only outside the cross-cut craters to avoid obscuring detail), and the white arrows indicate the direction to the centre of the volcanically infilled basin in each case. The volcanically infilled basins in each case are: (a) Unnamed (centre coordinates: 04°S, 123°W), 14 km diameter (images: EN1051949290M and EN0257562458M), (b) Pushkin (the crater that has been cut through by the basin-edge lobate scarp is Tsurayuki, 83 km diameter) (images: EN1066019121M, EN1066078737M and EN1066019149M), and (c) Durer, 31 km diameter (images: EN0211806621M, EN0227048749M and EN0211806621M).*

## 2.4. Discussion

### *2.4.1 Proposed formation mechanism*

Upon the basis of the location and morphology of the basin-edge lobate scarps, we propose the following formation sequence (depicted in Figure 10):

1. An impact event creates a basin.
2. As impacts continue on the surrounding region of the surface, regolith accumulates on the basin floor.
3. This basin is subsequently flooded by basaltic lavas that solidify to form a "smooth plains" unit (Strom *et al.*, 1975; Denevi *et al*., 2013). The interface between the basin floor and the base of the smooth plains unit may represent a mechanical discontinuity, especially if there had been time for an appreciable thickness of regolith to develop prior to flooding. The expectation is that regolith growth on Mercury is faster than on the Moon, since the median impact velocity at Mercury is approximately double that at the Moon (because Mercury is deeper in the Sun's gravity well (Langevin, 1997)). The observation of "ghost craters" visible within some of the smooth plains units (for example, Aneirin shown in Figure 2.3) indicates that a substantial period of time elapsed between basin creation and the most recent episode of volcanic plains emplacement in at least some cases (cf. Byrne *et al.* 2016).
4. As Mercury's crust shortens due to global contraction, fault nucleation occurs along the mechanically weak interface, and propagates along it before breaching the surface at the edge of the basin infill. The mechanically weak interface is at shallow crustal levels, where fault nucleation is most favourable within a stress field driving global contraction (Klimczak, 2015). A detachment fault, along which the overlying material slides, forms along the interface.
5. The smooth plains unit moves along the detachment fault, essentially as a hanging wall block, forming an arcuate lobate scarp (or scarps, since we observed examples where a basin-edge scarp has formed at opposite edges of the same volcanically filled basin) at the basin margin that approximately follows the inner edge of the original impact basin rim and, with increased amounts of shortening strains, over-thrusts it.

The mechanism we propose is comparable, although smaller in scale, to the basal décollement proposed by Rothery & Massironi (2010) beneath Beagle Rupes. Mechanical discontinuities within the crust of Mercury that have been suggested by Byrne *et al.* (2014) and hypothesised to be a contributing factor in the formation of Discovery and Adventure–Resolution Rupes (Watters *et al.* 2001). We observe that basin-edge scarps' vergence is always outwards facing, and that the scarps themselves follow the interior rim of the original basin without extending beyond it (except in examples where the smooth plains unit has overthrust the original rim). The mechanism we propose here accounts for these observations. When crustal shortening is localised along the interface between the basin floor and the base of the smooth plain infill (with a buried layer of regolith at some depth possibly also contributing, as discussed in point 3, above), that interface could constitute a detachment surface that would act as a stress guide into which thrust faults would be channelled (Zoback *et al.*, 2002). The smooth plains unit within the original basin is not fractured in this scenario, but instead is forced upwards along the detachment fault towards the rim of the original impact basin.

***Figure 2.10 (below): Cartoon depicting my proposed basin-edge lobate scarp formation mechanism. (a) The formation of an impact basin results in fracturing of the crust below and surrounding the impact basin (indicated by fine black lines). (b) A layer of regolith forms through continued impact bombardment (shown in green). (c) The basin is infilled by lava. (d) The large white arrows indicate direction of maximum compressive stresses in the lithosphere; as the crust is shortened, a fault (or faults) nucleate along the plane of weakness, resulting in movement along the interface between the basin floor and the base of the smooth plains unit. The example above depicts a basin with two lobate scarps (in this cross-sectional diagram: left and right). The cartoons are not to scale.***

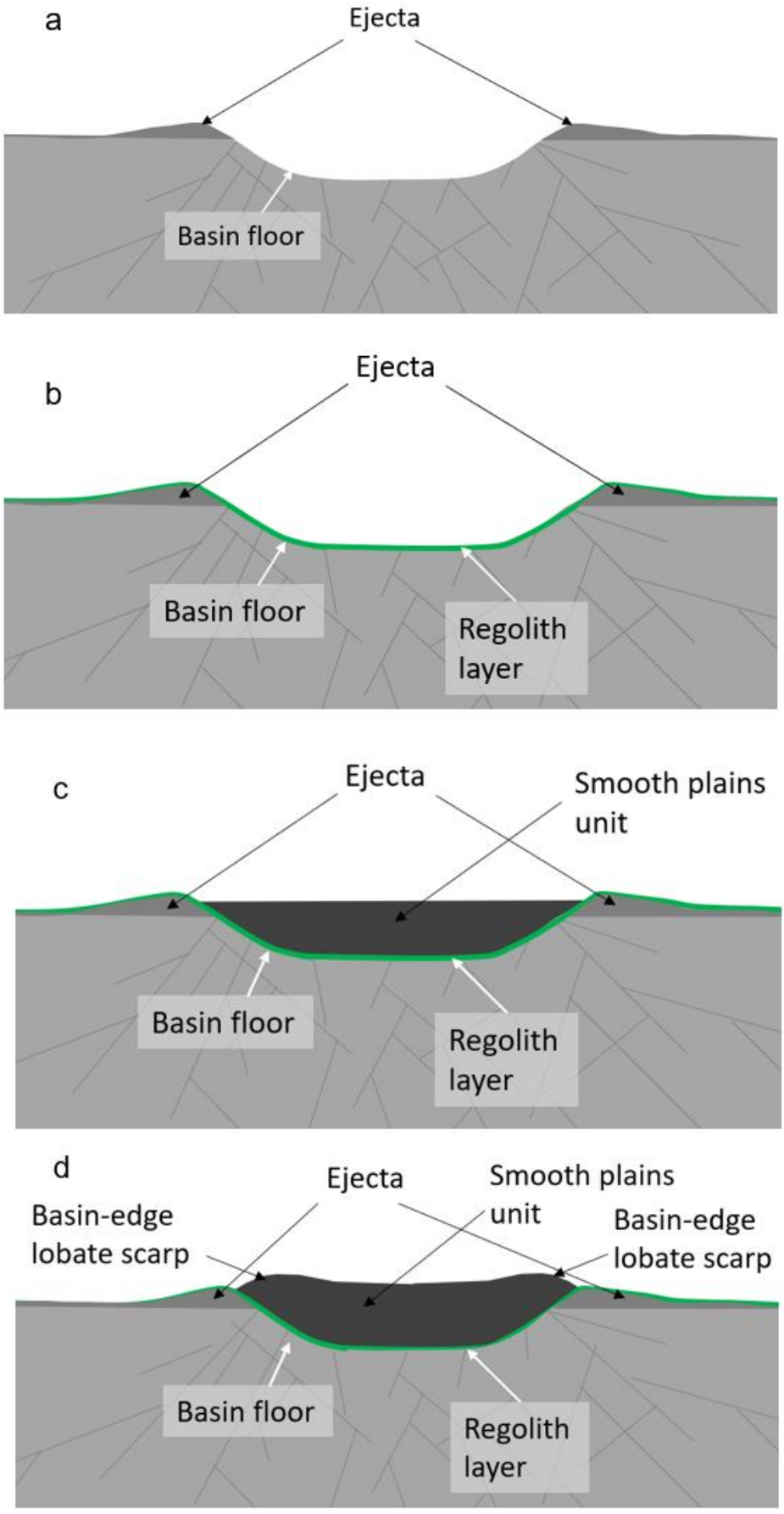
a
Ejecta
Basin floor
b
Ejecta
Basin floor
Regolith layer
c
Ejecta
Smooth plains unit
Basin floor
Regolith layer
d
Ejecta
Smooth plains unit
Basin-edge lobate scarp
Basin-edge lobate scarp
Basin floor
Regolith layer

### *2.4.2 Timing and locations of formation*

Volcanic activity on a very large scale (for example the northern volcanic plains and Caloris Plainitia) ended on Mercury by around 3.5 Ga (Byrne *et al*. 2016) with only smaller-scale volcanic flooding continuing thereafter (Prockter *et al.*, 2010; Marchi *et al.*, 2011; Byrne *et al.*, 2016). Our results indicate that volcanism of sufficient scale to cover basin floors of approximate areas of $8 \times 10^4$ km$^2$ (for basins with a diameter of 100 km) and above continued until at least approximately 1.5 Ga. Our youngest example (according to the model ages we calculated: see Table 2.1) with a basin-edge scarp is Shevchenko (1.5 ±0.2 Ga), and our youngest example without a basin-edge scarp is Khansa (0.9 ±0.1 Ga). These results are consistent with the findings of Marchi *et al.* (2011), who derived ages younger than ~1.0 Ga for the smooth plains fill of two basins (Raditladi and Rachmaninoff), though it is likely the fill in at least one of those cases is impact melt rather than volcanic lavas (Blair *et al.*, 2013). The ascent of magma is assisted by the fracturing created by impacts (Melosh, 2011; Klimczak, 2015; Byrne *et al.*, 2016) potentially accounting for how relatively large volcanic plains formed so late in Mercury's history despite ongoing global contraction.

The model ages we determined for the basin-edge lobate scarps lie between 0.6 and 1.1 Ga and they average to approximately 1 Ga (see Table 2.1). Under a scenario in which sufficient time elapsed between basin formation and volcanic infilling for a regolith to form on the original basin floor, then the presence of this regolith layer could constitute a detachment surface *(*Zoback *et al.*, 2002) However, although model age difference between basin formation and the youngest lava infill can sometimes be resolved (Marchi *et al.*, 2011; Ferrari *et al.*, 2015) it is not possible to determine the interval between the basin-forming impact and emplacement of the first volcanic fill, and therefore it is not possible to determine whether or not there was time for a sufficient thickness of regolith to form. However, we have observed several instances of ghost craters, such as those visible in Figure 2.3. The presence of these landforms suggests a significant time interval during which regolith could form, contributing themselves to the growth of regolith by way of their ejecta blankets.

## 2.5 Conclusions

Our results suggest that:

- Effusive volcanism of sufficient volume to extend across the floors of basins 100 km in diameter or greater continued until at least early Mansurian (approximately 1.5 Ga), possibly assisted by impact fracturing that allowed this relatively late ascent of magma to the surface despite Mercury's history of sustained global contraction.
- The use of the buffered method on tectonic features produces results consistent with the observed stratigraphy (Byrne *et al.*, 2016).
- Resolvable deformation accommodated by basin-edge lobate scarps appears to have ceased between ~1.1 Ga and ~0.6 Ga, in the mid-to-late Mansurian, at least as determined with our crater areal density surveys and our model ages.
- We suggest that the interface between the original basin floor and the base of the smooth plains units acts as a mechanical discontinuity along which detachment faulting could have occurred.

With regard to the orientation of basin-related lobate scarps we note that the results of our global survey are to first order, consistent with those of Watters *et al.* (2015) and Byrne *et al.* (2014), since we also observe a preference for north–south orientations at low latitudes and east–west at higher latitudes. However, our conclusions differ from those of Watters *et al.* (2015) since we found that the orientation/facing direction plots for structures in those same areas do not consistently show these preferences when the illumination direction is artificially varied. This strongly indicates to us that lighting bias cannot be ruled out when a north–south preference in orientation is detected on the surface of Mercury, as has been proposed by Byrne *et al.* (2014) and Klimczak *et al.* (2015).

## 2.6 Notes

In chapter 3, I present the additional work I carried out on the topic of basin-edge scarps that was not included in this paper.

# 3 Additional work on basin-edge scarps

## 3.1 Introduction

The work on basin-edge scarps that I presented in Chapter 2 was published in the journal Icarus (Fegan *et al*., 2017). However, I did related work on the topic of basin-edge scarps that I did not include in the published work. I include these additional sections in this chapter.

In addition to the Marchi *et al.* (2011) model production function that I chose for the publication, I also used two other model production functions. I applied some tests to examine the robustness of applying the buffered method for age dating linear features (Fassett *et al.,* 2008) to tectonic features on Mercury, rather than the channel floor features it was designed for. Finally, I include additional qualitative observations, and a section discussing further the limitations of the methods that I employed.

## 3.2 Model Production Functions

### *3.2.1 Neukum Production Function*

In Chapter 2, I presented my findings using the Marchi *et al.* (2011) model production function (MPF). In addition to this MPF, I also applied the Neukum Production Function method (Neukum *et al.,* 2001) to some of the basins I covered in Chapter 2. These two methods can produce absolute ages at variance with each other (Marchi *et al*., 2013), so my initial intention when obtaining model ages for all of my data using both methods was to investigate how great those differences were in these instances, and (using the visual verification, as presented in Chapter 2) attempt to identify which method produces results best matching my observations of the age of craters being cut by basin-edge scarps.

The Neukum *et al.* (2001) MPF method requires the same input as that of the Marchi *et al.* (2011), so no additional data collection was required. The processing of the SFD data from digitising the craters (using CraterTools plug-in for ArcMap 10.1) to creating the plots and fitting the model production curves (using the software CraterStats) is straightforward using the Neukum *et al.* (2001) MPF (particularly when working on areas rather than using the buffered

method), and possible for me to carry out myself. Neither of these is not the case when using the Marchi *et al.* (2011) method because there are too many variables and the code required hasn't been integrated into any of the software tools available to all. To obtain dates using the Marchi *et al.* (2011) method, the data must be sent to Marchi, who processes it and sends the absolute model ages and fit data back to the worker.

One example of the Neukum *et al.* (2001) MPF for basin volcanic fill and basin-edge scarp for Aneirin is shown in Figure 3.1. The remaining plots can be found in Appendix 2 (p.190 – 197), and the model ages are shown in Table 3.1.

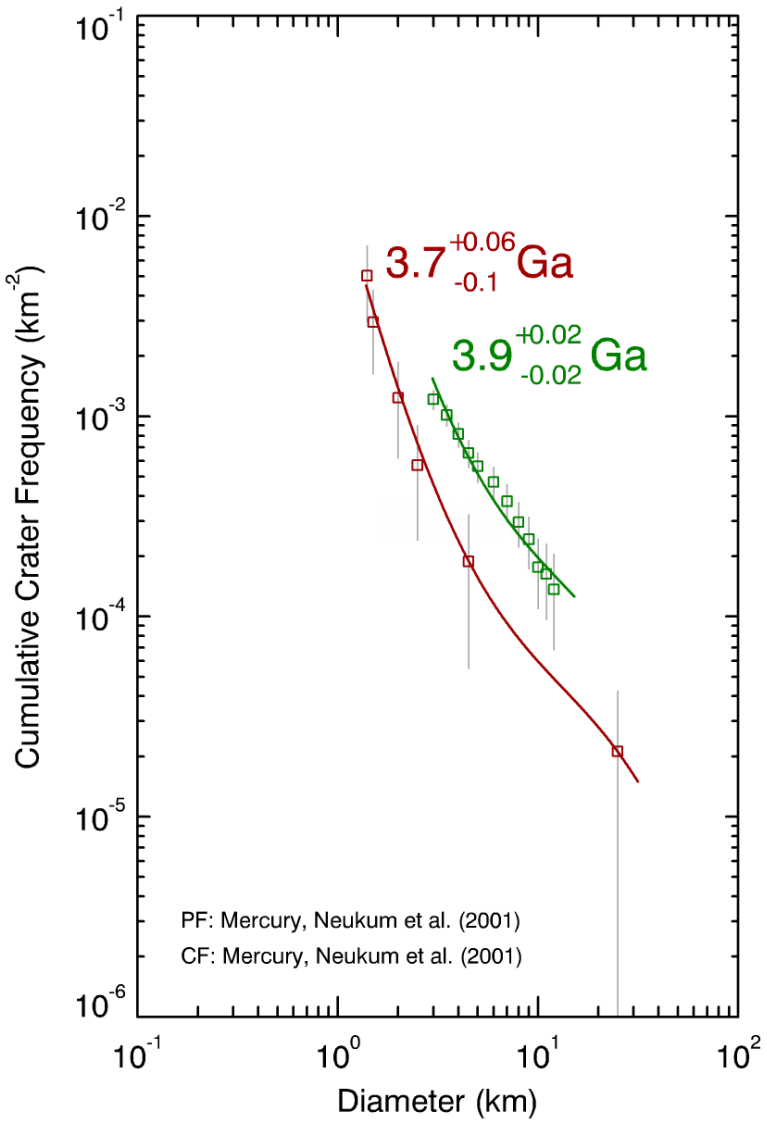


*Figure 3.1: A crater size-frequency plot, illustrating the fitting of the Neukum model production function to derive absolute ages for Aneirin basin fill (green) and the associated basin-edge scarp (red).*

**Table 3.1**: Comparison between Neukum and Marchi production function results for volcanic fills and lobate scarps. The unnamed basins are distinguished by the coordinates of their centre points in decimal degrees.

| | **Neukum Production Function model ages (Ga)** | | **Marchi *et al.* (2011) Production Function model ages (Ga)** | |
|---|---|---|---|---|
| | **Fill** | **Scarp** | **Fill** | **Scarp** |
| **Aneirin** | 3.9 | 3.7 | 2.2 | 0.6 |
| **Beethoven** | 3.9 | 3.9 | 3.5 | 1.0 |
| **Hafiz** | 3.9 | 3.7 | 2.9 | 1.0 |
| **Shakespeare** | 3.9 | 3.8 | 2.9 | 1.0 |
| **Shevchenko** | 3.7 | 3.6 | 1.5 | 1.1 |
| **Unnamed [40°S, 70°W]** | 3.9 | 3.9 | 3.9 | 1.1 |
| **Unnamed [91°N, 38°E]** | 3.8 | 3.8 | 3.9 | 1.1 |
| **Unnamed [150°N, 10°W]** | 3.9 | 3.9 | 3.0 | 1.1 |

As discussed in Chapter 2, for the Marchi *et al*. (2009) MPFs used in this work, the parameters applied were Hard Rock scaling (tensile strength: $2 \times 10^8$ dyne $cm^{-2}$), with no rheological layering and predominantly Near Earth Object population of impactors.

The differences between the model ages produced by the two different production functions are clear in Table 3.1. The NPF results in Table 3.1 indicate ages for both the fills and the associated lobate scarps of between 3.7 and 3.9 Ga, considerably older than the MPF ages. Although the input data are the same in each case, the model ages differ by up to two billion years. This is particularly noticeable in the model ages for the basin-edge scarps (those processed using the buffered count method).

Below I outline several differences between Neukum and Marchi MPF methods that might account for these differences, they are further detailed in Giacomini *et al.* (2015). For the Neukum MPF method, the lunar production function is altered (in terms of target gravitational acceleration) to apply to Mercury, and the impactor flux SFD is assumed stable throughout Solar System history (Neukum *et al.* 2001). In contrast, the Marchi MPF can account for impactor flux SFD variations throughout Solar System history: in the early Solar System it is assumed that impactors would be more likely sourced from Main Belt Asteroid (MBA), while more recently Near Earth Objects (NEO) would be the more likely source (Marchi *et al.* 2013). The MPF method also allows for the input of different target surface properties (with respect to tensile strength and density) as well as different crater scaling laws: Hard Rock or Cohesive Soil, the choice of which will also change the production function. We follow the example of Giacomini *et al*. (2015) in assuming the former case is unfractured rock and the latter to be rock with reduced strength due to fracturing. The target surface can also be rheologically layered in the MPF model, if the geology or crater SFD plot support the existence of layering in the crust (Marchi *et al*., 2013; Giacomini *et al.,* 2014)

The NPF method tends to over-estimate the age of younger surfaces and features, a problem which has been addressed by the MPF method according to Marchi *et al.* (2013). This is possibly what we observe in the results in Table 3.1, as the difference between and the overestimation of model ages derived from on the buffered (scarp) counts is in the billions of years. In addition, the NPF results shown in Table 3.1 suggest that (resolvable) activity on the basin-edge scarps ceased very shortly after volcanic infilling of the basins in all of the cases we examined using the NPF method.

The results in Table 3.1 show that the two methods cannot be used interchangeably. The evidence of morphologically Mansurian-age craters deformed by basin-edge lobate scarps (see Chapter 2) corroborates the late Mansurian model ages for cessation of scarp activity produced by the MPF method, which is the reason I chose to include the Marchi *et al.* (2011) model ages in Chapter 2 and not the Neukum *et al.* (2001) model ages.

### *3.2.2 Le Feuvre and Wieczorek Production Function*

Another modern model production function (MPF) is that of Le Feuvre & Wieczorek (2011). With the intention of using this alternative modern method to check the results I obtained using the Marchi Production Function (Marchi *et al.,* 2011) I re-calculate the model ages for the basins and basin-edge lobate scarps in Table 3.1 using this method. The Le Feuvre and Wieczorek (LeF&W) MPF allows the application of either porous or non-porous scaling. Whether the porous or non-porous scaling is appropriate depends upon the presence or lack, respectively, of a porous megaregolith on the surface of the body (Le Feuvre & Wieczorek 2011). We are not able to determine whether or not such a megaregolith is present, so we apply both porous (Table 3.2) and non-porous (Table 3.3) scaling to our data.

The crater SFD plots for one example of my application of LeF&W MPF to my crater SFD data is shown in Figure 3.2. The remaining SFD plots are provided in Appendices 3 (porous scaling) and 4 (non-porous scaling). All LeF&W results are shown in Tables 3.2 (porous scaling) and 3.3 (non-porous scaling).

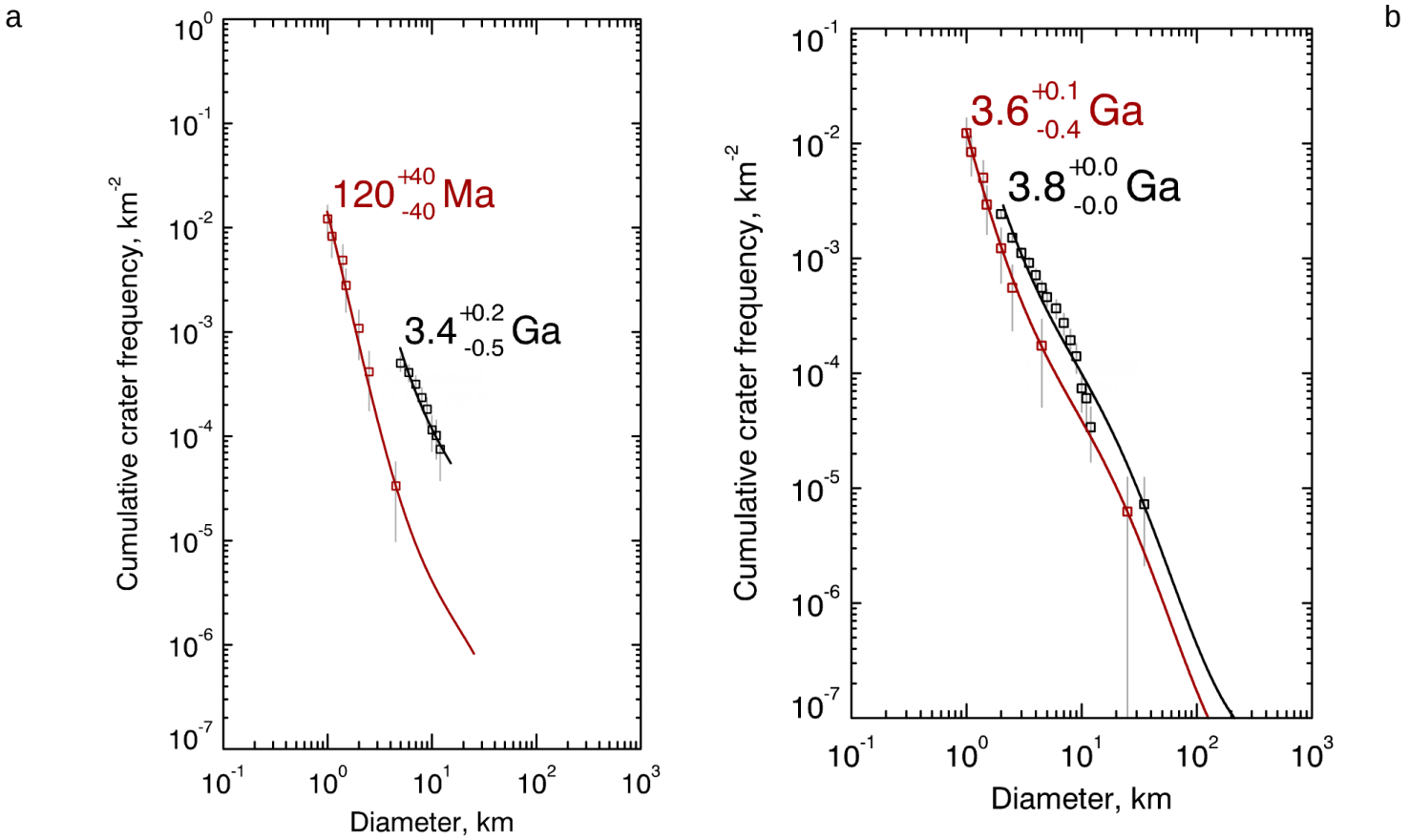


*Figure 3.2: LeF&W MPF results for Aneirin, black indicates the smooth plains, red indicates the basin-edge scarp. (a) uses the porous scaling, (b) uses the non-porous scaling.*

**Table 3.2**: LeF&W MPF results using the porous scaling. Note: craterstats quotes some errors as ±0 but stated here as ±0.1 to avoid giving the impression that the fit is entirely without uncertainty. Plots for the results for basins with basin-edge scarps can be found in Appendix 3 (p. 198 – 204).

| With basin-edge scarps | | | | | | Without basin-edge scarps | | | | |
|---|---|---|---|---|---|---|---|---|---|---|
| **Name** | **Count Area km$^2$** | **N(10) (conf. int.)** | **N(20) (conf. int.)** | **Fill (conf. int.) Ga** | **Scarp (conf. int.) Ga** | **Name** | **Count Area km$^2$** | **N(10) (conf. int.)** | **N(20) (conf. int.)** | **Fill (conf. int.) Ga** |
| Aneirin | 7.5x10$^4$ | 93 (±35) | 27 (±19) | 3.8 (±0.1) | 3.6 (+0.1 -0.4) | Mendelson | 4.4x10$^4$ | 45 (±32) | 23 (±23) | 3.7 (±0.1) |
| Beethoven | 1.6x10$^4$ | 88 (±23) | 31 (±14) | 3.8 (±0.1) | 3.8 (±0.1) | Hugo | 1.3x10$^3$ | 155 (±109) | N/A | 3.8 (±0.1) |
| Hafiz | 2.1x10$^5$ | 242 (±108) | 97 (±69) | 3.8 (±0.1) | 3.7 (±0.1) | Khansa | 4.6x10$^3$ | N/A | N/A | 2.3 (±0.4) |
| Shakespeare | 7.0x10$^4$ | 72 (±32) | 29 (±20) | 3.7 (±0.1) | 3.7 (±0.1) | Copland | 2.4x10$^3$ | N/A | N/A | 3.7 (±0.1) |
| Shevchenko | 6.1x10$^3$ | N/A | N/A | 3.6 (±0.1) | 2.5 (+0.8 -0.9) | Unnamed[-166, -25] | 4.0x10$^3$ | N/A | N/A | 0.4 (±0.06) |
| Unnamed[-40, -70] | 7.5x10$^4$ | 239 (±57) | 76 (±32) | 3.8 (±0.1) | 3.8 (±0.1) | Unnamed[154,67] | 3.8x10$^3$ | 261 (±261) | N/A | 3.7 (±0.1) |
| Unnamed[91, 38] | 1.8x10$^4$ | N/A | N/A | 3.7 (±0.1) | 3.7 (±0.1) | Unnamed[-69,0] | 8.0x10$^3$ | 126 (±126) | N/A | 3.6 (±0.1) |
| Unnamed[150, -10] | 1.4x10$^4$ | 138 (±97) | N/A | 3.8 (±0.1) | 3.8 (±0.1) | Unnamed[-13, -22] | 4.2x10$^3$ | 416 (±315) | N/A | 3.8 (±0.1) |

**Table 3.3**: LeF&W MPF results using the non-porous scaling. Note: craterstats quotes some errors as ±0 but stated here as ±0.1 to avoid giving the impression that the fit is entirely without uncertainty. Plots for the results for basins with basin-edge scarps can be found in Appendix 4 (p. 205 - 211).

| With basin-edge scarps | | | | | | Without basin-edge scarps | | | | |
|---|---|---|---|---|---|---|---|---|---|---|
| **Name** | **Count Area km²** | **N(10) (conf. int.)** | **N(20) (conf. int.)** | **Fill (conf. int.) Ga** | **Scarp (conf. int.) Ga** | **Name** | **Count Area km²** | **N(10) (conf. int.)** | **N(20) (conf. int.)** | **Fill (conf. int.) Ga** |
| Aneirin | $7.5x10^4$ | 93 (±35) | 27 (±19) | 3.4 (+0.2 -0.5) | 0.1 (±0.04) | Mendelson | $4.4x10^4$ | 45 (±32) | 23 (±23) | 0.5 (±0.05) |
| Beethoven | $1.6x10^4$ | 88 (±23) | 31 (±14) | 2.3 (±0.2) | 1.5 (±0.5) | Hugo | $1.3x10^3$ | 155 (±109) | N/A | 2.3 (±0.3) |
| Hafiz | $2.1x10^5$ | 242 (±108) | 97 (±69) | 2.3 (±0.6) | 1.4 (±0.7) | Khansa | $4.6x10^3$ | N/A | N/A | 0.05 (±0.01) |
| Shakespeare | $7.0x10^4$ | 72 (±32) | 29 (±20) | 2.5 (±0.5) | 0.4 (±0.2) | Copland | $2.4x10^3$ | N/A | N/A | 0.4 (±0.04) |
| Shevchenko | $6.1x10^3$ | N/A | N/A | 0.1 (±0.02) | 0.06 (±0.02) | Unnamed[-166, -25] | $4.0x10^3$ | N/A | N/A | 0.4 (±0.06) |
| Unnamed[-40, -70] | $7.5x10^4$ | 239 (±57) | 76 (±32) | 3.7 (±0.1) | 2.3 (±0.9) | Unnamed[154,67] | $3.8x10^3$ | 261 (±261) | N/A | 0.2 (±0.03) |
| Unnamed[91, 38] | $1.8x10^4$ | N/A | N/A | 0.8 (±0.3) | 0.6 (±0.2) | Unnamed[-69,0] | $8.0x10^3$ | 126 (±126) | N/A | 0.2 (±0.04) |
| Unnamed[150, -10] | $1.4x10^4$ | 138 (±97) | N/A | 0.6 (±0.08) | 0.5 (±0.1) | Unnamed[-13, -22] | $4.2x10^3$ | 416 (±315) | N/A | 0.7 (±0.07) |

Both the porous and non-porous scaling fit the size-frequency data, and produce different model ages, neither of which are comparable to those I obtained by applying the Marchi MPF. The porous scaling results are closer to the results of the Marchi MPF than the results of the non-porous scaling.

The porous scaling (Table 3.3) results in model ages for the smooth plains units within the basins with basin-edge lobate scarps (in both diameter bins) that all fall within the interval 3.6 – 3.8 Ga. For the basin-edge scarps, the model ages with porous scaling fall between 3.7 – 3.8 Ga with the exception of Shevchenko (in the smaller diameter bin), the basin-edge scarp of which has a model age of 2.5 Ga.

The non-porous scaling results in very different results from those of the porous scaling, and introduces a difference in the model ages of the smooth plains units within the large and small category basins. The model age of the smooth plains units within the large category fall between 2.3 – 3.4 Ga, and the associated basin-edge scarps model as 0.1 – 1.5 Ga. The corresponding intervals for the smaller diameter category are 0.1 – 3.7 Ga and 0.06 – 2.3 Ga. The model age results for Unnamed [-40, -70] in the small category are an outlier for that category, with model age results older than those of most of the larger category basins. However, the result is not necessarily suspect, because while smaller basins are more likely to be younger than larger ones, this is not universally the case.

Both the large and small categories of basins lacking basin-edge scarps have young model ages using the non-porous scaling, between 0.2 – 2.3 Ga.

Both porous and non-porous scaling results in good fits for the production function to the data in most cases, so we are unable to rule out one or the other on the basis of poor fit. Consequently, we cannot draw any conclusions upon the likelihood of the study areas having a megaregolith.

There are not currently sufficient examples in the literature using this new method for me to be able to determine whether I ought to apply the porous or non-porous scaling in these cases. I therefore present them for completeness with no additional analysis.

## 3.3 Tests of the buffered method

### *3.3.1 Test 1*

The method I used to carry out dating on the lobate scarps (see Section 2.3.2) was originally used on Martian channel floors (Fassett & Head 2008) rather than tectonic features and therefore I carried out a test to give confidence to my results. This is particularly important given the small separation in model ages for the volcanic fills and lobate scarps which deform them – it raises the question of whether this is a real result or simply comes about because the buffered method produces a model age for the fill the fault deforms rather than the lobate scarp itself.

The lobate scarp I chose is un-named and found at approximately 70 degrees north (see Figure 8). I chose it because it cuts through two different crater ejecta blankets – Nizami and Martial. I carried out crater counting on these two ejecta blankets and the intermediate terrain also deformed by the scarp, the count areas are delineated in Figure 8. I then followed the buffered crater counting method (described in section 2.3.2 and Fassett and Head (2008)) on the lobate scarp.

The results of the three crater counts and buffered count are presented on Figure 9. The model ages ought to reflect the superposition of Martial and Nizami crater ejecta onto the intermediate terrain and the lobate scarp deforming all three surfaces – making it the youngest feature.

The model ages for the lobate scarp (black) and Martial crater ejecta (orange) are identical within the error. However, the separation between the intercrater plains (green) and the ejecta of Nizami (red) is much clearer, which provides confidence that the buffered method is not simply dating the surface(s) across which the lobate scarp runs.

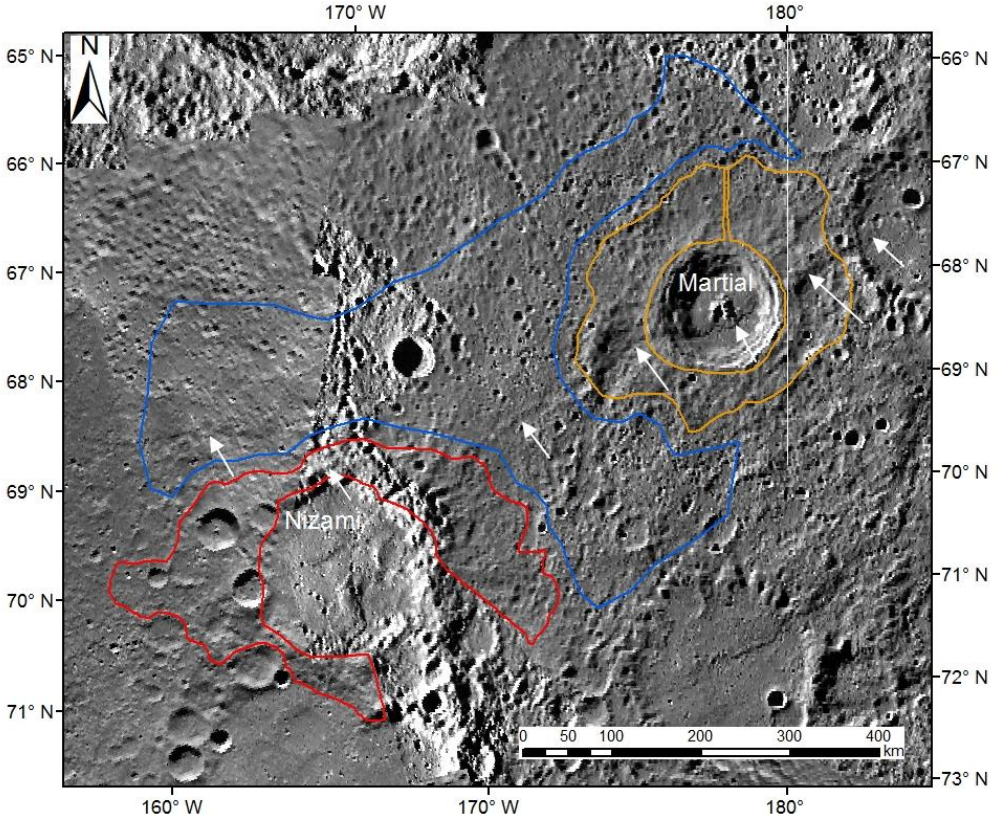


*Figure 3.3: Test 1 count areas (Nizami ejecta in red, Martial ejecta in orange, intercrater plains count area in blue), and lobate scarp indicated with white arrows. Image is polar stereographic projection of MDIS v9 global mosaic*.

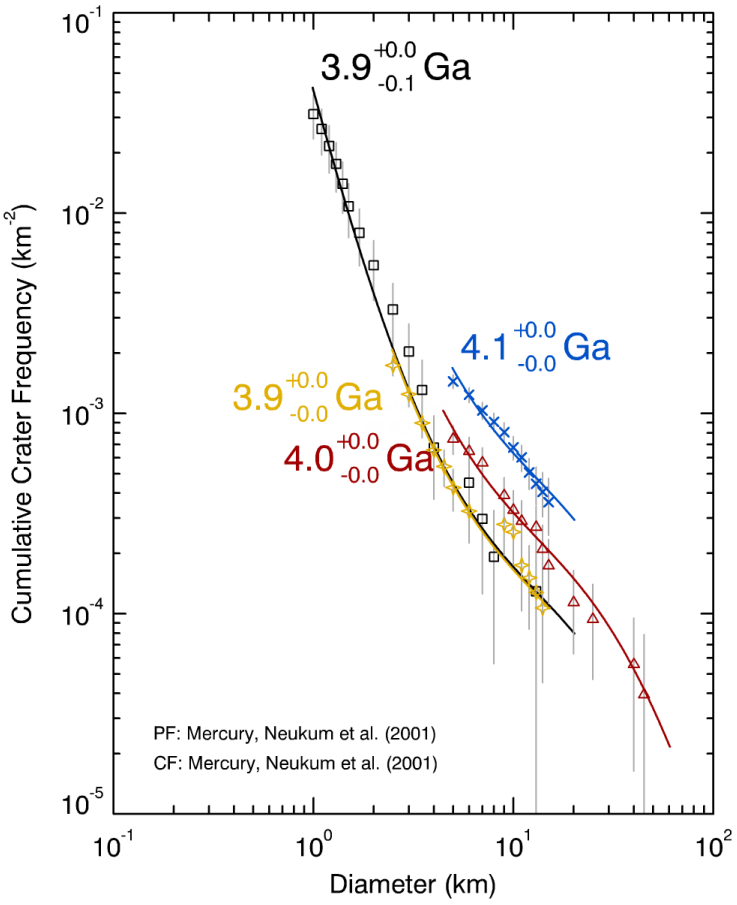


*Figure 3.4: Test 1 Results in order youngest to oldest: Black = lobate scarp, orange = Martial crater ejecta, red = Nizami ejecta and blue = intercrater plains.*

### *3.3.2 Test 2*

Using similar methodology to that I presented in section 3.3.1, I conducted crater SFD analysis on the Victoria Rupes area. The area is indicated in Figure 3.5, and the areas I carried out crater counting are: Intermediate Plains unit, Holbein crater fill, Holbein crater continuous crater ejecta, unnamed crater ejecta. I then also carried out buffered crater SFD analysis on the various sections of the Victoria Rupes. These areas are indicated on Figure 3.5.

My observations of this area indicate that the sequence of events shown by the relative ages of the areas/events ought to be: both Holbein and unnamed crater fills and ejecta (as relevant), then Victoria Rupes activity continuing after both of these impact features.

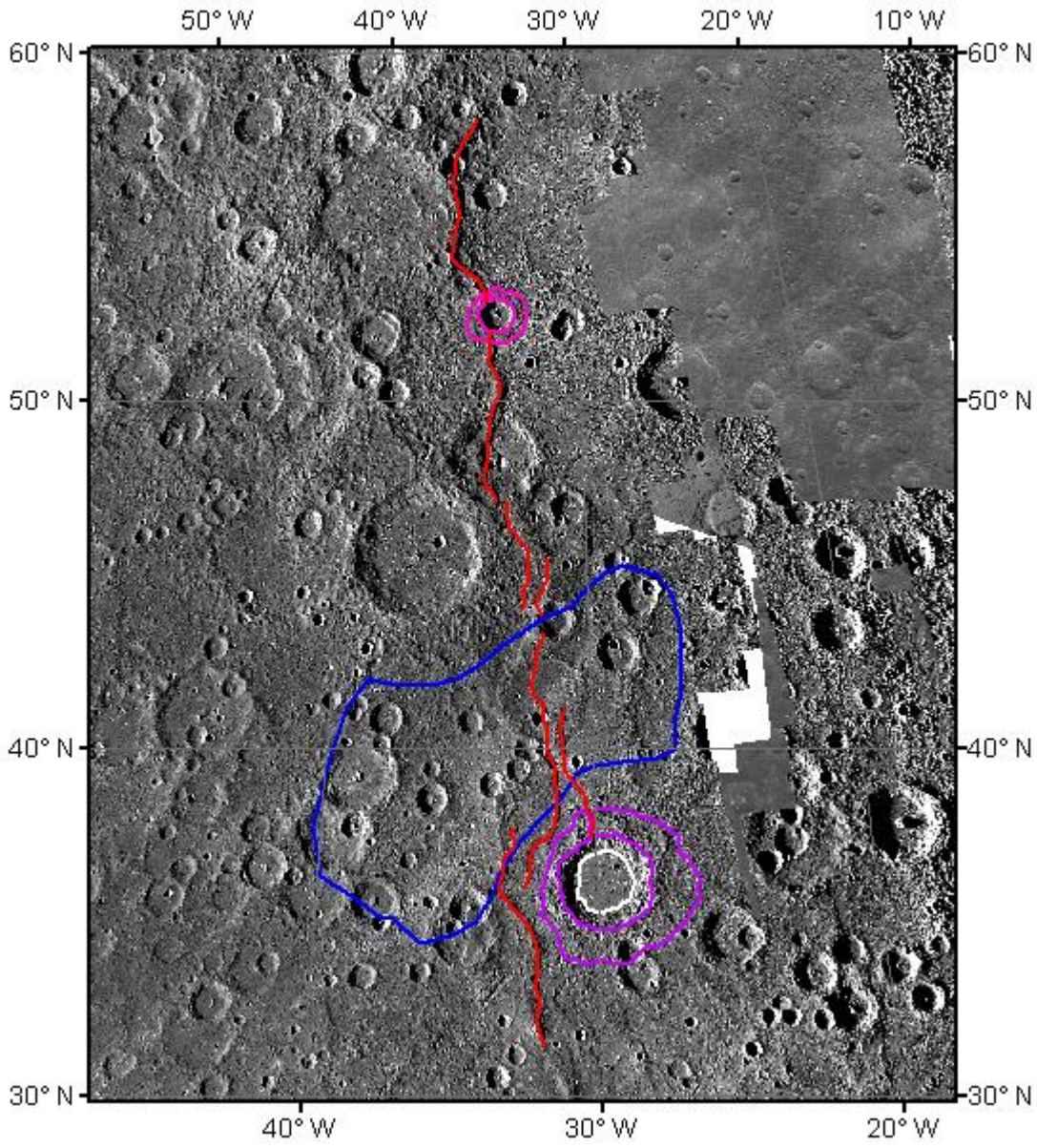


*Figure 3.5: Test 2 area: blue – plains, white – fill Holbeirn, purple – holbeirn ejecta, pink – unnamed ejecta, red – Victoria rupes.*

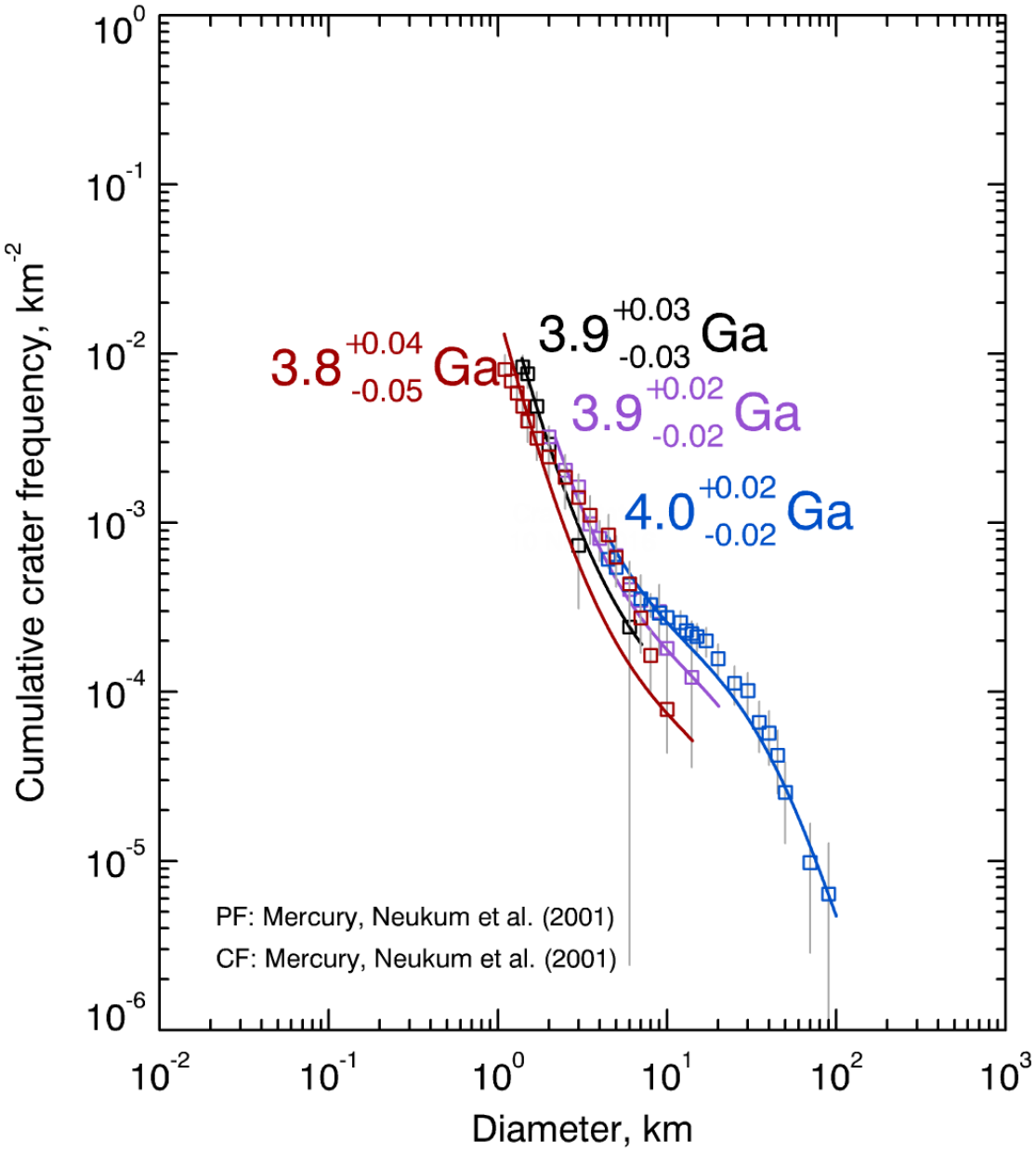


*Figure 3.6: Test 2 results - red = victoria rupes, blue = plains, purple = Holbein ejecta, black = Holbein fill.*

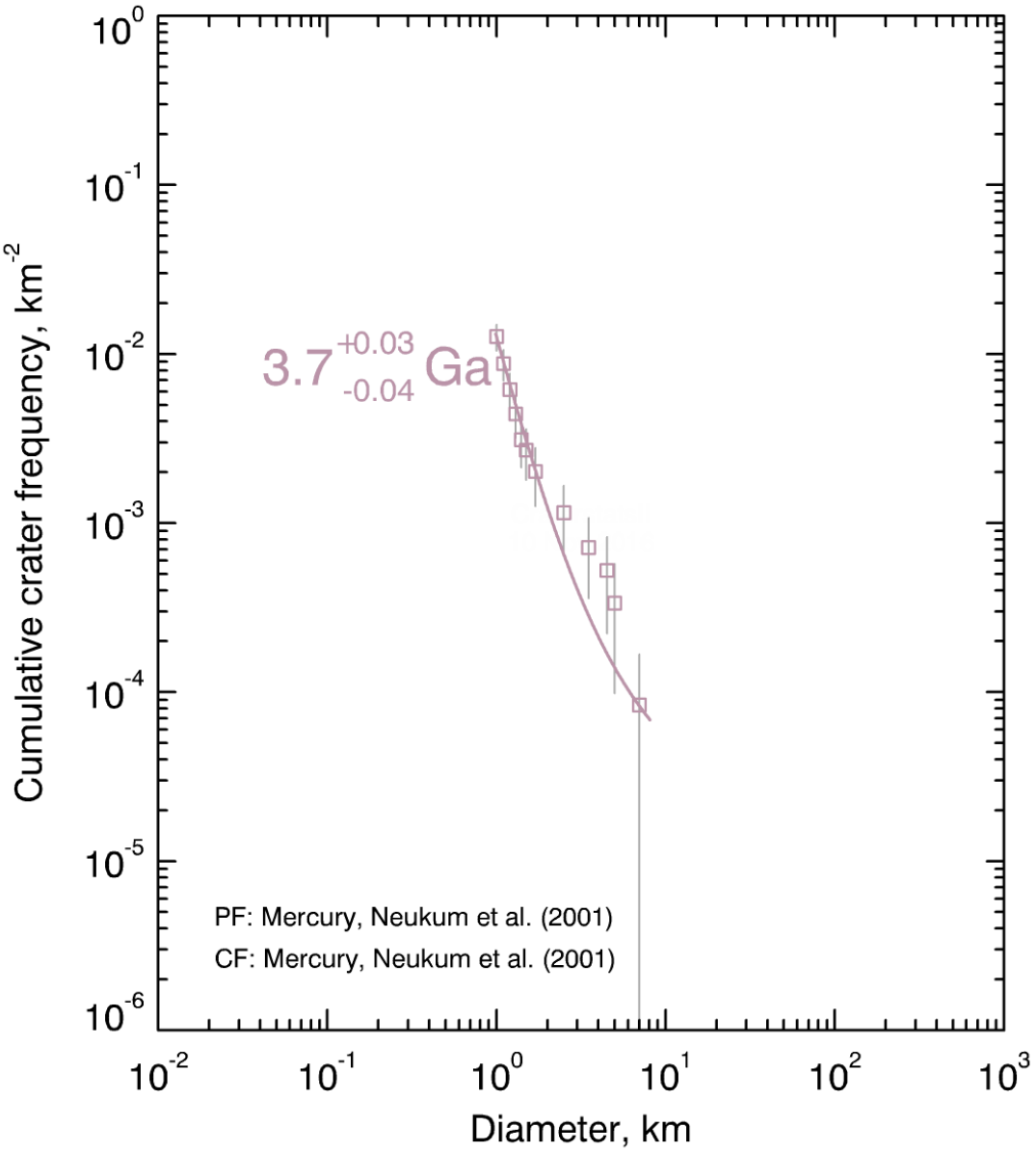


*Figure 3.7: Test 2 – unnamed crater ejecta.*

Figure 3.6 shows the crater and buffered crater SFD curves and their fits (using the Neukum Production Function), Figure 3.7 shows the crater SFD curve and fit for the unnamed crater's ejecta blanket (marked in pink on Figure 3.5) – it is shown on a separate plot because the fits were overlapping. The fits shown on these two plots indicates that the youngest of all of the features shows the following progression from oldest to youngest model ages:

- Plains unit
- Holbein ejecta
- Holbein fill (model age indistinguishable from Holbein ejecta)

- End of (resolvable) activity on Victoria Rupes
- Emplacement of unnamed crater ejecta blanket.

The ejecta of the unnamed crater ought to be older than the final (resolvable) activity on the fault, since it deforms the ejecta blanket as well as clearly cutting through the southern rim of the unnamed crater. This can clearly be seen in Figure 3.8. However, the model age obtained for the ejecta blanket of the unnamed crater is younger than that I obtained for Victoria Rupes. It is possible that the small area (2,296 $km^2$ – approximately half the size of the next smallest area, Holbein fill) of the ejecta blanket has resulted in errors in the SFD curve and, consequentially the model age.

Despite this one example of model age not agreeing with my observations of the stratigraphy, I think the use of buffered counting for linear tectonic features is still broadly supported by this second test. The use of small areas for crater statistics is likely to cause errors and ought to be avoided when possible – this is as much the case when using a mixture of crater SFD and buffered data as it is when applying model production functions to crater SFD curves alone.

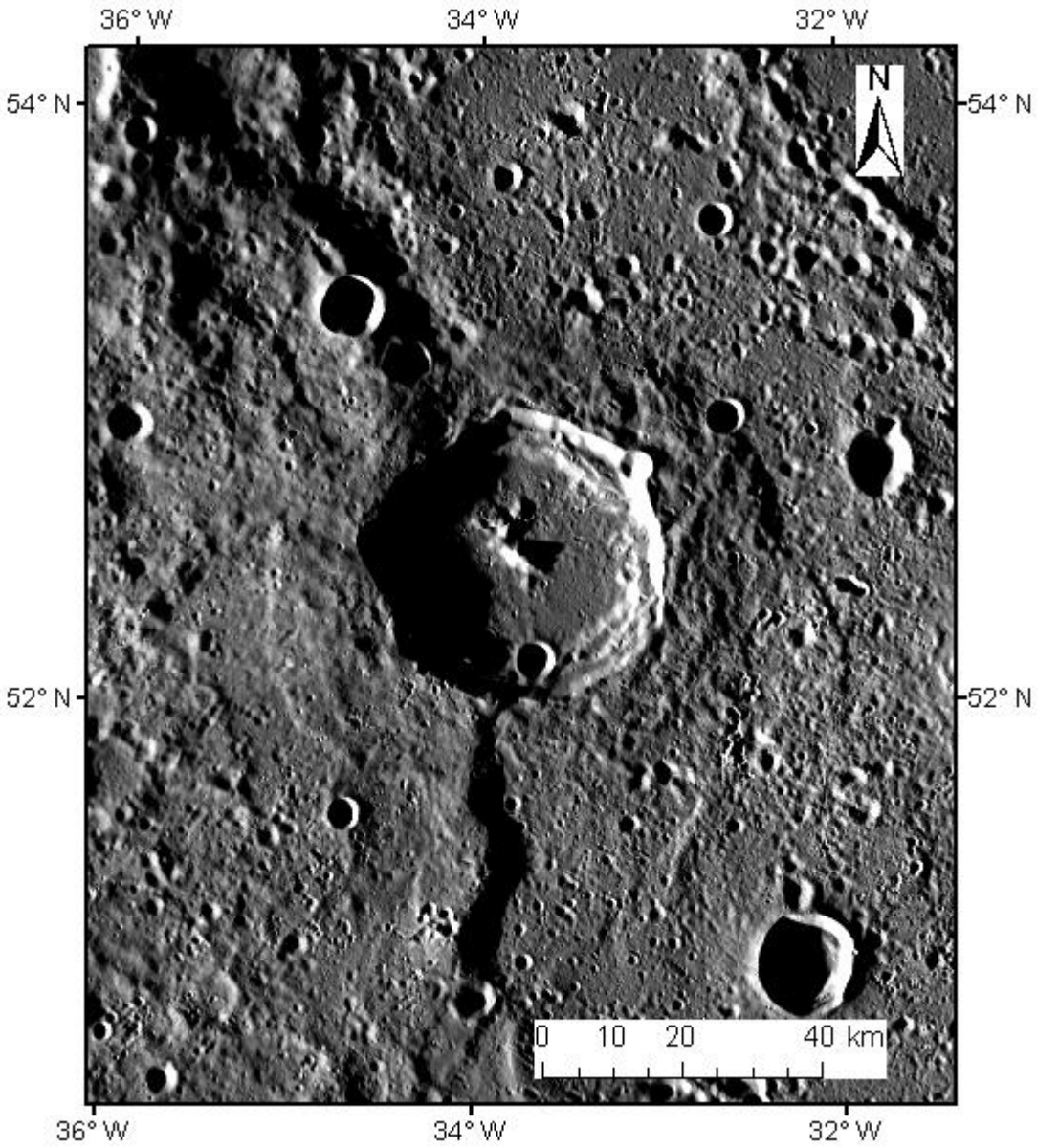


*Figure 3.8: Unnamed crater and ejecta blanket, cut through by Victoria Rupes (running approximately north to south).*

## 3.4 Other observations

During my global survey for basins with basin-edge scarps, I qualitatively observed that volcanic fill of basins is fairly common. However, basin-edge lobate scarps are not present in all cases of volcanically filled basins (although Mercury has undergone significant global contraction (Byrne *et al.,* 2014); 12% of basins in my survey (as presented in Chapter 2) with diameter >100 km exhibit basin-edge scarps. However, in basins with diameters of 200 km or

greater only, the percentage increases to 36% of basins exhibit basin-edge scarps.

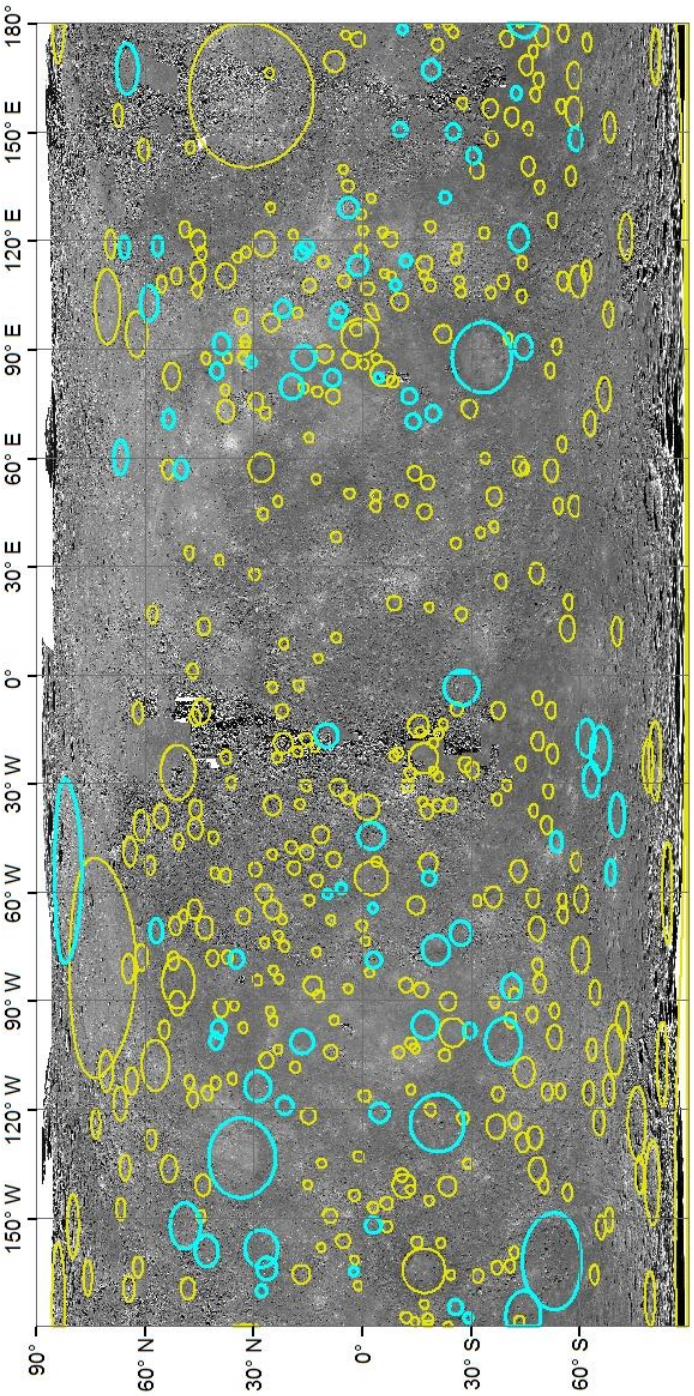


*Figure 3.9: MDIS v9 global mosaic with equirectangular projection. Survey results – basins outlined in yellow lack basin-edge scarps, those outlined in blue are those I have identified as having basin-edge scarps.*

**Table 3.4**: Number of basins with lobate scarps in total and by diameter category. Presence of basin-edge scarps is more common in the larger basin category.

| Diameter (km) | Total number of basins | Number with scarps | % basins with scarps |
|---|---|---|---|
| 100 – 199 km | 550 | 46 | 8% |
| >200 km | 90 | 32 | 36% |
| **Totals** | **640** | **78** | **12%** |

## 3.5 Limitation of methods

There are limitations to my methods, which I discuss and address where possible below.

- **The buffered method was originally used for the dating of Martian channels - features with a real, measurable width (W)**
  Lobate scarps have one clear edge (the base of the scarp slope), and one edge (the base of the lee slope) which has a more subjective and incidence angle-dependant placement. The value of W used in the equation to calculate buffer diameter (Equation 1 in Chapter 2) may therefore be in error, but we believe it unlikely to be more than a couple of km either way.

- **Buffered counting is reliant on few craters in the cases we look at in this work**
  This is due to the relatively small areas involved compared to other similar work on Mercury, e.g. (Giacomini *et al.,* 2015).

- **Crater count dating (using either method) is an indirect method of estimating the age of a surface or feature.**
  Crater size-frequency dating relies on a number of assumptions and the model dates can be used as estimates only – this is the case for all work

using these methods. An additional confounding factor for Mercury is that it is very difficult to ensure all secondary craters are removed. Our method relies on the judgement of the counter to remove secondaries from counts. This is very difficult on Mercury and it is highly unlikely that all secondaries have been excluded. It is also highly likely that some non-secondaries have been excluded.

# 4 Catenae

## 4.1 Introduction to Catenae on Mercury

Catenae are linear, curvilinear or curved/bent chains of craters on the surface of Mercury. There is very little currently in the literature discussing them although any worker spending time examining the surface of Mercury will have observed them. The references there are to catenae in the Mercury literature refer to them unequivocally as secondary impact chains (for example Gault *et al.,* 1975) presumably based purely upon their frequent collocation with impact basins, and do not generally use the name “catenae”.

A brief visual scan of any section of the surface will reveal many examples. However, there has been no previous work done to catalogue catenae, or question the assumption that they are secondary impact chains, despite similar features elsewhere in the solar system having alternative formation theories. Hermean catenae have varying morphology (further discussed in section 4.3.3); for example, the shared walls of consecutive pits may be either present, muted or entirely absent. The walls of the grooves may be slightly-to-very scalloped.

Features such as the one shown in Figure 4.1 can be seen in various locations on the surface of Mercury. Three features on Mercury are formally named Catenae in the USGS Planetary Nomenclature database (www4), for example Goldstone Catena (see Figure 4.2), and though these were initially named Valles, they are morphologically similar to the features indicated by the red arrows in Figure 4.1.

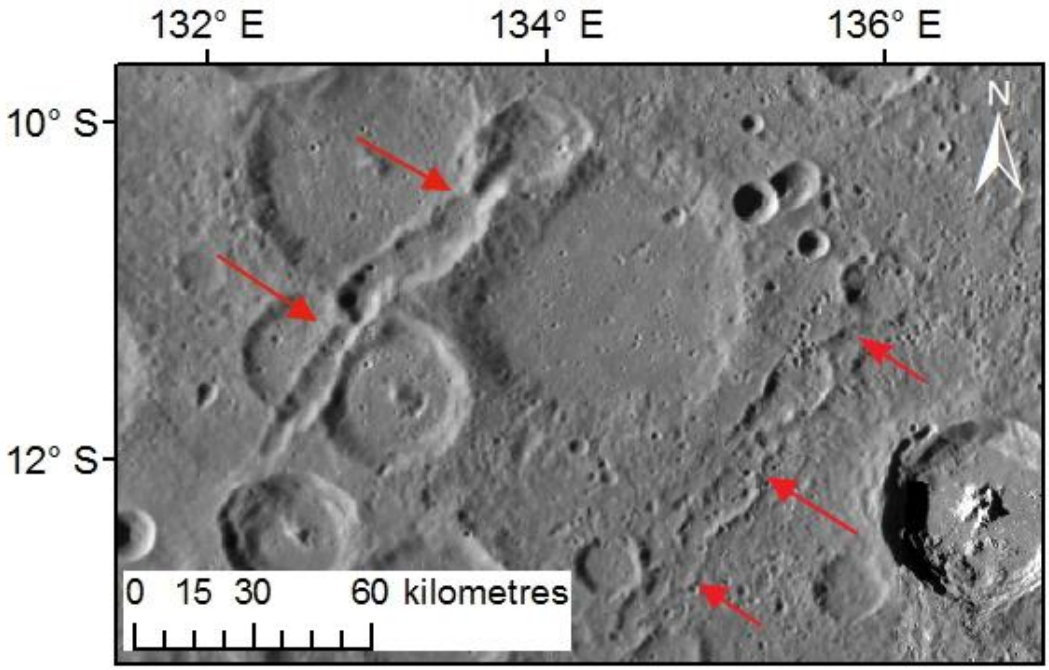


*Figure 4.1 (above): Two examples of (un-named) catenae on Mercury, which are somewhat atypical in morphology. MDIS mosaic, equirectangular projection.*

*Figure 4.2 (right): Goldstone Catena, Mercury, which is an archetypal catena. MDIS global mosaic, equirectangular projection.*

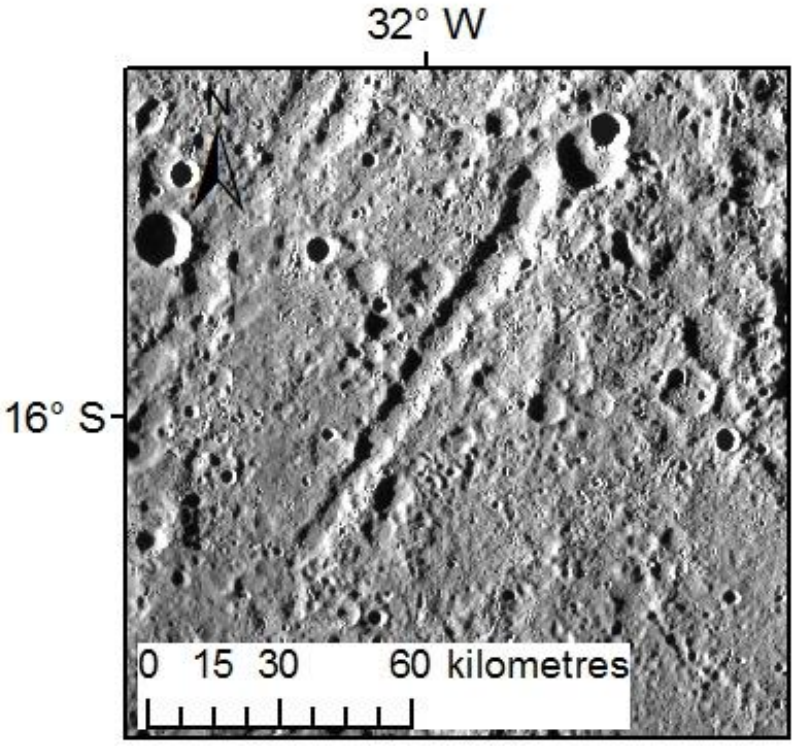

Because they are such a frequently-occurring feature, comprehensive interpretation of formation and history of alteration of the surface cannot said to be complete without an explanation for these features, including the process or processes that formed them.

The initial question I considered in the discussion of these features on the surface of Mercury is whether similar features are found elsewhere in the solar system, and by what mechanism(s) they are theorised to have formed. I have therefore carried out an investigation of the literature. As mentioned above, there is no literature specifically regarding catenae on Mercury. The features Byrne *et al.* (2013) identified and classified as Valleys (one of which was previously formally classified as a Catena in the Gazetteer Planetary Nomenclature) are an exception since they have many of the morphological requirements that would have lead me to include them in my survey. However, their edges have only a small degree of scalloping which is unusual for catenae. Byrne *et al*. (2013) theorised that these Valleys were formed by volcanic flows, and I do not include them in this work.

Gillis-Davis *et al.* (2009) wrote about features on Mercury they called pit-floor craters: irregular shaped depressions in the floor of certain craters, lacking rims and ejecta and therefore interpreted not to be impact-related. These features are relatively large, between 55 - 120 km in diameter. They are located upon smooth plains units within craters, and the long axes are frequently aligned concentric to the crater-rim. The authors believe that these features are due to the collapse of the surface into emptied near-surface magma chambers below, i.e. they are individual pit craters (they have not formed pit-crater chains as observed on other bodies).

## 4.2 Catenae on other bodies

Features similar in appearance to Hermean catenae have been observed on other terrestrial bodies (as discussed in detail below). However, these features have not always been named ‘catenae’ on these bodies; for example, similar-looking features have been referred to as grooves, crater chains, pit crater chains, graben, troughs, or furrows.

However, the word ‘catena(e)’ – as any other feature type under the planetary nomenclature - refers to the morphological characteristics only, it is not required that they have also been determined to form by the same mechanism**.** Because of this, when looking for comparable features on other planetary bodies and asteroids I have not limited myself only to features officially named Catena(e), but also included any linear or curvilinear grooves that have a beaded appearance in planform.

For these bodies, varying formation mechanisms have been invoked to explain catenae. The bodies where catenae (or features similar to catenae) have been observed are detailed below, along with a brief review of the formation mechanisms invoked in the literature in each case.

### *4.2.1 The Moon*

Schumm (1970) state that “crater chains” (and also crater clusters) observed on the Lunar surface appear to be of volcanic origin – specifically, venting of gas along fractures, fluidising the regolith overlying the bedrock. Schumm (1970) also carried out experimental work investigating the formation of pit crater chains by the drainage of regolith into underlying cavities (this is discussed in section 4.2.6).

McCauley and Wilhelms (1971), in their paper accompanying the geological map of the near side of the moon, state varying mechanisms for the formation of “crater chains” and “furrows”. Primarily they invoke volcanic or secondary impacts, but also in one case (radial to Imbrium basin), possible radial faulting from the impact. They also suggest the Rima Hyginus crater chain (or rille) as being a good candidate for volcanic origin, possibly collapse craters. Rima Hyginus crater chain is shown in Figure 4.3.

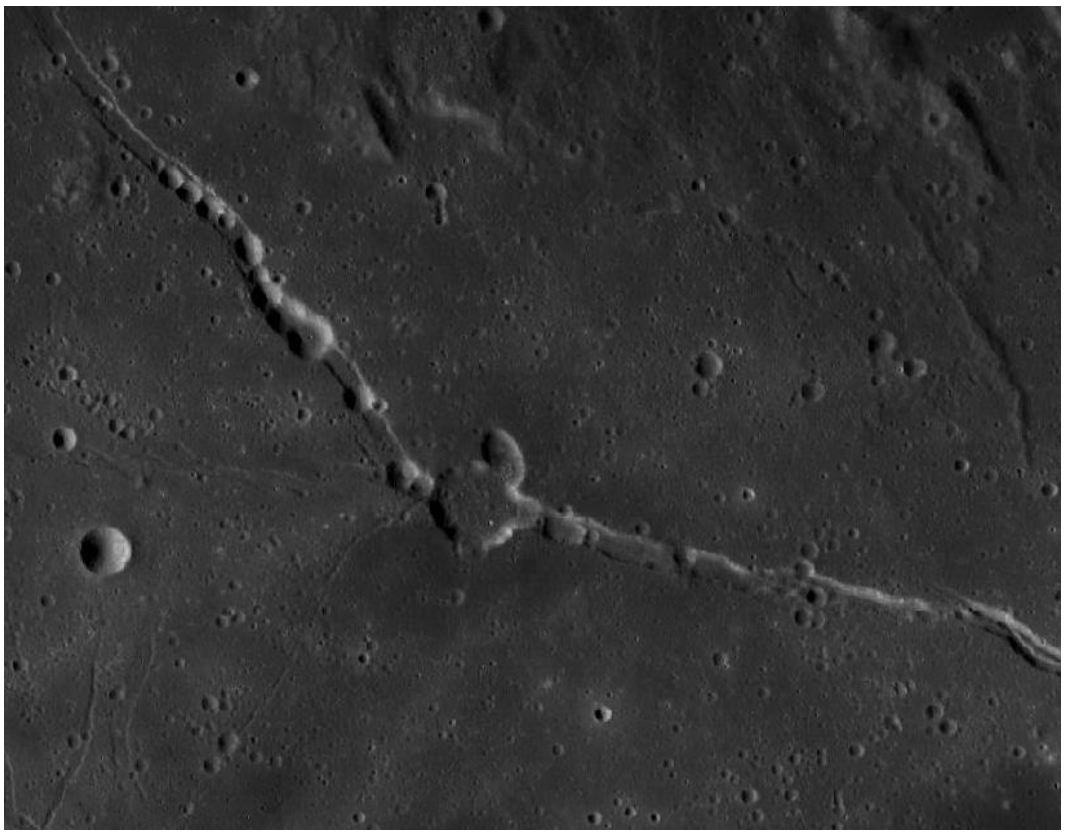

*Figure 4.3: Rima Hyginus rille on The Moon, obtained from Lunar Quickmap (www5), the centre of the image is 7°N, 7°E. The crater in the near-centre of the image is Hyginus 8.2 km in diameter.*

Schumm (1970) published an experimental investigation into the morphology of groove or crater chains formed due to the fluidisation of regolith. Fluidisation occurs due to volcanic vents beneath the regolith releasing gases that suspend the grains, therefore allowing the mass to flow like a medium-to-high viscosity liquid). This particular work was in reference to Lunar crater chains.

The result of the experiments investigating the morphology of pits/pit chains formed when the thickness of regolith is varied along the line concluded that the thicker the regolith layer, the more flat-floored craters formed, the deeper and wider the craters created by drainage of regolith (though beyond a certain point the regolith thickness vs volume of pit formed flattened out).

A single long vent below a regolith that varied in depth (wedge-shaped in cross section) along the long axis of the vent produced linear grooves with flat floors, scalloped edges but no internal shared rims, features that were similar in appearance to catenae on Mercury (albeit at a smaller scale). With regard to the

curves and bends in catenae observed on Mercury, Schumm (1970) was able to produce similar features when using a sufficiently thick layer of regolith, with a wedge-shaped cross-profile, over even a sharply angular linear pattern of vents.

Schumm (1970) also found that a series of discontinuous vents, in a roughly linear series, formed a continuous trough forms a continuous sinuous trough with highly scalloped edges, if a layer of coarse shattered material above the vent but below the fine regolith – most especially when there was a low degree tilt (3 degrees) to the experiment (see Figure 4.5) Schumm (1970) proposed Davy I and Rima Hyginus (see Figure 4.3) as potential sites of fluidisation grooves on The Moon. The latter was later suggested to be an area hosting crater chains of volcanic origin by Wilhelms and McCauley (1971), supporting Schumm's (1970) findings. Many of the features Schumm (1970) created in his experiments look morphologically similar (although scaled down) to catenae on Mercury, including the presence of raised rims in the craters and crater chains of his experimental results.

### *4.2.2 Mars*

Over 1500 grooves have been identified on the Martian surface, mostly in Tharsis region, ranging from 10 m – 4.5 km in length. Often found within graben, or transitioning into graben or normal faults. There are a number of suggested theories regarding the formation of grooves (most commonly referred to as pit crater chains in Martian literature), including the following: pressure drop due to volatile release from dykes (from Mège *et al*. (2003)), drainage into collapse magma chambers, drainage into extensional fractures, karst dissolution, dilational faulting (Wyrick *et al.*, 2009), and plinian eruption (Scott *et al.*, 2002).

Graben are differentiated from pit crater chains by morphology (for example they have straight edges and internal structure within their walls) (Wilson and Head, 2002), and are not a likely analogue for the features I refer to as 'catenae' on Mercury. However, pit crater chains are so frequently associated with graben (Mège *et al.,* 2003) it seems likely that – at least on Mars – there is a link between the two, meaning that Martian pit crater chains are linked in some way to extensional faulting. Scott *et al.* (2002) suggested that the graben

are found above above dykes emanating from a central volcanic edifice (the majority are found in the Tharsis region), and pit crater chains are formed within these graben.

Regarding terminology, Mège *et al.* (2003) refer to catenae, troughs and pit crater chains as morphologically separate, a feature being referred to as a ‘catena’ when ‘elongated U-shaped troughs’ and ‘pit crater chains’ align. The former feature the authors state are likely formed partly due to plinian eruption (the authors suggest the larger pits within chains that sometimes have slight rims), and partly volatile release along the faults in the graben. The latter (along with ‘small chasma’) they consider volcanic collapse, or collapse of surface material into tension cracks, as most likely origins. They also refer to Linear U-shaped troughs (similar to elongated U-shaped troughs but greater in length), that they also suggest are due to surface collapse above magma bodies.

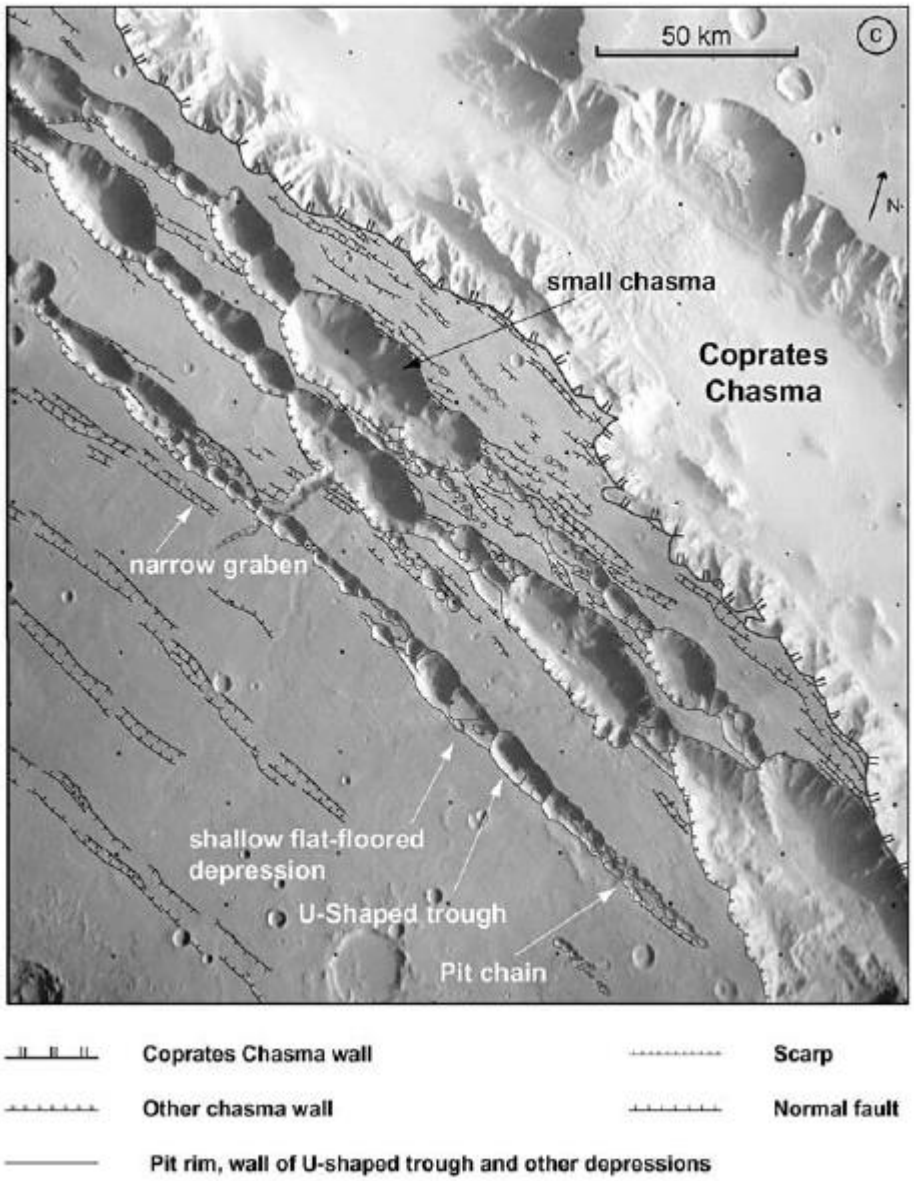


*Figure 4.4: (after Mège et al. (2003), Figure 3). The feature indicated variously along its length as Pit chain, U-Shaped trough and shallow flat floored depression is the most similar in morphology and scale to most of the features I have categorised as catenae on Mercury.*

On Mercury, it is not possible to examine catenae at a high enough resolution to discuss morphology to as great a degree as it is on Mars. It is possible to determine approximate length, width, and whether there are bends or kinks. Catenae rims would likely be visible in most cases, and ejecta (if present) might be visible in larger examples. However, Mege *et al.* (2003) suggest that all the categories form above dykes or magma bodies (or the low-pressure voids where magma bodies once were), and form due either to eruption or collapse.

It is noteworthy that I have not been able to find any suggestion in the Martian literature that pit crater chains could be created by secondary impacts.

### *4.2.3 Phobos*

The families of parallel grooves on the leading hemisphere of Phobos have been hypothesised to be secondary chains or rolling boulder tracks from the largest impact structure on the moon (Stickney), or possibly fractures from that impact or from tidal forces (Murray & Iliffe 2011).

Veverka and Duxbury (1977) state that Viking images allowed identification of various grooves upon the surface of Phobos that the authors divided into three categories based on their morphology and context: 1) chains of coalescing craters, with elongated or irregular form associated with impact crater Stickney (10 km diameter), and begin at its rim ; 2) chains of coalescing craters 50-200 m across, with elongated or irregular form that are not obviously associated with the Stickney impact (as one crosses the crater) that run parallel to the equatorial plane ; 3) At least 2 sets of parallel linear grooves of uncertain origin, 150-200 m wide and up to 5 km in length. Some of these have scalloped edges while others have straight edges.

The authors believed 1) are fractures likely formed by the Stickney impact, as initially suggested by Thomas *et al.* (1979). 2) they suggest have the morphology of secondaries (clustering, occasional herringbone patterning) but as Phobos is not believed to have sufficient gravity to result in ejecta striking the surface, they suggested that they might be ejecta propelled into Mars-orbit that then re-impacted on Phobos. This is based upon an earlier theory by Soter (1971). It is also possible that the Stickney impact created fractures, into which regolith drained after the event (Pollack *et al.,* 1973).

3) These striations, the authors suggest, might be (re-impacted) secondary chains (as 2) but not the same source and/or mechanism for re-impact due to the different distribution on the surface), original layering within Phobos itself, or they are cracks due to tensional stress. They considered the latter unlikely because tensional stress cracks would not present with a beaded appearance in planform. Alternatively, as suggested by Pollack *et al*. (1973), they could be formed by outgassing of volatiles along fractures, possibly formed by the Stickney impact.

Thomas *et al.* (1979) suggested that the grooves (up to 200 m in width and up to 30 km long) might be formed by the drainage of regolith into a fissure, possibly aided by venting of volatiles. The Stickney impact directly created those groves radial to the crater, and reactivated previous planes of weakness in the body, or caused further fractures due to the alteration in Phobos' rotation post-impact. Horstman and Melosh (1989) suggest that drainage of regolith into fractures (associated with Stickney impact) is the mechanism that fits the observations the best. They state that the venting hypothesis proposed by Thomas *et al.* (1979) would explain those grooves that cut the rim of Stickney – the venting of gas would allow the formation of the grooves for a period after the impact. Secondary crater chains would not be expected to cut the rim of the primary crater (which is why Veverka and Duxbury (1977) stated they did not believe those grooves that did cross-cut Stickney's rim were related to the crater).

Horstman and Melosh (1989) refer to previous work by Schumm (1970), that investigated the formation of crater pit chains and grooves by drainage of regolith into fissures beneath – previously detailed above. They also carried out their own experiments, and concluded that drainage into a fissure could certainly produce features with the correct morphology to explain the grooves on Phobos. They felt their results suggested that venting of gas was not necessary, but might play a minor role. They also stated that measuring the distance between the center of each pit in a chain can shed light upon the thickness of the unconsolidated regolith layer.

Murray *et al.* (1994) and Murray and Iliffe (2011) stated that since ejecta from Stickney would not attain sufficient velocity to form crater chains, and no boulders are found at the end of the chains, the authors propose that the grooves are secondary chains, where the primary impacts were on Mars. They believe that the morphology of the grooves is not indicative of the involvement of underlying fractures.

### *4.2.4 Galilean Moons and Enceladus*

The crater chains on the Jovian satellites Ganymede and Callisto are thought to be formed by the impact of fragments of a parent body which was split by Jupiter's tidal forces prior to impact (Melosh & Schenk, 1993; Melosh, 1998). The resulting landform resembles a chain of secondary craters, but is apparently unrelated to any primary impact structure. In addition, they are almost without exception found on the Jupiter-facing hemisphere of the tidally locked moons Callisto and Ganymede (Melosh & Schenk, 1993). From the physical characteristics of the catenae, estimations have been made about the mass and orbital trajectory of the parent comet/asteroid (Mckinnon & Schenk, 1995)**.**

Buczkowski *et al*. (2016) theorised that the pit crater chains of Enceladus, buried faults beneath regolith, dilation occurs and regolith falls into the fissure forming chains of craters and (eventually) these craters can merge forming grooves/troughs. Wyrick *et al.* (2010) also report dilational faulting as an existing theory for pit crater chains on Enceladus.

### *4.2.5 Asteroids*

Following the discovery of the grooves on Phobos, Thomas and Veverka (1979) predicted that between 1/12$^{th}$ and 1/4$^{th}$ of asteroids <100 km in diameter would also exhibit grooves. This is on the basis that the energy of the Stickney impact was sufficient to create extensive fractures into which regolith drains, but not sufficient to destroy the asteroid. This presupposes the grooves are due to impact-related fractures.

Grooves have been observed on the surfaces of other asteroids. Prockter *et al.* (2002) reported linear grooves among the linear features observed on S-class (silica-rich) asteroid Eros, as well as on asteroids Gaspra, Ida and Vesta Buczkowski *et al*. (2016). These grooves are either beaded or straight-edged in plan view, and one groove might grade from one to the other form along its length. The authors attributed them to drainage of regolith into fractures in the rock beneath.

Prockter *et al.* (2002) did not associate the grooves with any particular impact craters. However, Buczkowski *et al.* (2008) mapped 2141 grooves on Eros, and stated that the likely formation mechanism was either impact-related processes (they mention fractures related to impacts tend to be radial to the crater) or pre-existing fabric, but do not go into detail on the specifics of either mechanism. They examined whether the lineations were radial to impact craters, by examining which were radial to craters and present in at least a 45 degree arc around the crater centre-point. The poles of each radial set also clustered around the coordinates of the crater. They weren't able to assign all the grooves on Eros to these sets, but did find that 13 craters had radial grooves. There was no reported trend in crater size or locations that would indicate why these craters had radial grooves, while other craters didn't, although most of them are among the larger craters on Eros' surface.

In addition to the crater-radial sets, Buczkowski *et al.* (2008) identified at least 3 sets of grooves, based upon their strikes and locations, one of which ("set 1") they also attributed to large impacts. Sets 2 and 3 they stated were either due to an internal fabric or impacts, but where the primary crater was no longer visible (since Eros is a fragment of an original, larger, body the primary could have been on a separate section).

Buczkowski *et al.* (2016) reports grooves, kilometres in length, including named Catenae (although the name Samhain has been applied to a set of parallel grooves rather than an individual one) present on the surface of Ceres. While some are radial to impact craters, and therefore likely created due to "impact processes" (as Buczkowski *et al.* (2008) the authors do not elaborate as to whether this might be secondary impacts or drainage of regolith into impact-related fractures, or an additional mechanism). Buczkowski *et al.* (2016) state that the lack of raised rims on the Samhain Catenae preclude an origin as secondary impacts. They also observe that nearby polygonal craters have straight edges that align with the Catenae, suggesting a local fabric of fractures (since the shapes of polygonal craters are believed to be structurally controlled). Buczkowski *et al*. (2016) suggest that the proximity of Fractured Floor Craters (that form due to intrusion of low density material beneath them, resulting in doming and fractures) could mean that intrusion (possibly salt diapirism) could be responsible for the Samhain Catenae also.

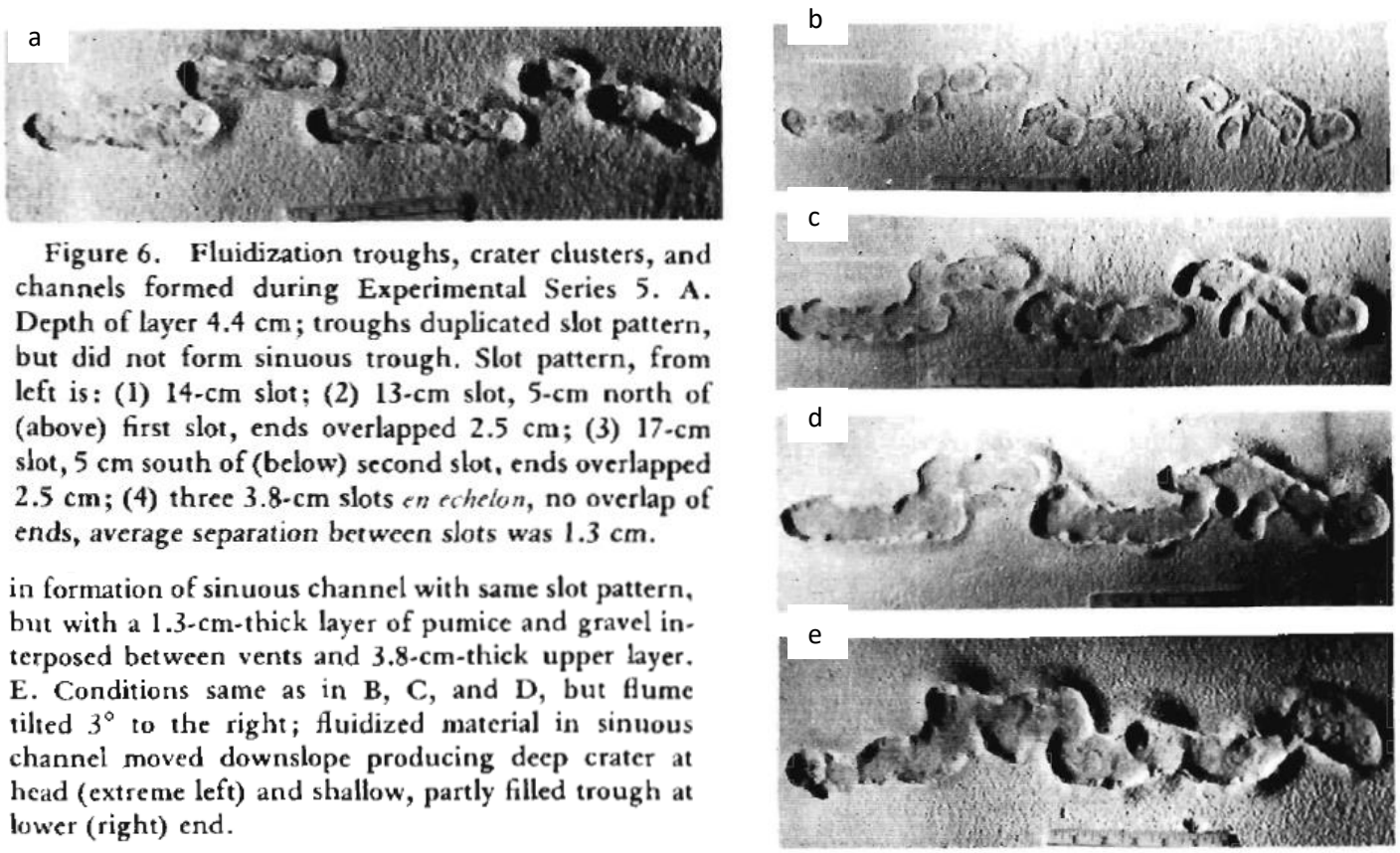


Figure 6. Fluidization troughs, crater clusters, and channels formed during Experimental Series 5. A. Depth of layer 4.4 cm; troughs duplicated slot pattern, but did not form sinuous trough. Slot pattern, from left is: (1) 14-cm slot; (2) 13-cm slot, 5-cm north of (above) first slot, ends overlapped 2.5 cm; (3) 17-cm slot, 5 cm south of (below) second slot, ends overlapped 2.5 cm; (4) three 3.8-cm slots *en echelon*, no overlap of ends, average separation between slots was 1.3 cm.

in formation of sinuous channel with same slot pattern, but with a 1.3-cm-thick layer of pumice and gravel interposed between vents and 3.8-cm-thick upper layer. E. Conditions same as in B, C, and D, but flume tilted 3° to the right; fluidized material in sinuous channel moved downslope producing deep crater at head (extreme left) and shallow, partly filled trough at lower (right) end.

*Figure 4.5: Schumm (1970) (page 2544) experimental results with discontinuous vents in a roughly linear series (as (a)) over a layer of coarse shattered material above the vent but below the fine regolith (b-d). (e) a low degree tilt (3 degrees) was added to the experiment.*

## 4.3 Catenae on Mercury

As discussed above, I observed many catenae across the surface of Mercury while carrying out earlier work. This section investigates the morphology and occurrence of catenae across the Hermean surface. A later section investigates whether they have a preferential orientation, or are more common on certain geologic units, as these data may help establish whether they are formed by impact processes.

### *4.3.1 Survey method*

In order to quantify and further examine the trends in distribution of these features, I carried out a global survey. I did this following a similar method I employed for the survey of tectonised basins (Chapter 2), using the MDIS v9 monochrome global mosaic as the basemap in ArcMap. I created a polygon shapefile into which I entered the outlines of all the catenae I observed, thereby digitising the global population.

My criteria for outlining a feature as a catena were: a groove longer than it is wide, if there are individual crater characteristics visible (e.g. scalloped edges of the catena formed by adjacent craters that have merged together into a groove) then there must be 3 or more craters in the chain/groove, the craters must be overlapping and have internal dividing walls either absent or minimal when compared to the rim of the catena as a whole. With the exception of these criteria, I outlined any groove-like feature that I observed, which was of sufficient width to be easily delineated at my maximum survey scale (1:1,000,000 or greater). This minimum width was approximately 2 km. While I observed groove-like features narrower than this, it was not practical to delineate each one of these when mapping on a global scale.

Since catenae might occur on any area of the surface, rather than being limited to the edge of infilled impact basins and craters, I had no framework to begin with in the way I did with the basin-edge scarps survey (where I directed my search initially by using the Fassett *et al.* (2012) basin database). Instead I surveyed by visual scanning of the MDIS mosaic in an equirectangular projection, beginning at 60°N at the western edge of the mosaic and surveying downwards (at a scale of 1:1,000,000) to 60°S.

I then moved the survey frame eastwards and scanned northwards in a strip parallel to the first. I continued with this until the mid-latitude and equatorial surface had been surveyed, then surveyed the poles at the high (60°N/S and above) using the MDIS v9 monochrome polar mosaics, which use polar stereographic projection. The minimum width of catenae included in this global survey is approximately 2 km (the narrowest catenae practicable to outline using ArcMap at the survey scale). I observed narrower groove-like features during this survey, and had the option to zoom in to outline them and include them in the survey. However, the extent of the area (they entire surface) I intended to cover meant that it was prudent to set a minimum threshold.

In addition to outlining each catena, I also included a separate shapefile within which I added a polyline feature for each catena. I drew each polyline along the centre line of each catena, along the long axis. This line feature shapefile was for the purposes of line density distribution (see section 4.3.4), and investigating the orientations of catenae on Mercury (see Chapter 5).

### *4.3.2 Survey results and qualitative observations*

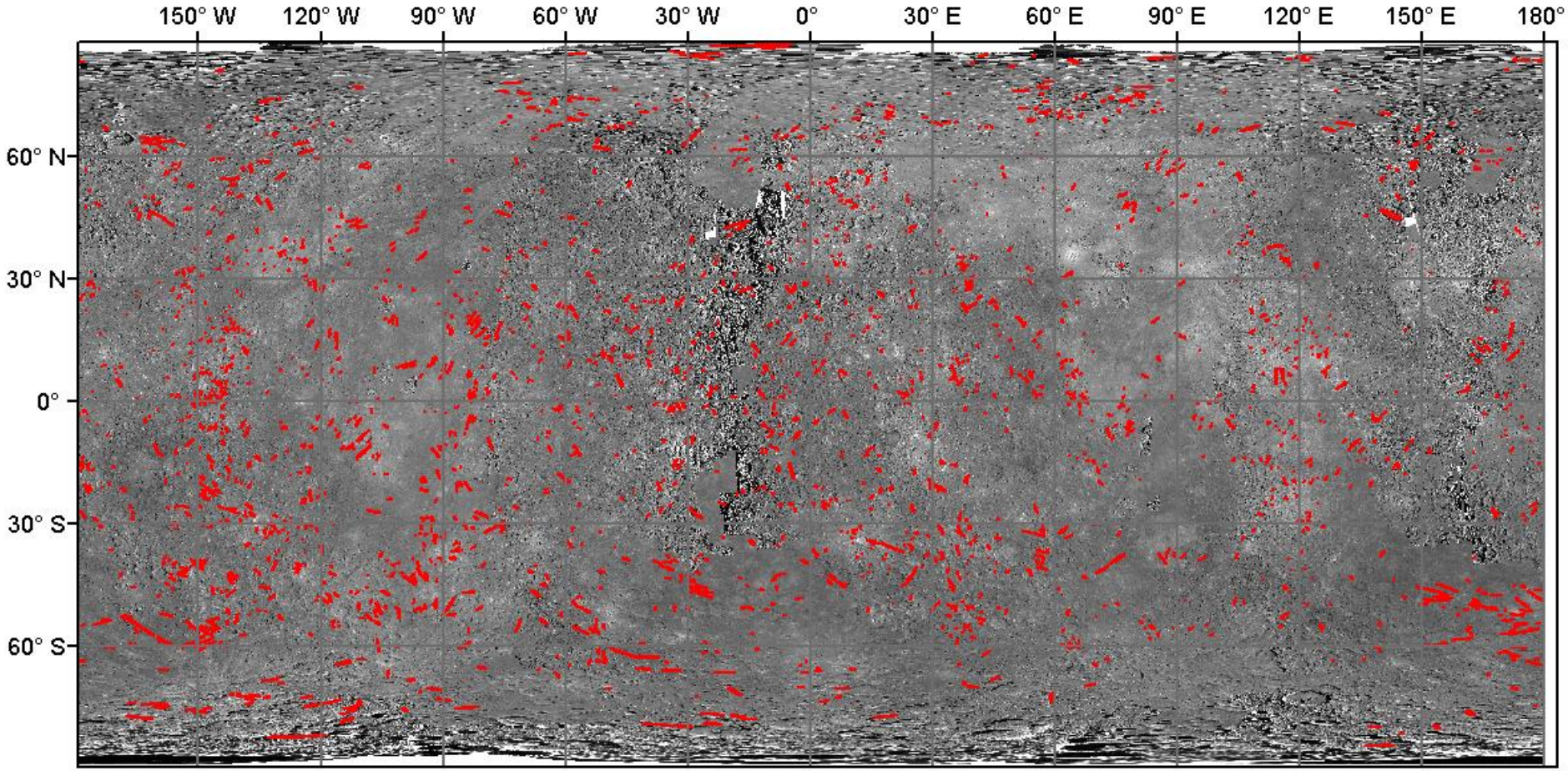


*Figure 4.6: Global survey of catenae (equirectangular plot, MDIS v9 monochrome mosaic)*

The survey results can be seen in Figure 4.6, and the shapefile can be accessed using the link provided in Appendix 5 (p. 212). My qualitative observations during the survey confirmed are as follows:

- catenae are present over the entire surface of Mercury;
- they appear to be more common on older, more heavily cratered surfaces than smooth volcanic plains which are lightly cratered and thus younger;
- the vast majority of the population have raised rims,
- they are frequently found radial to impact basins (for example Figure 4.7), but not in all instances;
- they are not all straight, some are looped curved or have kinks;
- some have larger craters at one end;
- they all lack visible ejecta blankets and obvious volcanic edifice/lava flows.

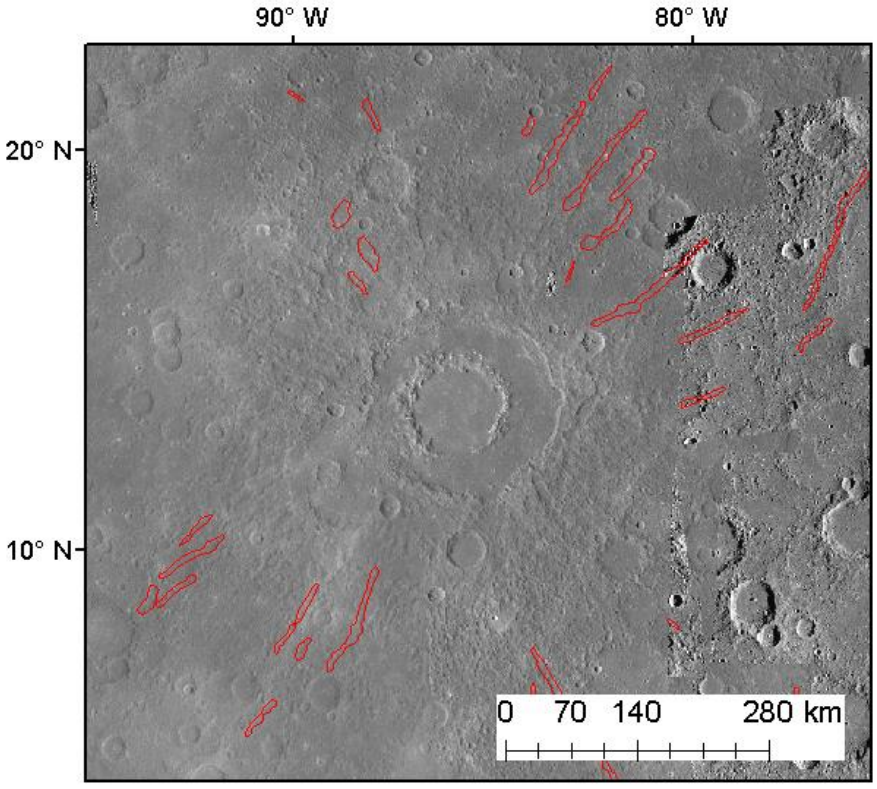


*Figure 4.7: Catenae radial to an impact basin*

### *4.3.3 Morphological types*

Within the survey criteria (as outlined in section 4.3.1), I observed a variety of morphologies. Figure 4.8 shows the most common type of catenae: slightly sinuous, scalloped edges, with raised rim and present but smaller internal walls. Figure 4.9 shows a catena with two less common (but still observed across a number of examples) morphological characteristics, a loop and a crater with considerably larger diameter at one end. Figure 4.10 shows a catena that appears to follow the internal rim of an impact crater. Catenae that appear to interact with other features are rare but this is not the only example; the western catenae in Figure 4.1 also appears to divert around the edge of an impact basin.

Figure 4.11 shows two catenae that cross each other, the older of the two (trending NNW-SSE) is muted but has no unusual characteristics. It is cross-cut by the other more recent catenae (the crisper example, trending NNE-SSE) which does exhibit some unusual characteristics. Catenae normally have fairly consistent widths of the individual craters along their length, and some examples have a wider crater at one end (as discussed above). The crisp catenae in Figure 4.11 has a wider crater midway along its length, with narrower craters towards each end. The individual craters vary considerably in depth, which is also unusual. The catena extends northwards partially into the impact crater; however, this section of the catena is much more muted and shallow than the rest of it.

Figure 4.12 is very unusual, with the eastern end of the catena having a shallow appearance, with wide, flat floor and vertical walls, but the west end having very much the appearance of the most common morphological type (as Figure 4.8). It is radial to a basin, which is to the west of this catena. It is possible that these are two separate features one of which directly overlies the other by coincidence, but the rims do align very closely if this is the case. Alternatively, this example (the only one like this I observed on Mercury) has certain characteristics in common with Rima Hygenus (Figure 4.3), which as discussed in section 4.2.1 is likely to be formed by the collapse of a lava tube.

However, across all of these types there is the common presence of raised rims.

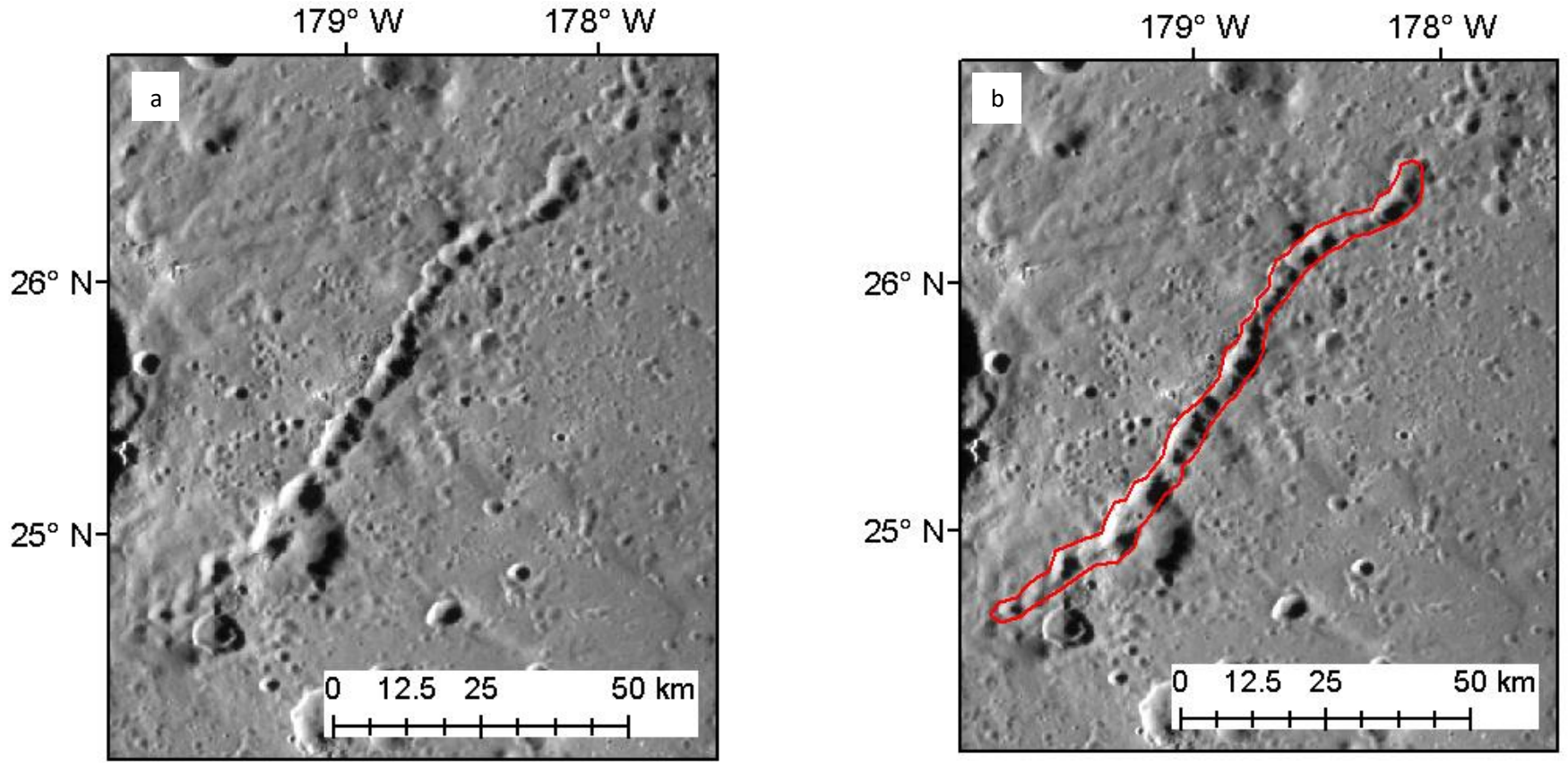


*Figure 4.8: (a) An archetypal catena, (b) delineated in red.*

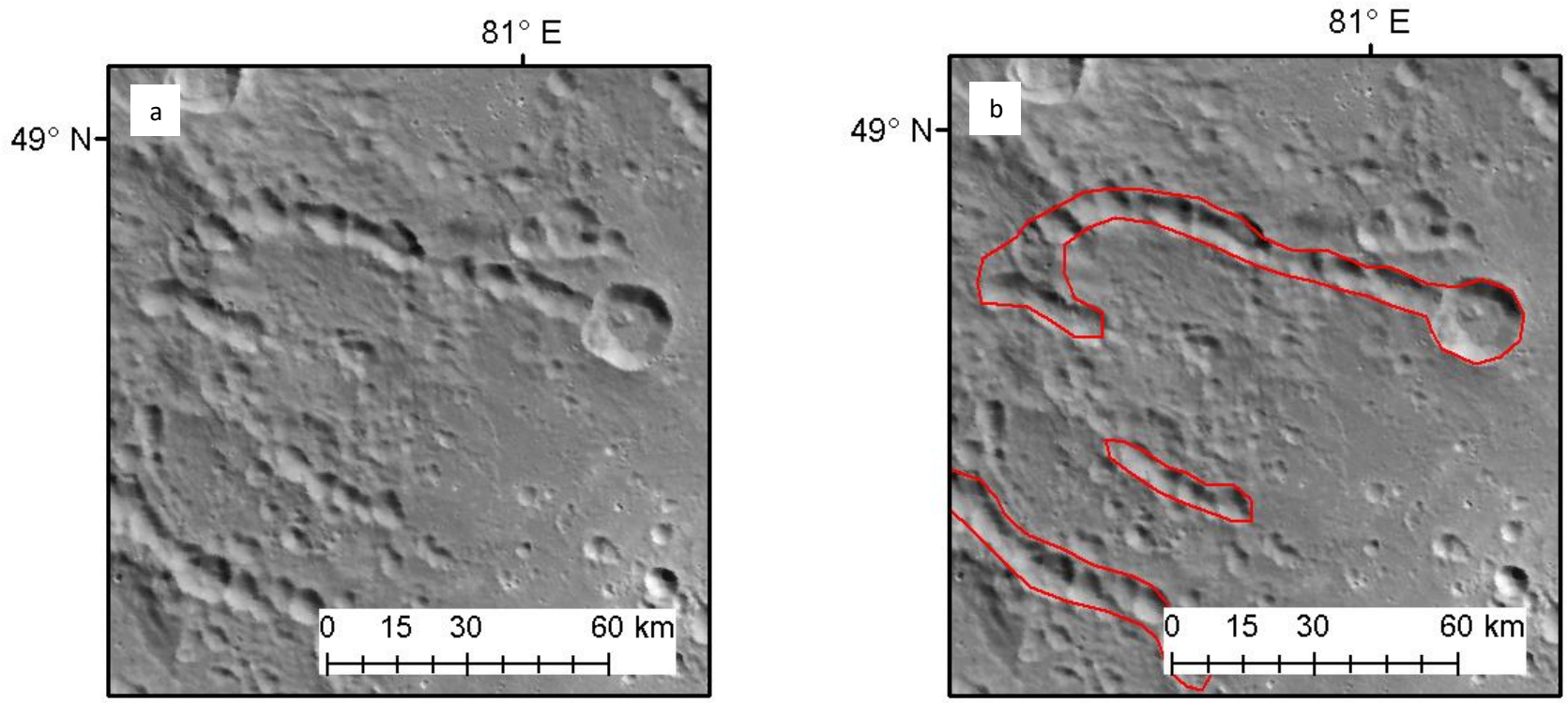


*Figure 4.9: (a) A curved catenae with a crater with greater diameter than the rest of the catena at the eastern end, (b) catenae delineated in red.*

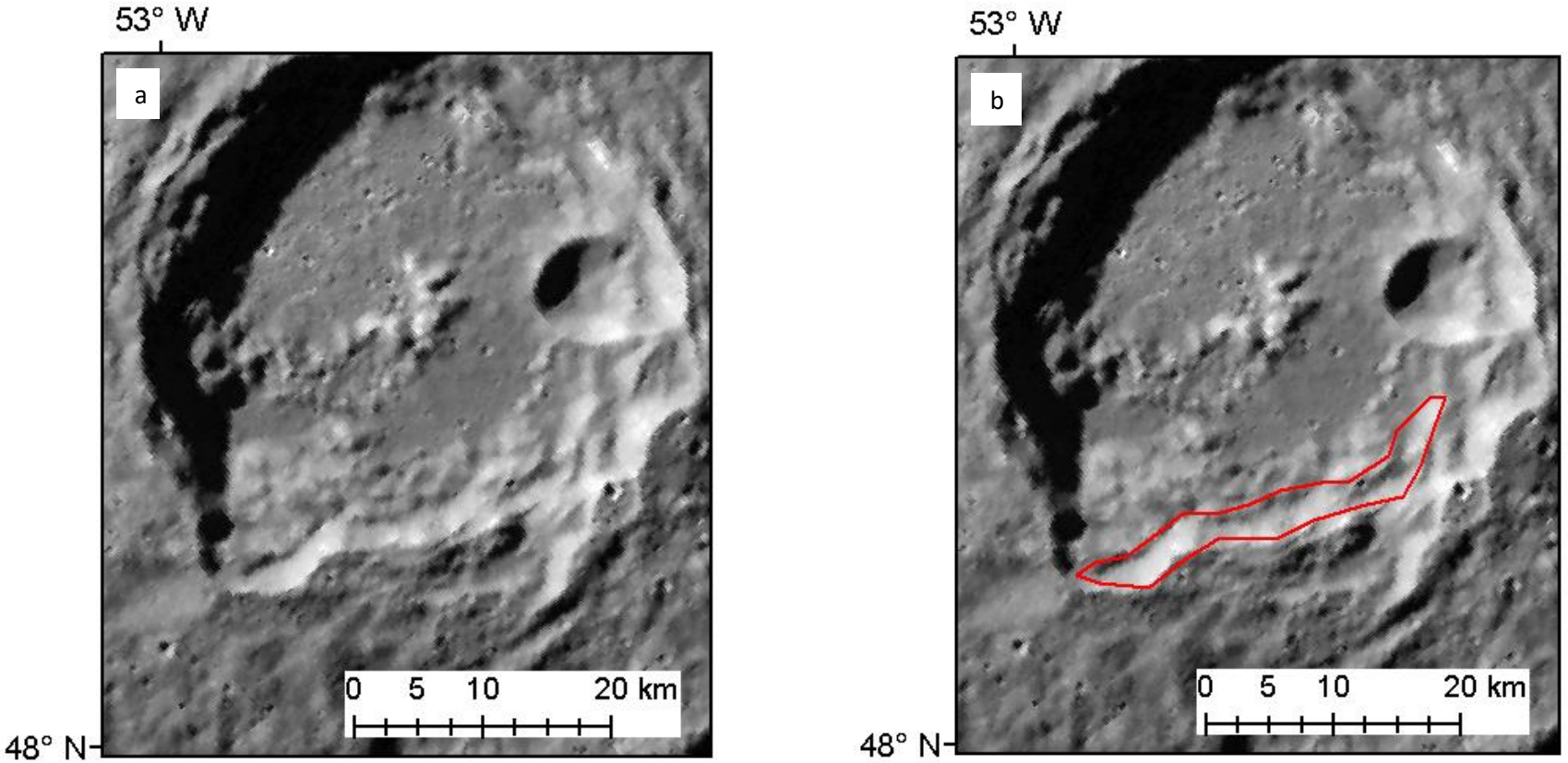


*Figure 4.10: (a) A curved catena that appears to follow the rim of an impact crater, (b) catena delineated in red.*

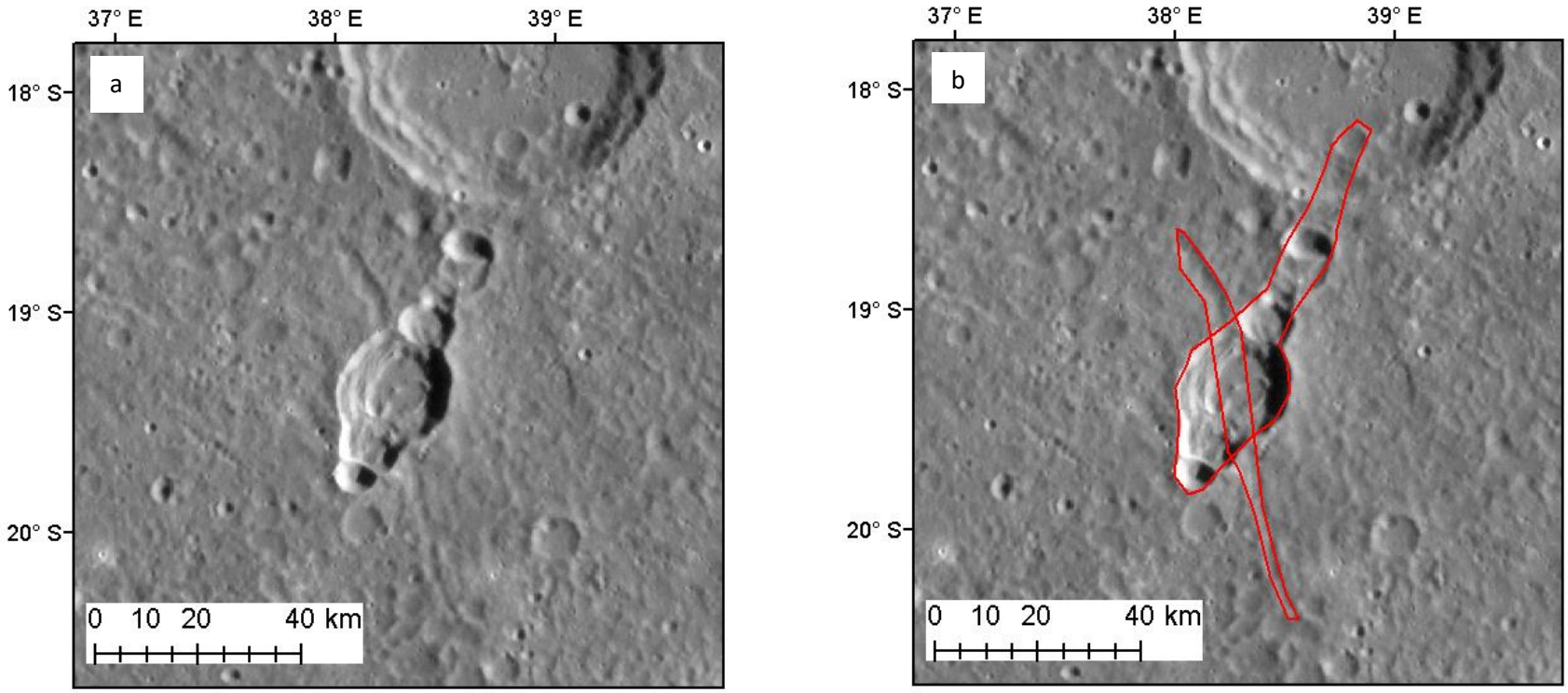


*Figure 4.11: (a) two catenae crossing, the nnw-sse trending catena is the older and the nne-ssw trending catena is younger because it cuts across the other. The older narrower catena is narrower and more of the archetypal variety, the younger catena is unusual in that the constituent craters are of very different diameters and depths. (b) catenae delineated in red.*

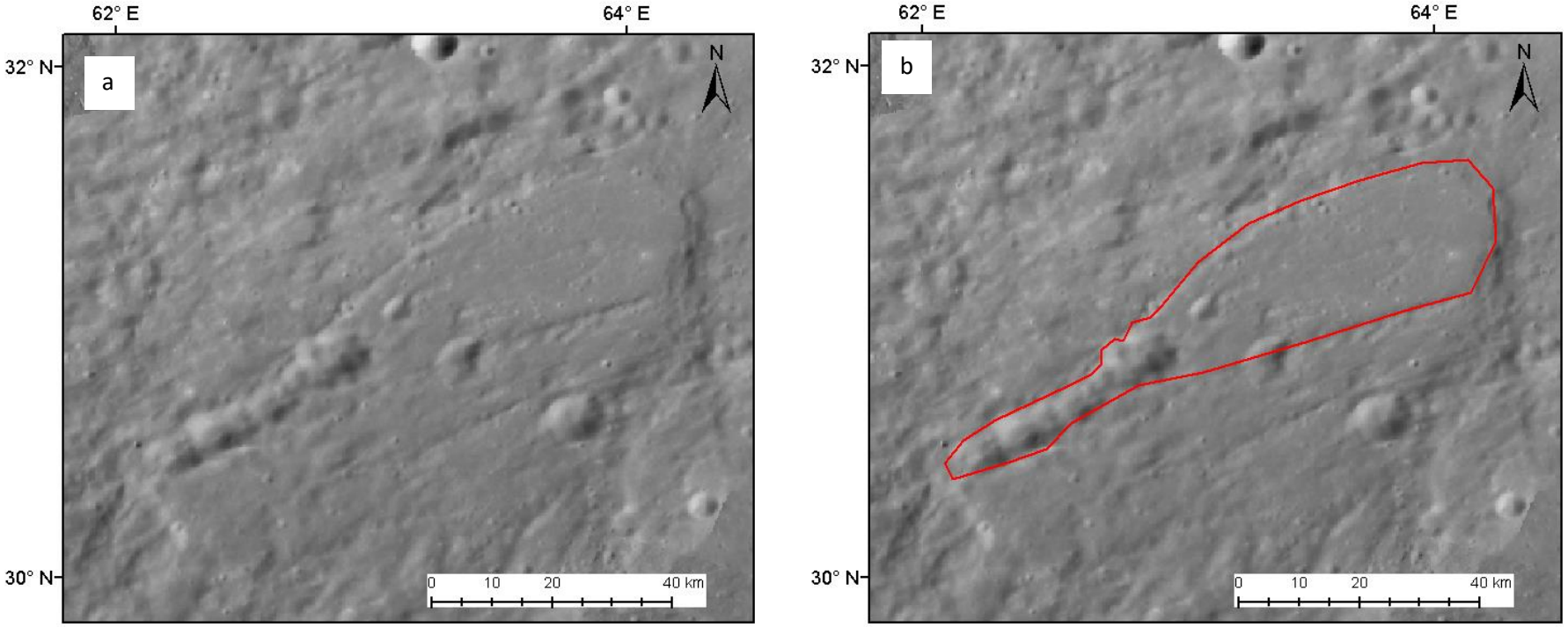


*Figure 4.12: (a) A catena that has a typical morphology to the south-west but appears to be linked to a shallower and wider section to the north-east. (b) Delineated in red.*

### *4.3.4 Quantitative observations and geological units*

The results of my global survey of catenae are shown in Section 4.3.2 (Figure 4.6). In total, I identified 2,365 catenae, distributed across the entire surface. Those I identified are between approximately 2-30 km in width and approximately 5 to 300 km in length. Initially, it appeared that catenae were spread over the whole surface and that there might be no apparent pattern to their occurrence, except that they are frequently observed radial to impact basins and craters. However, even a cursory initial survey indicated that they are less common on smooth plains (as mentioned above and discussed further at a later stage).

In order to provide some quantitative data with regard to the distribution of catenae, I applied the Line Density tool, within the Spatial Analyst toolbox of ArcMap. I used the line feature shapefile I produced along with the outlines shapefile as an input because the tool cannot process using polygon shapefiles. This tool determines the average density of catenae across the surface (within a specified radius around each raster cell, in this case approximately 240 m), in terms of length of line (km) per unit area ($km^2$). The output of this line density analysis is shown in Figure 4.13.

Figure 4.13 indicates that there are distinct areas of high catenae-concentration (0.0067 – 0.0076 km per $km^2$, depicted by the red areas in Figure 4.13) and areas where the density is low or there are no catenae present (0 – 0.0008 km per $km^2$, indicated by pale pink in Figure 4.13).To determine whether the clustering visible in Figure 4.13 is statistically significant, I used the Raster to Point tool in the ArcMap 10.1 Toolbox to create an attribute table that indicates the catenae line density value for every pixel in the raster (shown in Figure 4.13). I exported this to MS Excel and used the CHITEST function to compare the density value of each individual pixel to the mean value (given in the Properties table of the line density raster layer). This produced a P value of 1, which indicates that the clustering of catenae is very statistically significant.

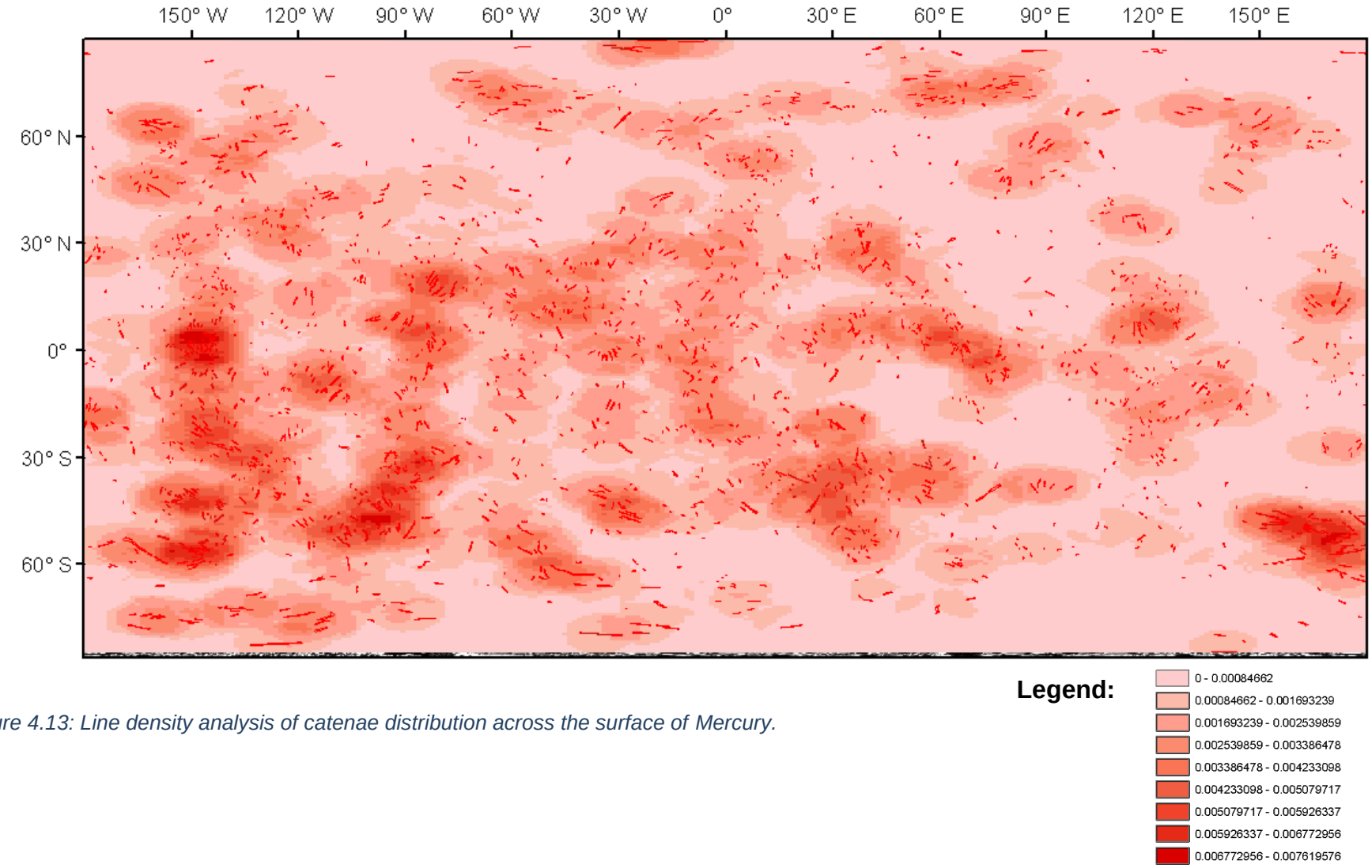


*Figure 4.13: Line density analysis of catenae distribution across the surface of Mercury.*

The fact that there are clusters of catenae, resulting in these high concentration areas in the line density analysis is not surprising, since I observed during the global survey that catenae are often found around impact basins. One such example, where an area of high line density is due to two neighbouring impact basins, each with a family of radial catenae, is shown in Figure 4.14. These high concentration clusters are therefore likely located around impact basins. However, the line density analysis also indicates that high concentration areas are generally found in the southern hemisphere, and slightly more commonly between 0° and 180°W than 0° and 180°E.

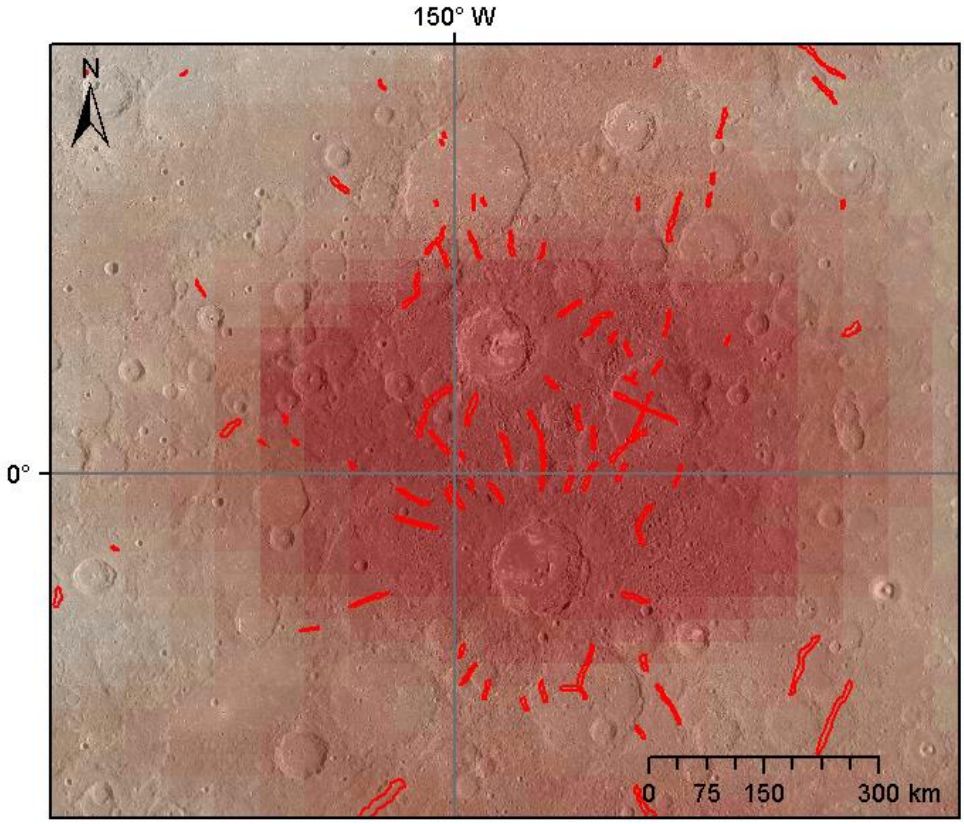


*Figure 4.14: Impact basins as a source of one high line density region for catenae.*

As my next step, it seemed reasonable to investigate whether catenae might be more common on some geological units than others. In order to investigate this possibility, I first obtained the ArcGIS shapefiles for the geological map of Mercury created from the Mariner 10 flybys (USGS (2010) Mercury Geology Downloads (www6). It should be noted that the Mariner 10 geological map covers 45% of the surface of Mercury, on account of the limited coverage of the

Mariner 10 flybys. I selected the units Smooth Plains (the youngest), Intermediate Plains and Intercrater Plains (the oldest, most heavily cratered unit) and selected the catenae from the global survey that were wholly or partially within each unit.

The results of this are shown in Table 4.1. In total, 41% of the catenae I identified in my survey were located entirely or partially on one of these three geological units. While considering that the Mariner 10 map omits 55% of the surface of the planet, it is still noteworthy that the greatest number of catenae are found upon the Intercrater Plains unit. This unit is the largest of the three I consider here (at 12 x $10^6$ $km^2$), and the small size of the Intermediate Plains (relative to the other two units) is likely reflected in the small (7%) share of the total population of catenae located upon that unit.

Table 4.1: Catenae populations on Mariner 10 map units.

| Geological unit | Areal extent ($km^2$) | Number of catenae | % total population | Mean Catenae density (number / $10^6$ $km^2$ area) |
|---|---|---|---|---|
| Smooth Plains | 10x$10^6$ | 333 | 14% | 33 |
| Intermediate Plains | 4.8x$10^6$ | 173 | 7% | 36 |
| Intercrater Plains | 12x$10^6$ | 467 | 20% | 39 |

Due to the different areas of the three units, the column on the right is the most indicative of “concentration” of catenae within each unit. The figure in each row is the number of catenae divided by $10^6$ $km^2$ unit area for each unit. These results show that the population of catenae per unit area is the lowest on the Smooth Plains unit, the highest on the Intercrater Plains and the Intermediate Plains unit has an intermediate catenae population per unit area. Therefore, the results in Table 4.1 indicate that catenae are more likely to be observed on the Intercrater Plains unit – the oldest and most heavily cratered unit of the three I

have included here. They are less likely to be found on the Intermediate Plains and least likely to be observed on the Smooth Plains unit.

To investigate whether the differences in catenae density between the three geological units is statistically significant, I carried out a chi-squared test. The calculations are set out in Table 4.2. For the “expected value” I applied the total areal density of catenae (the population of catenae, 2365, divided by the total surface area of Mercury (per $10^6$ $km^2$), 74.8). In addition to the three geological units in Table 4.1, I also included the rest of the surface of the planet and the portion of the catenae population not included in any of the three units in Table 4.1.

The hypothesis is that catenae density varies depending on geological area. The null hypothesis is that catenae density does not vary depending on geological unit.

**Table 4.2**: Chi squared analysis of the significance of catenae density on different Mariner 10 geological units

| Geological unit | Observed value | Expected value | Residual (Observed – Expected) | Residual squared | Component = Residual squared / Expected value |
|---|---|---|---|---|---|
| Smooth Plains | 33.3 | 31.6 | 1.68 | 2.83 | 0.09 |
| Intermediate Plains | 36.0 | 31.6 | 4.42 | 19.57 | 0.62 |
| Intercrater Plains | 38.9 | 31.6 | 7.30 | 53.28 | 1.68 |
| Rest of surface | 29.9 | 31.6 | -2.62 | 6.85 | 0.22 |
| | | | | **Chi-squared statistic:** | **2.61** |

The number of degrees of freedom (df) for the data in Table 4.2 is 3. For df = 3, the Critical Values (CV) for 5%, 10% and 50% are 9.49, 6.25 and 2.37 (respectively). The chi-squared statistic value in Table 4.2 is 2.61; greater than the CV50 value but less than the CV10 value.

Therefore, the null hypothesis (that the areal density of catenae does not vary depending on geological unit) cannot be rejected at the 10% significance level, but can be rejected at the 50% significance level. This indicates that the catenae areal density differences between the three geological units (and the rest of the surface) are not particularly significant. However, the geological units used in Tables 4.1 and 4.2 use the geological units derived from Mariner 10 data, which covered less than half of the surface area of Mercury. Geological maps covering the entirety of the surface (at greater resolution than produced from the Mariner 10 data) are currently in production. Once completed reliance of catenae areal density based upon geological area can be better assessed.

Denevi *et al.* (2013) produced a more modern map of the smooth plains, based upon MESSENGER data and covering the entire globe. The whole surface can therefore be divided into Smooth Plains and all other units (which will include Intermediate and Intercrater Plains, as well as smaller units such as ejecta material) based on this work.

When the global survey population of catenae is divided up upon this basis, the number of catenae located partially or entirely upon the smooth plains (which have a total area of $31 \times 10^6$ km$^2$) is 691, while 1,775 catenae are located wholly or partially on other units (adding to a total of 2466) (see Table 4.3). Note that the entire global population – as identified during this work – is 2,365. The reason for this discrepancy is that some catenae will straddle the contacts between smooth plains (as identified by Denevi *et al.* (2013)) and therefore be double-counted.

**Table 4.3**: Catenae populations on Denevi et al. (2013) map units.

| Unit | Areal extent | Number of catenae | Mean Catenae density (number / $10^6$ $km^2$ area) |
|---|---|---|---|
| Smooth Plains (as Denevi *et al.,* 2013) | 31 x $10^6$ $km^2$ | 691 | 22 |
| Other units | 44 x $10^6$ $km^2$ | 1775 | 40 |

These results also support the observation that catenae are less common on smooth plains units than on all other types of unit on the surface of Mercury. The line density of catenae on Smooth Plains (as Denevi *et al.* (2013)) is just over half that of the rest of the surface of Mercury (which includes Intermediate and Intercrater Plains, as a large portion of this remaining surface). Since the majority of the total area of smooth plains on Mercury are located in the northern hemisphere (Denevi *et al*., 2013) this accounts for the relative paucity of these features in the northern hemisphere compared with the southern hemisphere (as observed in Figure 4.13).

### *4.3.5 Quantitative Categorisation*

As previously discussed, during the global survey I observed that many catenae were not straight but instead are looped, kinked or curved. Some are radial to impact basins while a few are not, and some have a crater at one end that is significantly wider than the rest of the catenae. After digitising all of the catenae I observed during the survey, I next went systematically through this database and categorised each catena according to these attributes: The results of this survey can be found in Appendix 5 (p. 212 – 264).

- Identifiably radial to an impact basin (approximately radial to, and within 1 basin diameter of the edge of, the basin in question, assigned a value of 1 within the Attribute Table), or “orphaned” (not identifiably radial to or within 1 basin diameter of an impact basin, assigned a value of 0), or not possible to tell (these might be likely radial but in the vicinity of multiple basins so cannot be assigned to one or the other, or radial but too far

from the basin to be definitively linked to it, and are assigned the value 2).

- Whether straight (assigned a value of 0 in the Attribute Table), or bent curved or kinked (assigned a value of 1).

- Whether there is a crater at one end of the catena that is of double the width or greater compared with the rest of the catenae (assigned a value of 1) or the catena is of approximately the same width along its entire length (assigned a value of 0).

My findings are as follows. In terms of morphology, the majority of catenae are approximately straight, only 710 displayed loops, curves or kinks, which is 30% of the total surveyed population. 82% of the catenae population (as identified in this survey) were approximately the same width along their length. 426 (the remaining 18%) did have a larger crater at one end. These variations in morphology might be indicative of variables in the formation of catenae, and will be discussed further in section 4.4.2.

The majority of catenae were identifiably radial to an impact crater or basin, of the total population of 2,365 catenae only 377 (16%) could not be tied to an impact feature; these are “orphan” catenae. I marked 363 catenae as uncertain, either because they were potentially radial to more than one basin and so it was not possible to say for certain which one was the correct family to assign it to or there was a likely candidate ‘parent basin’ but outside the 1 basin diameter threshold I initially set. Both the radial and non-radial catenae are as widely distributed as the full global database.

## 4.4 Analysis and discussion

### *4.4.1 Distribution*

My observation that the majority of catenae can be associated with an impact crater or basin indicates that the impact process is closely involved in their formation. However, assuming this were to be the case then 100% of catenae should be associated with a crater or basin. My survey was not able to do this, however there is the possibility that in some cases the primary crater or basin

might be obscured beneath younger geological units. If this is the case, I would expect proportionally fewer catenae observed on the smooth plains (the youngest geological unit) compared with the rest of the surface, since some of the primary craters and basins for “orphan” catenae would be buried beneath the smooth plains units. (Some would also no-doubt be concealed beneath intermediate plains units and older volcanic units also, but the Smooth Plains are the easiest unit to check this theory against at this stage).

As I discussed in section 4.3.4, according to my results the population density of catenae on the smooth plains is lower (55%) than that of the rest of Mercury’s surface. Catenae are significantly less common on the surface of smooth plains units compared with the older units.

However, 133 out of 377 (35%) non-radial (“orphan”) catenae can be found on the Denevi *et al.* (2013) smooth plains. This percentage is comparable to the percentage of the surface of Mercury covered by the smooth plains, as mapped by Denevi *et al.* (2013) (which occupy approximately 41% of the surface). This implies that “orphan” catenae (the category I would consider likely to be proportionally under-represented on the Smooth Plains compared to the area of Mercury they cover) are not proportionally uncommon on the Smooth Plains unit (as identified by Denevi *et al.* (2013)). This implies that there is another factor involved.

One such factor might be that during the global survey I did not distinguish between catenae and “ghost” catenae. Similar to “ghost” craters, this latter category are features that are visible through a younger layer of lava and are therefore muted, sometimes with partial rather than complete rims and no or little depth.

Ghost catenae become relevant here, because I am looking at the presence or absence of catenae on smooth plains units as an indicator of the periods in Mercury’s history that they were forming. In some cases, catenae showing as being “partially or entirely on the Denevi smooth plains” might in fact be ghost catenae, visible through the smooth plains and consequently mapped within them during my initial survey, but emplaced beforehand. In this case some of those catenae on smooth plains units would effectively be “false positives” in this context.

As a check on this, I carried out a survey to evaluate the proportion of catenae on the Denevi smooth plains that are ghost catenae, or partially ghost catenae. The total population of catenae on the smooth plains was too great to re-survey within the time constraints, however the 133 “orphan” catenae on the Denevi smooth plains – the category of particular interest here - are a small enough population to visually re-survey. I have done this and found that the majority of the 133 catenae are not ghost catenae – I identified 6 out of this population as being ghost catenae or partially ghost catenae (4.5% of the resurvey population). In general, the catenae I recorded as being entirely or partially upon the Denevi smooth plains were indeed formed after the emplacement of those plains, as opposed to pre-existing features visible through the plains.

While none of the survey findings are conclusive when it comes to definitively indicating how these features formed, taken together some conclusions can be drawn. Primarily that they are almost certainly associated in a direct or close way with the formation of impact craters and basins. It is possible that these catenae might be chains of secondary impact craters. For example, those that are proximal, straight and radial (or nearly radial) to impact craters are difficult to interpret as other than chains of secondaries. However, the orphan catenae (assuming the case where there is an obscured primary basin) and those that I observed to bend or divert round the edges of older craters, as well as the particularly unusual morphology seen in Figure 4.12, are hard to reconcile with a conventional origin as chains of secondaries. This leaves open the possibility that a further factor might be involved. I discuss this further below.

Gault *et al.* (1975) state that they observed catenae (which they described as impact basins with diameter greater than ~150 km, however, I was able to quickly identify 14 examples of craters with diameters 50 – 100 km that have radial catenae. Catenae are therefore not limited to craters 150 km in diameter or greater. However, proportionally they do qualitatively appear rarer in smaller craters and basins which suggests to me that the size of the basin is a factor in whether catenae will be formed associated with it.

### *4.4.2 Comparative morphology*

In terms of morphology, the catenae that I have observed and recorded in my survey of Mercury have more in common with secondary impact crater chains than many of the features on other planetary bodies.

The lunar crater chain in Figure 4.3 has some similarities to some of the catenae I have surveyed on Mercury. However, the craters in the lunar example are found within a continuous groove, with straight edges (known as Rilles). I did not observe any morphologically similar straight-edged grooves on Mercury, with the sole exception of the feature shown in Figure 4.12. Some similarities are present between Hermean catenae and the some of the variously-named groove-like features on Mars which have a beaded appearance, are comparable in scale to catenae on Mercury and have rims in places. Mège *et al.* (2003) and Scott *et al.* (2002) suggest that Martian pit (crater) chains are associated with graben, and consequently volcanic activity or volatile release along faults.

It is not currently possible to observe catenae on Mercury to the same high resolution as on Mars (or the Moon), so in depth morphological comparison is not possible. However, catenae on Mercury almost always have identifiable rims, which is not the case with most Martian pit (crater) chains. Their likely association with graben on Mars also suggests a different formation of Mercury, despite there being some morphological similarities.

I found during my global survey that catenae on Mercury often cluster around impact basins. Consequently, using the Lunar Quickmap service online I looked at large craters (with fresh, crisp morphology to have the best change of observing preserved catenae) on the Moon. I identified some possible candidates in the area surrounding Copernicus impact crater. The Copernican catenae appear more muted than Copernicus crater, but most are radial or approximately radial and are similar in morphology to many Hermean catenae, although with a more muted appearance.

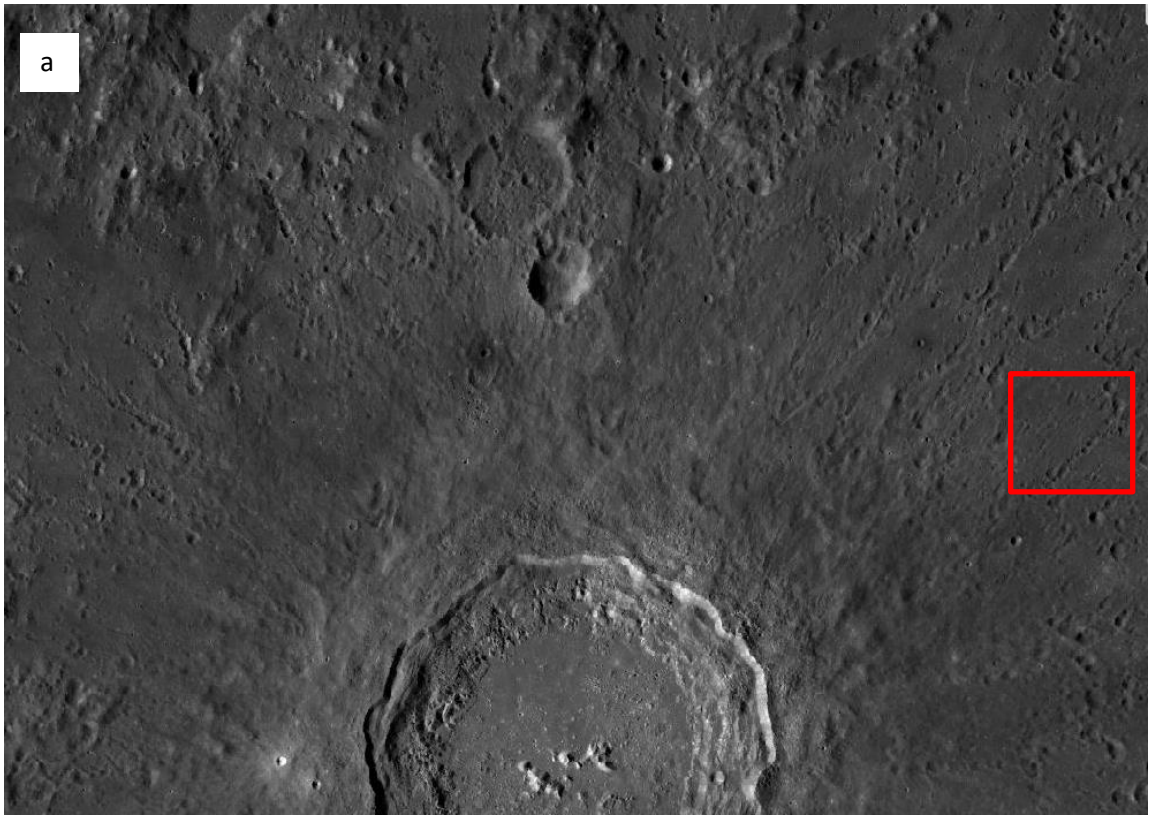


*Figure 4.15: a) Copernicus crater on the Moon and area immediately to the North, source: Lunar Quickmap (http://target.lroc.asu.edu/q3/#). Copernicus is 96 km in diameter, crater centre coordinates 10°N, 20°E. b) is an expanded view of the area within the red box in a), showing a crater chain radial to Copernicus.*

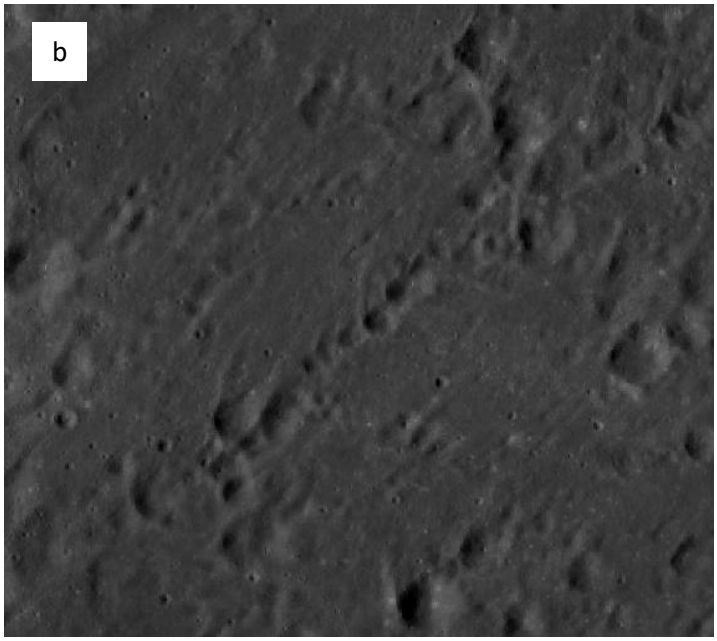


A second crater with some examples of radial groovelike features is Schrödinger. This 316 km diameter impact basin has two named Valles (Schrödinger and Planck Valles) radial to it, as shown in Figure 4.16. Schrödinger Vallis is very similar in morphology to catenae I included in my global survey of Mercury. There are several other named Valles on The Moon, but I have been unable to find anything in the lunar literature regarding the

formation of these features. While this observation does not assist me in identifying the formation mechanism for catenae on Mercury, I can state that similar features to Hermean catenae do occur on the Moon (although they are much rarer).

Schumm (1970) carried out experiments into the morphology produced by drainage of regolith analogues into underlying fractures (due to emission of gas from these fractures resulting in fluidisation) (discussed in more detail in section 4.2.6) and observed that the resulting landforms were strongly similar in morphology to Lunar crater chains. He stated that his results supported the theory that Lunar crater chains such as those within the graben Rima Hyginus (see Figure 4.3) were related to the faults of the graben. I observed that the experimental results of Schumm (1970) are comparable with the catenae on Mercury, notably the presence of rims. Rims are present in all catenae (where there is sufficient image resolution to distinguish them), and so any theory of formation needs to account for them. Rims are absent from most of the other (non-impact related) possibilities for the formation of crater chains (catenae) and so fluidisation drainage appears a strong contender.

In addition to the fluidisation experiment results of Schumm (1970), the crater chains of Phobos, the Galilean moons and Ceres are also similar in morphology to catenae on Mercury. The formation theories in these cases all indicate the involvement of impacts, whether they be secondary impacts, draining of regolith into impact-created fractures (which may include fluidisation processes) or the impact of fragmented comets. This – along with the clear association of the majority of catenae in my survey with impact basins –might lead me to suggest that most if not all the features I have included in my global survey of catenae on Mercury were formed by impact related processes. Given the long global contraction on Mercury (Byrne *et al.,* 2014; Klimczak *et al.,* 2015), one might consider the secondary impact hypothesis the more likely than the regolith draining hypotheses. However, the evidence that impact-related fractures may have assisted the formation of volcanic plains indicates that fractures do remain open for an extended period of time, leaving the possibility of a drainage/fluidisation process as a potentially viable option. It is possible that both of these processes are involved in forming the global population of catenae. .

Regardless of the exact process or combination of processes, the evidence suggests to me that catenae are closely linked to primary impact craters and basins. Gault (1975) observed that catenae form around basins approximately 150 km in diameter. According to Gault (1975), 80% of the impact craters between diameters 10 and 20 km that they examined exhibited central peaks, increasing to 93% in diameters greater than 20km (noting that they examined a limited number of impact craters). Pike (1988) also created the category “immature complex” impact craters for Mercury, of diameters 9.5 – 29.1 km. This category may have terracing and central peaks.

If catenae are chains of secondary impacts, I would expect that some would have craters in their chains that exhibit a central peak would assist in confirming their origin as being due to secondary ejecta impacts. However, the majority of catenae I identified during my global survey have maximum diameter (the diameter of the largest individual crater in the chain) of less than 8 km.

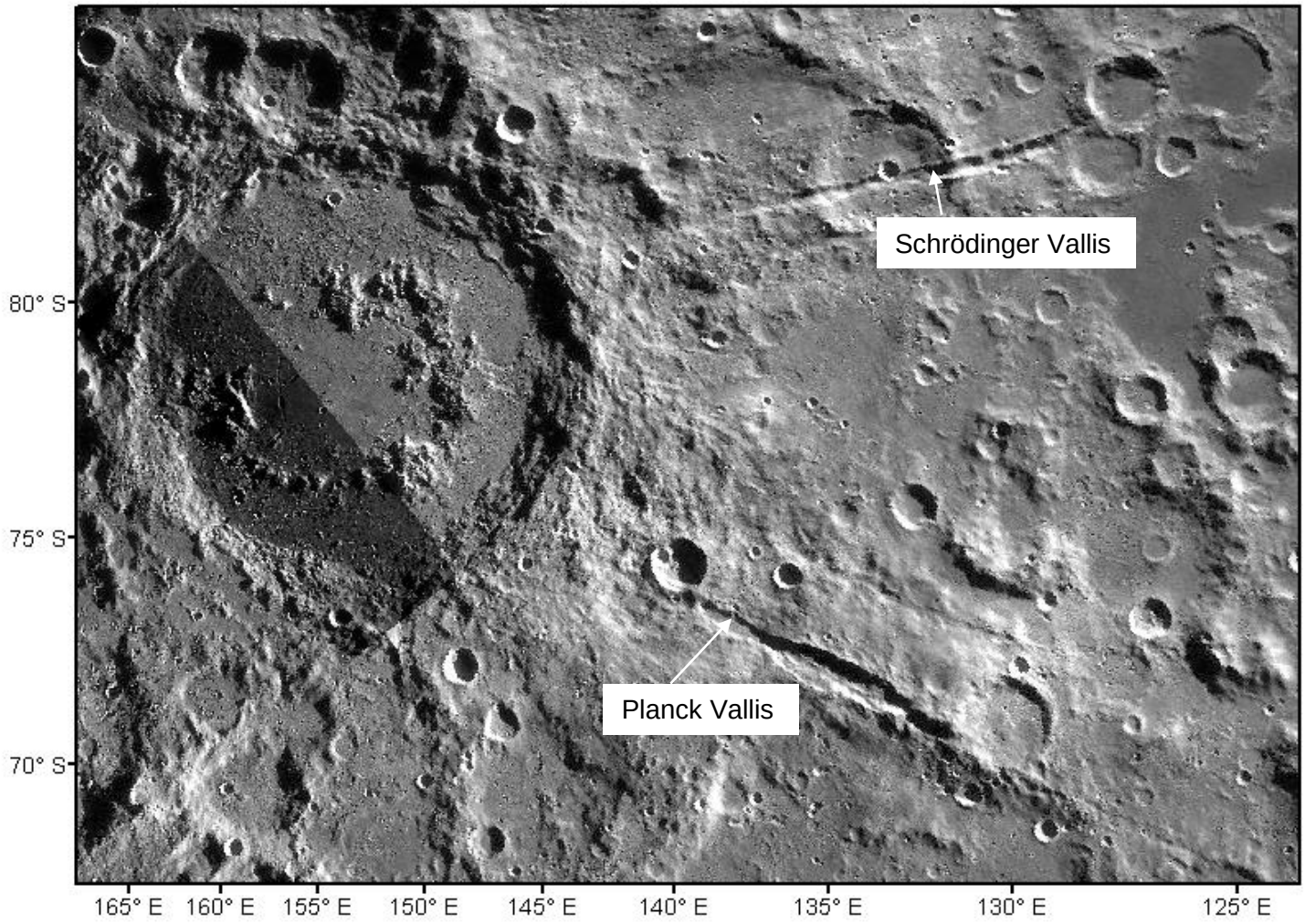


*Figure 4.16: Schrödinger basin, Schrödinger Vallis and Planck Vallis.*

I visually resurveyed the catenae in my global survey between 40°N and 40°S, and identified two catenae that appear to have one crater in the chain that has a central peak These are shown in Figures 4.11 and 4.17. In both cases, the largest crater in the catena is the one with the central peak – in Figure 4.11 the crater with the central peak has a diameter of 20 km. In Figure 4.17 the crater with the central peak has a diameter of 22 km. However, in the case of the latter it is possible that this crater is not part of the catena, but was simply formed on top of it. This is on the basis of its greater depth, and the clear rim between it and the next crater in the chain.

The fact that I have identified only a couple of craters in catenae that have central peaks does not rule out the secondary impact formation hypothesis because most craters forming catenae are too small for peaks to have formed.

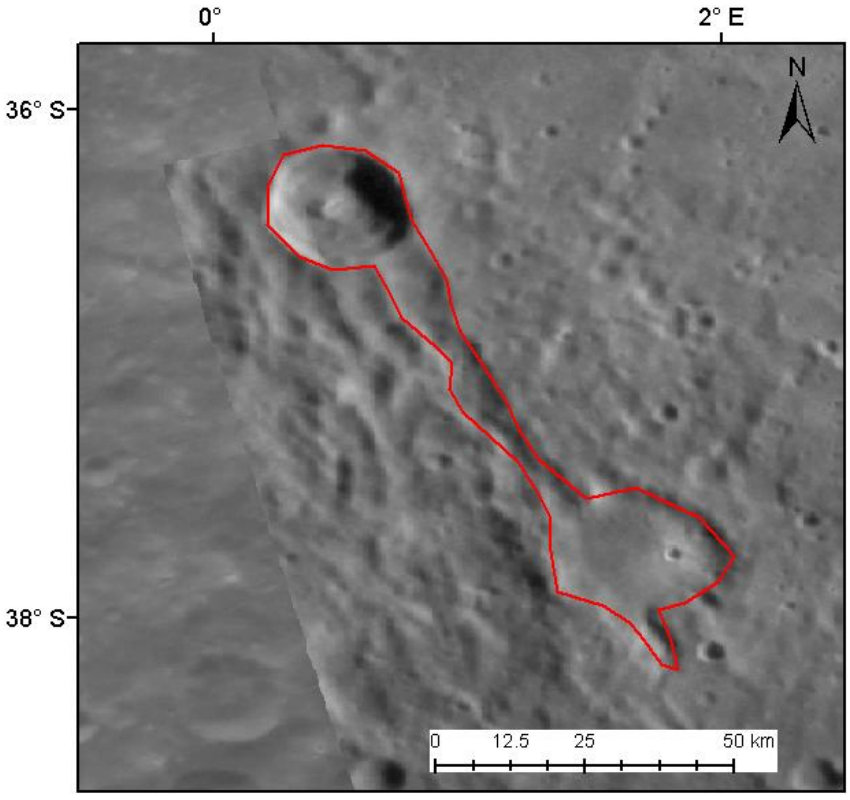


*Figure 4.17: Catena with possible central peak in one crater in the chain.*

### *4.4.3 Applications of catenae*

Given my conclusion in section 4.4.2 that catenae are directly related to impacts (whether formed by secondary impacts, or fluidisation drainage into impact-related fractures), I therefore assume that they formed at the same time or

within a geologically short time period thereafter. This being the case, they can be used for stratigraphic purposes. Catenae are still often visible after the continuous ejecta blankets become indistinguishable from the plains units, and where a catena and ejecta blanket (or two catenae) intersect, the one that is cross-cut will be the younger (and associated with the younger crater or basin) by the law of superposition. Additionally, the ejecta blanket covers the area immediately around the crater or basin while catenae extend into the continuous secondary facies and discontinuous secondary facies (as Xiao *et al.* (2014)). Catenae can be used to determine which of two neighbouring – but not superposed – craters or basins is the younger and therefore assist in establishing the history of an area.

# 5 Illumination bias

## 5.1 The illumination bias on Mercury

Authors investigating orientation trends of linear features on Mercury tend to mention in discussion or supplementary information that illumination bias is a problem that can affect observations (e.g. Byrne *et al.* (2014), Watters *et al.* (2015)). Some of these papers make note of what measures they took to minimise the effects (Watters *et al.*, 2015), and some also include evidence that they consider proves that the bias has not affected their data to any great degree (and therefore their conclusions are based upon robust observations), but not all do this. Klimczak *et al.* (2015) acknowledge the problem of illumination bias in their discussion, but draw conclusions from data regardless, stating that the trends observed in lobate scarp orientation support a particular model of Mercury's geological development "despite lighting bias". In fact, the illumination bias would accentuate the trends in orientation they are using as evidence, rather than minimise them, making it likely they would observe those trends whether or not their favoured model was correct.

I observed an apparent trend in the orientation of both of the types of features under investigation. Among the scientific community the response to these apparent trends in orientation have been to attribute them to the problem of illumination bias on Mercury. This prompted me to investigate the orientations of the global populations of basin-edge scarps and catenae and investigate the effect (if any) of the illumination bias upon orientation surveys of basin-edge scarps and catenae.

Any real trends in orientation of basin-edge scarps are potentially of great interest in the context of Mercury's geological history (as detailed in Chapter 2, which also includes some results of global orientation surveys of basin-edge scarps). Real trends in the population of catenae would be of interest to me due to the potential implications about how this feature type forms. My work on documenting the trends I observed, and testing the extent to which they are artificially created trends due to the illumination bias, is set out in this chapter. A smaller section on the orientation of basin-edge scarps already covered in Chapter 2.

## 5.2 Data used from global mapping

Until the global Digital Elevation Map (DEM) was released in mid-2016 the MDIS mosaics were the only available planet-wide dataset to carry out mapping of lobate scarps and other structural features. When carrying out global surveys of topographical features on Mercury, workers typically use the global mosaics (either the monochrome morphology mosaic, such as the one I have used throughout, the colour mosaic or enhanced colour mosaic). There are two monochrome mosaics recently made available at time of writing, one composed of the highest resolution images available with medium incidence angle, and therefore medium level of shadowing, which is the most appropriate for identifying topographical features (Di Achille *et al.,* 2012; Watters *et al.,* 2015; Watters *et al.,* 2016).This mosaic has recently been published, and has a greater resolution than the MDIS v9 monochrome mosaic I have used throughout this project (166 m/pixel compared to 250 m/pixel), the MDIS v9 global mosaic, Watters *et al*. (2016) have stated that a minimum resolution of 200m/pixel is helpful for identifying lobate scarps. The use of global mosaics is convenient for investigating large areas or the entire globe, as it avoids the need to identify, download, process and mosaic each individual image covering the area of interest.

As mentioned in Chapter 2, Mercury's near-zero obliquity (Yseboodt and Margot, 2006; Byrne *et al.,* 2014) means that for a given point on the surface the solar azimuth will be either east or west (depending on the time in the Hermean day the image was taken), but with no other notable variation in illumination geometry. For a given point on the equator, the solar azimuth (the compass bearing for the sub-solar point on the surface (Watters *et al.,* 2015) will be either due East or due West and for one at low latitudes the solar azimuth will be either approximately east or approximately west. For a given point at high latitudes the solar azimuth will be either north-east or north-west (for southern high latitudes, or south-east or south-west for northern high latitudes).

Features trending parallel to the illumination direction are at greater risk of being overlooked (Melosh and McKinnon, 1988; Watters *et al.,* 2004), particularly with solar incidence angles of <75° (as measured from the zenith) (Klimczek *et al*., 2015). Therefore, topographical features with trends aligned with the solar

azimuth would be less likely to be observed than features perpendicular to the illumination azimuth. Any given point on a planetary body with a degree of obliquity, such as Mars (with a large orbital obliquity of 25°) or the Moon (with a small orbital obliquity of 7°) will have varying illumination azimuths depending upon the season. This provides opportunity for an orbiter to obtain images with varying illumination geometry, which allows for topographic features of various orientations to be observed. For this reason, illumination bias is more likely to have a significant impact on observations of topographic features on Mercury than on Mars or the Moon or other planetary bodies with a degree of obliquity.

In order to address this, Klimczek *et al.* (2015) have suggested that the use of topographic models produced from stereo imaging (such as those produced by Preusker *et al.* (2011)) would be a useful resource for mapping tectonic landforms on Mercury, in addition to using the MDIS imagery. I have employed this approach in the following sections with the aim of determining whether the preference in orientation for the global populations of basin-edge lobate scarps and catenae I observed using MDIS images alone are real or artefacts of the illumination bias.

## 5.2 Basin-edge lobate scarps

I introduced basin-edge lobate scarps (shortened to “basin-edge scarps”) in Chapter 2. A full description of these features can be found therein, but briefly: Basin-edge scarps are curvilinear features with one steep limb and one gently dipping limb, found at the edges of the volcanic fill of certain basins on Mercury. The steep scarp invariably faces outwards, away from the centre of the basin. Lobate scarps on Mercury are commonly interpreted as the surface expressions of thrust faults (Strom *et al*., 1975; Watters *et al.*, 2004; Byrne *et al.*, 2014), and in Chapter 2 my co-authors and I propose a similar mechanism of formation for basin-edge lobate scarps.

In Chapter 2 I also made the first mention of the potential impact of illumination bias on the detectability of linear and curvilinear features on the surface of Mercury, in this case specifically basin-edge scarps.

### *5.2.1 Global survey method*

The methods I employed to investigate whether the global population of lobate scarps exhibited any trends in orientation were briefly outlined in Chapter 2, but will be set out in more detail here. I surveyed on the MDIS monochrome global mosaic v9, using an equirectangular projection to survey from 60°S to 60°N and northern and southern polar projections to survey the polar areas. The mapping performed as part of the global survey of basin-edge scarps (carried out using ArcGIS 10.1) produced a polyline shapefile layer, indicating the centreline all of the basin-edge scarps I observed during the survey. The survey was based upon visual observation of each of the basins (which I defined as >100 km diameter impact craters) in a database. That database is another shapefile of polygons (circles), largely created by (Fassett *et al.*, 2012) with two additions by me where I identified basins missing from that survey.

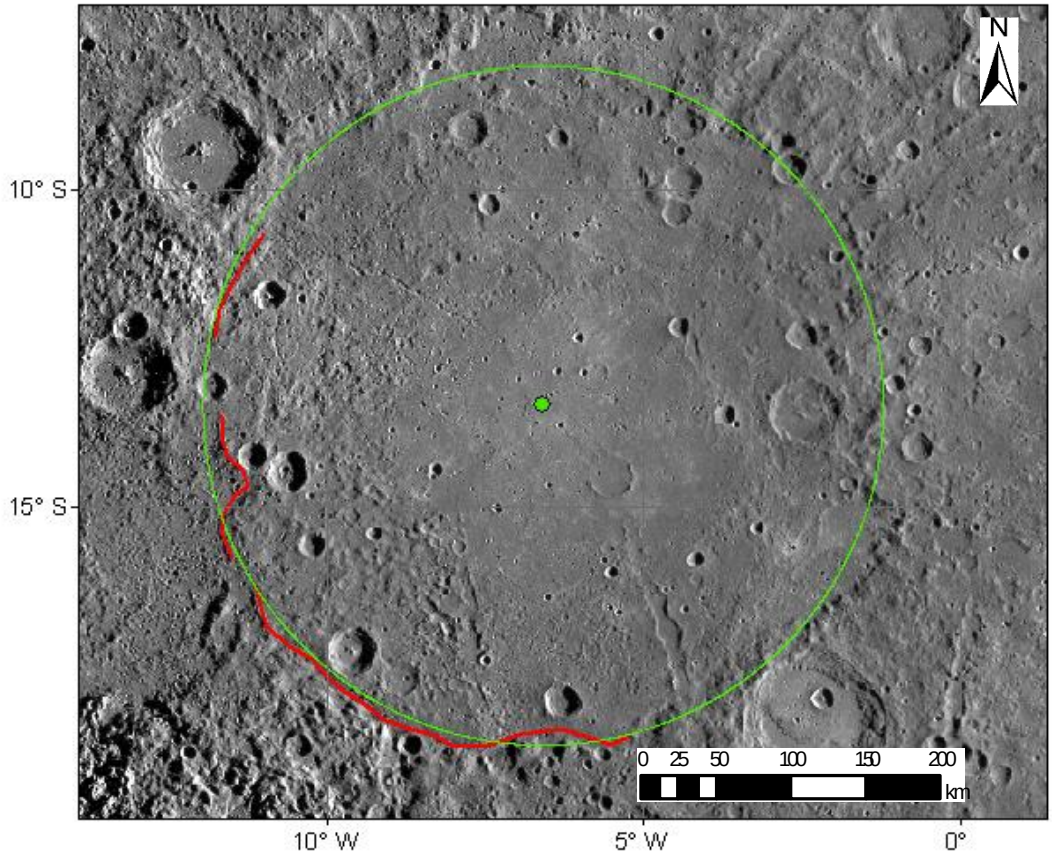


*Figure 5.1: Sanai basin, shown in green, with the three sections of basin-edge scarp I identified at the edge of the smooth plains unit within the basin rim delineated in red. The centroid of the basin is the green dot.*

In order for the following process to work correctly, any overlapping basins must be sorted into separate non-overlapping circle-type polygon shapefiles (and

their corresponding basin-edge scarp polylines similarly separated into separate shapefiles). The procedure will not necessarily assign each basin-edge scarp polyline to the correct basin, in any situation where the basins overlap. The series of steps outlined below are performed for each pair of polygon-polyline shapefile layers individually.

Using a Feature to Point Tool (from the Data Management Toolbox in ArcMap 10.1), I created a shapefile layer of centroid points for each of the circles outlining the basins and a separate layer of centroids for the basins that were overlapping and removed from the original shapefile. The shapefile of points to be analysed was the input for the Euclidean Direction tool within the Spatial Analyst Toolbox. I also input the extent the tool was to cover, which needs to be a minimum of the distance in km of the shortest radius between the centroid and associated basin-edge scarp (I chose 150 km, 3 times the radius of the smallest basin in this work but large enough to ensure the raster for each centroid includes the associated polylines). If the extent is smaller than this minimum radius, the raster produced by the Tool, which is based upon the location of the centroids and the distance specified by the extent input, will not reach the polylines delineating the basin-edge scarps. In order to output useful statistics results at the end of this process, I assigned each polyline a unique identifier.

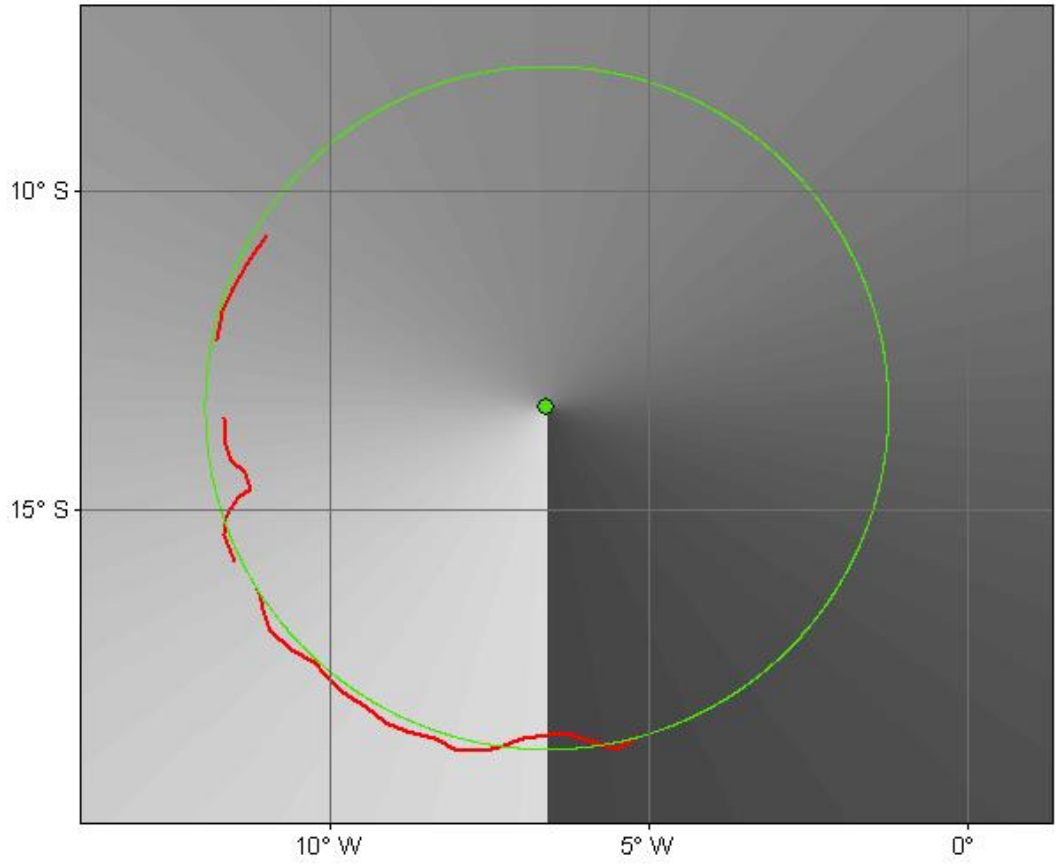


*Figure 5.2: An example of the output of the Euclidean Direction Tool. The increments of grey radial to the green centerpoint represent the degrees of a circle, lightest shade bring 0-1°, darkest shade being 359-360°.*

The Euclidean Direction tool outputs a raster containing angles radial to each central point, clockwise from due south. An example is shown in Figure 5.2, and several can be seen in the Figure 5.3. This is the input for the next stage, the Zonal Statistics tool which I used to extract statistics from rasters (in this case the Euclidean Direction output) based upon the Zone Data input. In this case, the resulting output is the minimum and maximum value from the raster around the relevant centroid point (the point created to indicate the centre of the basin around which each basin-edge scarp is situated) for each individual polyline. Since the Euclidean Direction tool measures 000° as due south, the outputs from the Zonal Statistics tool each need 180° adding on to them. Another is that polylines that cross “000°” (actually, 180°) result in a minimum bearing of 000° and a maximum of 360°. In these cases, which are the minority of the global population, I measured the bearing pixel value of both ends of each polyline on the original raster produced by the Euclidean Direction Tool manually.

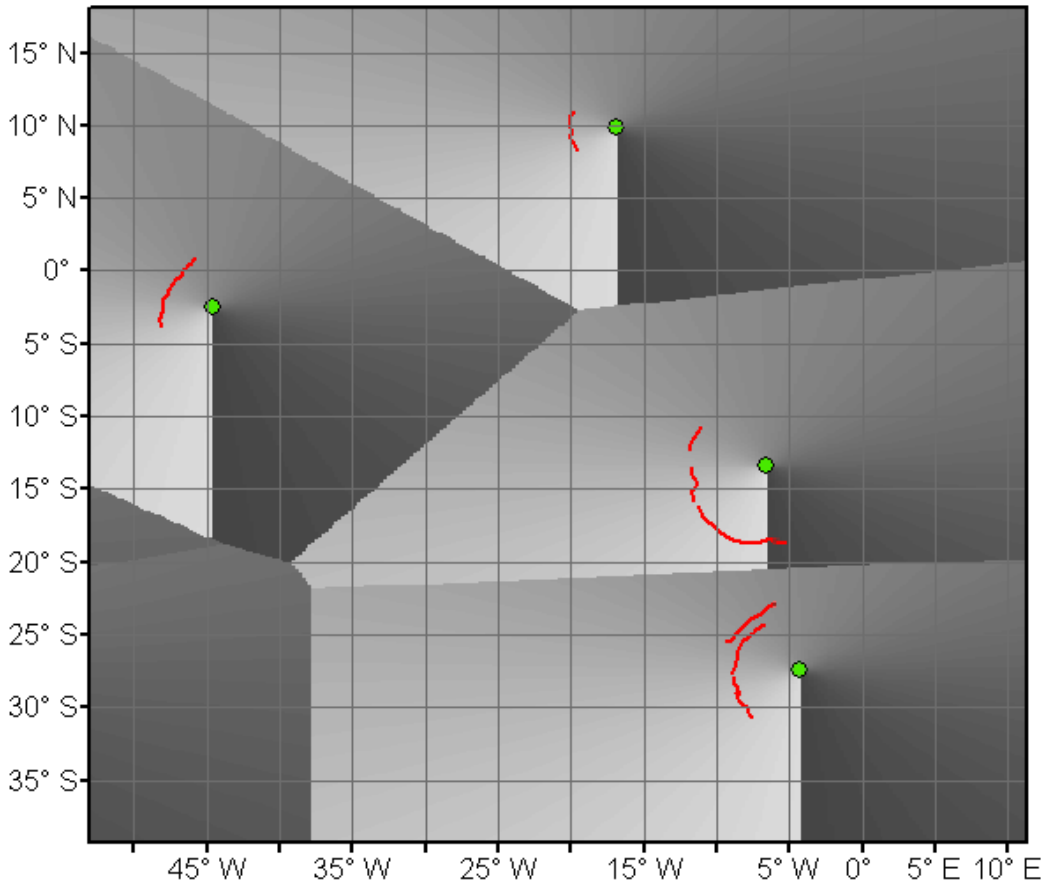


*Figure 5.3: A few examples of the output of the Euclidean Direction Tool. The "000°" in each case is due south (180°), which means the results need 180° to be added before they are accurate. The grey shading is as in Figure 5.2.*

The result of this procedure is a list of each individual polyline (representing the individual sections of basin-edge scarp I identified in my global survey, see Chapter 2) and the minimum and maximum compass bearing (two numbers between 0 and 359) for each of them. In order to best graphically represent the data, an additional stage is required. I tallied the frequency of a section of basin-edge scarps for every single-degree bin between 000° and 359°. For example, the degree 089-090° will have one tally for every section of scarp that passes through it. A scarp section with a minimum bearing of 010° and a maximum bearing of 015° will result in one tally in each bearing bin 010-011°, 011-012°, 012-013°, 013-014° and 014-015°.

The resulting table, of 359 single-degree bins and a tally number, can be plotted as a radial plot therefore graphically representing the orientations of basin-edge scarps across the surface of Mercury (in the case of the global survey data).

### *5.2.2 Global survey results*

The radial plot for the global survey is shown in Figure 5.4 (also in Chapter 2).

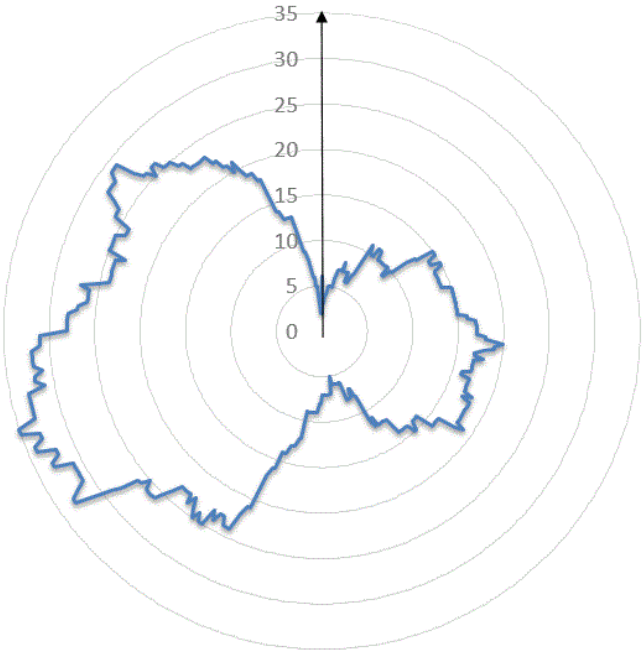


*Figure 5.4: A radial plot displaying the facing directions of the global population of basin-edge scarps (n = 142). The black arrow denotes north; the radial axis indicates frequency of lobate scarp facing direction occurrence (per degree of bearing). This plot indicates a north–south alignment of scarps, which are more commonly west-facing than east-facing.*

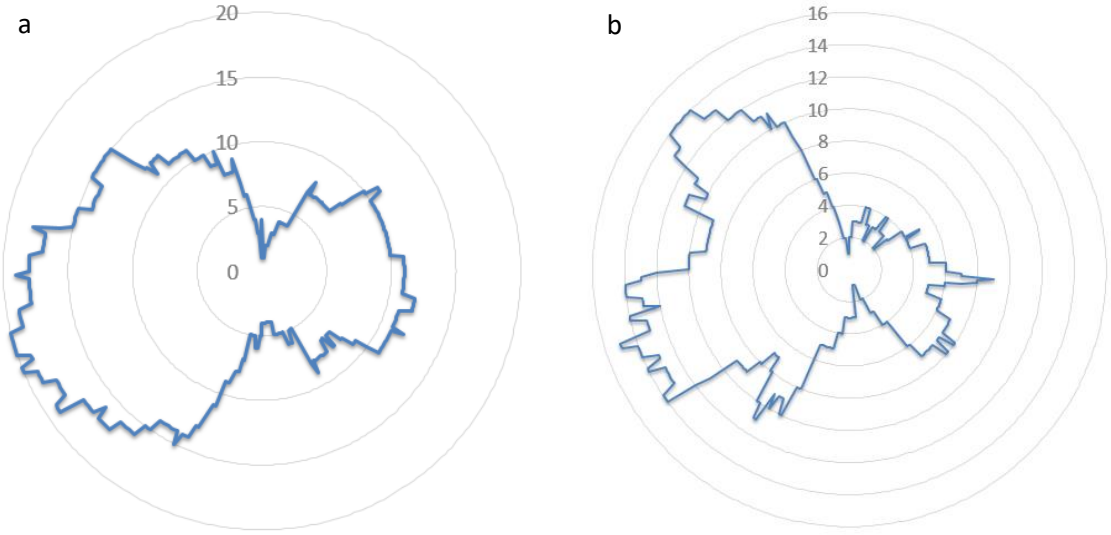


*Figure 5.5: (a) Small category (n= 66) . 5.5 b: Large category (n= 76)*

While not included in the final version of the paper, my work on basin-edge scarps initially divided those scarps peripheral to basins of diameter 100-199 km (“small category”) from those peripheral to basins of diameter >200 km (“large category”). The results of the small category global survey of the orientations of basin-edge scarps are shown in Figure 5.5a, those for the large category are shown in Figure 5.5b.

There is very little substantive difference between the global radial plot (for all basins of diameter greater than 100 km) and those for the small and large category radial plots; both show a strong preference for north-south orientations and both exhibit a preference for basin-edge scarps on the west edge of the basins as opposed to the east. The main noticeable difference between the large and small category plots and the global plots is that the large category plot is more asymmetric than the other two. In other words, proportionally more of the large category basin-edge scarps were observed on the west edge of basins (as opposed to the east edge of basins) than for the small category or the global population.

### *5.2.3 Artificially illuminated shaded-relief models*

At the time of this work the global DEM (released in April 2016) was not available, and the Mercury Laser Altimeter (MLA) data covers the northern hemisphere only, and with the highest resolution in the north polar regions (Zuber *et al.,* 2012). In order to look at how the orientation trends of basin-edge scarps might vary with illumination orientation I require a shaded-relief model upon which I could impose various illumination conditions. The minimum horizontal resolution required to resolve basin-edge scarps is approximately 200m/pixel.

Preusker *et al.* (2011). produced 3 DEMs produced from MDIS stereo images with a resolution of approximately 220m/pixel. None of these are centred in the southern hemisphere, but there is one that covers a very low-latitude portion of the southern hemisphere and extends up to 60°N. Having the greatest possible range of latitudes allows me the greatest chance to investigate global (as opposed to local) variations in This is the DEM named “M2”, which covers an

irregular-shaped area of approximately 13 x $10^6$ $km^2$. The whole of the DEM area is used in the next section of this work.

Using the Hillshade tool in ArcMap 10.1, I created shaded relief surfaces (hillshade models) for two lighting azimuths (000° and 090°) from the M2 DEM raster. The shading of the models is determined by the topography from the DEM and the illumination azimuth chosen. It is this latter variable that makes the Hillshade tool of interest when it comes to examining the effect of illumination azimuth on the apparent orientation of linear topographic features. It seems reasonable to think that features that trend perpendicular to the direction of illumination are most likely to be observed and recorded on a visual survey, but ones that trend parallel to the direction of illumination are more likely to be overlooked.

In order to provide the best comparison between the global survey and the results of the surveys I undertook using the shaded-relief models, I cropped the global survey results down to the same area as the shaded relief model. The results of the global survey (undertaken on the global monochrome mosaic v9) as cropped to the survey area are depicted in Figure 5.6, with the results divided into small and large categorised in Figures 5.7a and b (respectively).

To carry out the surveys, I followed the same procedure as I initially followed for the global survey (as outlined in Chapter 2), using the same database of basins of diameter >100 km but with the database cropped to the same area as the M2 DEM.

When the global survey is cropped to the area of the M2 DEM shaded-relief model, the results differ slightly from the original global results. The full survey results indicate the scarps lie preferentially along the direction north-south, but indicate that the preference for basin-edge scarps is for the east edge of the basins rather than the west edge (as in Figure 5.8). The plots for small and large categories (Figures 5.9a and b) agree with the Figure 5.8 result, also showing a preference for the east side of basins, that is more noticeable in the large category plot.

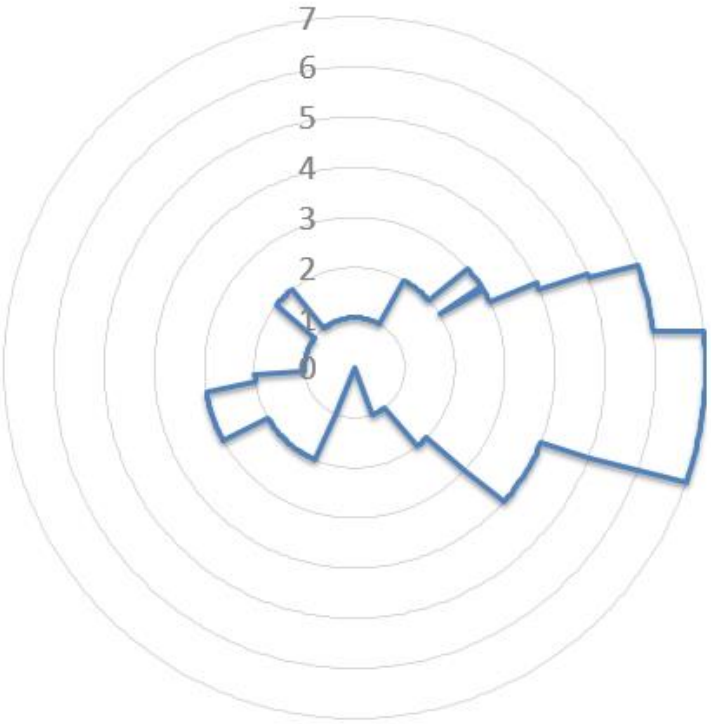


*Figure 5.6: The global survey cropped to the shaded-relief model survey area (n=11).*

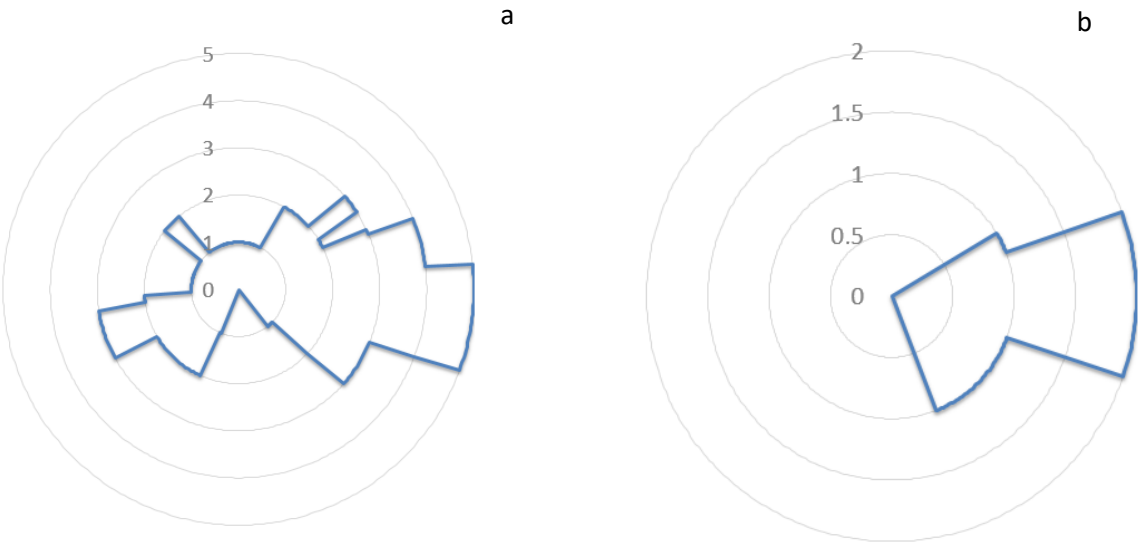


*Figure 5.7: The global survey cropped to the shaded-relief model survey area, by size category. (a) Small (n=9).(b) Large (n=2).*

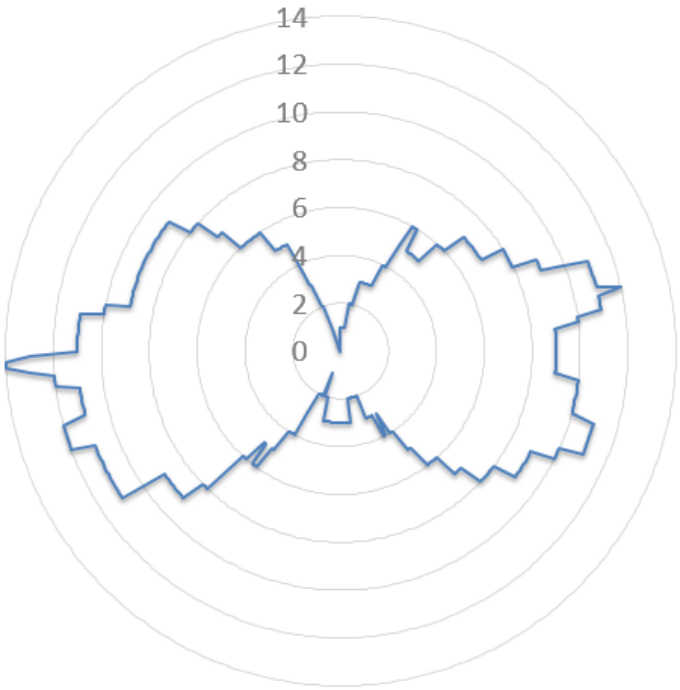


*Figure 5.8: Radial plot of facing directions produced from hillshade models artificially illuminated from the east (n = 40). The scarps show strong preferences for east- or west-facing directions.*

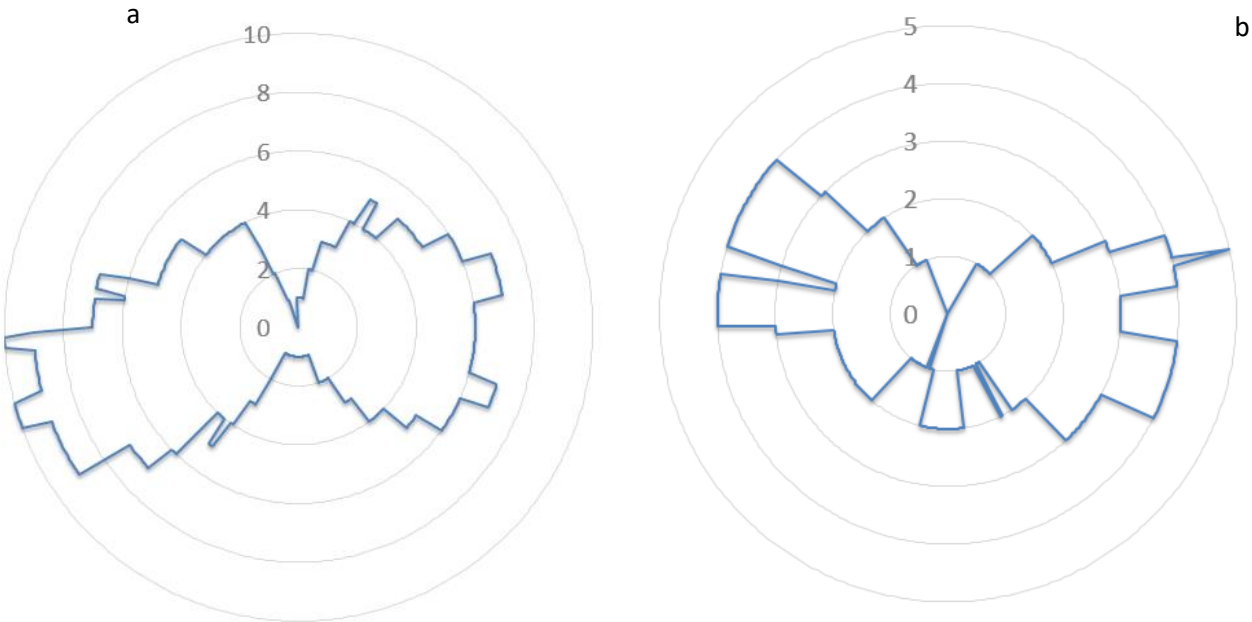


*Figure 5.9: Radial plot of facing directions produced from hillshade models artificially illuminated from the east. (a) Small (n= 24). (b) Large (n= 16).*

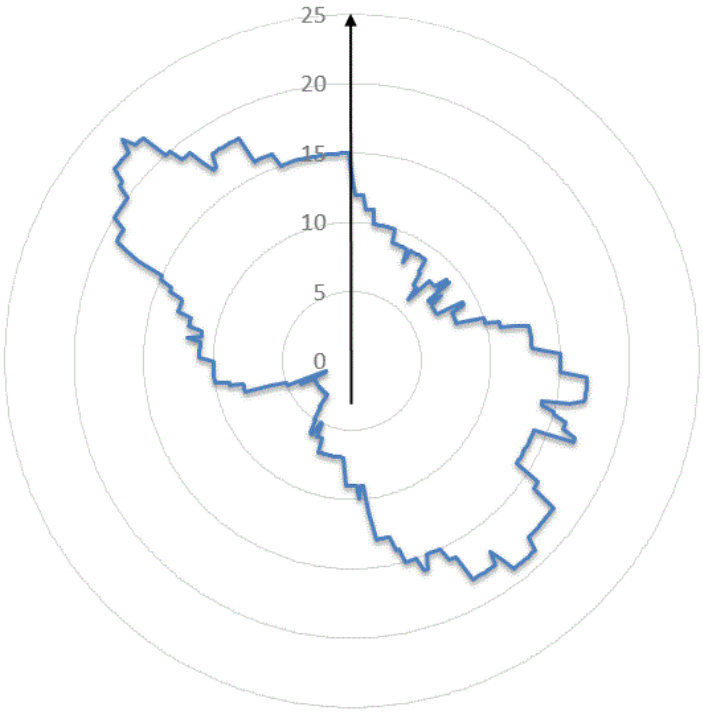


*Figure 5.10: Radial plot of facing directions produced when hillshade model was artificially illuminated from the north (000°) (n = 56), yielding preferential scarp facing directions to the northwest and southeast.*

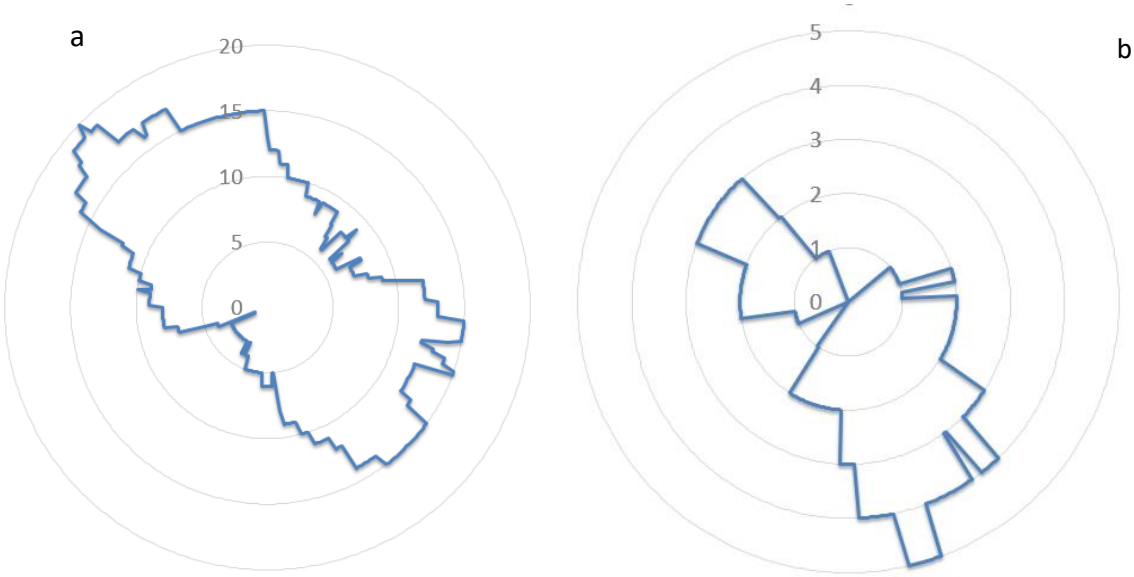


*Figure 5.11: Survey when hillshade model was illuminated from north (000°). (a) small (n=44). (b) large (n=12).*

However, it should be noted that the number of basin-edge scarps within the hill-shaded area (according to the initial global survey) is rather small: only 11 scarp sections in total, only 2 of which are in the large category, compared to 142 basin-edge scarp sections in the entire global survey. This is just below 8% of the total global population, and thus is below a statistically significant population, which I would consider to be 10% minimum in this case. However, the survey area with varying illumination is limited to the extent of the M2 DEM, which was the best option available at the time.

Figures 5.8 and 5.10 show the surveys I undertook on the shaded-relief models when illumination azimuth was 090° (Figure 5.8) and 000° (Figure 5.10). Figures 5.9 a and b and Figures 5.11 a and b are the small and large category break-downs of the surveys in Figures 5.8 and 5.10.

The radial plots for the results of my survey with illumination azimuth 090° (total survey, small and large categories) all indicate the same results: a preference for NS orientation, with a more symmetric distribution between east and west edge of basin volcanic fills than displayed in the global survey (Figure 5.4, 5.5 a and b and 5.6, 5.7 a and b). Except for the more symmetric distribution between east and west, the results are the same as those of the global survey (a preference for north-south strikes). This is not surprising given the predominant illumination azimuth on the global MDIS mosaic is also approximately 090°. The population of the survey I undertook on the shaded-relief model is higher than that of the global survey results on the same area (n=40 as opposed to n=11). I believe the reason for this is simply that the smaller survey area (and resulting smaller number of basins in the survey population) resulted in greater focus on each basin within the survey area, and a greater amount of time spent visually examining each basin. It is also possible that the lower resolution of the shaded-relief models created from the M2 DEM resulted in more “false-positive” identification of scarp sections.

The radial plots for the results for my survey with illumination azimuth 000° are different from any of the previous survey plots. All three of the azimuth 000° plots display the same trend; a preference in scarp strike for NE-SW. This trend is different from the NS preference apparent in the previous global survey

(entire globe or cropped to the same area as the shaded-relief models), or the shaded-relief model survey with illumination azimuth 090°.

### *5.2.4 Uncertainly estimation for global surveys*

The global surveys I undertook to map the distribution and locations of basin-edge scarps (Chapter 2) and Catenae (Chapter 4) are unlikely to have included all of the respective features, due to the scope of the area I was covering and the resolution at which I was mapping in order to cover such an area, as well as the unavoidable restrictions resulting from the illumination bias that is the subject of this Chapter.

Since the method set out in section 5.2.3 involves resurveying for basin-edge scarps within a smaller area than the entire surface area of Mercury, only 13 x $10^6$ $km^2$, the area of the M2 DEM, rather than 75 x $10^6$ $km^2$ (the surface area of Mercury). When focussing only upon this smaller area, I identified a greater number of basin-edge scarps than within the corresponding area of the global survey. When the DEM was artificially lit from azimuth 090° I identified 40 basin-edge scarps, and when lit from azimuth 000° I identified 56. Within the same area, I identified only 11 basin-edge scarps in my initial global survey.

This allows me to tentatively place an uncertainty estimate upon my global population figure, which applies to catenae as much as to basin-edge scarps, since the same mapping procedure and drawbacks apply to both types of feature. It is possible that the global populations might be 3.5 – 5 times larger than my surveys in Chapters 2 and 4 have indicated. These additional features may become apparent when mapping the surface at a greater resolution than I was able to during this project, and applying multiple illumination conditions to hillshade models created from DEMs (when global DEM coverage of sufficient resolution is available for Mercury), in order to reduce the impact of illumination bias.

### *5.2.5 Conclusions (basin-edge scarps)*

I believe that this variation in the results of surveys undertaken on the same area but with different illumination azimuths indicates that the apparent results of visual surveys of basin-edge scarps (and similar linear or curvilinear features) undertaken on MDIS mosaics will not provide a complete picture of the population of such features. Features running parallel with the illumination

azimuth are more likely to be missed, according to my findings. This means that investigations in the orientation trends (and subsequent scientific conclusions drawn from such observations) will be based upon incomplete and biased raw data, unless surveys on hillshade models are also incorporated.

## 5.3 Orientations of catenae

Straight, curvilinear or looped grooves on the surface of Mercury are referred to in this project as catenae (an example is shown in Figure 5.12). The global distribution and possible formation mechanisms, based upon locations and morphology, are discussed further in Chapter 4. As part of my investigation into their possible formation mechanisms I have investigated whether there are any identifiable trends in orientation. This is because if all catenae are secondary crater chains radiating from primary impacts, one would expect a stochastic orientation distribution. Therefore, a lack of random distribution of orientations might indicate an alternative formation theory (or a combination of theories) is required to explain these features on Mercury. The survey method I followed is as described in section 5.2.1, with the exception that the location of impact basins was assumed to be of no relevance for the survey initially. The results of the global catenae survey are further described in Chapter 4.

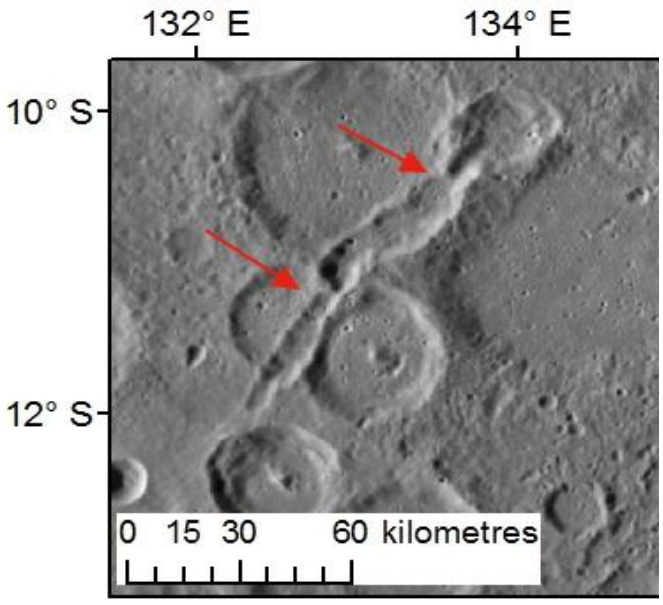


*Figure 5.12: An unusual un-named catena on Mercury, indicated by red arrows. MDIS mosaic, equirectangular projection. A landslide in the crater at the southern end of the catena may have been triggered by its emplacement.*

### *5.3.1 Method*

I was not able to apply the same method I used for the basin-edge lobate scarps, because by definition the basin-edge scarps are found circumferential to basins, meaning that they can be described in terms of number of degrees around the circumference they cover. Catenae can occur at any location on the surface, and are not circumferential to any point (such as the centre of a basin) so the same method cannot be applied to determine their orientations.

Initially I examined the orientations of the global orientation of catenae from the survey I carried out on the monochrome global mosaic (see Chapter 4). As discussed in Chapter 4, the catenae are outlined as polygons in a shapefile in ArcMap 10.1. To determine the trend of each catena, it was necessary to construct a new shapefile layer and draw polylines for each catena polygon. These polylines run along the centre of each polygon's long axis, equidistant between the two sides. I then took the coordinates of both ends of each polyline, and used trigonometry to determine the compass bearing (trend) between the two. This method does not account for any bends or kinks in the catenae, it assumes they are straight lines. However, it gives a representative idea of the general trends.

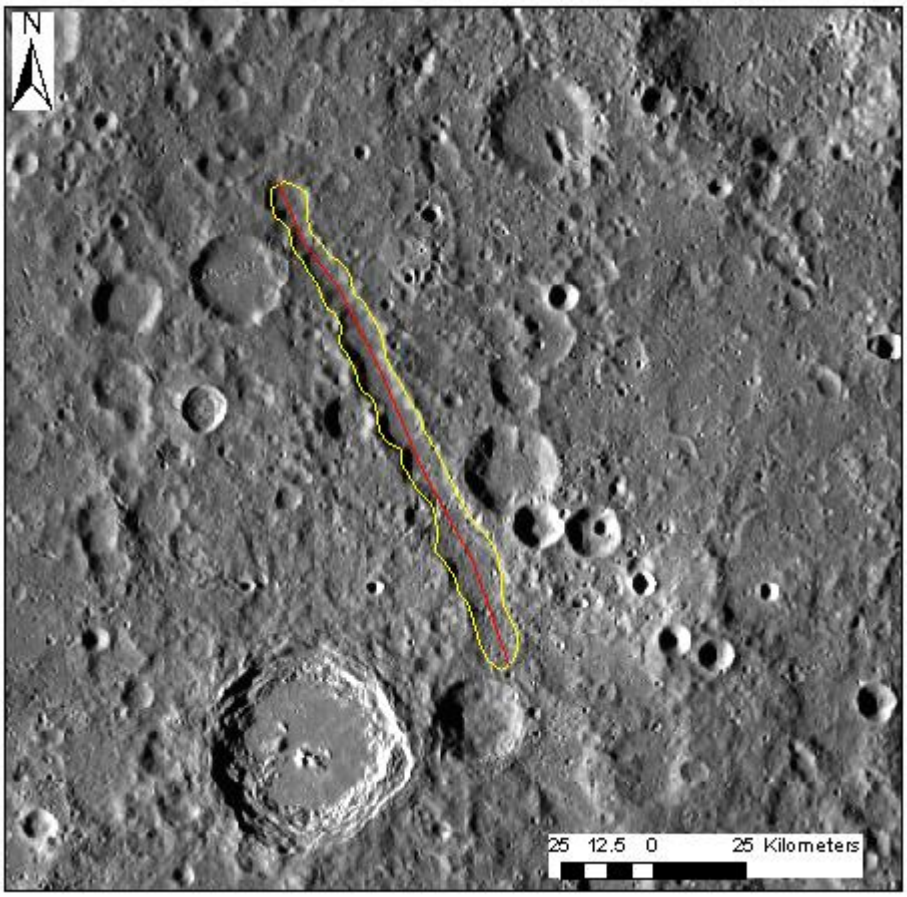


*Figure 5.13: Catenae digitisation: an example of a polygon (in yellow) and the equivalent polyline (in red). I used the coordinates of each end of the red polyline to calculate the straight-line trend of the catena using trigonometry.*

### *5.3.2 Global results*

The results for the global orientations of catenae are shown in Figure 5.14. Note that trends were measured between 0 and 180° rather than 0° and 360° since it would be meaningless to determine which direction to assign to most catenae, when there is no clear primary crater. Therefore, measuring and displaying data as if catenae had a vector value rather than purely a compass bearing value for their trends might be misleading. Figure 5.14 indicates that the global population of catenae (as surveyed in Chapter 4) has an apparent preference in trend for and SSE-NNW; essentially a north-south preference in trends. This is not in agreement with the assumption that the global population of catenae are secondary crater chains, which as stated earlier would result in a random distribution of trends around the compass.

It is therefore necessary to attempt to determine whether this north-south preference in catenae trends is a real observation that might then lend itself to the interpretation of how these features formed (perhaps casting doubt upon whether they are indeed all secondary impact chains), or if the observed preference is simply an artefact of the lighting bias described earlier in this chapter (see Section 5.1). Although the effect of lighting orientation is known to cause problems in the detection of features on Mercury's surface, due to the large size of these features we did not anticipate lighting bias to affect the results to a large degree. However, the apparent orientation of basin-edge scarps - also large features - appear to be affected so it is certainly a possibility with catenae. Unlike basin-edge scarps, which are by definition always located around the rims of impact basins, catenae can occur anywhere on the surface which makes them harder to detect when surveying large areas.

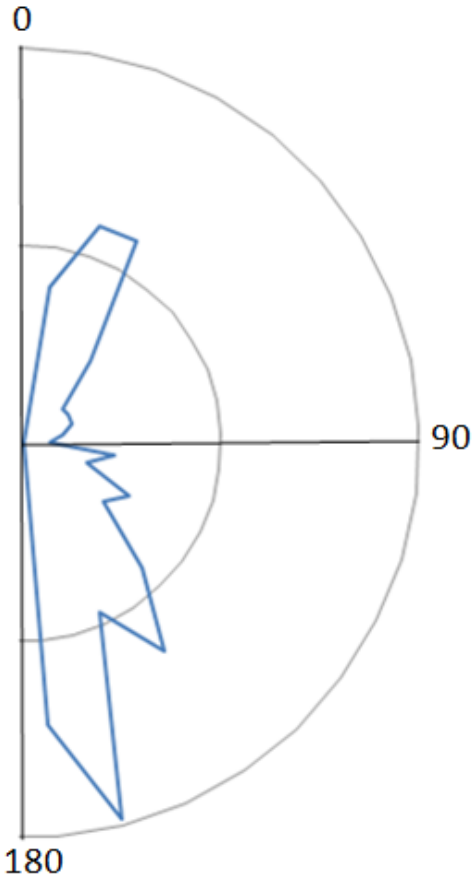


*Figure 5.14: The orientation of catenae on the surface of Mercury, according to my global survey using the MDIS mosaic.*

I therefore resurveyed catenae within a selected area using artificially-generated lighting, using two different illumination azimuths (as described in

detail below). The aim of this investigation was to see if the apparent orientation trend observed in each artificially-lit survey would be the same as each other, and as the global catenae population survey (shown in Figure 5.14), or would vary with different lighting azimuths, and vary from the global survey on the MDIS v9 global mosaic.

### *5.3.3 Artificially illuminated shaded-relief models*

The method I employed for this section of the investigation was the same as that set out in Section 5.2.3. However, there are a far greater number of catenae within the M2 DEM area (shown in Figure 5.15) than there are basins of diameter >100 km with basin-edge scarps. Therefore, in order to keep the duplicate survey time reasonable, instead of surveying across the entire DEM (as I did in Section 5.2.3), I chose to limit the surveys to a rectangular region, superimposed upon the DEM in Figure 5.15. This study area has an area of 9.8 x $10^6$ $km^2$, which is slightly greater than 13% of the total surface area of Mercury.

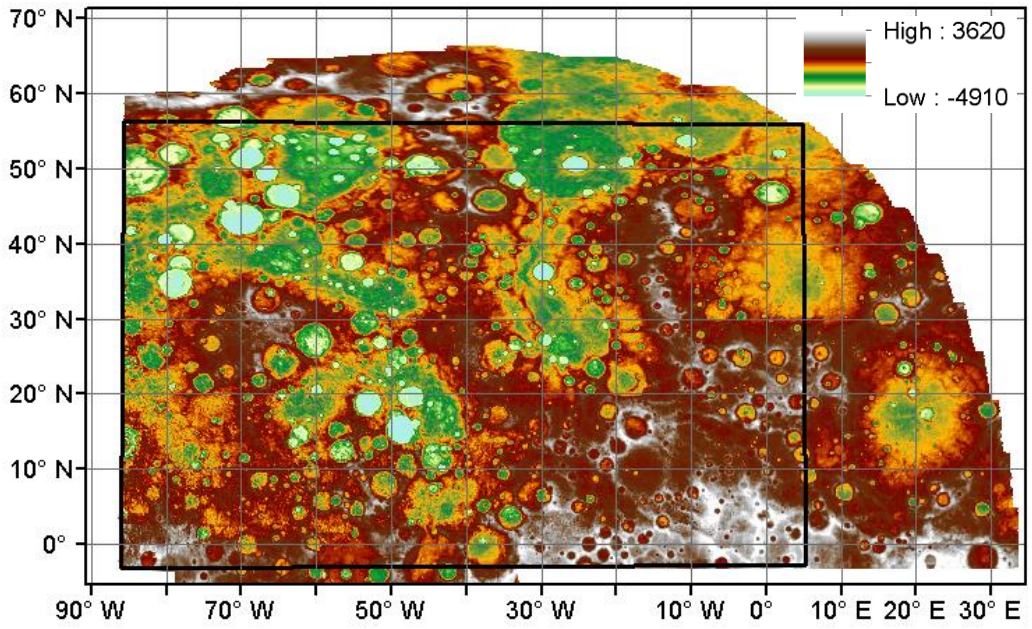


*Figure 5.15: M2 DEM where the pale blue indicates the lowest elevation and the white indicates the highest (as per the Legend at the top right of the Figure). The area surveyed using shaded-relief models is shown in black.*

As set out in section 5.2.3, I created shaded-relief surfaces (hillshade models) for two lighting azimuths from the M2 DEM raster (000° and 090°), using the Hillshade tool in ArcMap.

To best show topographical features, a lower elevation angle of illumination is likely to show the lowest possible elevation features, so I initially tried an illumination elevation of 25° on the shaded relief model. reconstructed from M2 DEM.

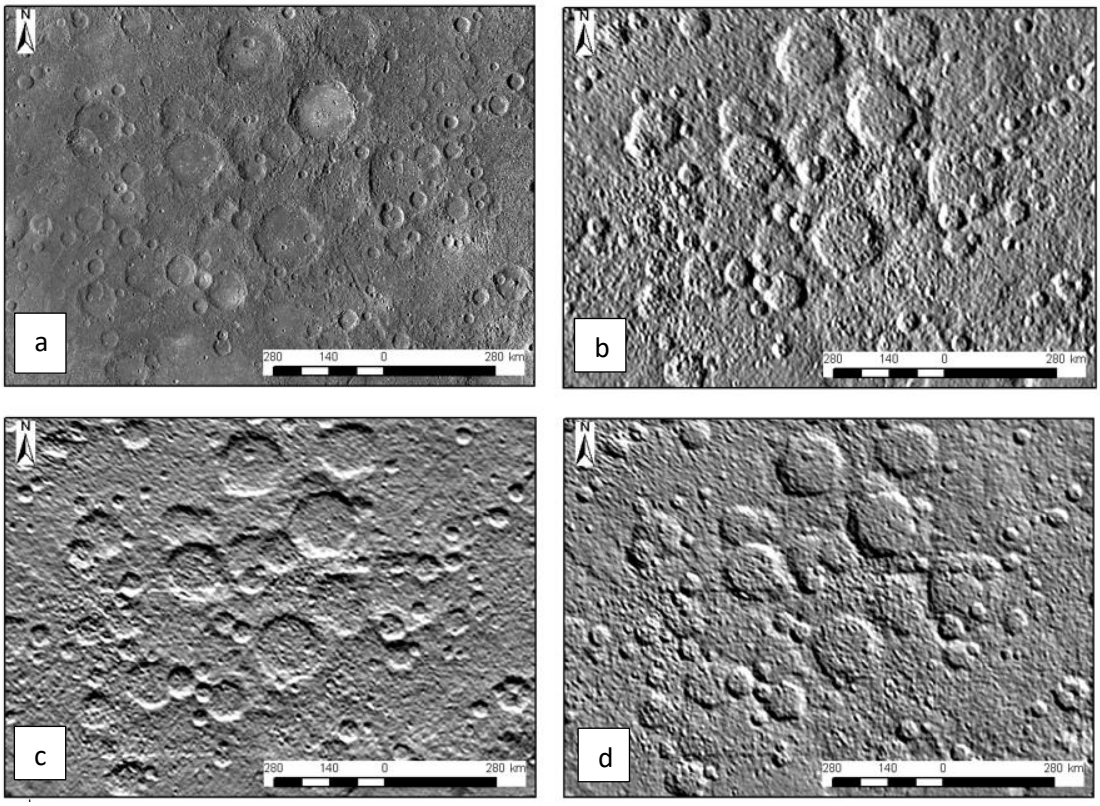


*Figure 5.16: (a) Global mosaic of an example area of the M2 DEM region. (b) a section of the M2 DEM with artificial illumination azimuth of 90°. (c) the same section with an illumination azimuth of 0° (d) the same section with an illumination azimuth of 225°. Scalebar is 200 km, center coordinates: 52°W 10°N.*

Figure 5.16 b-d are the shaded relief models produced from the M2 DEM, using an illumination elevation of 25° and illumination azimuths of 090°, 000° and 225° (respectively). Figure 5.16 a is the same area of the MDIS v9 monochrome global mosaic, for comparison.

The shading in each shaded relief model is correct, however the low angle of artificial illumination has resulted in the highlighting of even minor hollows and rises, making the model very visually ‘noisy’. This results in difficulties when it comes to scanning a model for catenae, as there is the risk of the eye being distracted into missing features that are there and seeing features which are not.

This visual noise can be seen in Figures 5.16 b-d, when compared to Figure 5.16 a that shows the same area of the MDIS v9 monochrome global mosaic. In Fig 5.16a, there are a number of radial catenae south of the fresh-looking basin at the north edge of each figure, which are not clearly visible in the subsequent images. This is likely partly to do with the noise of the shaded-relief models when lit from this elevation, but the lower resolution (1 km/pixel) of the shaded-relief models compared with the global mosaic (250 m/pixel) also no doubt contributes. On the other hand, in Fig 5.17c and d (lit from azimuths 000° and 225°, respectively) there is a long feature running east-west along the middle of the figures that is not at all visible in either the global mosaic or the shaded-relief model lit from 090°.

The catenae that are visible appear different to when observed on the global mosaic, again likely due to the lower resolution when surveying on the hillshade models. For example, scalloping of edges nearly impossible to make out, and the shallower catenae either appear very faintly or not at all (even when the lighting azimuth is favourable for their observation).

Despite this, I conducted a survey for catenae (long, narrow and shallow grooves that might have straight or scalloped edges, and might be straight, curvilinear or bent in planform) on each of the three shaded relief models. In each survey I referred only to the relevant hillshade model (with no reference to the catenae global survey shapefile layers, previous surveys on the other shaded relief models or the MDIS global mosaic).

The smallest scale I used on this (and all subsequent) hillshade model surveys was 1:2,500,000; larger than the minimum scale used on the global survey (see Chapter 4). This is because the resolution of the M2 DEM – and therefore the models produced from it - is not great enough to justify zooming in any further than this.

Due to these surveys being more localised, I drew the catenae polyline layers and exported the results to GNU Image Management Program (GIMP) then used the Measure tool to measure the compass bearing of each catenae by hand. The measure tool measures angles northwards from either due west or due east rather than as compass bearings (which would measure the trends of the lines from 000°), so additional processing was required. I exported each bearing to MS Excel, rounding to the nearest whole number, listing angles measured from due east and those measured from due west separately. I then calculated the actual compass bearing of those measured from due east (090°) by subtracting the measured value from 90°. To obtain the compass bearing of the trends measured from the angles measured from due west (270°), I added 90° on to the measured value.

This method that has the advantage of avoiding the trigonometry involved in the method described in section 5.3.1, which is time consuming, but is only possible due to the limited area being studied in this Section and the lower resolution resulting in fewer catenae being identified to measure. It would not be a practicable method to apply to the global survey due to the sheer number of features that would have to each be measured by hand.

Next I sorted the processed values into 10 degree bins, and plotted on a radial frequency plot for each shaded relief model. It is possible to observe and survey catenae using these hillshade models, but as stated earlier it is not easy to see them. In addition, the ‘noise’ results in false positives as the high contrast can trick the eye into seeing groove where they likely do not exist.

### *5.3.4 Shaded-relief model - 25° illumination elevation*

My results from surveying for catenae on a shaded-relief model with a 25° illumination elevation and lit from 090° and 000° generally indicate a preference in trend ESE-WSW, with the survey on the model lit from the east showing a slightly less strong preference (an additional peak in frequency to the NNE-SSW, in the orientation bin 120-139°). This suggests that the variation in illumination elevation has an effect on catenae survey findings, but it is not sufficiently severe to prevent the correct conclusions from being drawn with respect to preferential orientation. In this case, the results appear to suggest that catenae do have a preferential trend, for ESE-WSW (between 120° and 139°).

The results of the survey on the shaded relief model with an illumination angle of 25° are in fact similar to the results of my survey of the orientations of the global population (see Figure 5.14), with the exception of the secondary frequency peak around the 0-19° bins (observed in the global survey, see Figure 5.14) is only present in the 090° azimuth radial plot, not in the 000° and 225° azimuth plots.

When resurveying the same area multiple times there is a risk of becoming familiar with where the features of interest are located in the area of interest – or remember where they were from the global survey on the MDIS monochrome mosaic, which I carried out prior to this work. In order to attempt to provide a check on this, I hosted a placement student, Kupa Mugwagma (KM) and tasked him with repeating some of my surveys. The idea of this was that if his results were similar to mine, it is likely that I was not seeing what I expected to see, since the student had no expectations. If his observations and results were notably different from my own, then this would call into question how reliable my data are. The student had no previous experience with catenae, ArcGIS/ArcMap 10.1 or any background in remote sensing for planetary science, but was introduced to catenae on Mercury and the software packages at the start of his placement, which lasted 7 working days. His results are shown in Figure 5.19.

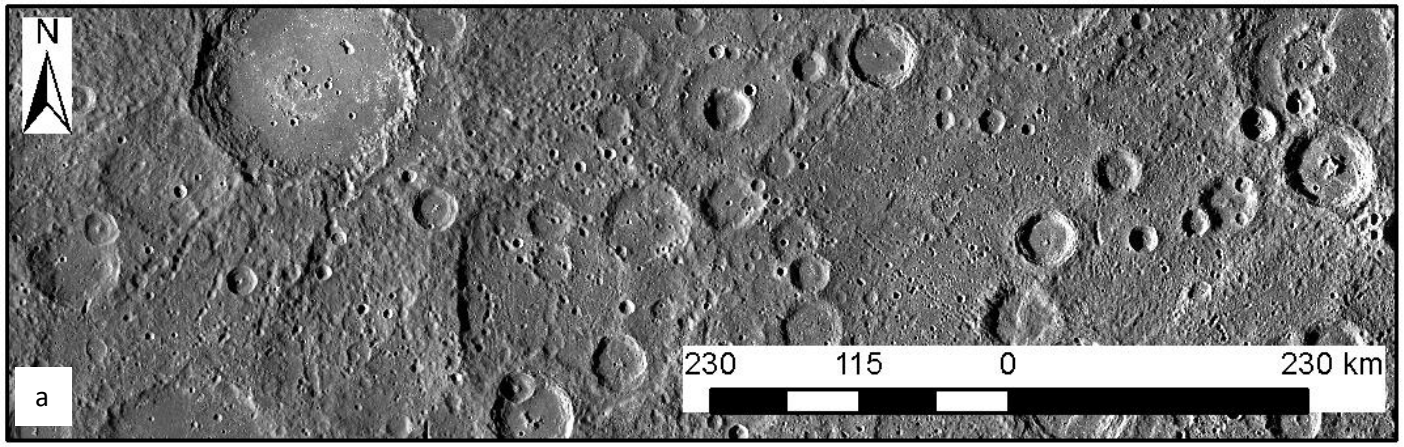
N
230
115
0
230 km
a

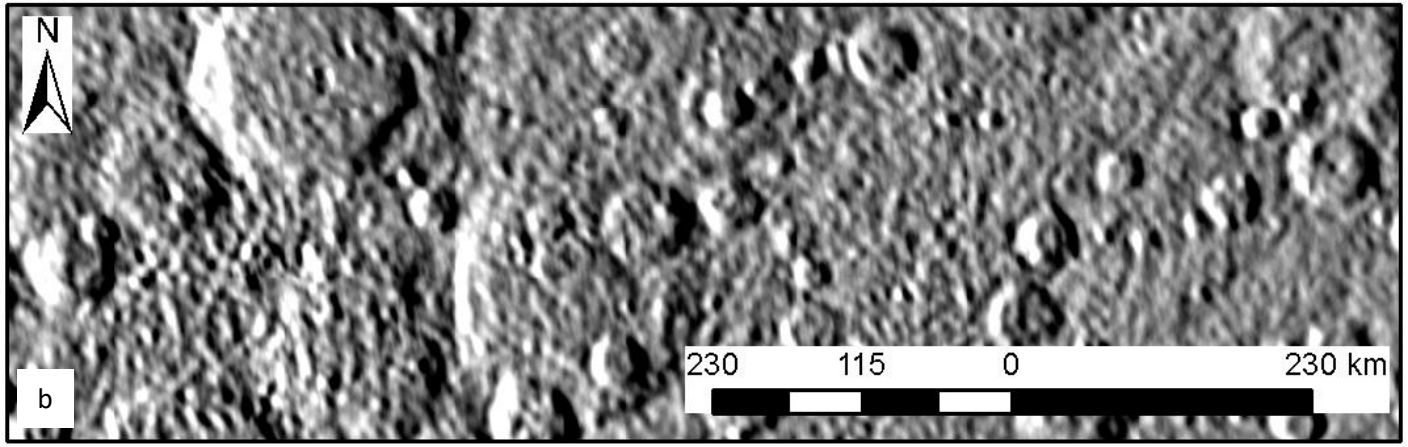
N
230
115
0
230 km
b

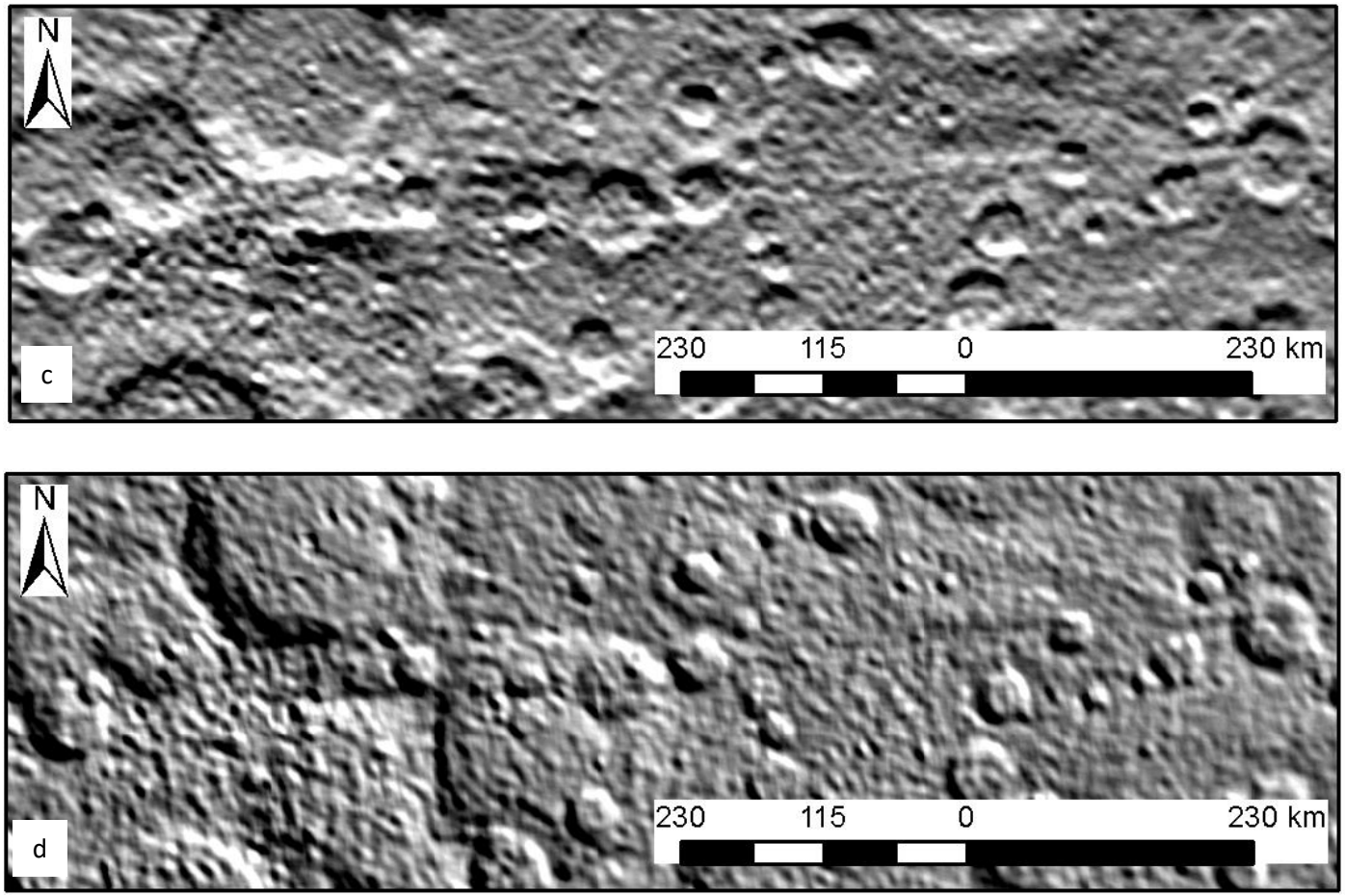


*Figure 5.17: (a) Global mosaic of an example area of the M2 DEM region. (b) a section of the M2 DEM with artificial illumination azimuth of 90°. (c) the same section with an illumination azimuth of 0°. (d) the same section with an illumination azimuth of 225°. Center coordinates: 38W 12N.*

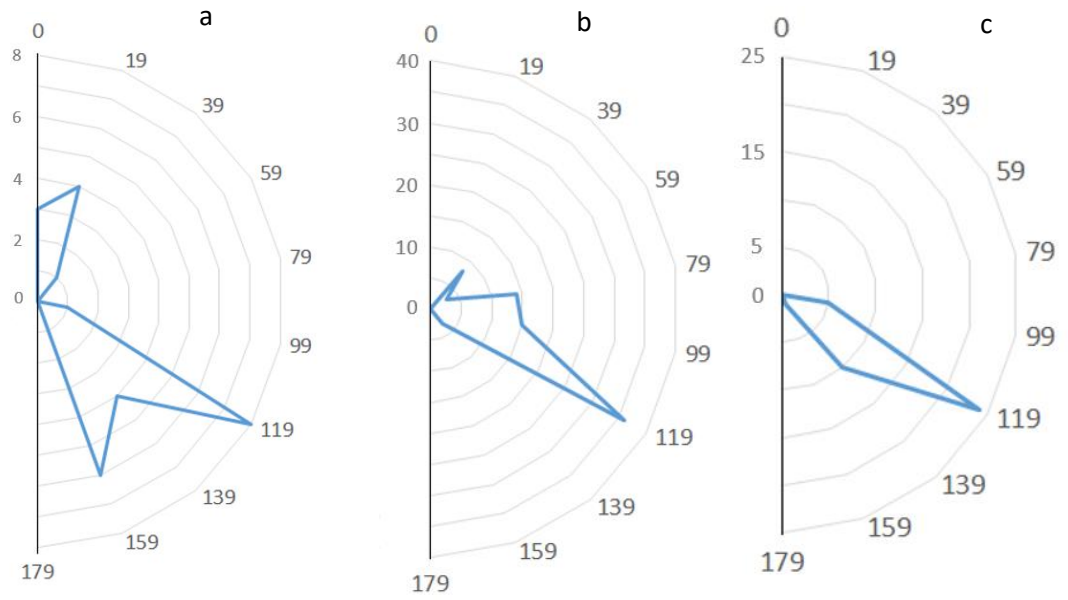


*Figure 5.18: 25° elevation artificial illumination, catenae survey by me. (a) Artificial lighting from 090°. (b) artificial lighting from 000°. (c) artificial lighting from 225°.*

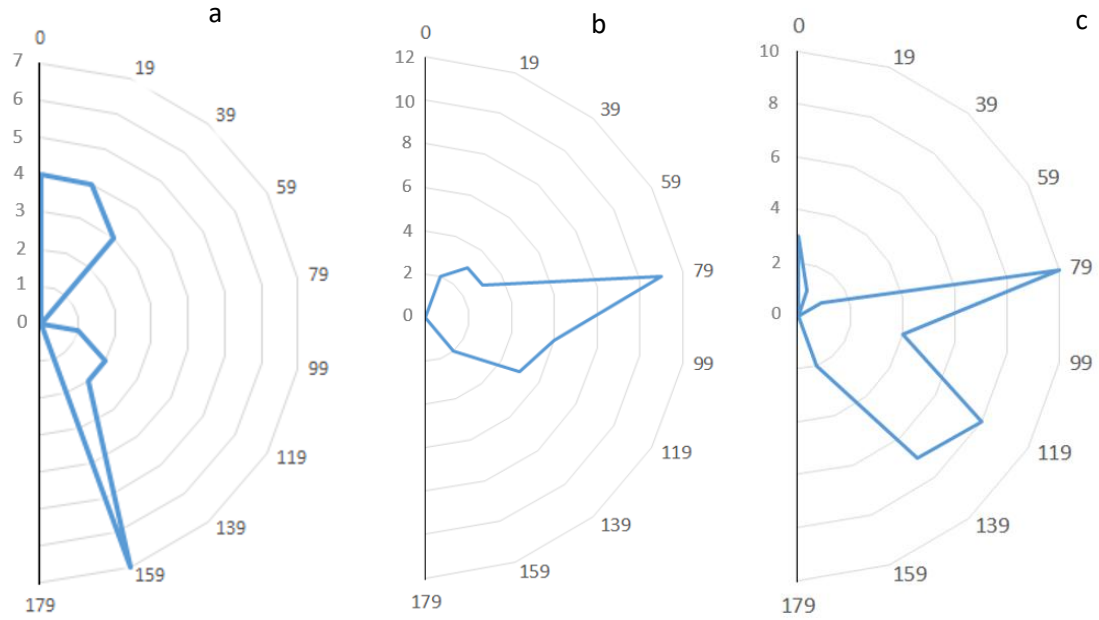


*Figure 5.19: 25° elevation artificial illumination, catenae survey by Kupa Mugwagma. (a) Artificial lighting from 090°. (b) artificial lighting from 000°. (c) artificial lighting from 225°.*

Figure 5.19 a-c indicate KM's survey results on each of the models within the study area shown in Figure 5.15, and Figure 5.18 a-c show my survey results.

KM's findings (Figures 5.19 a-c) are broadly in agreement with my own findings (Figures 5.18 a-c), in as much as the surveys on the shaded relief models lit from the north and the south west indicate a strong preferential orientation approximately east-west compared with the survey on the shaded relief model lit from the east. KM's surveys on the models lit from 000° (Figure 5.19b) and the 225° (Figure 5.19c) indicated a preferential orientation for ENE-WNW. KM's results when he surveyed on the model lit from the east (Figure 5.19a) are different from my equivalent findings (Figure 5.18a); he found catenae on that shaded relief model appeared to have a preferential trend for approximately north-south. He found no peak in the frequency in the 120-139° bin in any of his surveys, while that peak occurred in all three of my surveys.

It is worth noting that in both mine and KM's surveys, the results (in terms of gross trends rather than fine detail) for surveys on the models lit from 000° and 225° are essentially the same. This isn't surprising (and is in fact reassuring), since it would be expected that surveys with illumination azimuths 180° apart (directly opposite) would yield the same results. 000° - 225° is only 45° different from being a 180° separation, which appears not to be sufficient to make a noticeable difference in the overall results.

Figures 5.20a-c show KM's results on each of the three shaded-relief models, indicating the different catenae he observed and recorded within the same area when the model had different illumination azimuths. This figure depicts the reason that altering the illumination azimuth affects the trends in the orientation radial plots. These examples are all good examples of catenae that KM correctly identified. There are other examples among his survey that I do not believe to be actual catenae, which is to be expected given he had only a week to become accustomed to the features and the software package. However, overall I do think that his results support my own, and therefore lend more weight to the theory that changes in illumination azimuth do indeed result in differing orientation trends.

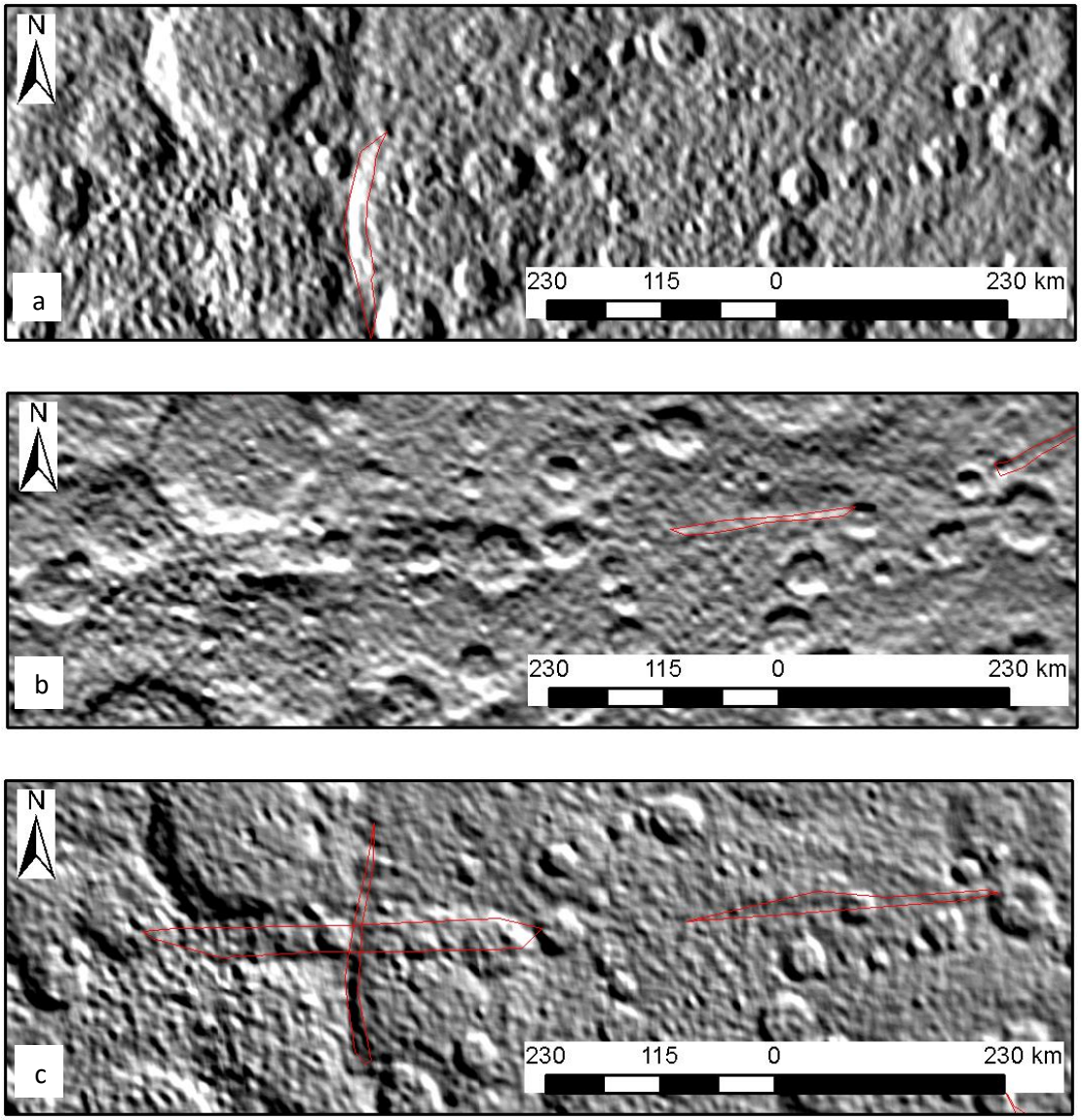


*Figure 5.20: A section of KM's survey on the three hillshades with different illumination azimuths. (a) Illumination azimuth of 90°. (b) Illumination azimuth of 0°. (c) Illumination azimuth of 225°.*

### *5.3.5 Shaded-relief model – higher elevation of illumination*

While low elevation illumination is better for surveying topographic features in theory, the high degree of noise in the shaded-relief models (for example Figure 5.20a) makes visual scanning problematic. Therefore, I repeated the survey on the study area two further times, using illumination elevations 35° (medium elevation set) and 45° (high elevation set). Because it was apparent from the results in section 5.3.3 that the results from 000° and 225° illumination azimuths do not produce materially different survey results for the purposes of this

investigation, I surveyed on just 2 different illumination azimuths for each of these sets; 000° and 090°.

The shaded-relief models using higher illumination elevations produces results with less extreme variation in relief, meaning it is less disturbing to the eye and easier to scan for catenae. However, there was the possibility that a significant proportion of catenae would no longer appear in the medium and high elevation illumination surveys, since they are relatively shallow features and higher angle lighting would result in less obvious differences in shading.

The results of my surveys on the hillshades with medium elevation illumination are shown in Figures 5.21 a and b, while those from the hillshades with high elevation illumination are shown in Figure 5.22 a and b. In all 4 figures there is a primary peak in frequency between 100° and 159° and a secondary, considerably smaller, peak in frequency between 000° and 039°.

The only notable difference between the 000° and 090° illumination azimuth radial plots (for both illumination elevations) is that the secondary frequency peaks are smaller in the results from the hillshade models lit from 000°. This not is a surprising result because, as mentioned above, I expected that features perpendicular to the illumination direction would show up best, and the secondary peaks are approaching parallel to the illumination azimuth in the 000° radial plots.

The only notable difference between the medium and high illumination elevation models is that the secondary peak in the 045° set is much larger in the plot of the results on the model with the 090° illumination azimuth.

While I had considered the risk that a higher elevation of illumination on the shaded-relief models would result in fewer catenae being apparent compared to the low elevation models, the opposite appears to have been the case. I recorded a considerably higher total population in the medium and high illumination angle models than in the 25° illumination angle model. This is probably due to the visual noise in the latter models making it difficult to see any but the deepest and/or largest features, while the higher elevation models are less visually disturbing so the smaller and more subtle features are easier to detect.

The medium and high elevation model survey results agree well with the global population trends in orientation, and the low elevation model results when the illumination azimuth is 090° also agree with the global population results (though the low elevation survey with illumination azimuths 000° and 225° agree less well, with the same primary frequency peak but lacking a notable secondary frequency peak).

A question arises from the fact that the results for 090° and 000° azimuth surveys (for both higher elevation shaded-relief models) are relatively similar, as described above. Are the surveys picking up the same catenae, or different ones that have (as a population) the same orientation trends?

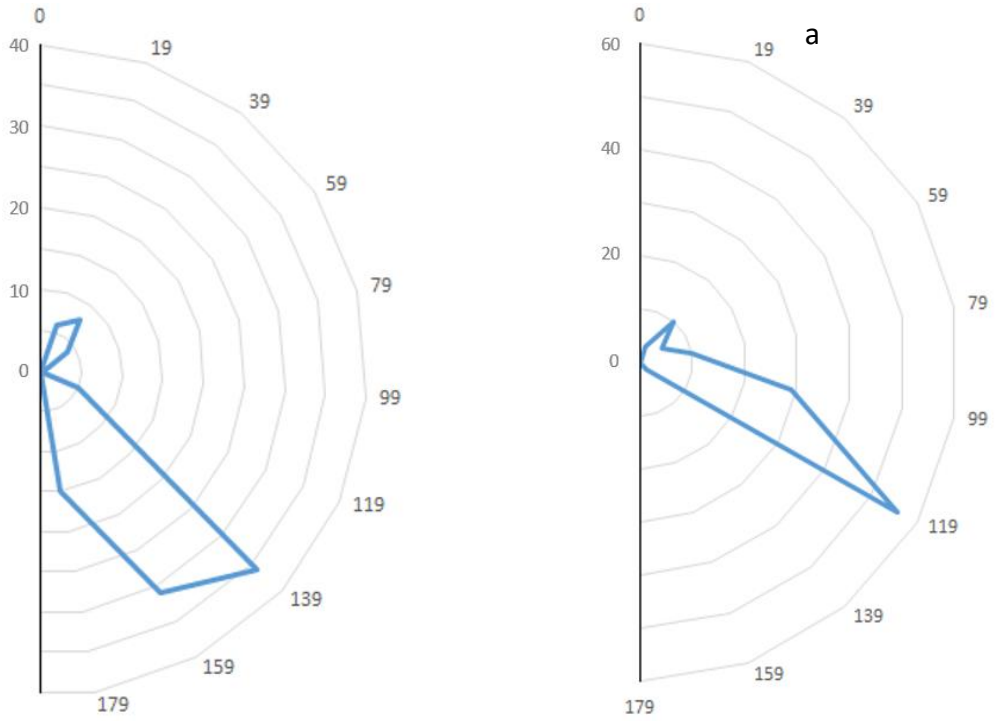


*Figure 5.21: Medium (35°) elevation artificial illumination.(a) Artificial lighting from 090°. (b) artificial lighting from 000°.*

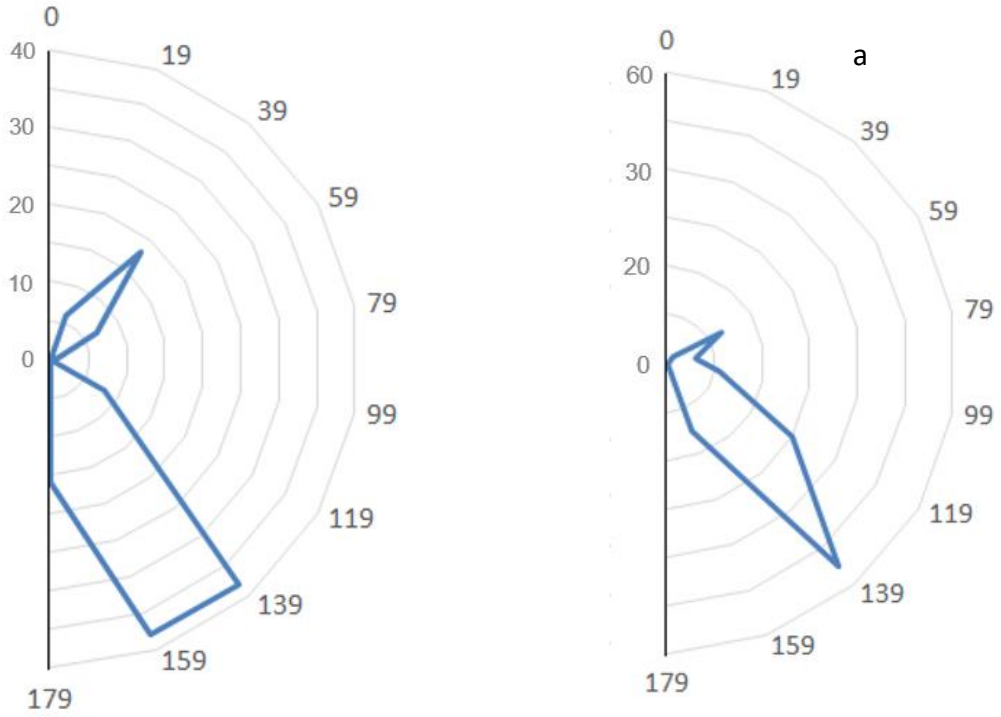


*Figure 5.22: High (45°) elevation artificial illumination. (a) Artificial lighting from 090°. (b) artificial lighting from 000°.*

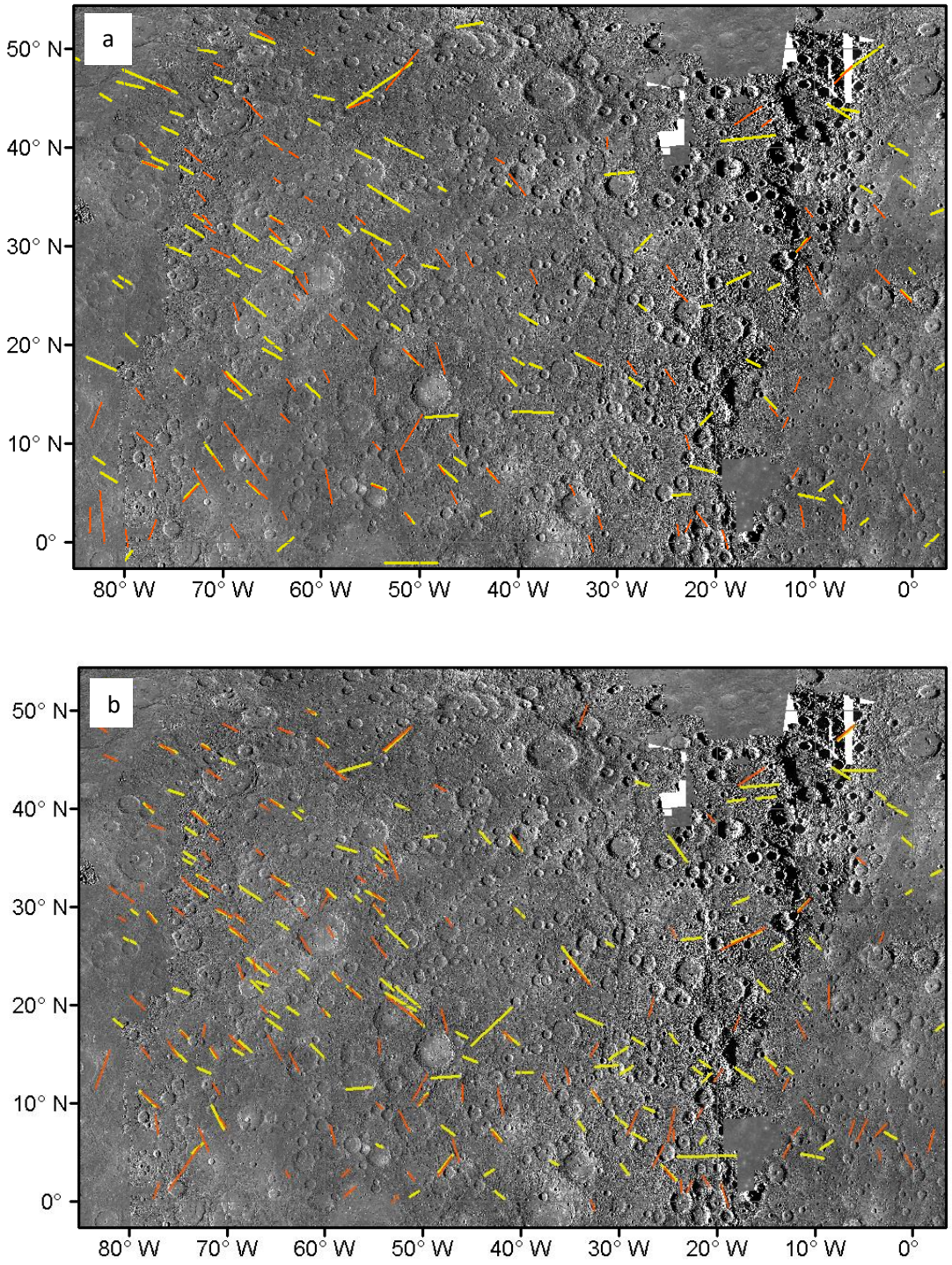


*Figure 5.23: Yellow lines are the survey results for azimuth 000°, orange lines are the survey results for azimuth 090°. (a) 35° illumination elevation. (b) 45° illumination elevation.*

Figures 5.23 a and b show the trends of catenae when surveyed on hillshade models illuminated from 000° (yellow lines) and 090° (orange lines), with medium illumination angle (Figure 5.23 a) and high illumination angle (Figure 5.23 b). In Figures 5.23 a and b the orange and yellow lines coincide in some, but not the majority of cases. This indicates that the 000° and 090° azimuth

surveys mostly did not pick up the same features. When using hillshades for surveying catenae it therefore might be prudent to do multiple surveys with different illumination azimuths and combine the results from each.

Regarding catenae, I cannot at this point explain what might cause chains of secondary impact craters (as I concluded in Chapter 4 that catenae most likely are) to exhibit actual preferential orientations on a global scale. While individual impacts might have ejecta material distributed preferentially in certain directions, when taken across the entire surface of the planet ejecta debris ought to be oriented equally in all directions. However, impact physics is outside of the scope of this project, and I will have to leave that topic to future workers. It is also possible that catenae are too shallow to be easily distinguished in DEM-derived hillshade models, particularly those made from DEMs that might themselves be affected by the illumination bias having been produced from stereoimages.

### *5.3.6 Conclusions (catenae)*

From this work investigating the effect of illumination azimuth and elevation I can draw the following conclusions:

- The global population of catenae appear to have an orientation preference for NNE and SSE.
- Low elevation illumination (in this case 25°) produces shaded-relief models with a high level of 'visual noise' unsuited to visual surveying for catenae, since it appears to result in a high proportion of shallow and small catenae not being observed and recorded.
- The medium (35°) and high (45°) illumination elevation shaded-relief models are suitable for surveying for catenae, and do not obscure small and shallow features as much as I had originally assumed.
- The medium and high elevation model survey results agree well with the global population trends in orientation, suggesting that the preference of catenae in the global survey in Chapter 4 for NNE and SSE is in fact a true observation and not an artefact of the illumination bias on Mercury. I cannot

explain this, as if catenae are formed by secondary impacts it would be expected to find a global lack of preferred orientation.

- My low elevation illumination results were confirmed by an independent survey, with the caveat that a lot of his observations were artefacts rather than catenae. In future, the low elevation hillshades would be better left to more experienced surveyors purely because the amount of visual noise.
- When surveying for catenae, including multiple surveys on hillshade models, with different illumination azimuths, would be helpful since features were apparent on the hillshades that were not visible on the global mosaic (for example in Figure 5.17 c and d), and surveys using different illumination azimuths revealed different populations of features. I suggest that surveying on the global mosaic, and hillshades with illumination azimuths 0° and 90° and combining results would be the minimum required to ensure a high proportion of the total population were represented in the results.
- With the previous point in mind, it is not realistic to assume that the global survey detailed in Chapter 4 is in fact the entire population of catenae on Mercury, since it was carried out only on the global image mosaic without using elevation data.

## 5.4 Limitations of the method

There are certain limitations inherent in the methods used in this Chapter, which apply to both the method applied to the basin-edge scarp orientation and the catenae orientation studies.

- Due to working on the M2 DEM, my work on the shaded-relief models is limited to the extent of this DEM. In the case of catenae this is sufficient, but a larger area would have been beneficial for the basin-edge scarps investigation. Note that since doing the work set out in this Chapter, I made hillshade models using the global DEM. In future the global DEM potentially allows similar investigations to be carried out across the entire surface of Mercury. However, the quality of shaded-relief models produced from the global DEM have a “blocky” appearance, less suited for surveying than those produced from the M2 DEM for this work.

- All of the work here, and the original global surveys were done by visual scanning of the MDIS mosaic, or shaded-relief models. This introduces the possibility of missing some features, or seeing features that are not in fact present. To attempt to quantify this problem, I had a placement student repeat my methods (section 5.3.4), in order to compare the difference between our results. However, he was previously unfamiliar with planetary geology in general and the features I am investigating in particular, as well as ArcGIS software, and he had 7 days to learn the methods and carry out the work. Therefore, the value of his additions (through no fault of his own) are questionable.
- My method of investigating the effect of varying the illumination azimuth (and illumination angle) involved resurveying the same area multiple times. This means that there is the possibility of my having remembered where I saw features before and then recording on other hillshade models. This was another reason for attempting to have another worker duplicate my methods.

## 5.5 Discussion - Implications for the literature

As stated in Chapter 2, the matter of preferential orientation of thrust faults has been covered in the literature a number of times as a result of its importance in the matter of the interaction between global contraction and tidal despinning. While in the early Mercury literature predictions were made as to the observable indicators of despinning on the tectonic features (for example Melosh (1977) predicted the relaxation of the equatorial bulge as Mercury's rotation rate decreased would produce an equatorial province of lobate scarps with north-south trends, a province of strike-slip faults at mid-latitudes and a polar province of east-west trending thrust faults). However, as yet no worker has conclusively demonstrated the impact of tidal despinning on the surface of Mercury.

Cordell and Strom (1977) were the first to publish the observation that the majority of lobate scarps were oriented within ±45° of due north, and to attribute this to the illumination bias. Dzurisin (1976), Dzurisin (1978) and Melosh and McKinnon (1988) all identified a possible preference for north-south oriented tectonic features, after examining the Mariner 10 images. They attributed this

preference to faults exploiting pre-existing lines of weakness within the Hermean crust, created due to the stresses due to tidal despinning.

More recently, Watters *et al.* (2004) noted a lower population of lobate scarps in areas of Mercury's surface where the solar incidence angle is <50° (the subsolar point would have an incidence angle of 90° while at the terminator it would be 0°) when they surveyed on Mariner 10 images.

Byrne *et al.* (2014) carried out a global survey of shortening features (including both lobate scarps and smaller features named wrinkle ridges). Byrne *et al.* (2015) observed variations in frequency of occurrence in lobate scarps with longitude, with concentrations at 0°, 90°, 180°, 270°E but they attribute these to the longitudinal bands of high incidence angle on the MDIS mosaic they used.

Figure 5.24 shows the results of Byrne *et al.* (2014) orientation results, by 30° latitude bins. My orientation findings of basin-edge lobate scarps agree with the findings of Byrne *et al.* (2014), and similarly to my conclusions Byrne *et al.* (2014) stated that the north-south preference of orientations at low and mid-latitudes coincides with the results that one would expect given the east or west illumination azimuths. As a result of this, they drew no conclusions from the apparent preferential orientations.

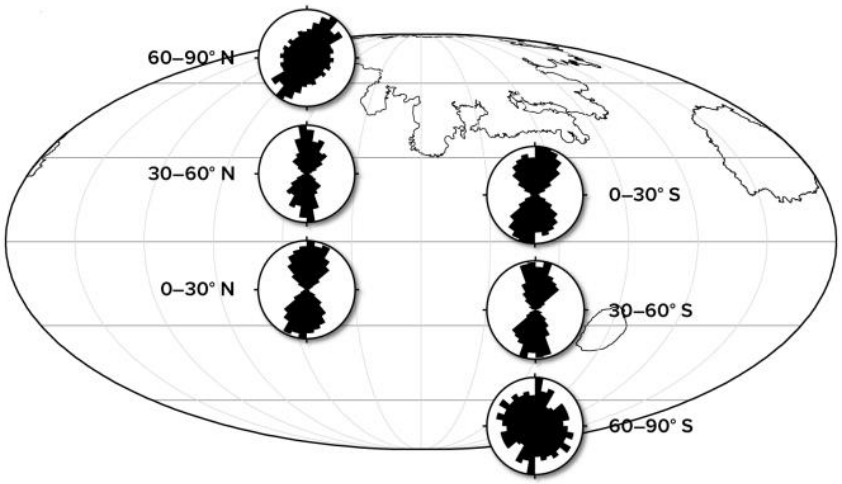


*Figure 5.24: Byrne et al. (2014) lobate scarp orientation results.*

As previously discussed in Chapter 2, Klimczak *et al.* (2015) carried out a more modern approach to modelling the results of global contraction and despinning,

using rock strength and deformation properties appropriate for Mercury. They reason that despinning either happened very early, before contraction began (but imposed a fabric on the lithosphere that is still a factor in determining the orientation of later features), or there was an overlap between the two processes. In the former, the models of Klimczak *et al.* (2015) predict a global system of jointing in the former case, and in the case of the latter a global population of thrust faults oriented north-south at the poles but of more random orientations at increasing latitudes. They also mention the issue of limited variation in illumination azimuth and that areas of low incidence angle (<75° measured from zenith) present on the MDIS mosaic they used mean that east-west oriented lobate scarps are missing from the global survey they used (that of Byrne *et al.* (2014)).

Klimczak *et al.* (2015) conclude that the observations strongly support the case where despinning and global contraction coincided, despite the certain impact of the illumination bias. However, the illumination bias would in fact accentuate the features that they use to draw their conclusions, which is why in Chapter 2 my coauthors and I did not draw any conclusions from the apparent preference on orientation, particularly between 60°N and 60°S.

Watters *et al.* (2015), using MESSENGER MDIS images as a base map confirmed the findings of Watters *et al.* (2004), in as much as there are longitudinal bands of low-frequency occurrence of lobate scarps, which they are of the opinion are actual observations but Byrne et al. (2014) attributed to observational bias. They also noted the same preference in orientations that I observed and discussed above, which they noted could be due to observational bias. However, they state that they used images with large incidence angles, and furthermore they also surveyed on DEMs (generated from Mercury Laser Altimeter data and stereo images) merged with the MDIS images. They state that they identified a number of east-west oriented lobate scarps, and from that assume that their survey is equally representative of features oriented in all directions. My co-authors and I (from our work in Chapter 2) disagree with this.

## 5.6 Conclusions

Conclusions specific to basin-edge scarps and catenae are presented in sections 5.2.4 and 5.3.6 (respectively). More generally speaking, my results indicate that the detection of linear/curvilinear features does appear to be affected by illumination bias, and that when doing surveys with the particular intention to identify and trends in orientation – and then draw scientific conclusions based upon any trends identified – it would be advisable to survey on shaded-relief models with at least two illumination azimuths in addition to the MDIS images or mosaics. In addition, the two illumination azimuths should be perpendicular, since the results when two illumination azimuths were (effectively) 45° were very similar so the same features would be missed in both cases.

# 6 Study area mapping

## 6.1 Study area and context

The features discussed in previous chapters (basin-edge scarps, Chapters 2 and 3, and catenae, Chapter 4) are of interest in their own rights, and separate areas of study. However, both types of feature also have the additional interest of being useful for stratigraphic mapping and for interpreting the finer details of the history of local areas of the surface of Mercury. This chapter aims to investigate and demonstrate these uses.

Basin-edge scarps form at the edges of smooth plains, meaning that the smooth plains volcanic unit will have had to be emplaced prior to the compression that led to the creation of the basin-edge scarp. Catenae are, in most cases, likely secondary crater chains and therefore can be tied in location and timing to the formation of their primary basin. They extend beyond the continuous ejecta blanket (in some cases considerably beyond the ejecta blanket) and can therefore be of help in determining the relative timing of emplacement of neighbouring impact features and ejecta blankets.

In order to demonstrate the potential of these features to assist in the identification of stratigraphic relationships, I selected an area to map (Figure 6.1) that includes examples of both basin-edge scarps and catenae. The mapping area, outlined in red in Figure 6.1, is in the low southern latitudes. It spans parts of 4 quadrangles: H-6 Kuiper, H-10 Derain, H-11 Discovery and H-14 Debussy (Figure 6.2). This spread of the area over several quadrangles is not problematic, since the aim of this mapping work is not to map a quadrangle, but to create a more detailed stratigraphic map of a smaller area. Moreover, this approach is less likely to miss pertinent stratigraphic relationships (particularly regarding the relationship between basins Aneirin and Sanai, since they fall into separate quadrangles) than a study confined to any of the quadrangles in isolation.

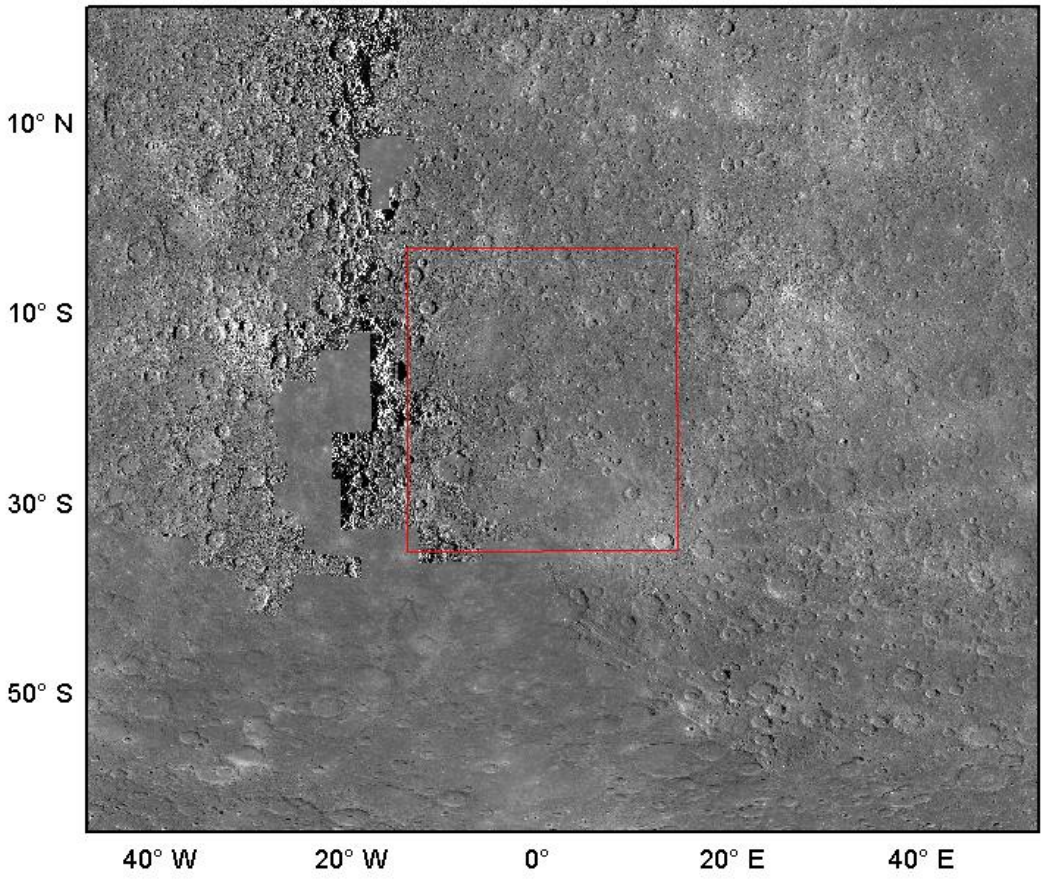


*Figure 6.1: Mapping area (shown outlined in red) and context. MDIS monochrome mosaic v9, Mercator projection.*

The study area is slightly south of the equator (spanning 3° to 35° South) and covers 14° west to 14° east. It is located to the south of the Northern Volcanic Plains, but includes two basins with smooth plains volcanic infill. Both of the basins have been previously mentioned in this thesis – Aneirin and Sanai – since they both have basin-edge scarps. I chose this area in order to focus on impact basins Aneirin, Dario and Sanai, their immediate and associated features, and their local context. The mapping area covers 1,644,061 $km^2$, which is approximately $1/10^{th}$ the size of a standard quadrangle.

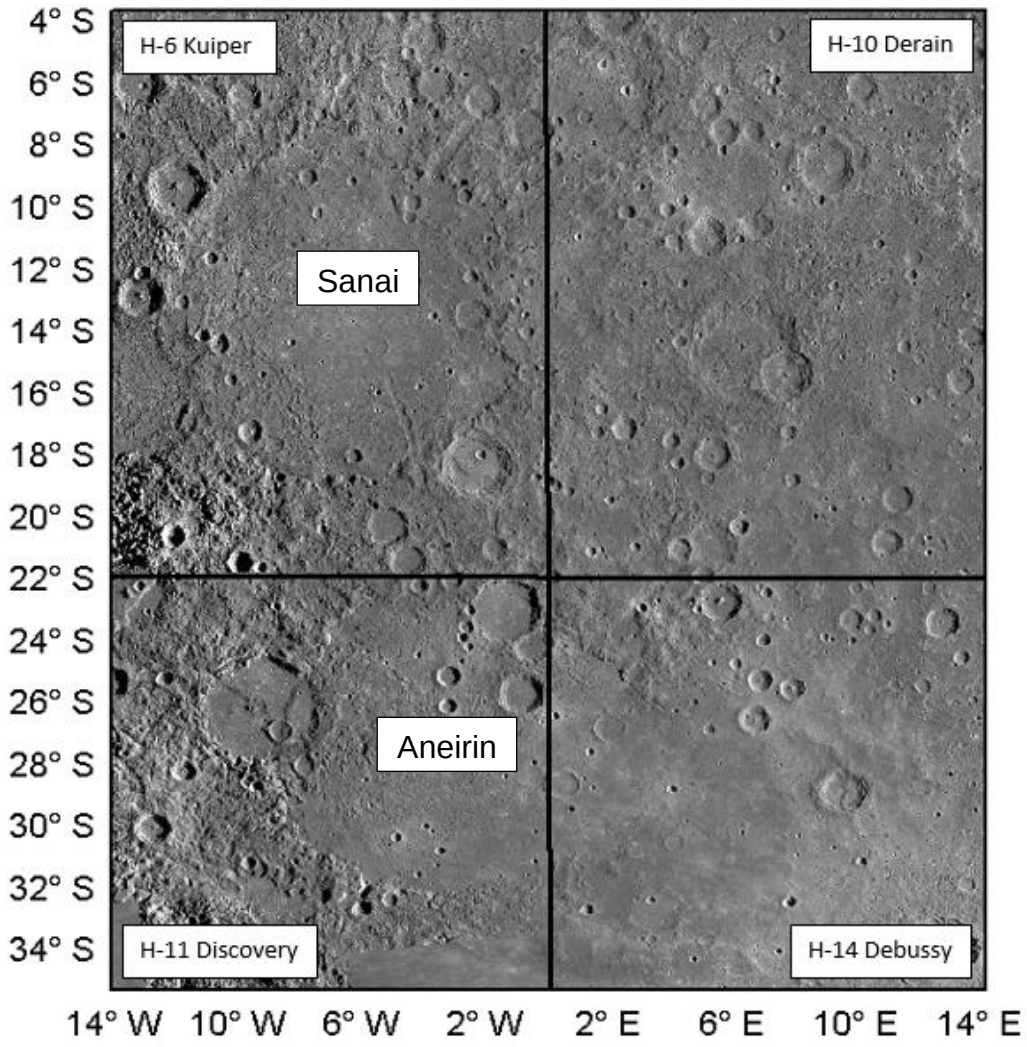


*Figure 6.2: The mapping area, MDIS monochrome mosaic v9 (Mercator projection) and the boundaries between four quadrangles the area spans. Basins Sanai and Aneirin are labelled.*

## 6.2 Methods

### *6.2.1 Mapping approach*

With certain exceptions (discussed below), and with amendments to suit my aims and timescale, I followed the mapping approach set out in Galluzzi *et al.* (2017). The basemap I used to map structures and units was the MDIS v9 monochrome mosaic (with a resolution of 250m per pixel). Additionally, I made use of the Global DEM to assist the identification of structures, features and contacts of sufficient size and relief to be visible (source: www7), since it became available prior to my beginning work on this chapter (although it was not available during my work on any previous chapters).

I also used the enhanced colour mosaic (source*:* www8) to assist in identifying the differences between units, when the monochrome imagery and topography wasn't conclusive, in the same way Galluzzi *et al*. (2017) used the eight colour and three colour multispectral reduced data record global mosaics. However, I did not use the enhanced colour mosaic to map units based specifically on geochemistry or composition (as indicated by colours on the multispectral mosaics), since that is outside the scope of this work.

I also follow the example of Galluzzi *et al.* (2017) by classifying craters and crater material (ejecta blankets and central peaks etc) based upon their state of degradation – as identified by morphology - and chose to apply the same crater classification method: the three-category method, which recognises three classes of degradation. This is as opposed to the five-category classification, which is also currently in use for Mercury (e.g. (Kinczyk *et al.*, 2016)). The three-category classification is as follows: C1 (the oldest and most degraded category); C2 (intermediate stage of degradation); C3 (most recent fresh, crisp craters).

The three-category method is more straightforward and quicker to use, which suits my purposes for this work, and I agree with Galluzzi *et al.* (2017) that the five-category method has the potential to confuse. The reason for this is that, because smaller impact craters degrade faster than larger impact craters, impact craters that appear more degraded in their morphology can overlay (larger) craters that appear fresher. In the five-category classification this can lead to the paradoxical result of a crater classified as older overlying a crater classified as younger. The three-category method decreases the likelihood of this occurring, on account of the larger span (in terms of age and state of degradation) of the categories.

Unlike Galluzzi *et al*. (2017) – and other workers creating geological maps of quadrangles - I have chosen not to include wrinkle ridges or lobate scarps (with the exception of basin-edge lobate scarps) because these have been globally mapped to the same scale by (Byrne *et al.*, 2014). I also have opted to use the same colour to depict smooth plains areas within and exterior to basins. In the cases where the smooth units within impact basins are almost certainly volcanic in origin, they are not necessarily part of a single contiguous unit that includes

smooth plains units exterior to impact basins. However, in the case of Aneirin within my mapping area, it  is not possible to distinguish between the volcanic unit that filled the basin and other smooth plains exterior to the basin. On the basis of this, I opted to use the same colour to depict all smooth plains units, whether interior or exterior to impact basins.

In order to address the potential for bias when mapping, Galluzzi *et al.* (2017) made use of mosaics with different lighting azimuths. As per my own recommendations in Chapter 5, I created shaded relief models from the global DEM, using two different illumination azimuths (separated by greater than 45°): I chose to use azimuths 180° and 270°, both with an illumination elevation of 35°. I used the two shaded relief models to resurvey my mapping area, particularly with respect to catenae and basin-edge scarps.

### *6.2.2 ArcGIS methodology*

After importing the base maps (listed in section 6.2.1), and choosing and outlining my mapping area, my next step was to choose an appropriate map projection. Because of the location of the area, close to the equator, I opted to use a Mercator projection with the central meridian of 0° (since the mapping area spans 14° on either side of the equator), and a Standard Parallel of -22° (mid-way between the north-most and south-most extent of the mapping area). The Mercator projection has the advantage of preserving distances, angles and small areas (within an area as small as this mapping area). Larger areas are less well preserved, but since the main aim of this mapping exercise is stratigraphic, the direct comparison of the size of areas within the mapping region is not a necessity.

Having chosen the Mercator projection, I used the Project Raster tool within the ArcMap 10.1 Toolbox to reproject all of my basemaps, and all new layers used in this work were also created with the same projection.

According to the literature, the surface of Mercury is composed of successive flood basalt plains that – depending upon their age – have been subjected to varying degrees of degradation and cratering (Denevi *et al.,* 2009; Marchi *et al.,* 2013). There is literature to the effect that the threshold between Intercrater Plains and Intermediate Plains is less than clear-cut (for example, Denevi *et al.*

(2013) and Whitten *et al.* (2014)). However, this is beyond the scope of this investigation, and I have chosen to follow Galluzzi *et al.* (2017) in this respect. Since I observed examples of smooth plains, very heavily cratered regions and areas that fall in between these two end members, I have delineated three geological units within the mapping area (see Figure 6.3). These units, and their definitions (as per the relevant literature), are as Section 1.4:

- Intercrater Plains: “level to gently rolling ground between and around large craters and basins” (Trask and Guest (1975)).

- Intermediate Plains: “planar to undulating surfaces that have higher crater density than smooth plains material, but are less heavily cratered than intercrater plains material” (Spudis & Prosser, 1984).

- Smooth Plains: “relatively flat, sparsely cratered material” (Spudis and Guest, 1988; Strom, Trask and Guest, 1975; Trask and Guest, 1975) “that displays sharp boundaries with adjacent regions and is level to gently sloped over a baseline of ~100–200 km” (Denevi *et al.,* 2013).

The order of the list above reflects the chronology of the formation of these provinces, with the oldest type at the top (the Intercrater Plains) and the youngest at the bottom (Smooth Plains).

I identified and outlined the impact craters and basins by the highest points of their rims, and this also applies to catenae (in order to be classed as a catena a chain of craters needs to have a minimum of 3 constituent craters).

Due to my work in previous chapters, I had already created global surveys of basin-edge scarps (Chapter 2) and catenae (Chapter 4), and had the shapefile layer of basins with diameter >100 km (based upon the database of Fassett *et al.* (2012). I cropped all of these (using the Clip to Extent Tool) to the mapping area and reprojected them. These then provided a starting point for my mapping. To create the map itself, however, I opted for a geodatabase (within which were “feature classes” containing my mapping data), rather than using multiple shapefile layers. I used two line-type feature classes, one to delineate geological contacts (certain and uncertain) and one to indicate linear features that are not contacts, as follows: basin-edge scarps; catenae; crater rims (for

craters of diameter >15 km); “ghost” catenae; “ghost” craters; crater rims (for craters of diameter 8 – 14.9 km).

I began mapping the linear features first, starting with outlining the rims of impact basins. The basin database shapefile I imported initially indicated each impact basin using a circle. For mapping purposes, the exact outline of the basin and crater rims need to be delineated, but the shapefile allowed me to use the ‘zoom to’ function to move quickly from basin to basin when drawing, which made the process faster. In addition to the basins in the imported database, I delineated smaller impact features within the mapping area, to a minimum diameter of 8 km. This minimum size threshold was based upon the size below which the features become likely to be secondary impact craters (Strom *et al.,* 2008).

I distinguished between “small” and “large” craters (with the diameter threshold between the two categories being 15 km) because I decided to map the ejecta blankets – where identifiable – of the larger category only. Galluzzi *et al.* (2017) mapped ejecta blankets for impact craters of diameter 20 km and greater. However, since I had a smaller area to map, and am mapping at a greater resolution (Galluzzi *et al.* (2017) produced a map with a scale 1:3,000,000 while my map is 1:1,500,000) I opted to identify ejecta blankets for craters with the smaller minimum diameter 15 km and above – where I was able to identify them.

My global survey of catenae required me to refine their boundaries so it was necessary for me to re-draw all of the catenae within the mapping area (using the survey as a template). While mapping at the smaller scale of 1:500,000 compared to my global survey (which for catenae was at a minimum of 1:800,000) I identified additional basins and catenae that were excluded previously due to the global scale of the original survey.

When mapping, all linear features, and the rims of features such as craters/basins and catenae were all outlined as line-class features. Having outlined the impact craters and basins, catenae, “ghost” craters and “ghost” catenae (features that are still visible but have been partially obscured by later smooth plains/volcanic deposits) and basin-edge lobate scarps, the next step was to map the stratigraphic contacts within the mapping area. When mapping

contacts, it was important that – while also mapped as line-class features – these features formed closed shapes. If the lines did not join up, to form a closed shape, the next step would not be successful.

Having outlined both linear features and contacts within the two feature classes in the geodatabase, I converted the lines within the contacts feature class into polygons, using the Feature to Polygon tool. I saved the resulting polygon shapefile within the geodatabase.

Within the same geodatabase I created an attribute domain which contains all of the units within the mapping area. I imported this attribute domain into the polygon shapefile outlining the units and assigned a colour palette to it. I then selected the appropriate unit for each polygon from a list under the Attributes menu in ArcMap.

## 6.3 Stratigraphic Map and results

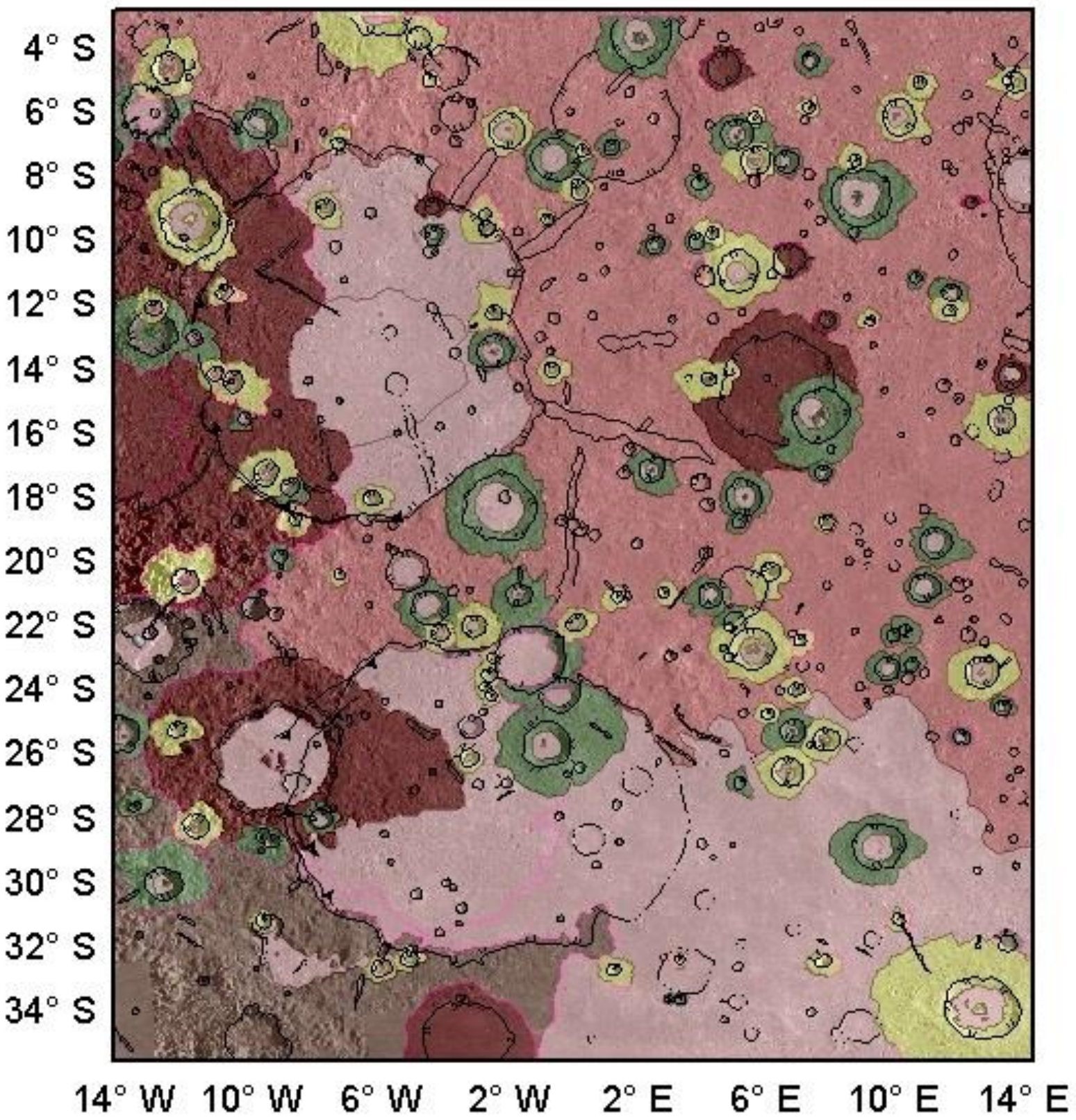


*Figure 6.3: Stratigraphic map of the mapping area*

**Legend:**

**Contacts**

- Certain
- Uncertain

**Linear Features**

- Basin edge scarps
- Catenae
- Crater rims (>15 km)
- Ghost catenae
- Ghost craters
- Small craters (>8 km)
- Wrinkle ridges

**Lithology**

- C1 (degraded craters)
- C2 (intermediate craters)
- C3 (fresh craters)
- Intercrater Plains
- Intermediate Plains
- Smooth Plains

The mapping area is dominated by Intermediate Plains, with areas of the more heavily cratered, older unit Intercrater Plains to the west and an extended area of lightly cratered, younger Smooth Plains in the southern half of the area. In addition to the extended area of Smooth Plains, many of the impact craters and basins within the mapping area are also infilled by smooth plains material, including Sanai (the northern of the two large basins within the mapping area, with a centre approximately 15° S) and Aneirin (the southern of the two large basins in the mapping area, with a centre approximately 25°S). It is the latter of these two that prompted my decision to apply the same colour to the areas representing the smooth plains within impact basins and the areas of Smooth Plains exterior to impact features.

The area has two examples of basin-edge scarps (associated with Sanai and Aneirin), and 90 identified catenae. The latter are more common on the Intercrater and Intermediate terrains, though a few can be observed on the Smooth Plains to the south as well. This observation is reflective of the global distribution of catenae (described in Chapter 4).

There are 49 examples of “ghost” craters (indicated on Figure 6.3 using pink), 23 of which are found in the Smooth Plains or within volcanically filled basins (which for the purpose of this work I have mapped as the same type of unit).

There are also 7 examples of “ghost” catenae, which like their crater equivalents are catenae that have been flooded by a volcanic unit but remain partially visible, though subdued with obscured rims and shallower depth. Good examples of ghost catenae can be seen though the volcanic unit filling Sanai, and are discussed in section 6.4.3.

## 6.4 Discussion

### *6.4.1 Geological Units*

The eastern rim of Aneirin has been entirely submerged beneath a smooth plains unit, such that it is impossible to distinguish between the volcanic unit that infilled the original basin and the volcanic unit that flooded the area to the east and south of Aneirin, and the eastern portion of the basin. Rothery *et al.* (2017) observed another example of ambiguity between volcanic plains interior to an impact basin and those external to the impact basin, at Caloris (Area 4 in their paper). However, the difference in the case of Area 4 was that it was possible to distinguish between interior and exterior plains by use of MDIS colour mosaic and X-Ray Spectrometer (XRS) images. While I have not used the XRS data, I did examine the area of plains covering the eastern rim of Aneirin using the MDIS colour mosaic, and there was no difference in colour between the plains to the east of where I interpret Aneirin's eastern rim is flooded and those to the west (inside the basin).

The ghost craters show that the underlying surface or basin floor was exposed for a sufficient length of time to accumulate several impact craters before the emplacement of the final smooth plains unit within the basin. The plains unit therefore cannot be impact melt from the basin-forming impact. The ghost craters were flooded by the plains unit but were either not totally obscured or have been partially revealed due to the subsidence of the surface as the lava cooled.

### *6.4.2 Crater classification*

It was relatively straightforward to classify all of the impact basins and craters into the three categories C1 (the oldest, most degraded) – C3 (the most recent and fresh). The different classes are indicated by the colours of the areas on Figure 6.3 (the polygons I drew cover the continuous ejecta blankets, where I was able to identify and delineate them, and the crater rim and walls. The crater floors are also included, if the crater has not been later infilled by lava. The two largest basins within the area shown in Figure 6.3 are both C1-class, which is unsurprising given that the largest of Mercury's craters were emplaced early in the history of the solar system.

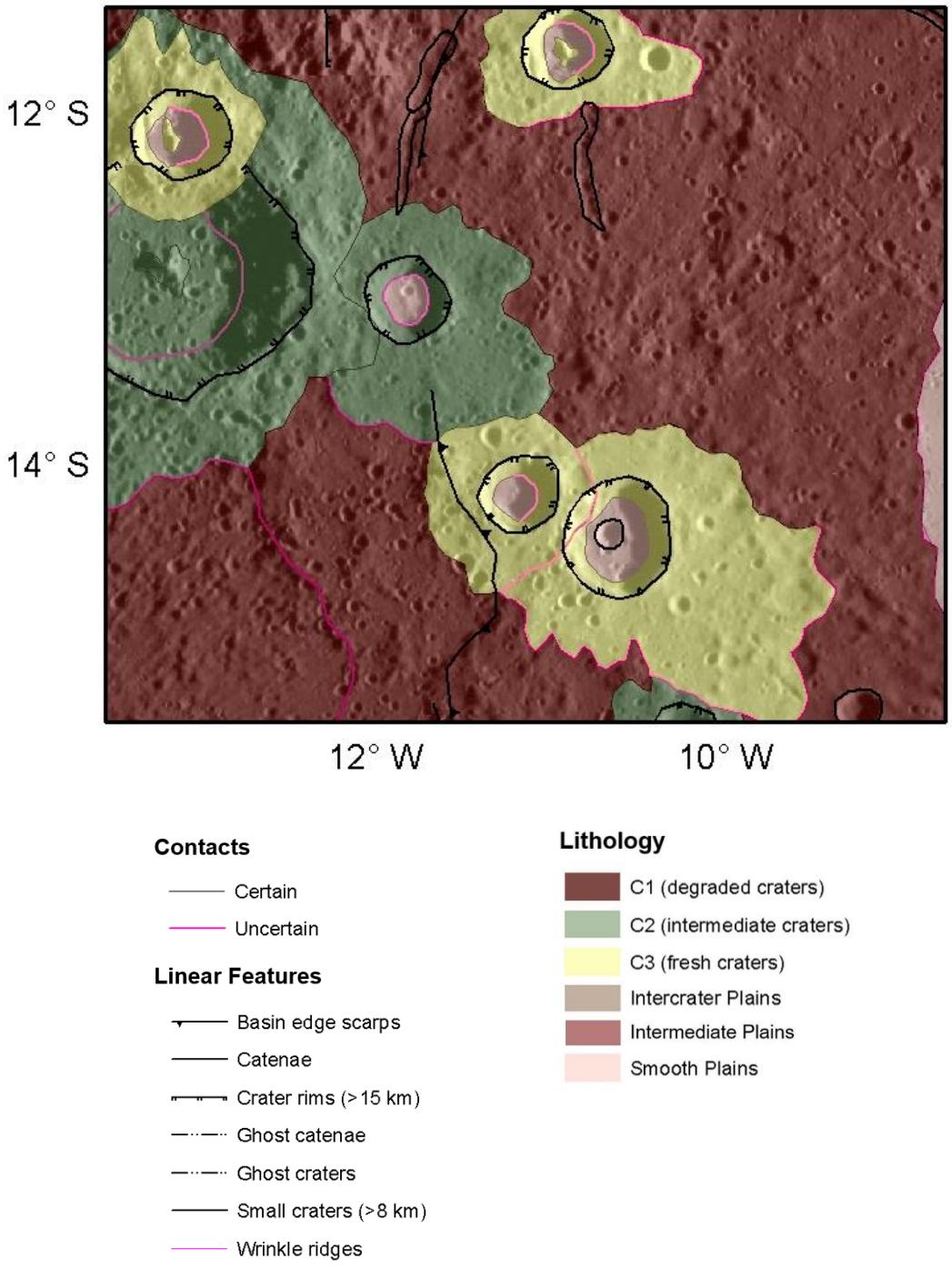


*Figure 6.4: An example of overlapping C3-class craters. The western C3 crater also slightly covers the southern edge of a C2-class crater.*

I did not encounter any instances of older-in-appearance craters overlying younger ones. There are, however, several examples of two or more C2-class (of intermediate degradation and age) craters or their ejecta over-lapping or overprinting each other. One such example is shown in Figure 6.4.

Figure 6.4 depicts two overlapping C3-class craters. Assuming that the ejecta blankets are emplaced at the time of crater formation, which is the case with the continuous ejecta blankets and the assumption I make throughout this project, the observations match what I would expect. Namely, the craters that are less degraded in appearance over-lie the more degraded C2-class craters and ejecta blankets.

### *6.4.3 Shaded-relief models*

The two shaded-relief models I created to assist with the identification of topographical features were helpful in the identification of the edge of ejecta blankets, when examination of the MDIS mosaic proved inconclusive. Figure 6.5 shows the MDIS v9 monochrome mosaic, which was my primary basemap for identifying linear features and contacts. Figure 6.6 shows the same area, with the shaded-relief model with illumination azimuth of 270° and illumination elevation of 35°. The white arrow on Figure 6.5 indicates where I perceive the edge of the continuous ejecta blanket, using the MDIS v9 mosaic. The white arrow on Figure 6.6 is in the same location, but using the shaded-relief model (as illuminated from due-west) I placed the boundary of the continuous ejecta for that crater in a different location, further west (as indicated by the red arrow, and as per the section of the stratigraphic map in Figure 6.6).

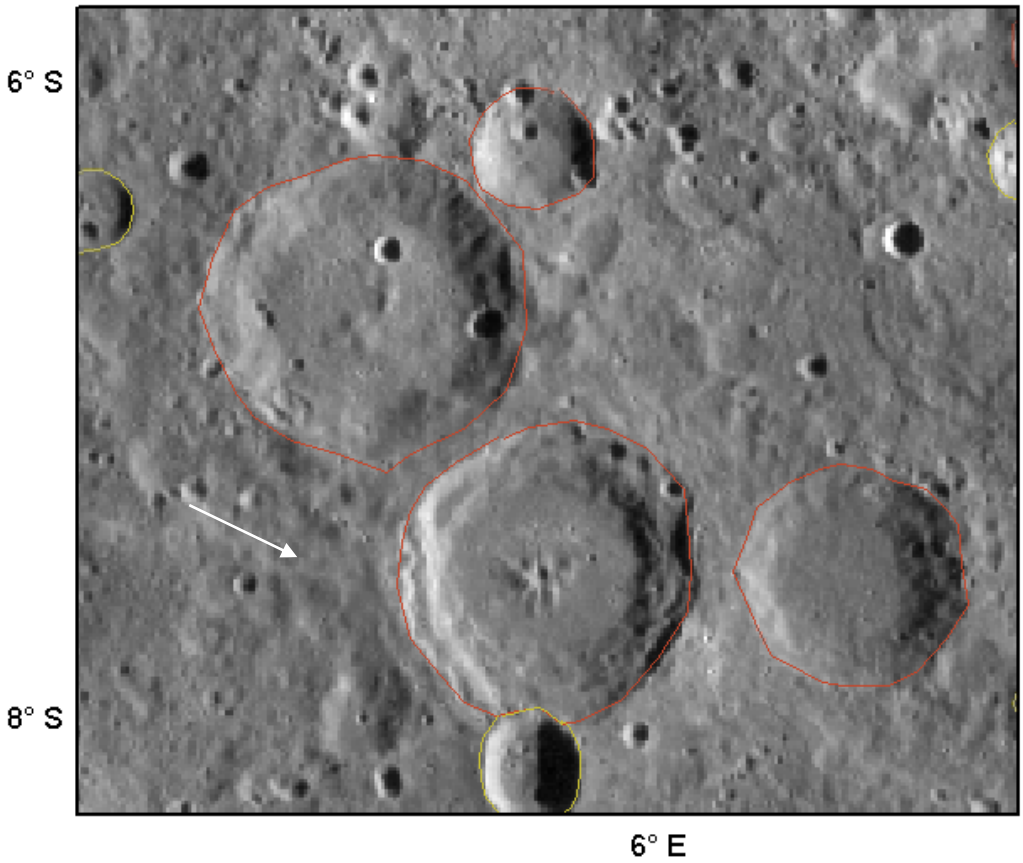


*Figure 6.5: MDIS mosaic basemap. Crater rims indicated (red indicating craters with diameters >15 km and yellow indicating craters with diameters between 8 and 14.9 km). White arrow indicates where I would tentatively put the edge of the ejecta blanket using only the basemap.*

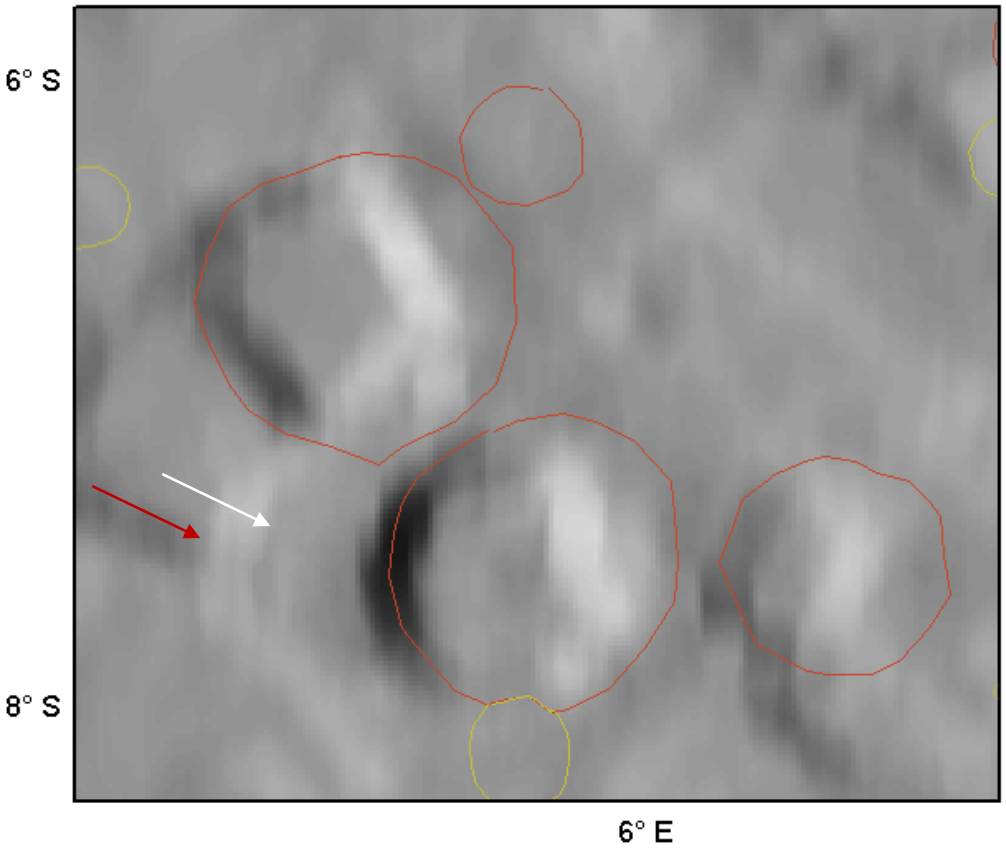


*Figure 6.6: Area as in Figure 6.5, with the hillshade model (illumination azimuth of 270°) rather than the MDIS mosaic. The white arrow is in the same location as in Figure 6.5, the red arrow shows where the edge of the ejecta blanket is – further west than I would have placed it based on the MDIS mosaic.*

In addition to assisting me in identifying the edges of ejecta blankets in cases where I was uncertain, the hillshade models also lead me to add a couple of catenae to the area map, which I had missed in the first pass using the MDIS mosaic. However, I found them less helpful in identifying basin-edge scarps. I was able to identify the scarps I was already aware of (due to my work in Chapter 2) in Aneirin and Sanai (although because I was already familiar with them I knew where to look) but I did not identify any others within the mapping area. This might be because there are not any, or because their relief is insufficient to cast shadows in the shaded-relief models created using the global DEM (as opposed to the M2 flyby DEM that I used in Chapter 5).

### *6.4.4 The use of catenae and basin-edge scarps in stratigraphy*

The relationships between Aneirin, Dario and Sanai basins and their associated (infilling) volcanic units, ejecta, basin-edge scarps and catenae allow the identification of their relative ages and therefore the sequence of events in the geological history of the area. The relationships between these various features and units demonstrate the use of catenae and basin-edge scarps for assisting in interpretation of the sequence of events in local areas, according to the primary aim of this Chapter. My interpretation of the sequence of events and justifications are as follows (beginning with the earliest event I can determine from the current surface).

1) Of Aneirin and Sanai basins, Sanai was the earlier to be formed: based upon the units around Sanai, I believe that the Intermediate Plains unit was emplaced prior to the formation of the impact basin. This is based on the fact that the rim of Sanai cuts the Intercrater Plains. At the same time as Sanai basin was formed, an ejecta blanket would have been deposited, however none of it survives to be observed in the current data. This is not unsurprising given that age and level of degradation of many C1 craters. However, catenae radial to Sanai are still observable, as seen in Figure 6.3.

2) After the Sanai basin was formed, I conclude that the original floor of the basin was left exposed for a relatively long period of time (geologically), based upon the ghost craters and ghost catenae visible beneath the later infilling volcanic unit. These mean that the floor was exposed for long enough to accumulate both impact craters/basins and catenae (which are likely secondary crater chains from near to medium distance large impacts).

3) The 230 km diameter C1-class basin immediately to the west of Sanai was formed and the ejecta appears to have extended into the western portion of the basin. The original eastern rim of this basin, where it cuts into Sanai) is no longer observable due to the cluster of younger (C2 and C3-class) craters.

4) After the creation of Sanai, Aneirin impact basin was formed. At approximately the same time an ejecta blanket would have been deposited (although, like Sanai, Aneirin is a C1-class basin that has no identifiable surviving ejecta blanket). However, at the same time as both the impact and the formation of the continuous ejecta blanket, the secondary ejecta from the Aneirin impact formed secondary crater chains and secondary crater grooves (catenae) by means of ejecta propelled away from the primary basin. Some of the catenae have survived to the present day, as identifiable by being radial to Aneirin and (based upon stratigraphic relationships and degradation) roughly the same age.

   Two examples of catenae of the approximately correct age, distance and radial distribution relative to Aneirin that have survived have become “ghost” catenae within the plains infilling Sanai basin. These two catenae are indicated in Figure 6.7, with white arrows. One of these catenae (to the east) clearly cuts across the rim of Sanai, meaning it was formed after the formation of that basin. The fact that the second catena, to the west, is parallel to the first one therefore – even though it does not cut the rim of Sanai – I assume that it is also a secondary crater chain from the emplacement of Aneirin.

5) The next stage in the geological history of the area was the completion of the volcanic flooding of Sanai. This flooding may have been a single large event, or an infilling that happened in stages over geological time, but the emplacement of the Aneirin-radial catenae (see 4) finished prior to the completion of the flooding of Sanai basin. The volcanic infill appears to onlap onto the ejecta blanket of the C1-class basin to the west of Sanai. Only the eastern portion of Sanai basin is volcanically infilled with smooth plains.

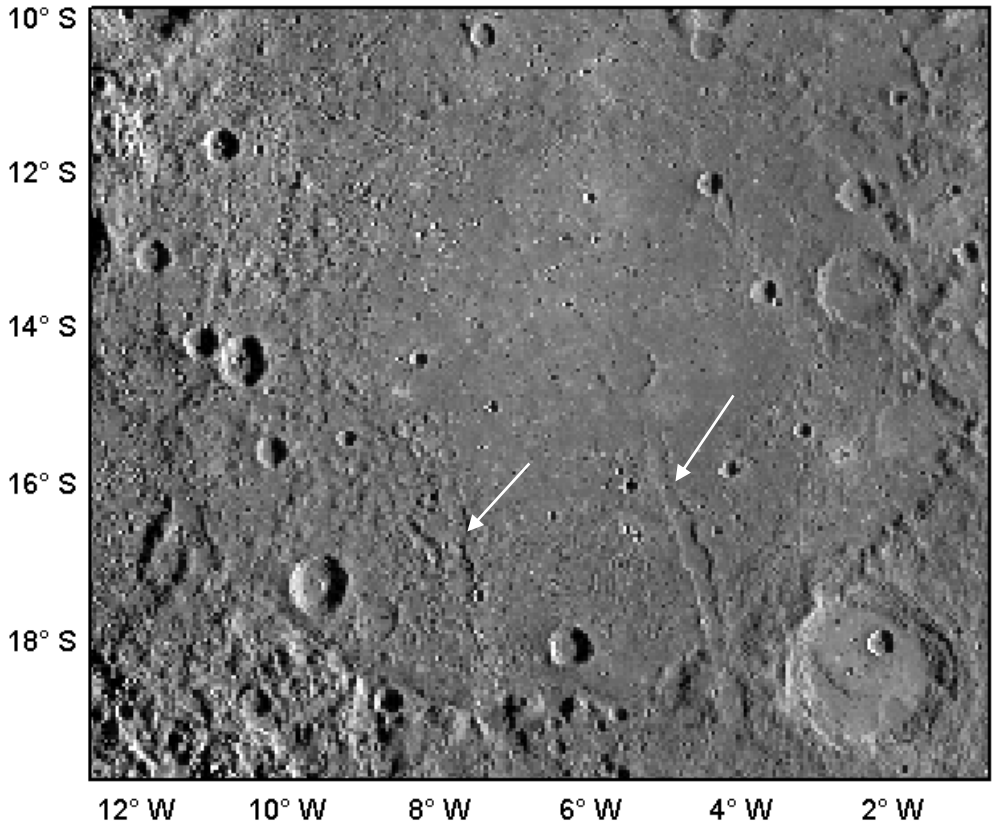


*Figure 6.7: Sanai basin and two catenae from the formation of Aneirin basin (to the south). The catenae are shown using the two white arrows.*

6) The next geological event in this local area was the completion of volcanic infilling of the Aneirin impact basin. As with the volcanic fill of Sanai, this may have occurred in stages or as a single event**.**

7) Next, Dario basin was emplaced, cutting across part of Aneirin's rim. It is not possible to say how long the interval was based only on the stratigraphic relationships. However, Dario's ejecta covers the volcanic fill of Aneirin, meaning that the Dario impact likely occurred after the volcanic fill had been emplaced.

8) Dario was then filled with a smooth plains unit. This unit extends into Aneirin, covering the area where a section of the western rim was prior to the Dario impact. Once again it is not possible to tell in this case whether infill of Dario began prior to the formation of the ghost crater, and continued afterwards (i.e. several stages of volcanic flooding occurred),

or whether it was a single event.

9) I have identified two areas of smooth plains material that appear more sparsely-cratered than the rest. One occupies the centre of Sanai, and another covers the south-eastern rim and section of Aneirin, and extends along the southern and south-western outer edge of Aneirin's interior. Based upon their smooth appearance, I interpret that these were emplaced more recently than the rest of the smooth plains units, as second (or final) stages of volcanism in each case. I have delineated these and marked them with "2" to distinguish them from the older smooth plains units, which are shown in the same colour on the map. In the case of Sanai, two "ghost" catenae can be observed crossing into this central, smoother region (indicated by white arrows in Figure 6.7). In this central region they appear to become more obscured than they were in the less-central areas of Sanai's interior, until in the centre of the basin they are no longer visible.

10) While it cannot be determined when formation of the Sanai basin-edge scarp began, resolvable activity on the scarp ended at some point after the emplacement of the (initial) volcanic plains and the present. The stratigraphic relationships indicate that the scarp was forming at the time or after the emplacement of the C2-class crater to the west of Sanai, since the scarp cuts through the ejecta blanket. This indicates that the scarp was forming until geologically relatively recently – but not into geologically recent history, since a C3 crater abuts the northern end of the Sanai scarp. This which would support certain of the crater size-frequency statistics already detailed (see Chapter 3).

11) The formation of the basin-edge scarp of Aneirin was completed (for the process of formation see Chapter 2). This lobate scarp cuts through the rim of Dario, the volcanic infill and the ghost crater visible through the volcanic infill of Dario. The scarp also deforms the "second stage" smooth plains unit at the far south-western edge of Aneirin's interior. This indicates that activity on this scarp continued after the emplacement of this unit, the youngest within the mapping area. The basin-edge scarp of

Sanai may also have been active at this time, and/or at the time of emplacement of the “second stage” smooth plains unit within Sanai but it is not possible to tell this based upon stratigraphy.

Aneirin and Dario were included in the large basins survey conducted by Fassett *et al*. (2012), under the designations “b37” and “b38” respectively. Rothery *et al*. (2013) featured Aneirin (still designated “b37” at that time) and its basin-edge scarp in their paper, which also discussed their interpretations of the sequence of events in the formation and volcanic filling of Aneirin and Dario based upon superposition relationships. Their interpretation was that Aneirin was formed, and then volcanically filled. Afterwards, Dario (referred to by Rothery *et al.* (2013) as an unnamed 140 km diameter crater) was formed and then infilled, then the formation of the 30 km diameter crater within Dario. Rothery *et al*. (2013) refer to this 30 km diameter crater as infilled, though based on its morphology I interpret it as a ghost crater, see 8), that was formed before the volcanic unit within Dario. Rothery *et al.* (2013) state that the latest relevant event was the formation of the lobate scarp. My investigation of this area has confirmed the sequence of events between Anerin, Dario and the Aneirin basin-edge scarp though as investigated and discussed in Chapter 2, the nature of lobate scarps only permit me to state that the scarp remained active until after the formation of both basins and volcanic units. Activity may well have been occurring on the basin-edge scarp throughout, and only ceasing afterwards.

Rothery *et al.* (2013) also identified Sanai (referred to as “b38”) in their initial identification of basin-edge scarps on Mercury. Both Aneirin and Sanai are C2-class basins, but the my use of catenae – on the basis that they are secondary crater chains (see Chapter 4) – for stratigraphic purposes has allowed me to state that Sanai is the older of the two. While the crater SFD analysis work I undertook in Chapters 2 and 3 support this, these analyses were carried out on the surface of the volcanic fills of both basins. They therefore do not provide any data on the relative timings of the basin-formation events themselves, while my use of catenae as indicators has been able to do so.

It should be noted that the work I undertook for Chapters 2 and 3 was carried out prior to this in-depth mapping. I had not identified the “second stage”

smooth plains within Sanai and Aneirin (see point 9) above) when that work was carried out. As a result, the areas I chose to carry out crater counting in both of these cases covered both smooth plains and “stage two” smooth plains – which are separate geological units. In the case of Aneirin this is likely why the crater size-frequency distribution (SFD) curve for the volcanic infill exhibits a kink. Kinks are commonly observed when the crater count analysis area covers more than one geological unit (or there has been resurfacing). Since the unit in question is a volcanic unit filling an impact basin, I knew to expect some indication of resurfacing in the SFD curve so did not – at that point – inquire further as to the source of that kink.

## 6.5 Conclusions

In this chapter I aimed to establish the stratigraphic history of the study area including impact basins Aneirin/Sanai. Furthermore, I hoped to establish the usefulness of basin-edge scarps and catenae (based upon my finding in Chapter 4 that the latter are most likely secondary impact chains) in the stratigraphic mapping process.

I have found that both basin-edge scarps and catenae are of help when carrying out stratigraphic mapping. The former can only cut across features that were in place prior to the cessation of fault activity, thus indicating a sequence of formation. The latter are useful because they can often (though not always, see Chapter 4) be linked back to a particular basin, and persist longer than ejecta blankets do. Catenae are therefore of particular use when establishing the relative ages between an impact basins or craters when, morphologically, they appear of similar age. For example, I have been able to demonstrate that Sanai is older than Aneirin. I also identified during the mapping work that both large impact basins in the mapping area (Aneirin and Sanai) appear to have undergone multiple events of volcanic infilling.

My summary of the geological history of the mapping study area is as follows:

- Emplacement of volcanic units that later become the Intercrater Plains
- Emplacement of volcanic units that later become the Intermediate Plains
- Sanai C1-class basin formed

- C1-class basin immediately to the west of Sanai is formed, ejecta blanket covers and fills the western section of Sanai basin.
- Aneirin C1-class basin formed
- Sanai basin volcanically infilled.
- C1-class crater formation ceases, C2-class crater formation begins
- Aneirin basin volcanically infilled.
- Dario C2-class basin formed
- Some further C2-class craters formed (including the “ghost” crater within Dario)
- Emplacement of Dario infilling smooth plains
- Emplacement of “second stage” Smooth Plains unit (flooding Aneirin’s east rim and south-eastern, far southern and south-western interior)
- Cessation of resolvable activity on the Aneirin basin-edge scarp (after deforming both smooth plains and second stage smooth plains units, Dario’s rim, infilling smooth plains unit and ghost crater).
- C2-class crater formation ends, C3-class crater formation begins.
- Cessation of resolvable activity on the Sanai basin-edge scarp Further emplacement on C3 craters.

# 7 Summary of findings

In this chapter I summarise my findings and conclusions from each chapter of this thesis, and discuss – where relevant – where the next mission to Mercury (BepiColombo) might be able to provide data allowing progression or additional ground-truthing of my work. BepiColombo is currently planned to launch in July 2016, and the Mercury Planetary Orbiter (MPO) will carry a payload of 11 instruments that will operate once in orbit (Benkhoff *et al*., 2010; Rothery, 2015).

The instruments I expect to be of particular relevance to the features I have examined are: BepiColombo Laser Altimeter (BELA) and Spectrometer and Imagers for MPO BepiColombo Integrated Observatory System (SIMBIO-SYS). Mercury Thermal Infrared Spectrometer (MERTIS) will provide data on the mineralogy of the surface. These three instruments' data are also likely to be of great use when investigating any type of surface feature, and producing further stratigraphic maps.

## 7.1 Basin-edge scarps

My work on basin-edge scarps, recently published in Icarus (Fegan *et al.,* 2017) investigated that sub-type of lobate scarps on Mercury initially identified by Rothery *et al.* (2013). My aims when doing so were to map the occurrence of basin-edge scarps on Mercury; investigate when they were tectonically active, and the age of the volcanic plains they deform, and when activity on them ceased; form a theory as to how they have likely formed, and how they fit into their local contexts and might contribute to the understanding of Mercury's geological history. In addition to the Marchi Production Function (as Marchi *et al.* (2011)) results presented in Chapter 2, I also applied the Neukum Production Function (Neukum *et al.,* 2001) and the Le Feuvre and Wieczorek Model Production Functions (Le Feuvre & Wieczorek, 2011)) during this work. These results are presented in Chapter 3.

In addition, prior to writing the paper (Chapter 2 ), I carried out tests the buffered crater size-frequency distribution (SFD) method initially published by Fassett *et al.* (2008), as applied to linear tectonic features on Mercury (see Chapter 3). The initial intended use of the buffered method was to provide ages for the floors of valleys on Mars, and at the time of my beginning my work there was little precedent in the literature for its use on linear features of questionable

width rather than features with measurable and definite width. Furthermore, activity on the lobate scarps was not a single event, as discussed in Chapter 2, meaning that that the method would not be dating a single event, but rather when activity (or activity resolvable by the method) ceased.

However, the tests that I carried out on the buffered method (Chapter 3) in which I compared buffered results, crater SFD results for plains areas, ejecta blankets e.t.c., and my observations of the stratigraphic relationships both supported my use of the buffered SFD method on lobate scarps on Mercury. Subsequent to this work (but prior to my papers' publication) other workers have published work on Mercury using the buffered method for similar purposes (e.g. Giacomini *et al*. (2015))**.**

My conclusions from my work in Chapters 2 and 3 on basin-edge scarps and associated units are as follows:

- The mechanism my co-authors and I considered most likely to explain the formation of basin-edge scarps is that the interface between the original basin floor and the base of the smooth plains units acts as a mechanical discontinuity along which detachment faulting could have occurred.
- Volcanism of sufficient volume to extend across the floors of basins >100 km in diameter or greater continued until at least early Mansurian (approximately 1.5 Ga). I suggested in Chapter 2 that magma ascent may have been assisted by impact fracturing given the location of the volcanic smooth plains within impact basins and the prolonged and potentially ongoing global contraction of Mercury
- The use of the buffered method on tectonic features produces results consistent with the observed stratigraphy with regard to basin-edge scarps and both of the tests I carried out on other curvilinear tectonic features and associated units.
- Resolvable deformation accommodated by basin-edge lobate scarps appears to have ceased between ~1.1 Ga and ~0.6 Ga, in the mid-to-late Mansurian.

- Neukum, Marchi and Le Feuvre and Wieczorek (employing both porous and non-porous scaling) Model Production Functions produce four different sets of results between them, and cannot be used interchangeably.
- There is not yet sufficient use of the Le Feuvre and Wieczorek Model Production Function in the Mercury literature to establish whether the porous or non-porous scaling is more appropriate for smooth plains units on Mercury.

I anticipate that the visible-spectrum imager of the BepiColombo MPO spacecraft (SYMBIO-SYS) will be of great help in identifying examples of basin-edge scarps that may not be included in my survey due to the limits of the MESSENGER dataset. The laser altimeter (BELA) is also likely to be useful in as much as the global coverage will allow the creation of a global DEM created from direct measurement rather than a mix of direct measurement (northern hemisphere) and stereo imaging (southern hemisphere), as is the current global DEM created from MESSENGER data. This will allow the creation of hillshade models that have a lower risk of being affected by the illumination bias. They can therefore be used with high confidence in support of imagery surveys and mapping of linear/curvilinear features such as basin-edge scarps.

## 7.2 Catenae

Catenae, chains of 3 or more craters, are commonly observed on the surface of Mercury. While the assumption has been that they are chains of secondary impact craters (for example, Gault (1975))**,** this has not been previously examined in the literature. My aims were to map the occurrence of catenae on Mercury, down to a scale of 1:800000 (the minimum width of catenae I can reliably distinguish at this resolution was approximately 800 m); identify the most likely mechanism for their formation, based on the literature for similar features and their morphology and occurrence; investigate how catenae fit into and can assist in the interpretation of the geological and stratigraphic history of Mercury (both globally and locally).

Thus, in Chapter 4, I determined that the evidence supports the assumptions in the literature and amongst my peers, and that catenae do appear to be closely

linked to primary impact craters and basins. They appear to be either secondary impact chains, or possibly chains of collapse pits forming above impact fractures. It seems to be a reasonable assumption that they formed either at the same time or in the period shortly after the formation of the primary basin. This being the case, they are potentially of help when creating stratigraphic maps. Some catenae remain visible radial to degraded C2 and even C1-class craters and basins are still often visible after the continuous ejecta blankets can no longer be observed. I also observed catenae extending beyond the continuous ejecta into the continuous secondary facies and discontinuous secondary facies (as Xiao *et al.* (2014)). Where catenae exhibit cross-cutting relationships, they can therefore be used to determine which of two otherwise-not-superposed craters is the older (as I did in Chapter 6).

BepiColombo MPO might be able to further test my hypothesis that catenae are formed by secondary impacts. I discussed in Chapter 4 the possibility of identifying catenae craters with central peaks, if they are indeed formed by impacts. However, this effort was hampered by the fact that catenae on Mercury tend to have diameters of <10 km (small enough that central peaks would not be very likely to form in impact craters). However, if catenae are formed by impacts, one would expect ejecta blankets to be formed surrounding them, though these blankets would not be very large in extent. In young catenae, this ejecta material may not have been consolidated to the same extent as the surrounding surface, in which case the thermal inertial properties may also be different. This difference might be resolvable by the MERTIS instrument, providing the ejecta blanket is large enough (the resolution of MERTIS will be 500m/pixel).

## 7.3 Illumination bias

Both basin-edge scarps (Chapters 2 and 3) and catenae are tens or hundreds km scale curvilinear topographic features. Both global surveys produced data that indicated preferential orientations. Due to the scale of the features involved, I had initially expected lighting bias not to have a notable effect. In both cases, any global trends in their orientations would be of interest in interpreting either their origins (in the case of catenae) or drawing inferences about the history of Mercury (in the case of basin-edge scarps).

However, Mercury's near-zero obliquity means that (particularly at low latitudes) linear features on Mercury suffer from illumination bias due to the illumination azimuth being either east or west but with no other variation. This means that (at low latitudes) east-west trending curvilinear features would be likely to be under-represented in the global population, while this would not be the case for north-south trending features. At high latitudes, as there is more variation in illumination azimuth, this is less of a problem.

In both surveys, I observed a preference for north–south orientations at low latitudes and east–west at higher latitudes. Having determined this, my aim in Chapter 5 was to assess whether my surveys on the MDIS global mosaic of basin-edge scarp and catenae have been affected by this illumination bias, by resurveying on a number of differently artificially illuminated shaded-relief models. My results from my investigation into basin-edge scarps indicates that their detection does appear to be affected by illumination bias. However, in the case of catenae, the global survey results appear to have revealed a true preference in orientation (NNE-SSW), possibly since by definition catenae have slopes (that would cast shadows) facing in all four cardinal directions making them less prone to the illumination bias.

My general finding is that, when surveying on shaded-relief models, it would be preferable to survey on hillshade models with at least two illumination azimuths in addition to the MDIS images or mosaics. In addition, the two illumination azimuths should be perpendicular, to ensure the illumination is sufficiently different each time, and creating the hillshade models with a medium (35°, measured from the surface towards the zenith) or high (45°) illumination elevation is preferable, since the low illumination elevation (25°) produced a 'noisy' model.

Regarding catenae, my findings in Chapter 5 were that the preferences in orientation that I observed in my global survey data are not due to the illumination bias. I am not able to explain what might cause a preference in the orientation of secondary ejecta chains, and leave this to be investigated in future work. It is also possible that the resolution of the hillshade models that I was resurveying on in order to compare with my survey on the MDIS mosaic was too low for me to be able to identify catenae that are unfavourably aligned with the illumination direction. As the M2 DEM I used was produced from

stereoimaging, it is possible that the illumination bias inherent in the source images were carried over into the DEM, and therefore into the hillshade models I created.

As discussed above, BELA will provide global topographic coverage, allowing the creation of DEMs that are not affected by illumination bias. Higher resolution images (from SYMBIO-SYS) will also assist, but any orbital imaging of Mercury will be affected by the same illumination bias as described in Chapter 5. The laser altimeter data, and the DEMs and shaded-relief models created from it, will not be and therefore will provide an excellent complement to visual surveying, to capture those features aligned with illumination direction (as described in Chapter 5).

## 7.4 Mapping

My aims when carrying out stratigraphic mapping of the Aneirin/Sanai area in Chapter 6 were to investigate the geological history of that area, and to investigate and demonstrate the applications of basin-edge scarps and catenae when carrying out stratigraphic mapping. My investigation of this area has confirmed the sequence of events between Anerin, Dario and the Aneirin basin-edge scarp as initially proposed by Rothery *et al.* (2013), and discussed in Chapter 2. My use of catenae (based upon the model that they are secondary impact crater chains) provided the evidence required to establish that out of C2-class basins Sanai and Aneirin, Sanai is the older.

I therefore found that catenae are of use when establishing stratigraphic relationships between impact basins, due to the fact that they tend to extend further away from the primary basin than the ejecta blanket, and also tend to remain observable for longer.

I also identified during the mapping work that Aneirin appears to have had multiple volcanic infilling events. I arrived at this conclusion at the end of this project, so I carried out the crater size-frequency distribution work in Chapters 2 and 3 assuming that the top-most surface of the Aneirin smooth plains unit was emplaced at the same time.

The improved instrumentation of BepiColombo MPO will be invaluable when carrying out stratigraphic mapping. SYMBIO-SYS, MIXS, MGNS and MERTIS will provide imagery and information on the physical mineralogical and elemental composition of the surface. This will allow checking and testing of hypotheses, and refinement of the work carried out using MESSENGER data, including this thesis.

## References


Di Achille, G., Popa, C., Massironi, M., Mazzotta Epifani, E., Zusi, M., Cremonese, G. and Palumbo, P. (2012) 'Mercury's radius change estimates revisited using MESSENGER data', *Icarus*, 221(1), pp. 456–460. doi: 10.1016/j.icarus.2012.07.005.

Arvidson, R., Boyce, J., Chapman, C., Cintala, M., Fulchignoni, M., Moore, H., Neukum, G., Schultz, P., Soderblom, L., Strom, R., Woronow, A. and Young, R. (1979) 'Standard Techniques for Presentation and Analysis of Crater Size-Frequency Data', *Icarus*, 474, pp. 467–474.

Banks, M. E., Xiao, Z., Braden, S. E., Marchi, S., Chapman, C. R., Barlow, N. G. and Fassett, C. I. (2016) 'Revised age constraints for Mercury's Kuiperian and Mansurian systems', *LPSC 47*, 2943.

Benkhoff, J., Casteren, J. Van, Hayakawa, H., Fujimoto, M., Laakso, H., Novara, M., Ferri, P., Middleton, H. R. and Ziethe, R. (2010) 'BepiColombo — Comprehensive exploration of Mercury : Mission overview and science goals', *Planetary and Space Science*, 58(1–2), pp. 2–20. doi: 10.1016/j.pss.2009.09.020.

Beuthe, M. (2010) 'East–west faults due to planetary contraction', *Icarus*, 209(2), pp. 795–817. doi: 10.1016/j.icarus.2010.04.019.

Blair, D. M., Freed, A. M., Byrne, P. K., Klimczak, C., Prockter, L. M., Ernst, C. M., Solomon, S. C., Melosh, H. J. and Zuber, M. T. (2013) 'The origin of graben and ridges in Rachmaninoff, Raditladi, and Mozart basins, Mercury', *Journal of Geophysical Research: Planets*, 118(1), pp. 47–58. doi: 10.1029/2012JE004198.

Blewett, D. T., Denevi, B. W., Ernst, C. M., Chabot, N. L. and Neish, C. D. (2014) 'Mapping of optical maturity on Mercury', Abstract no. 1131, *45th LPSC*.

Buczkowski, D. L., Schmidt, B. E., Williams, D. A., Mest, S. C., Scully, J. E. C., Ermakov, A. I., Preusker, F., Schenk, P., Otto, K. A., Hiesinger, H., O'Brien, D., Marchi, S., Sizemore, H., Hughson, K., Chilton, H., Bland, M., Byrne, S., Schorghofer, N., Platz, T., Jaumann, R., Roatsch, T., Sykes, M. V., Nathues, A., De Sanctis, M. C., Raymond, C. A. and Russell, C. T. (2016) 'The geomorphology of Ceres', *Science*, 353(6303). doi: 10.1126/science.aaf4332.

Byrne, P. K., Klimczak, C., Celal Sengor, A. M., Solomon, S. C., Watters, T. R. and Hauck, S. A. (2014) 'The global contraction of Mercury', Abstract no. 2525*, 45th LPSC*, pp. 7–8.

Byrne, P. K., Klimczak, C., Şengör, A. M. C., Solomon, S. C., Watters, T. R. and Hauck, S. A. (2014) 'Mercury's global contraction much greater than earlier estimates', *Nature Geoscience*, pp. 301–307. doi: 10.1038/NGEO2097.

Byrne, P. K., Klimczak, C., Williams, D. a., Hurwitz, D. M., Solomon, S. C., Head, J. W., Preusker, F. and Oberst, J. (2013) 'An assemblage of lava flow features on Mercury', *Journal of Geophysical Research: Planets*, 118(6), pp. 1303–1322. doi: 10.1002/jgre.20052.

Byrne, P. K., Ostrach, L. R., Denevi, B. W., Chapman, C. R., Fassett, C. I., Whitten, J. L., Klimczak, C., Mazarico, E., Hauck, S. a, Head, J. W. and Solomon, S. C. (2015) 'Near-synchonous end to global-scale effusive volcanism on Mercury', Abstract no. 1731, *46th LPSC,* doi: 10.1016/j.icarus.2014.11.010.

Byrne, P. K., Ostrach, L. R., Fassett, C. I., Chapman, C. R., Denevi, B. W., Evans, A. J., Klimczak, C., Banks, M. E., Head, J. W. and Solomon, S. C. (2016) 'Widespread effusive volcanism on Mercury likely ended by about 3.5 Ga', *Geophysical Research Letters*, pp. 7408–7416. doi: 10.1002/2016GL069412.Received.

Chabot, N. L., Ernst, C. M., Denevi, B. W., Harmon, J. K., Murchie, S. L., Blewett, D. T., Solomon,

S. C. and Zhong, E. D. (2012) ‘Areas of permanent shadow in Mercury ’s south polar region ascertained by MESSENGER orbital imaging’, *Geophysical Research Letters*, 39, pp. 1–6. doi: 10.1029/2012GL051526.

Collins, G. S., Melosh, H.J. and Osinski, G. R. (2012) 'The impact-cratering process', *Elements*, 8 (1), pp. 25-30, doi:10.2113/gselements.8.1.25

Cordell, B. M. and Strom, R. G. (1977) ‘Global tectonics of Mercury and the moon’, *Physics of the Earth and Planetary Interiors*, 15(2–3), pp. 146–155. doi: 10.1016/0031-9201(77)90027-9.

Davies, M. E., Dornik, S. E., Gault, D. E. and Strom, R. G. (1978) *Atlas of Mercury*. National Aeronautics and Space Administration.

Denevi, B. W., Ernst, C. M., Meyer, H. M., Robinson, M. S., Murchie, S. L., Whitten, J. L., Head, J. W., Watters, T. R., Solomon, S. C., Ostrach, L. R., Chapman, C. R., Byrne, P. K., Klimczak, C. and Peplowski, P. N. (2013) ‘The distribution and origin of smooth plains on Mercury’, *Journal of Geophysical Research: Planets*, 118(5), pp. 891–907. doi: 10.1002/jgre.20075.

Denevi, B. W., Robinson, M. S., Solomon, S. C., Murchie, S. L., Blewett, D. T., Domingue, D. L., McCoy, T. J., Ernst, C. M., Head, J. W., Watters, T. R. and Chabot, N. L. (2009) ‘The evolution of Mercury’s crust: a global perspective from MESSENGER.’, *Science (New York, N.Y.)*, 324(5927), pp. 613–8. doi: 10.1126/science.1172226.

Dombard, A. J. and Hauck, S. a. (2008) ‘Despinning plus global contraction and the orientation of lobate scarps on Mercury: Predictions for MESSENGER’, *Icarus*, 198(1), pp. 274–276. doi: 10.1016/j.icarus.2008.06.008.

Dzurisin, D. (1978) ‘The tectonic and volcanic history of mercury as inferred from studies of scarps, ridges, troughs, and other lineaments’, *Journal of Geophysical Research*, 83(B10), p. 4883. doi: 10.1029/JB083iB10p04883.

Fassett, C. I. and Head, J. W. (2008) ‘The timing of martian valley network activity: Constraints from buffered crater counting’, *Icarus*, 195(1), pp. 61–89. doi: 10.1016/j.icarus.2007.12.009.

Fassett, C. I., Head, J. W., Baker, D. M. H., Zuber, M. T., Smith, D. E., Neumann, G. A., Solomon, S. C., Klimczak, C., Strom, R. G., Chapman, C. R., Prockter, L. M., Phillips, R. J., Oberst, J. and Preusker, F. (2012) ‘Large impact basins on Mercury: Global distribution, characteristics, and modification history from MESSENGER orbital data’, *Journal of Geophysical Research: Planets*, 117(E12), doi: 10.1029/2012JE004154.

Fegan, E. R., Rothery, D. A., Marchi, S., Massironi, M., Conway, S. J. and Anand, M. (2017) ‘Late movement of basin-edge lobate scarps on Mercury’, *Icarus*, 288, pp. 226–234.

Ferrari, S., Massironi, M., Marchi, S. and Cremonese, G. (2015) ‘Age relationships of the Rembrandt basin and Enterprise Rupes , Mercury’, in Platz, T., Massironi, M., Byrne, P. K., and Hiesinger, H. (eds) *Volcanism and Tectonism Across the Inner Solar System*. Geological Society, London, Special Publications, pp. 159–172. doi: 10.1144/SP401.20.

Le Feuvre, M. and Wieczorek, M. a. (2011) ‘Nonuniform cratering of the Moon and a revised crater chronology of the inner Solar System’, *Icarus*. Elsevier Inc., 214(1), pp. 1–20. doi: 10.1016/j.icarus.2011.03.010.

Flamini, E., Capaccioni, F., Cremonese, G., Palumbo, P., Formaro, R., Mugnuolo, R., Debei, S., Veltroni, I. F., Dami, M., Tommasi, L. and SIMBIO-SYS Team (2016) ‘SIMBIO-SYS for BepiColombo : status and issues’, *Memorie della Societa Astronomica Italiana*, 87(171), pp. 171-171.

Galluzzi, V. (2015) 'Structural analysis of the Victoria Quadrangle (H2) of Mercury based on NASA MESSENGER data', Università degli Studi di Napoli "Frederico II", Dipartimento di Scienze

della Terra, dell Ambiene e felle Risorse, Scuola di Dottorato in Scienze della Terra - XXVII Circlo.

Galluzzi, V., Guzzetta, L., Ferranti, L., Achille, G. Di, Rothery, D. A., Palumbo, P., Guzzetta, L., Ferranti, L., Achille, G. Di, Rothery, D. A. and Palumbo, P. (2017) 'Geology of the Victoria quadrangle ( H02 ), Mercury'. Taylor & Francis, 5647(January). doi: 10.1080/17445647.2016.1193777.

Gasselt, Van S. and Neukum, G. (2011) 'Chronology, cratering and stratigraphy', in M. Gargaud, W. M. Irvine, R. Amils, H. J. Cleaves, D. L. Pinti, J. Cernicharo Quintanilla, M. Viso (eds.), *Encyclopedia of astrobiology*, pp. 304–313. Berlin/Heidelberg: Springer-Verlag.

Gault, D. E., Guest, J. E., Murray, J. B., Dzurisin, D. and Malin, M. C. (1975) 'Some Comparisons of Impact Craters on Mercury and the Moon of Mercury', *Journal of Geophysical Research,* 80(17), pp. 2444–2460, doi: 10.1029/JB080i017p02444.

Giacomini, L., Massironi, M., Marchi, S., Fassett, C. I. and Achille, G. Di (2014) 'Dating tectonic structures on Mercury : new clues to understand the planet's thermal evolution', *Geophysical Research Abstracts*, 16, EGU2014-12194.

Giacomini, L., Massironi, M., Marchi, S., Fassett, C. I., Nazionale, I., Astronomico, O., Nazionale, I., Astronomico, A., Nazionale, I. and Astronomico, O. (2015) 'Age dating of an extensive thrust system on Mercury : implications for the planet's thermal evolution', in Platz, T., Massironi, M., Byrne, P. K., and Hiesinger, H. (eds) *Volcanism and Tectonism Across the Inner Solar System*. Geological Society, London, pp. 291–311.

Gillis-Davis, J. J., Blewett, D. T., Gaskell, R. W., Denevi, B. W., Robinson, M. S., Strom, R. G., Solomon, S. C. and Sprague, A. L. (2009) 'Pit-floor craters on Mercury : Evidence of near-surface igneous activity', *Earth and Planetary Science Letters*, 285(3–4), pp. 243–250. doi: 10.1016/j.epsl.2009.05.023.

Hawkins, S. E., Boldt, J. D., Darlington, E. H., Espiritu, R., Gold, R. E., Gotwols, B., Grey, M. P., Hash, C. D., Hayes, J. R., Jaskulek, S. E., Kardian, C. J., Keller, M. R., Malaret, E. R., Murchie, S. L., Murphy, P. K., Peacock, K., Prockter, L. M., Reiter, R. A., Robinson, M. S., Schaefer, E. D., Shelton, R. G., Sterner, R. E., Taylor, H. W., Watters, T. R. and Williams, B. D. (2007) 'The Mercury Dual Imaging System on the MESSENGER Spacecraft', *Space Science Reviews*, 131(1–4), pp. 247–338. doi: 10.1007/s11214-007-9266-3.

Head, J. W., Murchie, S. L., Prockter, L. M., Solomon, S. C., Chapman, C. R., Strom, R. G., Watters, T. R., Blewett, D. T., Gillis-Davis, J. J., Fassett, C. I., Dickson, J. L., Morgan, G. a. and Kerber, L. (2009) 'Volcanism on Mercury: Evidence from the first MESSENGER flyby for extrusive and explosive activity and the volcanic origin of plains', *Earth and Planetary Science Letters*, 285(3–4), pp. 227–242. doi: 10.1016/j.epsl.2009.03.007.

Horstman, K. C. and Melosh, H. J. (1989) 'Drainage Pits in Cohesionless Materials : Implications for the Surface of Phobos', *Journal of Geophysical Research*, 94(B9), pp. 12433–12441.

Kiefer, W. S. and Murray, B. C. (1987) 'The Formation of Mercury's Smooth Plains', *Icarus,* 491(4417), pp. 477–491, doi: 10.1016/0019-1035(87)90046-7.

Kinczyk, M. J., Prockter, L. M., Chapman, C. R. and Susorney, H. C. M. (2016) 'A Morphological Evaluation of Crater Degradation on Mercury : Revisiting Crater Classification With MESSENGER Data', Abstract no. 1573, 47th *LPSC*.

Klimczak, C. (2015) 'Limits on the brittle strength of planetary lithospheres undergoing global contraction', *Journal of Geophysical Research : Planets*, pp. 2135–2151. doi: 10.1002/2015JE004851.

Klimczak, C., Byrne, P. K. and Solomon, S. C. (2015) 'A rock-mechanical assessment of

Mercury's global tectonic fabric', *Earth and Planetary Science Letters*, 416, pp. 82–90. doi: 10.1016/j.epsl.2015.02.003.

Kneissl, T., van Gasselt, S. and Neukum, G. (2011) 'Map-projection-independent crater size-frequency determination in GIS environments—New software tool for ArcGIS', *Planetary and Space Science*, 59(11–12), pp. 1243–1254. doi: 10.1016/j.pss.2010.03.015.

Langevin, Y. (1997) 'The regolith of Mercury: present knowledge and implications for the Mercury Orbiter mission', *Planetary and Space Science*, 45(1), pp. 31–37. doi: 10.1016/S0032-0633(96)00098-0.

Marchi, S., Bottke, W. F., Cohen, B. A., Wünnemann, K., Kring, D. A., McSween, H. Y., De Sanctis, M. C., O'Brien, D. P., Schenk, P., Raymond, C. A. and Russell, C. T. (2013a) 'High-velocity collisions from the lunar cataclysm recorded in asteroidal meteorites', *Nature Geoscience*, 6(4), pp. 303–307. doi: 10.1038/ngeo1769.

Marchi, S., Bottke, W. F., Cohen, B. A., Wünnemann, K., Kring, D. A., McSween, H. Y., De Sanctis, M. C., O'Brien, D. P., Schenk, P., Raymond, C. A. and Russell, C. T. (2013b) 'High-velocity collisions from the lunar cataclysm recorded in asteroidal meteorites', *Nature Geoscience*, 6(4), pp. 303–307. doi: 10.1038/ngeo1769.

Marchi, S., Chapman, C. R., Fassett, C. I., Head, J. W., Bottke, W. F. and Strom, R. G. (2013) 'Global resurfacing of Mercury 4.0-4.1 billion years ago by heavy bombardment and volcanism.', *Nature*, 499(7456), pp. 59–61. doi: 10.1038/nature12280.

Marchi, S., Chapman, C. R., Fassett, C. I., Head, J. W., Bottke, W. F. and Strom, R. G. (2013) 'Global resurfacing of Mercury 4.0-4.1 billion years ago by heavy bombardment and volcanism.', *Nature*, 499(7456), pp. 59–61. doi: 10.1038/nature12280.

Marchi, S., Massironi, M., Cremonese, G., Martellato, E., Giacomini, L. and Prockter, L. (2011a) 'The effects of the target material properties and layering on the crater chronology: The case of Raditladi and Rachmaninoff basins on Mercury', *Planetary and Space Science*, 59(15), pp. 1968–1980. doi: 10.1016/j.pss.2011.06.007.

Marchi, S., Massironi, M., Cremonese, G., Martellato, E., Giacomini, L. and Prockter, L. (2011b) 'The effects of the target material properties and layering on the crater chronology: The case of Raditladi and Rachmaninoff basins on Mercury', *Planetary and Space Science*, 59(15), pp. 1968–1980. doi: 10.1016/j.pss.2011.06.007.

Marchi, S., Mottola, S., Cremonese, G., Massironi, M. and Martellato, E. (2009) 'a New Chronology for the Moon and Mercury', *The Astronomical Journal*, 137(6), pp. 4936–4948. doi: 10.1088/0004-6256/137/6/4936.

Massironi, M., Cremonese, G., Marchi, S., Martellato, E., Mottola, S. and Wagner, R. J. (2009) 'Mercury's geochronology revised by applying Model Production Function to Mariner 10 data: Geological implications', *Geophysical Research Letters*, 36(21), p. L21204. doi: 10.1029/2009GL040353.

McCauley, J. F. and Wilhelms, D. E. (1971) 'Geological Provinces of the Near Side of the Moon', *Icaurus*, 15, pp. 363–367.

Mckinnon, B. and Schenk, P. M. (1995) 'Estimates of comet fragment masses from impact crater chains on Callisto and Ganymede', *Geophysical Research Letters,* 22(13), pp. 1829–1832, doi: 10.1029/95GL01422.

Mège, D., Cook, A. C., Garel, E., Lagabrielle, Y. and Cormier, M.-H. (2003) 'Volcanic rifting at Martian grabens', *Journal of Geophysical Research*, 108(E5). doi: 10.1029/2002JE001852.

Melosh, H. J. (1977) 'Global Tectonics of a Despun Planet', *Icarus*, 31, pp. 221–243.

Melosh, H. J. (1998) 'Craters unchained', *Nature*, 394, pp. 221-223, doi: 10.1038/28271

Melosh, H. J. (2011) *Planetary Surface Processes*. 1st edn. Cambridge: Cambridge University Press.

Melosh, H. J. and Dzurisin, D. (1978) 'Mercurian Global Tectonics : A Consequence of Tidal Despinning?', *Icarus*, 35, pp. 227–236.

Melosh, H. J. and McKinnon, W. B. (1988) 'The Tectonics of Mercury', in Vilas, F., Chapman, C., Matthews, M. (eds.), *Mercury*, University of Arizona Press, pp. 374–400.

Melosh, H. J. and Schenk, P. (1993) 'Split comets and the origin of crater chains on Ganymede and Callisto', *Letters to Nature*, 365, pp. 731–733.

Murchie, S. L., Watters, T. R., Robinson, M. S., Head, J. W., Strom, G., Chapman, C. R., Solomon, S. C., Mcclintock, W. E., Prockter, L. M., Domingue, D. L. and Blewett, D. T. (2008) 'A View from MESSENGER Geology of the Caloris Basin , Mercury ':, *Science*, 321(5885), pp. 73–76.

Murray, B. C., Strom, G. and Trask, N. J. (1975) 'Surface History of Mercury and Implications for Terrestrial Planets', *Journal of Geophysical Research*, 80(17), pp. 2508–2514.

Murray, J. B. and Iliffe, J. C. (2011) 'Morphological and geographical evidence for the origin of Phobos' grooves from HRSC Mars Express images', *Geological Society, London, Special Publications*, 356(1), pp. 21–41. doi: 10.1144/SP356.3.

Murray, J. B., Rothery, D. A., Thornhill, G. D., Muller, J., Iliffe, J. C., Day, T. and Cook, A. C. (1994) 'The origin of Phobos ' grooves and crater chains', *Planetary and Space Science*, 42(6), pp. 519–526.

Neukum, G., Ivanov, B. A. and Hartmann, W. K. (2001) 'Cratering records in the inner solar system in relation to the lunar reference system', *Chronology and Evolution of Mars*, 96, pp. 55–86.

Neukum, G., Oberst, J., Ho, H., Wagner, R. and Ivanov, B. A. (2001) 'Geologic evolution and cratering history of Mercury', *Planetary and Space Science,* 49, pp. 1507–1521.

Oberbeck, V. R., Quaide, W. L., Arvidson, R. E. and Aggarwal, H. R. (1977) 'Comparative Studies of Lunar , Martian , and Mercurian', *Journal of Geophysical Research*, 82(11), pp. 1681–1698.

Ostrach, L. R., Robinson, M. S., Whitten, J. L., Fassett, C. I., Strom, R. G., Head, J. W. and Solomon, S. C. (2015) 'Extent, age, and resurfacing history of the northern smooth plains on Mercury from MESSENGER observations', 250, pp. 602–622. doi: 10.1016/j.icarus.2014.11.010.

Pechmann, J. B. and Melosh, H. J. (1979) 'Global fracture patterns of a despun planet: Application to Mercury', *Icarus*, 38(2), pp. 243–250. doi: 10.1016/0019-1035(79)90181-7.

Pike, R. J. (1988) 'Geomorphology of impact craters on Mercury', in Vilas, F., Chapman, C., Matthews, M. (eds.), *Mercury*, pp. 165-273. University of Arizona Press.

Pollack, J. B., Veverka, J., Noland, M., Sagan, C., Duxbury, T. C. and Smith, B. A. (1973) 'Mariner 9 Television Observations of Phobos and Deimos', *Journal of Geophysical Research*, 78(20), pp. 4313–4326.

Preusker, F., Oberst, J., Head, J. W., Watters, T. R., Robinson, M. S., Zuber, M. T. and Solomon, S. C. (2011) 'Stereo topographic models of Mercury after three MESSENGER flybys', *Planetary and Space Science*, 59(15), pp. 1910–1917. doi: 10.1016/j.pss.2011.07.005.

Prockter, L. M., Ernst, C. M., Denevi, B. W., Chapman, C. R., Head, J. W., Fassett, C. I., Merline, W. J., Solomon, S. C., Watters, T. R., Strom, R. G., Cremonese, G., Marchi, S. and Massironi, M. (2010) 'Evidence for young volcanism on Mercury from the third MESSENGER flyby.', *Science,*

329(5992), pp. 668–71. doi: 10.1126/science.1188186.

Prockter, L., Thomas, P., Robinson, M., Joseph, J., Milne, A., Bussey, B., Veverka, J. and Cheng, A. (2002) 'Surface Expressions of Structural Features on Eros', *Icarus*, 155, pp. 75–93. doi: 10.1006/icar.2001.6770.

Rothery, D. A. and Massironi, M. (2013) 'A spectrum of tectonised basin edges on Mercury', Abstract no. 1175, 44th *LPSC*.

Rothery, D. A. (2015) *Planet Mercury: From pale pink dot to dynamic world*. Springer Praxis Books.

Rothery, D. A., Mancinelli, P., Guzzetta, L. and Wright, J. (2017) 'Mercury ' s Caloris basin : Continuity between the interior and exterior plains', *Journal of Geophysical Research*. doi: 10.1002/2017JE005282.

Rothery, D. A. and Massironi, M. (2010) 'Beagle Rupes – Evidence for a basal decollement of regional extent in Mercury's lithosphere', *Icarus*, 209(1), pp. 256–261. doi: 10.1016/j.icarus.2009.12.009.

Ruiz, J., López, V. and Egea-González, I. (2013) 'Paleo-heat flows, radioactive heat generation, and the cooling and deformation history of Mercury', *Icarus*, 225(1), pp. 86–92. doi: 10.1016/j.icarus.2013.02.033.

Schumm, S. A. (1970) 'S. A. SCHUMM Department of Geology, Colorado State University, Fort Collins, Colorado 80521 Experimental Studies on the Formation of Lunar Surface Features by Fluidization', *Geological Society of America Bulletin*, 81, pp. 2539–2552.

Scott, E. D., Wilson, L. and Head, J. W. (2002) 'Emplacement of giant radial dikes in the northern Tharsis region of Mars', *Journal of Geophysics*, 107(E4), 5019, doi: 10.1029/2000JE001431

Siegfried, R. W. and Solomon, S. C. (1974) 'Mercury : Internal Structure and Thermal Evolution', *Icarus*, 205, pp. 192–205.

Solomon, S. C. (2003) 'Mercury: the enigmatic innermost planet', *Earth and Planetary Science Letters*, 216(4), pp. 441–455. doi: 10.1016/S0012-821X(03)00546-6.

Solomon, S. C. (2011) 'A new look at the planet Mercury', *Physics Today*, 64(1), p. 50. doi: 10.1063/1.3541945.

Soter, S. (1971) *The dust belts of Mars*. CRSR Rept. No. 462, Cornell University, available at: http://hdl.handle.net/1813/36286

Spudis, P. D. and Prosser, J. . (1984) *Atlas of Mercury - Geologic map of the Michaelangelo (H-12) Quadrangle of Mercury*. USGS.

Spudis, P. D. and Guest, J. E. (1988a) 'Stratigraphy and geologic history of Mercury', *Mercury University of Arizona Press*, 1, pp. 118–164.

Spudis, P. D. and Guest, J. E. (1988b) 'Stratigraphy and geologic history of Mercury', *Mercury University of Arizona Press*, 1, pp. 118–164. Available at: http://adsabs.harvard.edu/abs/1988merc.book..118S.

Strom, R. G., Banks, M. E., Chapman, C. R., Fassett, C. I., Forde, J. a., Head, J. W., Merline, W. J., Prockter, L. M. and Solomon, S. C. (2011) 'Mercury crater statistics from MESSENGER flybys: Implications for stratigraphy and resurfacing history', *Planetary and Space Science*, 59(15), pp. 1960–1967. doi: 10.1016/j.pss.2011.03.018.

Strom, R. G., Chapman, C. R., Merline, W. J., Solomon, S. C. and Head, J. W. (2008) 'Mercury

cratering record viewed from MESSENGER's first flyby.', *Science,* 321(5885), pp. 79–81. doi: 10.1126/science.1159317.

Strom, R. G. and Neukum, G. (1988) 'The Cratering Record on Mercury and the Origin of Impacting Objects', in Vilas, F., Chapman, C., Matthews, M. (eds.), *Mercury*, pp. 336–373. doi: 10.1103/PhysRevB.53.15485.

Strom, R. G., Trask, N. J. and Guest, J. E. (1975) 'Tectonism and volcanism on Mercury', *Journal of Geophysical Research*, 80(17), pp. 2478–2507. doi: 10.1029/JB080i017p02478.

Thomas, P. (1979) 'Surface Features of Phobos and Deimos', *Icarus*, 40, pp. 223–243.

Thomas, P. and Veverka, J. (1979) 'An Analysis of Mariner 9 and Viking Data', *Journal of Geophysical*, 84(B14), pp. 8131–8146.

Trask, N. J. and Guest, J. E. (1975) 'Preliminary Geologic Terrain Map of Mercury The methods used fo r geologic mapping of the moon have', *Journal of Geophysical Research*, 80(17), pp. 2461–2477.

Veverka, J. and Duxbury, T. C. (1977) 'Viking Observations of Phobos and Deimos Preliminary Results', *Journal of Geophysical Research*, 82(28), pp. 4213–4223.

Watters, T. R., Cook, a. C. and Robinson, M. S. (2001) 'Large-scale lobate scarps in the southern hemisphere of Mercury', *Planetary and Space Science*, 49(14–15), pp. 1523–1530. doi: 10.1016/S0032-0633(01)00090-3.

Watters, T. R., Daud, K., Banks, M. E., Selvans, M. M., Chapman, C. R. and Ernst, C. M. (2016) 'Recent tectonic activity on Mercury revealed by small thrust fault scarps', 9, pp. 743–747. doi: 10.1038/NGEO2814.

Watters, T. R., Robinson, M. S., Bina, C. R. and Spudis, P. D. (2004) 'Thrust faults and the global contraction of Mercury', *Geophysical Research Letters*, 31. doi: 10.1029/2003GL019171.

Watters, T. R., Schultz, R. A., Robinson, M. S. and Cook, A. C. (2002) 'The mechanical and thermal structure of Mercury ' s early lithosphere', *Geophysical Research Letters*, 29(11), pp. 1–4.

Watters, T. R., Selvans, M. M., Banks, M. E., Hauck II, S. A., Becker, K. J. and Robinson, M. S. (2015) 'Distribution of large-scale contractional tectonic landforms on Mercury: Implications for the Origin of Global Stresses', *Geophysical Research Letters*, 42, pp. 3755–3763. doi: 10.1002/2015GL063570.Received.

Watters, T. R., Solomon, S. C., Robinson, M. S., Head, J. W., André, S. L., Hauck, S. a. and Murchie, S. L. (2009) 'The tectonics of Mercury: The view after MESSENGER's first flyby', *Earth and Planetary Science Letters*, 285(3–4), pp. 283–296. doi: 10.1016/j.epsl.2009.01.025.

Whitten, J. L., Head, J. W., Helbert, J. and Solomon, S. C. (2014) 'Rembrandt basin: distinguishing between volcanic and impact-produced smooth plains deposits on Mercury', *45th LPSC*.

Wilhelms, D. E. (1976) 'Mercurian Volcanism Questioned', *Icarus*, 28, pp. 551–558.

Wilson, L. and Head, J. W. (2002) 'Tharsis-radial graben systems as the surface manifestation of plume-related dike intrusion complexes : Models and implications', *Journal of Geophysical Research*, 107(E8).

Wyrick, D. Y. and Smart, K. J. (2009) 'Dike-induced deformation and Martian graben systems', *Journal of Volcanology and Geothermal Research*, 185, pp. 1–11. doi: 10.1016/j.jvolgeores.2008.11.022.

Xiao, Z., Strom, R. G., Chapman, C. R., Head, J. W., Klimczak, C., Ostrach, L. R., Helbert, J. and D'Incecco, P. (2014) 'Comparisons of fresh complex impact craters on Mercury and the Moon: Implications for controlling factors in impact excavation processes', *Icarus*, 228, pp. 260–275. doi: 10.1016/j.icarus.2013.10.002.

Yseboodt, M. and Margot, J.-L. (2006) 'Evolution of Mercury's obliquity', *Icarus*, 181, pp. 327–337. doi: 10.1016/j.icarus.2005.11.024.

Zoback, M. D., Townend, J. and Grollimund, B. (2002) 'Steady-State Failure Equilibrium and Deformation of Intraplate Lithosphere', *International Geology Review*, 44(5), pp. 383–401. doi: 10.2747/0020-6814.44.5.383.

Zuber, M. T., Smith, D. E., Phillips, R. J., Solomon, S. C., Neumann, G. a, Hauck, S. a, Peale, S. J., Barnouin, O. S., Head, J. W., Johnson, C. L., Lemoine, F. G., Mazarico, E., Sun, X., Torrence, M. H., Freed, A. M., Klimczak, C., Margot, J.-L., Oberst, J., Perry, M. E., McNutt, R. L., Balcerski, J. a, Michel, N., Talpe, M. J. and Yang, D. (2012) 'Topography of the northern hemisphere of Mercury from MESSENGER laser altimetry.', *Science,* 336(6078), pp. 217–20. doi: 10.1126/science.1218805.

## Online references

www1: http://sci.esa.int/bepicolombo/58591-bepicolombo-launch-rescheduled-for-october-2018/ Author: European Space Agency, page last updated 26th November 2016 [accessed 30th January 2018].

www2: http://messenger.jhuapl.edu/Explore/Images.html#global-mosaics Author: The Johns Hopkins University Applied Physics Laboratory LLC [accessed 30th January 2018].

www3: https://www.nasa.gov/mission_pages/messenger/spacecraft/index.html , Author: National Aeronautics and Space Administration, page last updated: Aug. 4, 2017, Page Editor: Tricia Talbert, NASA Official: Brian Dunbar [Accessed 3rd January 2018].

www4: https://planetarynames.wr.usgs.gov/nomenclature/SearchResults Author: International Astronomical Union (IAU) Working Group for Planetary System Nomenclature (WGPSN) [accessed 30th January 2018].

www5: http://target.lroc.asu.edu/q3/ [accessed 30th January 2018].

www6 http://webgis.wr.usgs.gov/pigwad/down/mercury_geology.htm Author: US Geological Survey, page last updated May 2010 [accessed 30th January 2018].

www 7: https://astrogeology.usgs.gov/search/map/Mercury/Topography/MESSENGER/Mercury_Messenger_USGS_DEM_Global_665m Author: USGS Astrogeology Science Center, page last updated 16th May 2017 [accessed 30th January 2018].

www8 https://astrogeology.usgs.gov/search/map/Mercury/Messenger/Global/Mercury_MESSENGER_MDIS_Basemap_EnhancedColor_Mosaic_Global_665m Author: Johns Hopkins Applied Physics Laboratory, page last updated 16th May 2017 [accessed 30th January 2018].

# Appendix 1

Model production function plots for the model ages presented in Chapter 2 Table 2.1.

**A1a**: Marchi *et al.* (2009) MPF plot for the smooth plains unit (black) and basin-edge scarp (red) of Aneirin.

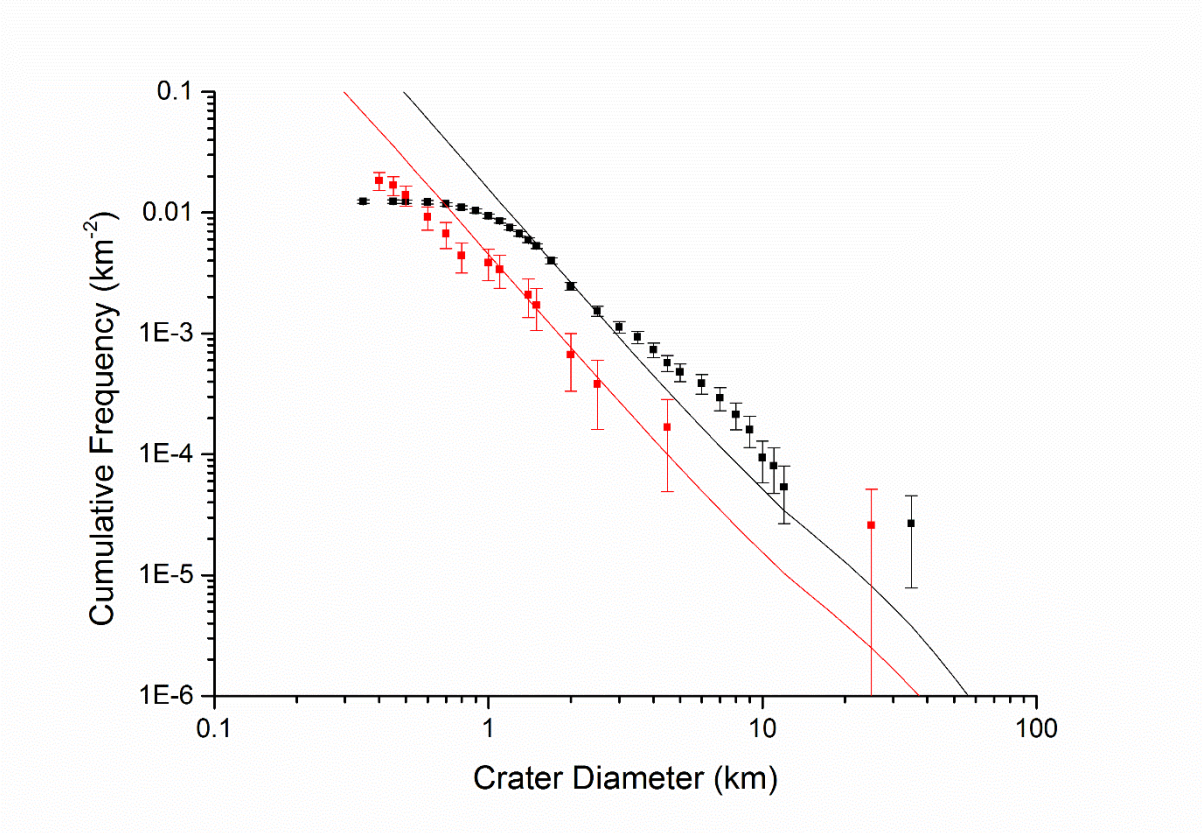

**A1b** : Marchi *et al.* (2009) MPF plot for the smooth plains unit (black) and basin-edge scarp (red) of Beethoven.

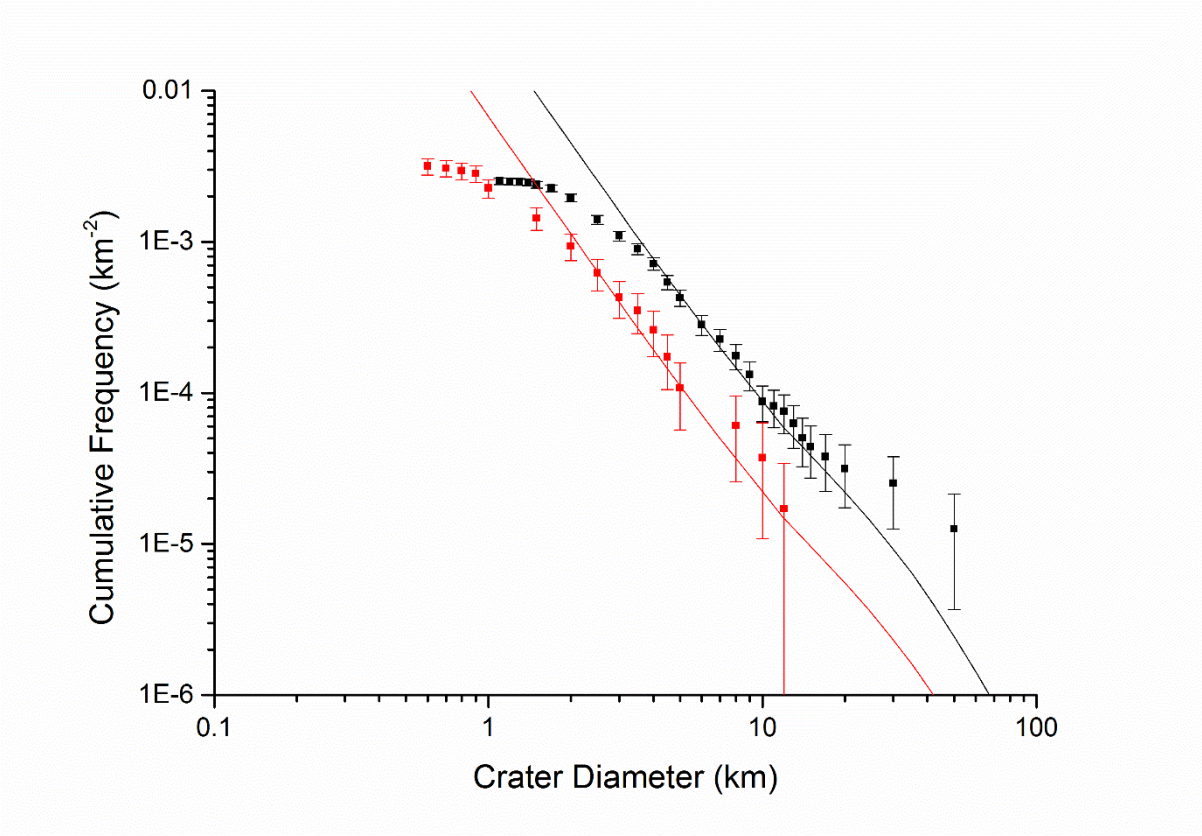

**A1c:** Marchi *et al*. (2009) MPF plot for the smooth plains unit (black) and basin-edge scarp (red) of Hafiz.

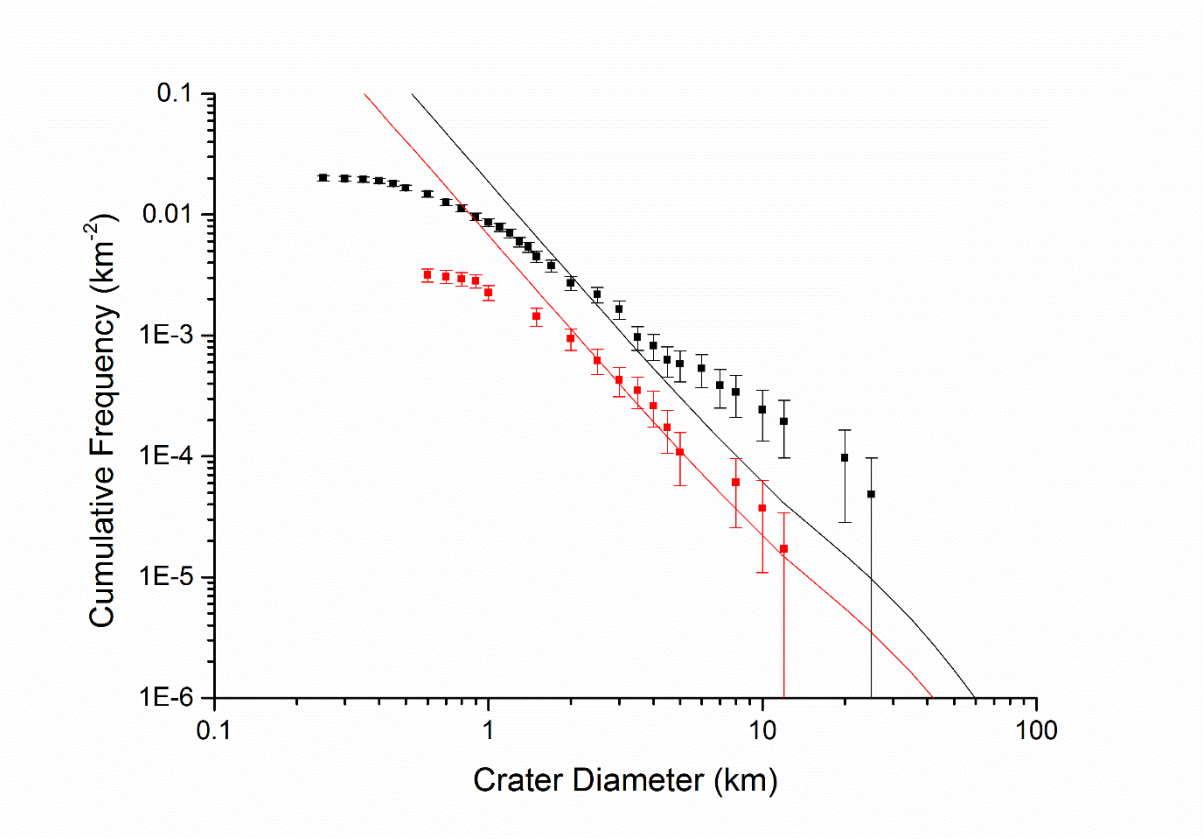

**A1d:** Marchi *et al*. (2009) MPF plot for the smooth plains unit (black) and basin-edge scarp (red) of Shevchenko.

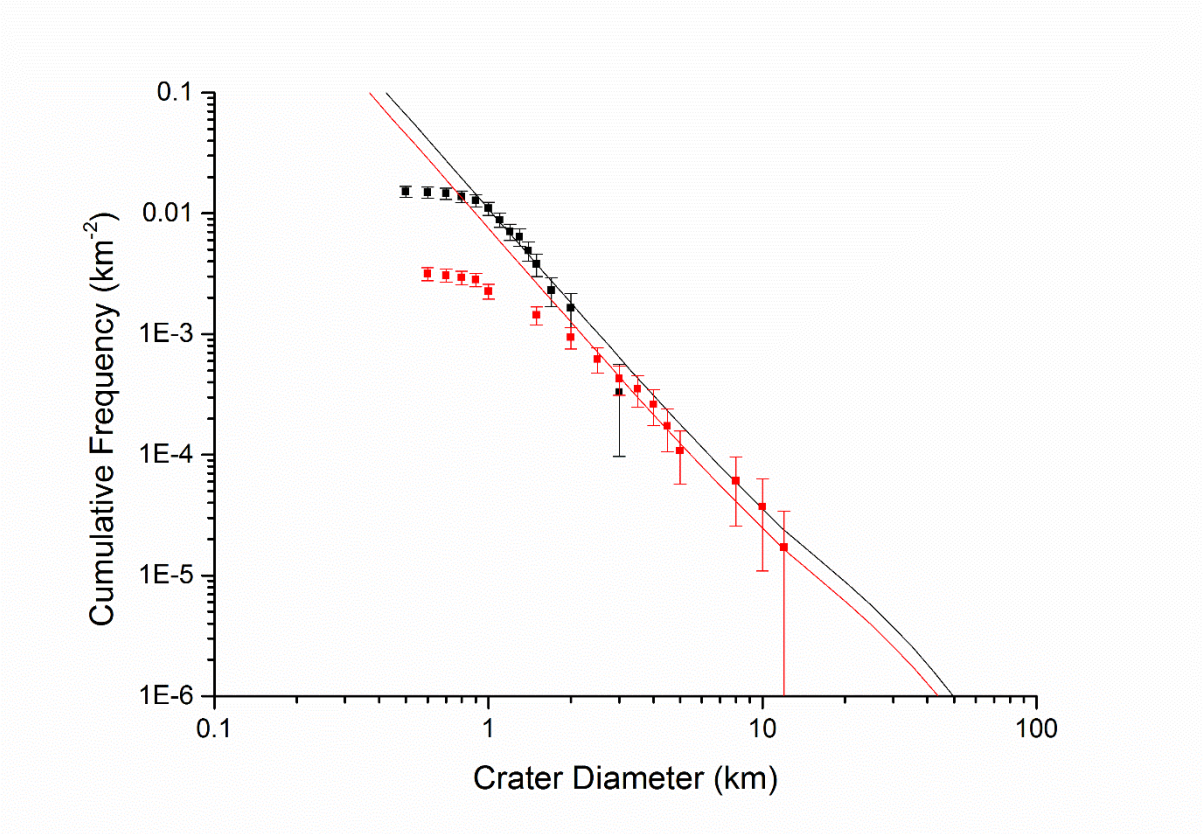

**A1e**: Marchi *et al.* (2009) MPF plot for the smooth plains unit (black) and basin-edge scarp (red) of Unnamed [-40, -70].

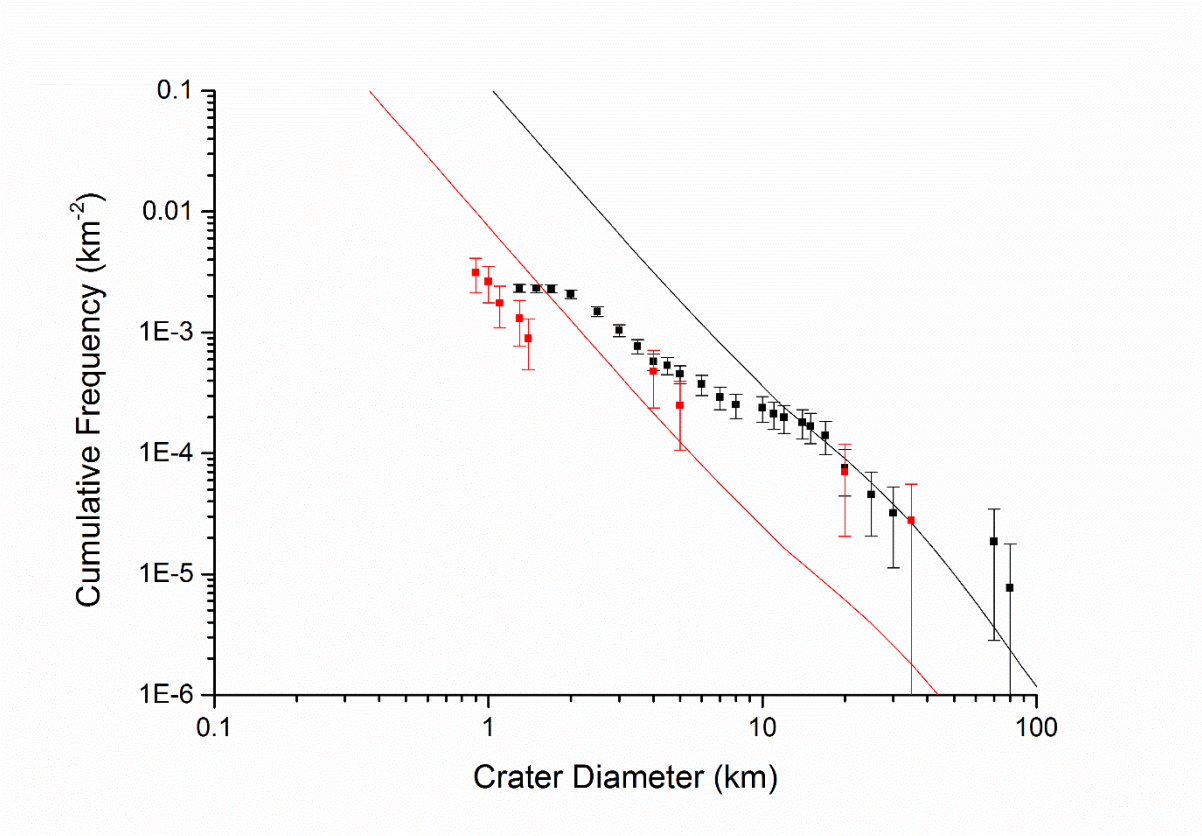

**A1f:** Marchi *et al.* (2009) MPF plot for the smooth plains unit (black) and basin-edge scarp (red) of Unnamed [91, 38].

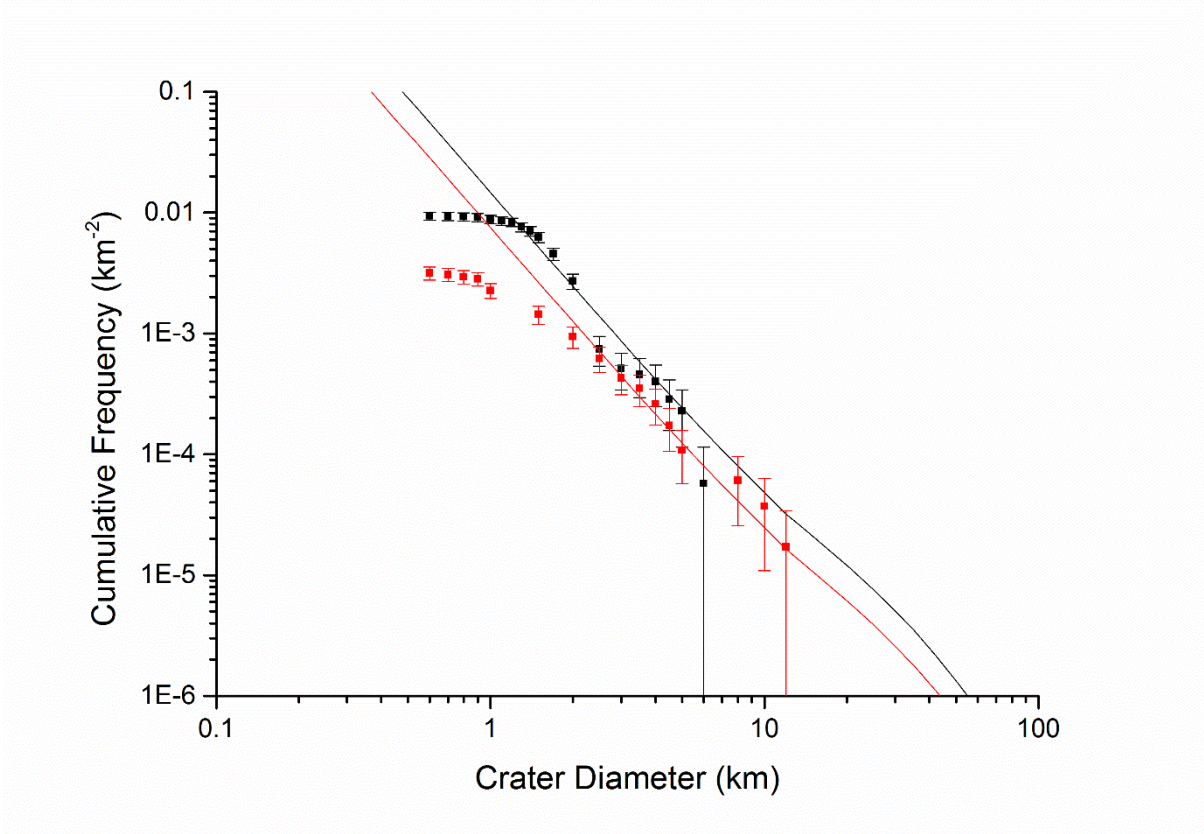

**A1g:** Marchi *et al.* (2009) MPF plot for the smooth plains unit (black) and basin-edge scarp (red) of Unnamed[150, -10].

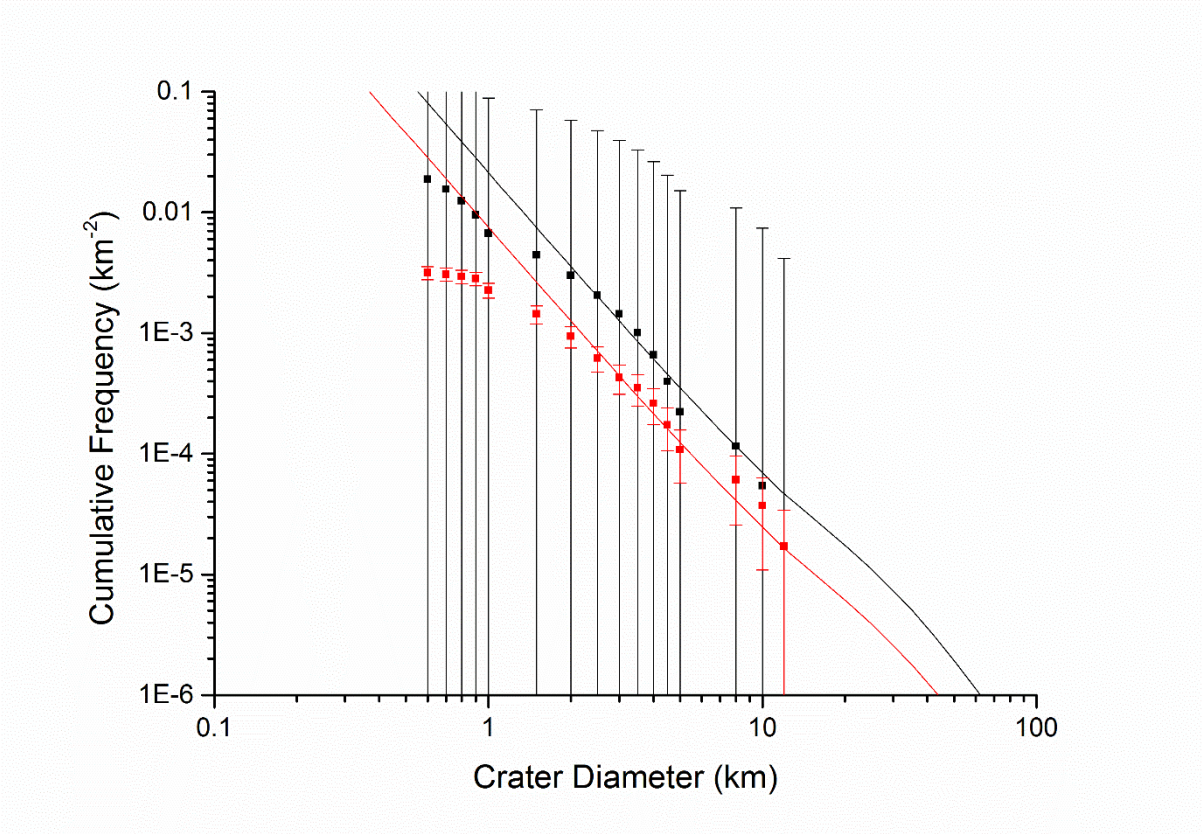

**A1h:** Marchi *et al.* (2009) MPF plot for the smooth plains unit of Mendelson.

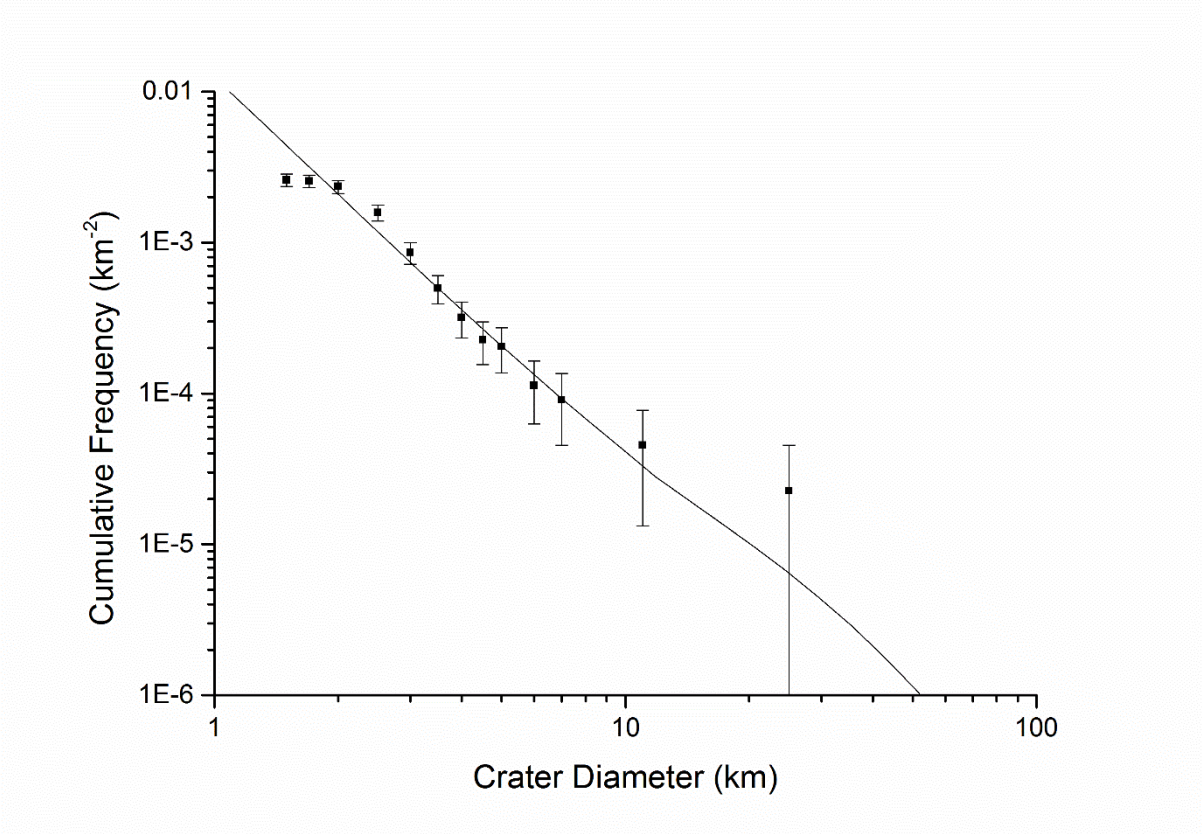

**A1i:** Marchi *et al.* (2009) MPF plot for the smooth plains unit of Hugo.

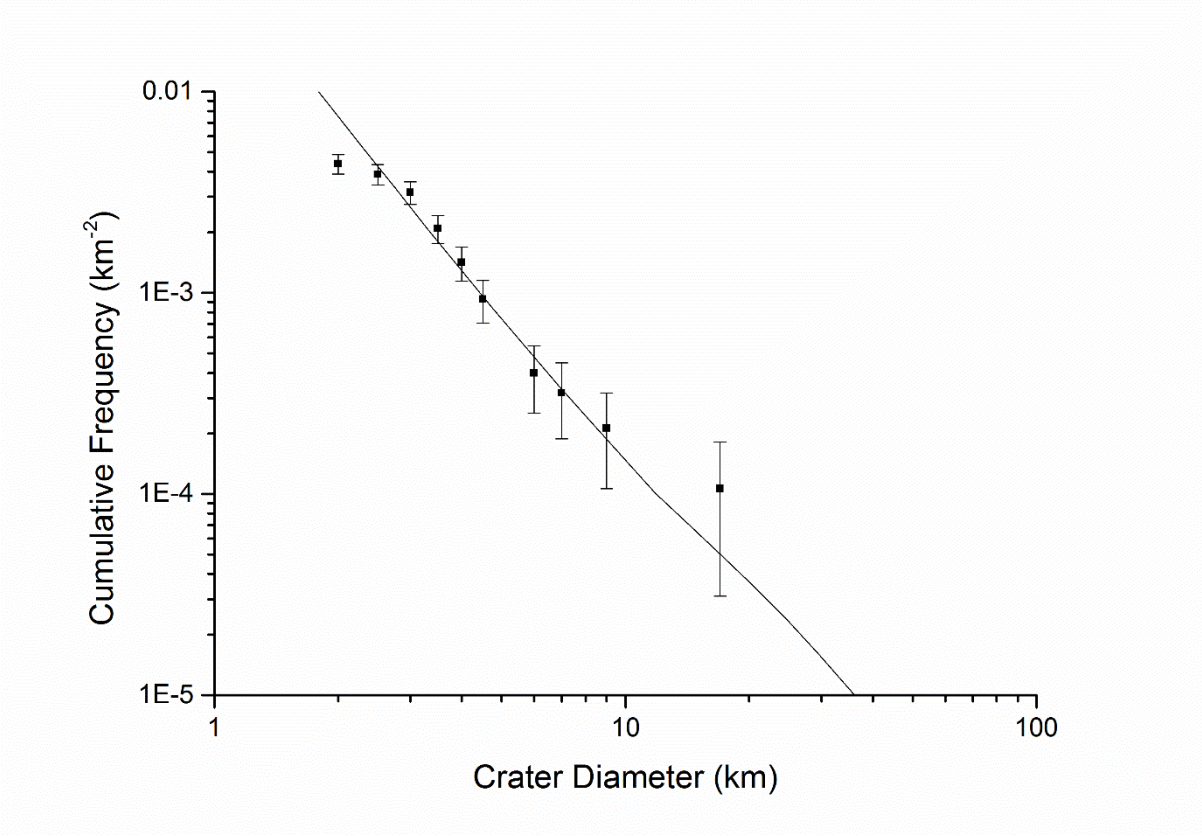

**A1j**: Marchi *et al.* (2009) MPF plot for the smooth plains unit of Khansa.

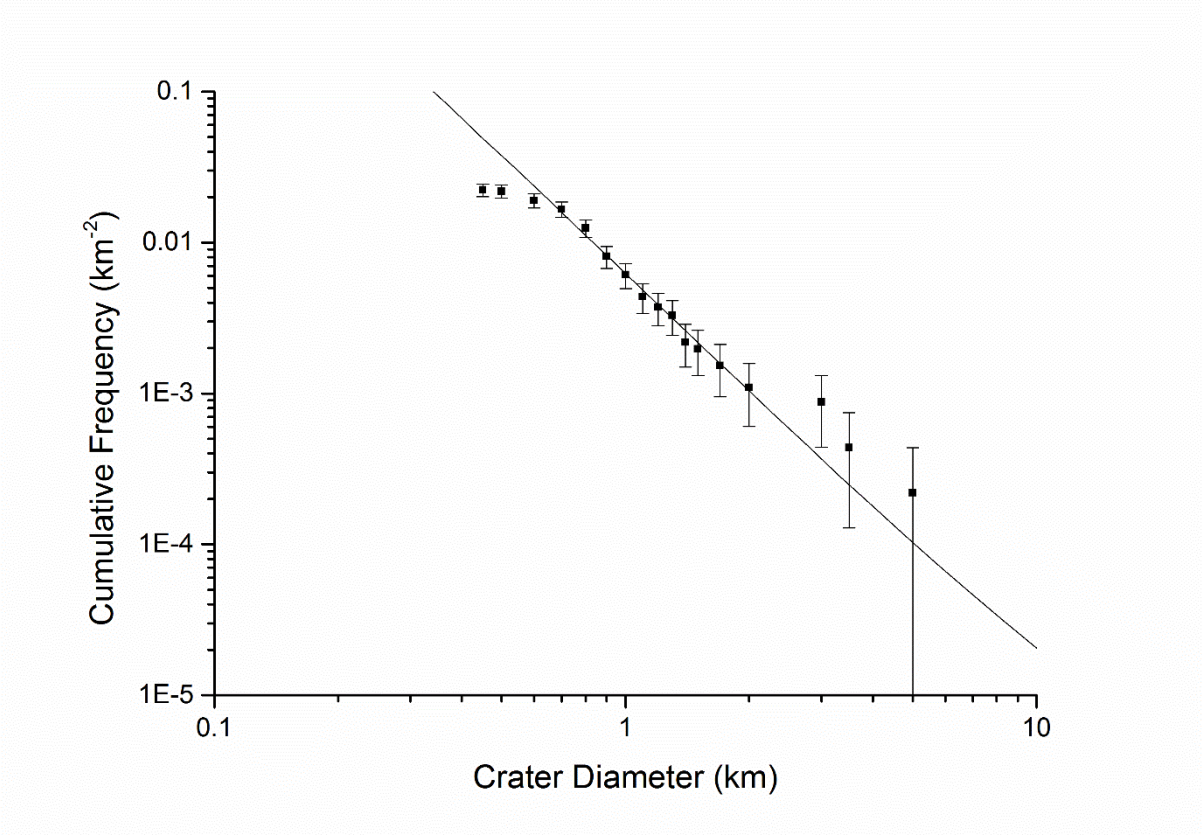

**A1k:** Marchi *et al*. (2009) MPF plot for the smooth plains unit of Copland.

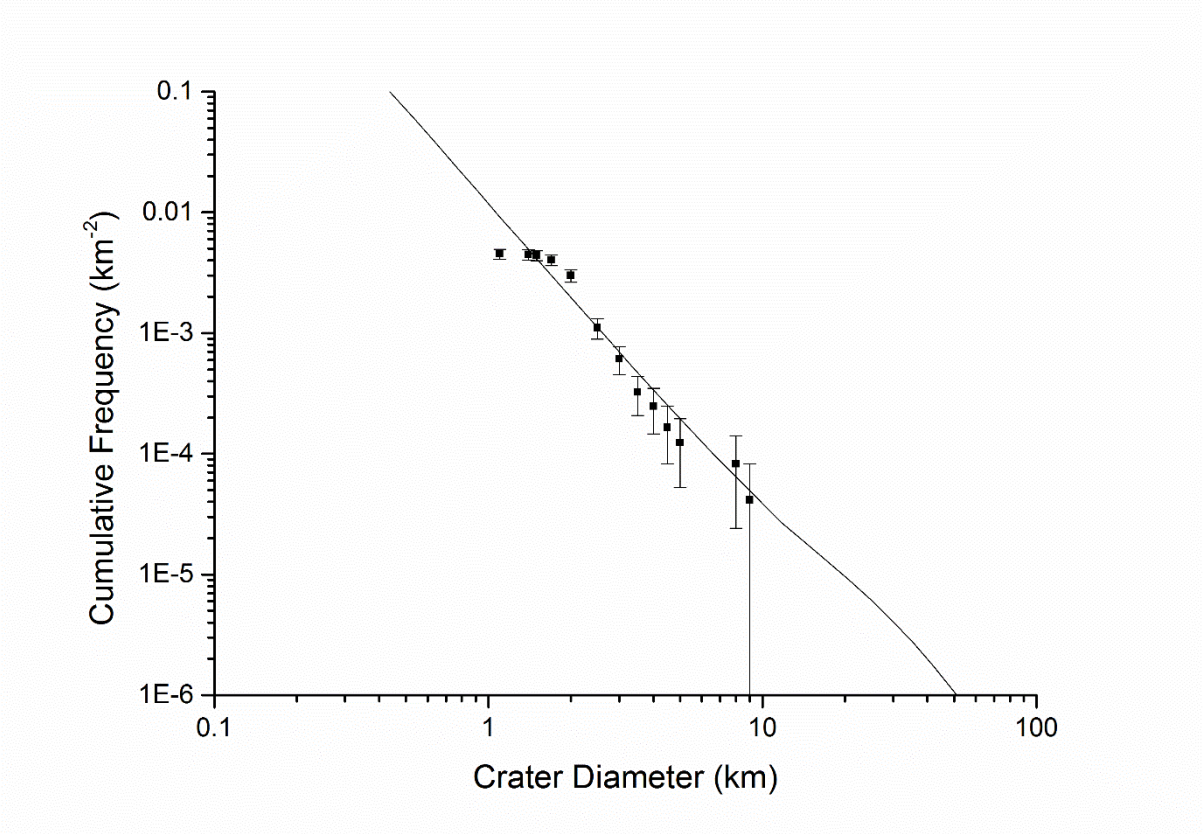

**A1l:** Marchi *et al.* (2009) MPF plot for the smooth plains unit of Unnamed [-166,-25].

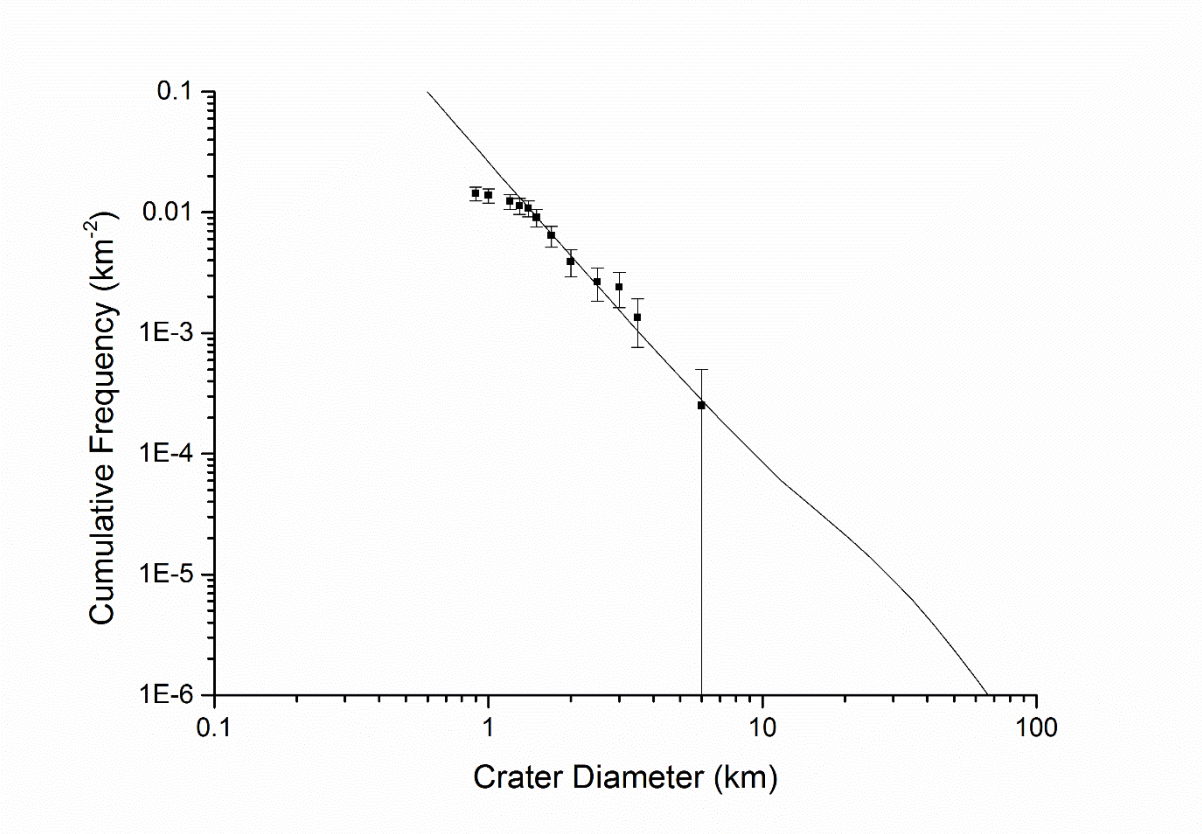

**A1m:** Marchi *et al.* (2009) MPF plot for the smooth plains unit of Unnamed [154,67].

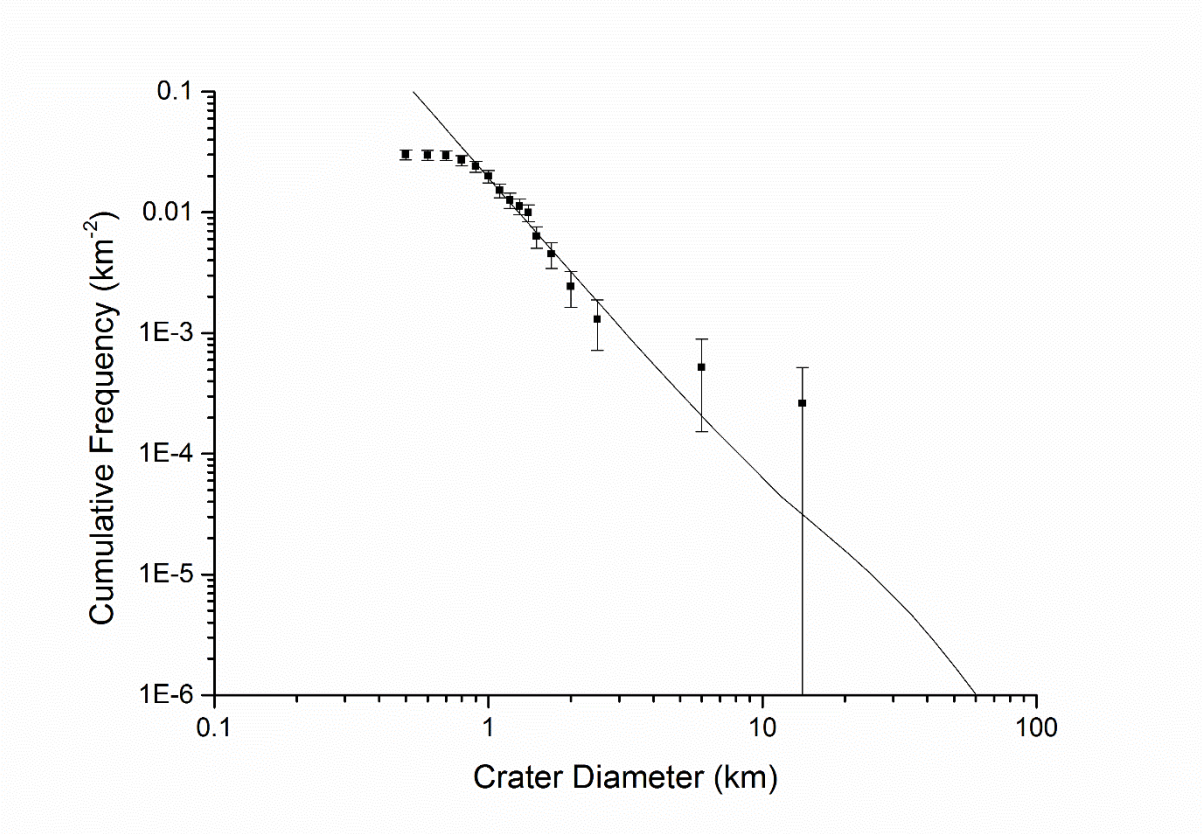

**A1n:** Marchi *et al.* (2009) MPF plot for the smooth plains unit of Unnamed [-69,0].

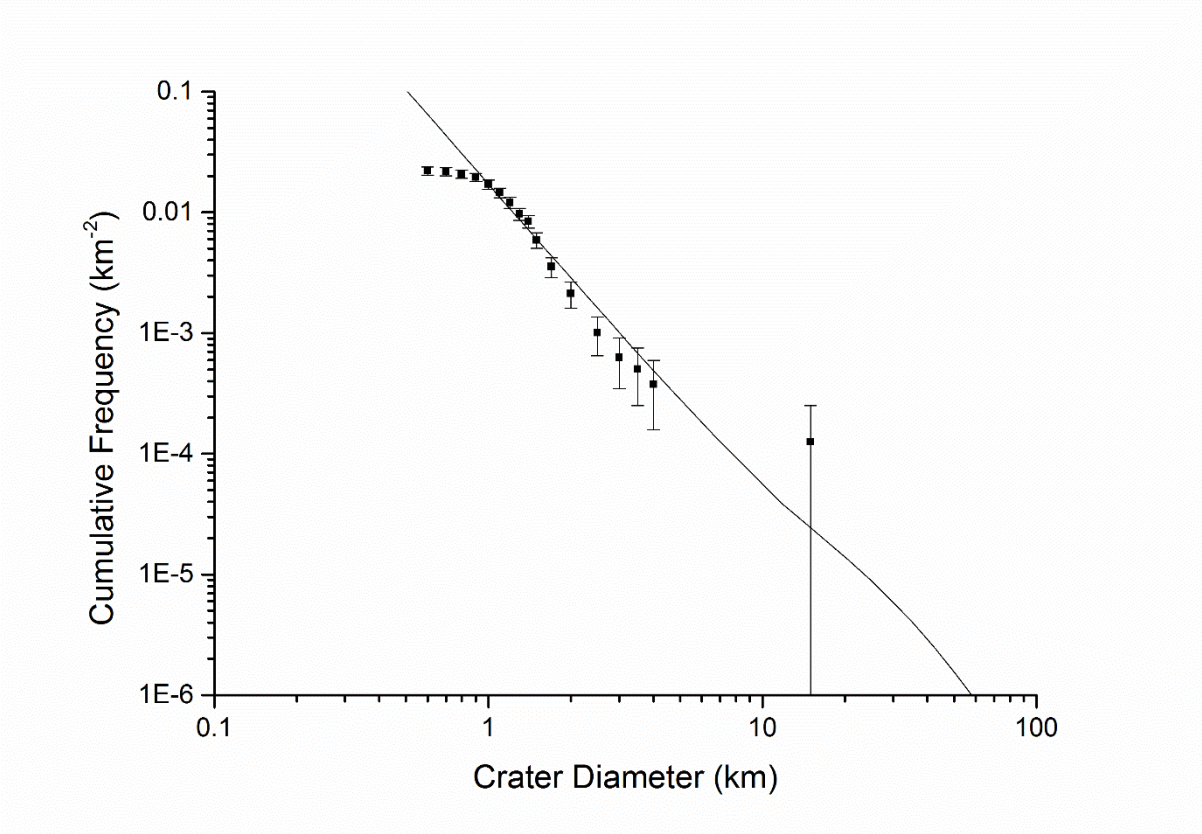

**A1o:** Marchi *et al.* (2009) MPF plot for the smooth plains unit of Unnamed [-13,-22].

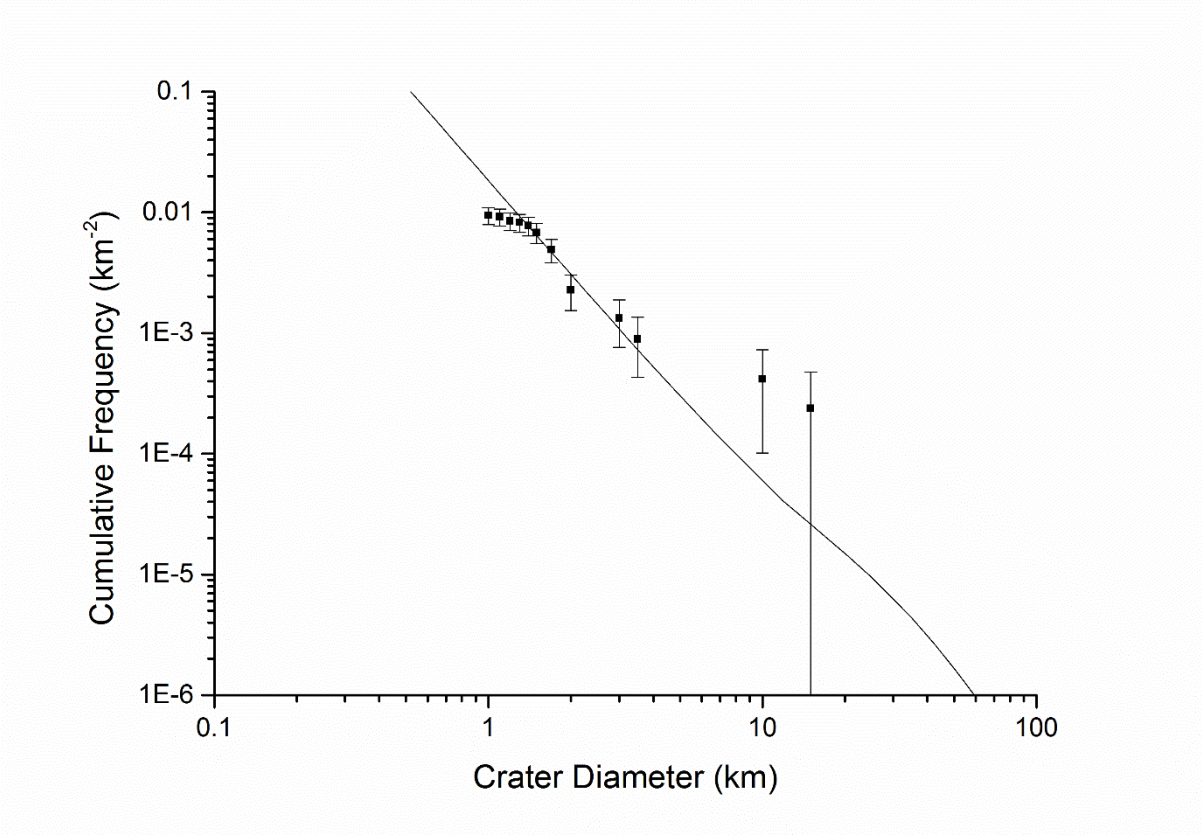

## Appendix 2

Model production function (MPF) plots for the model ages presented in Chapter 3 Table 3.1.

**A2a**: Neukum *et al.* (2001) MPF plot for the smooth plains unit (green) and basin-edge scarp (red) of Beethoven.

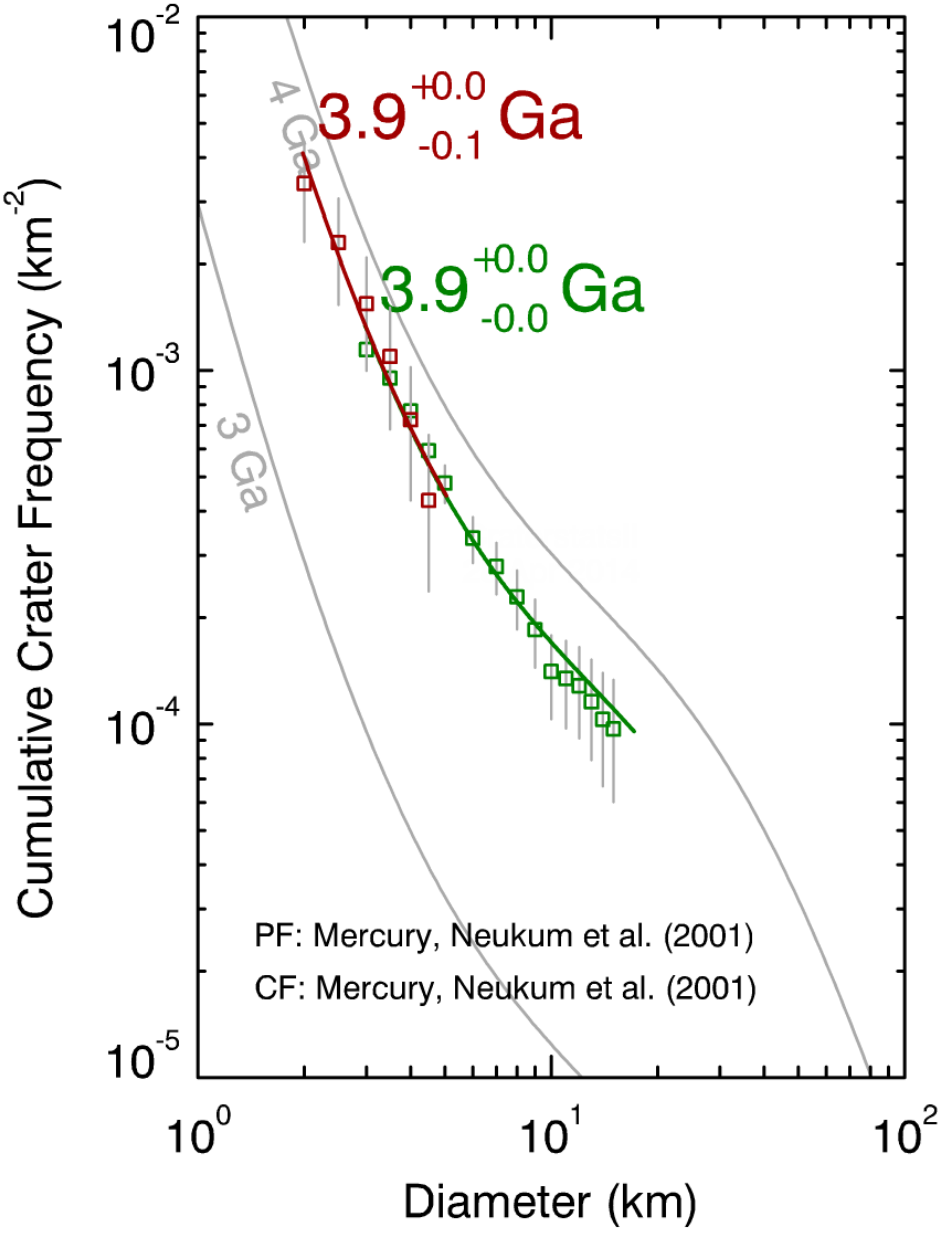

**A2b**: Neukum *et al.* (2001) MPF plot for the smooth plains unit (black) and basin-edge scarp (red) of Hafez.

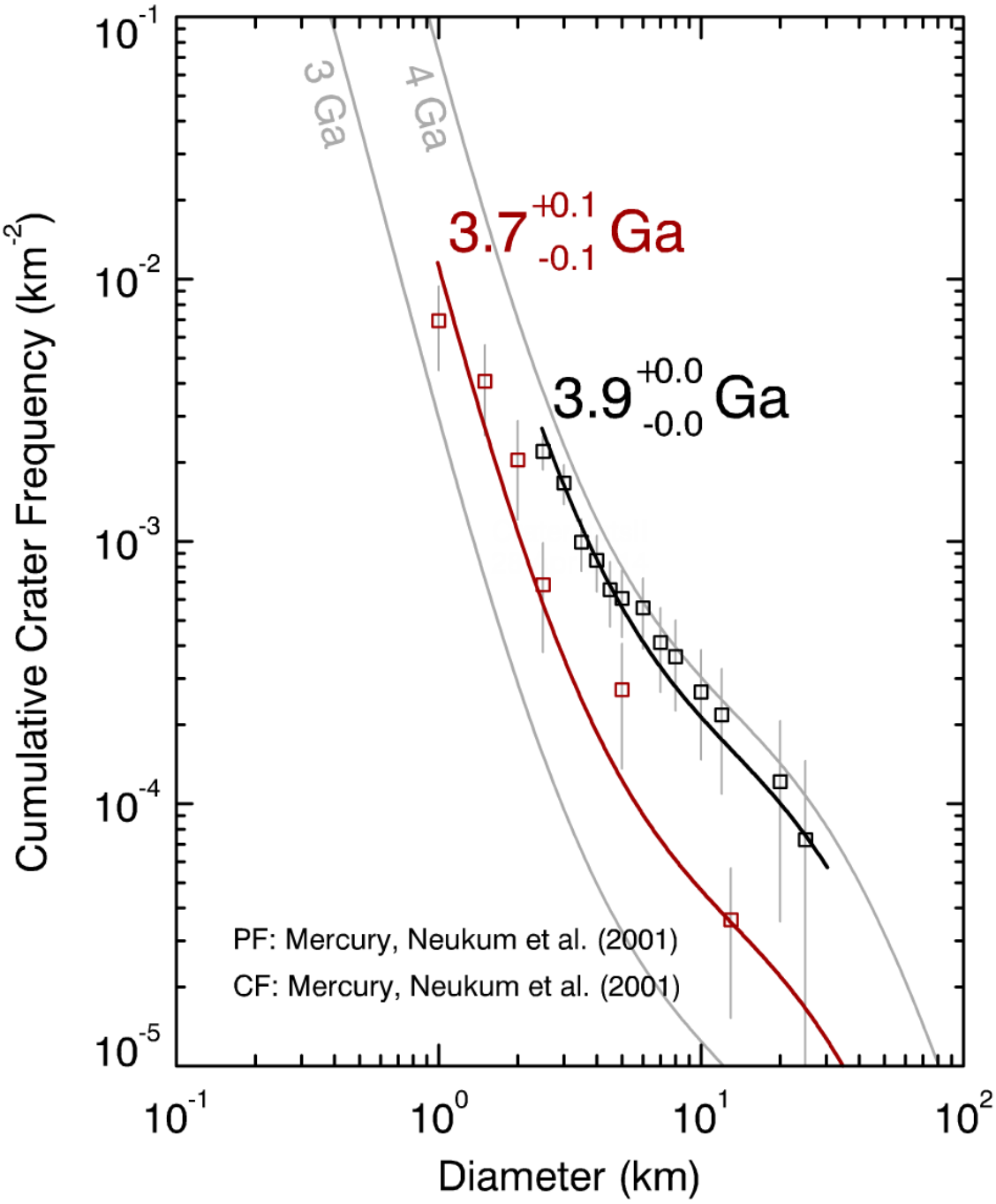

**A2c:** Neukum *et al.* (2001) MPF plot for the smooth plains unit (black) and basin-edge scarp (red) of Shakespeare.

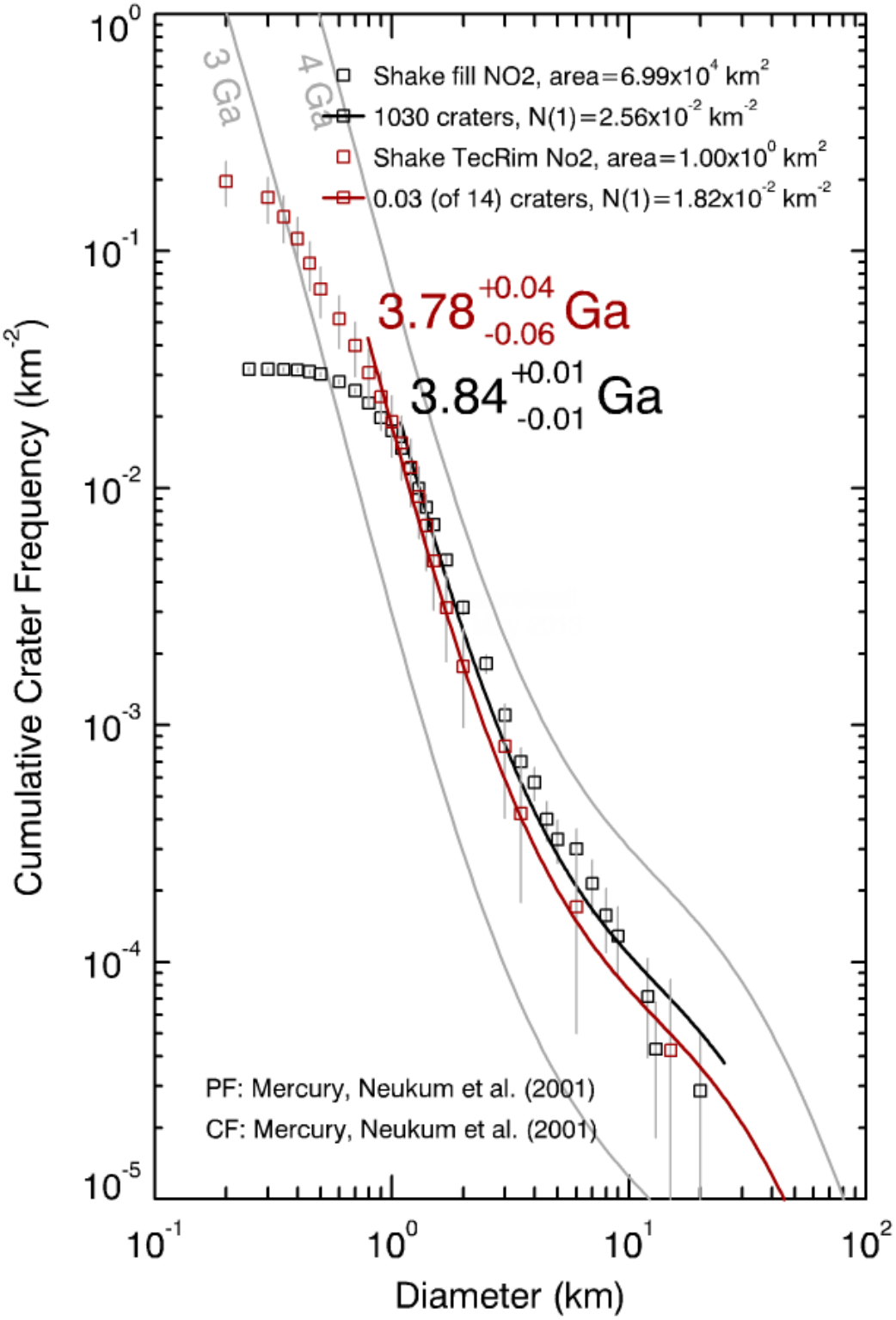

**A2d:** Neukum *et al.* (2001) MPF plot for the smooth plains unit (black) and basin-edge scarp (red) of Shevchenko.

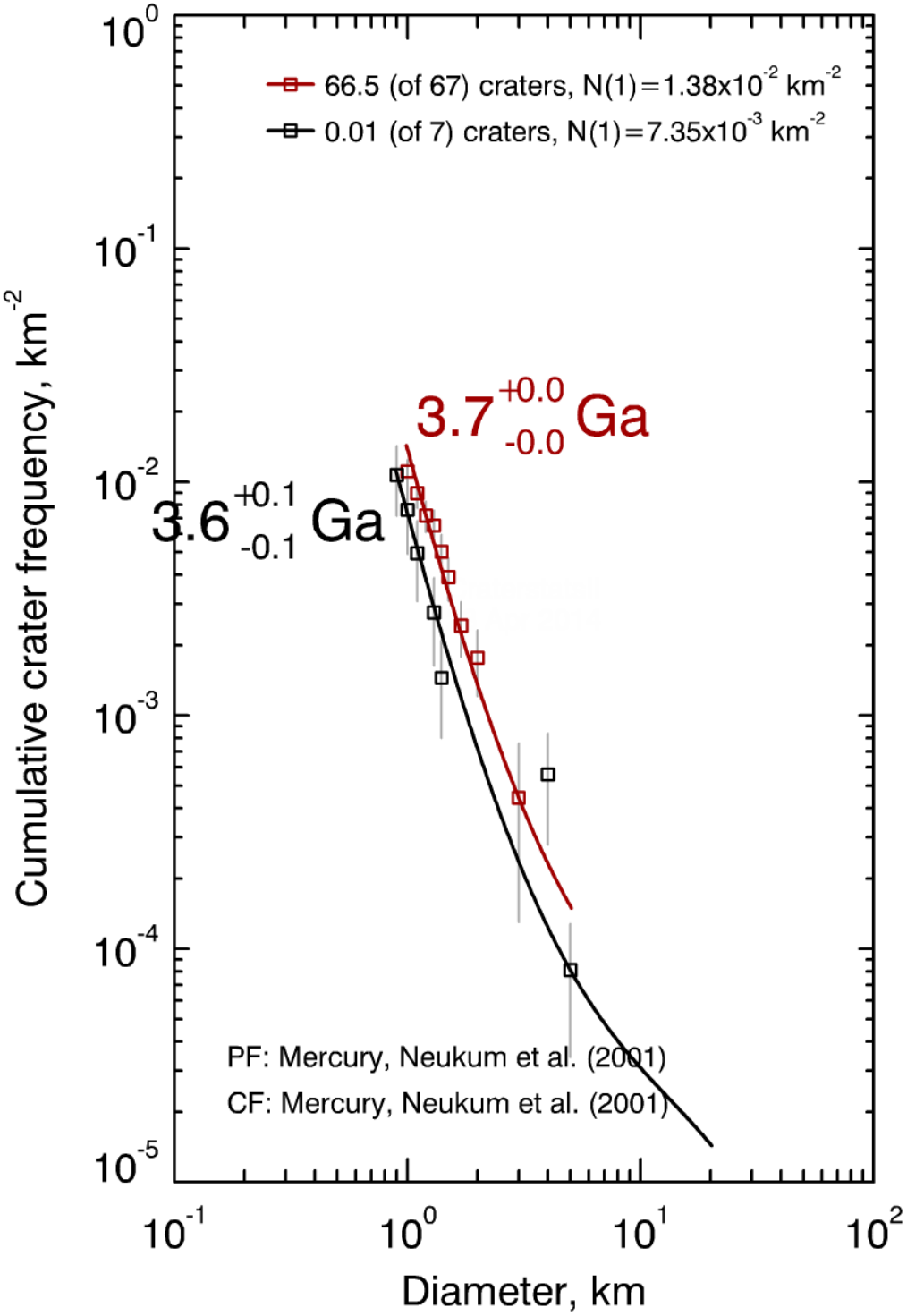

**A2e**: Neukum *et al.* (2001) MPF plot for the smooth plains unit (black) and basin-edge scarp (red) of Unnamed [40°S, 70°W].

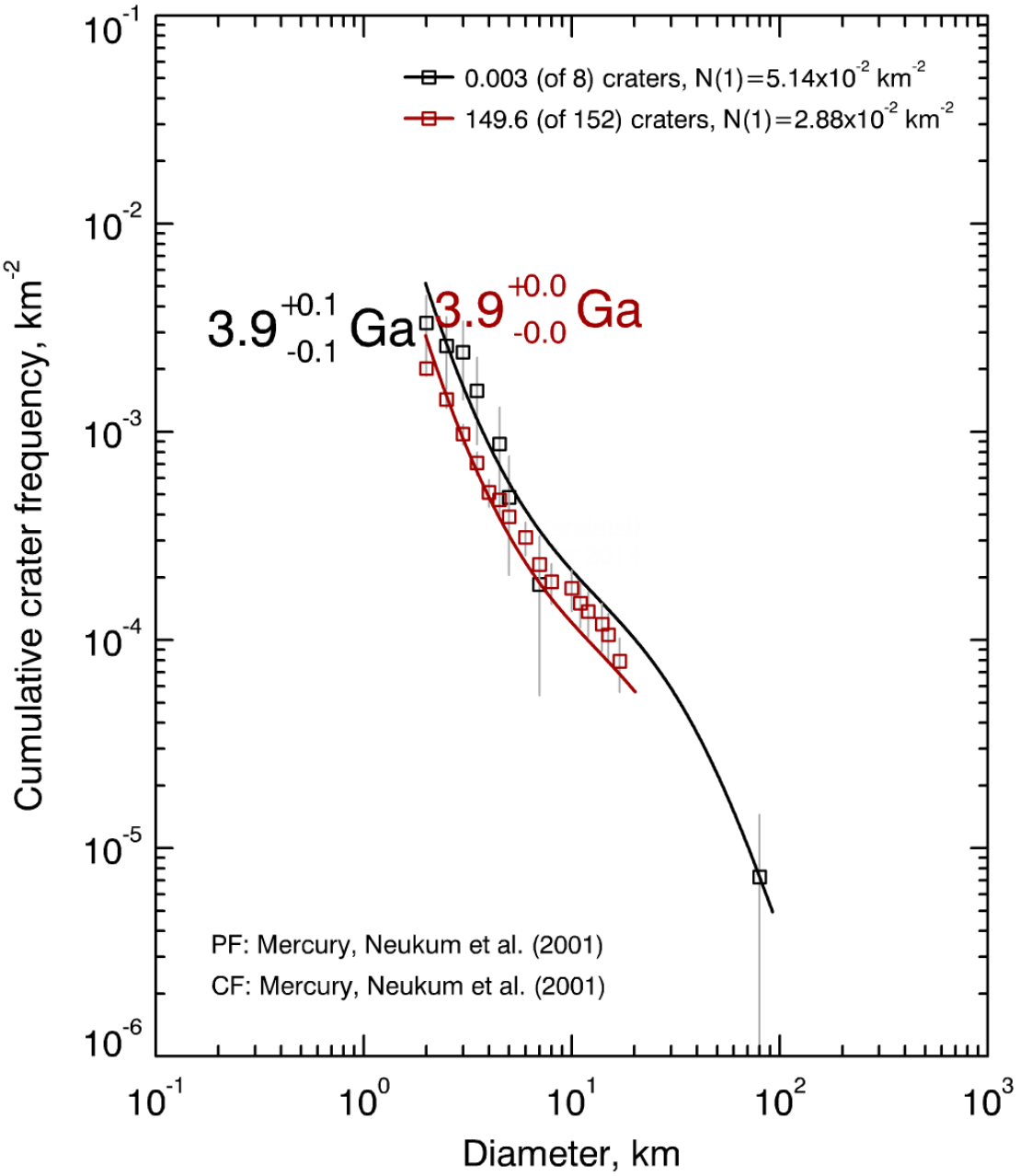

**A2f**: Neukum *et al.* (2001) MPF plot for the smooth plains unit (black) and basin-edge scarp (red) of Unnamed [91°N, 38°E].

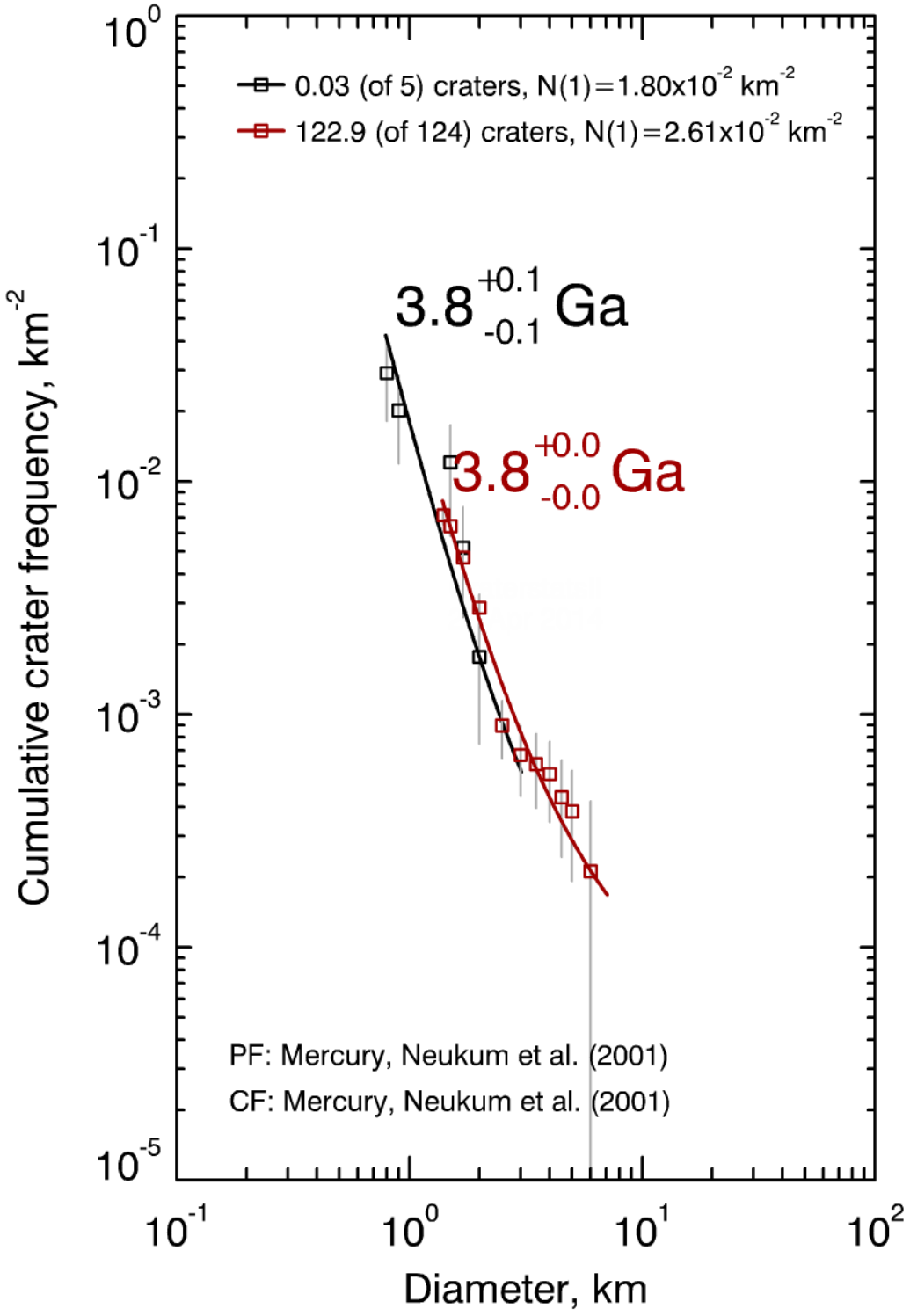

**A2g**: Neukum *et al.* (2001) MPF plot for the smooth plains unit (black) and basin-edge scarp (red) of Unnamed [91°N, 38°E].

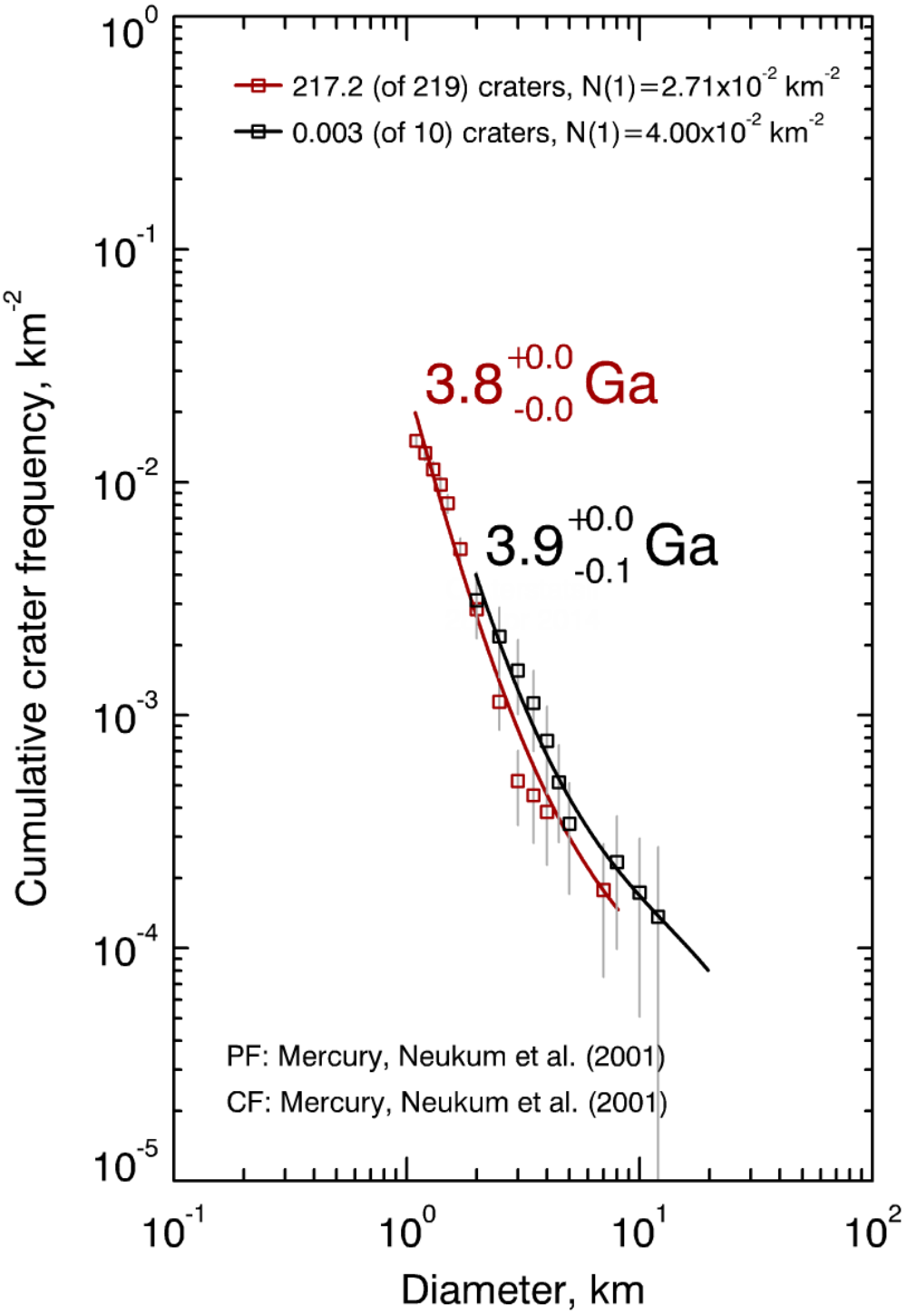

**A2h**: Neukum *et al.* (2001) MPF plot for the smooth plains unit (black) and basin-edge scarp (red) of Unnamed [150°N, 10°W].

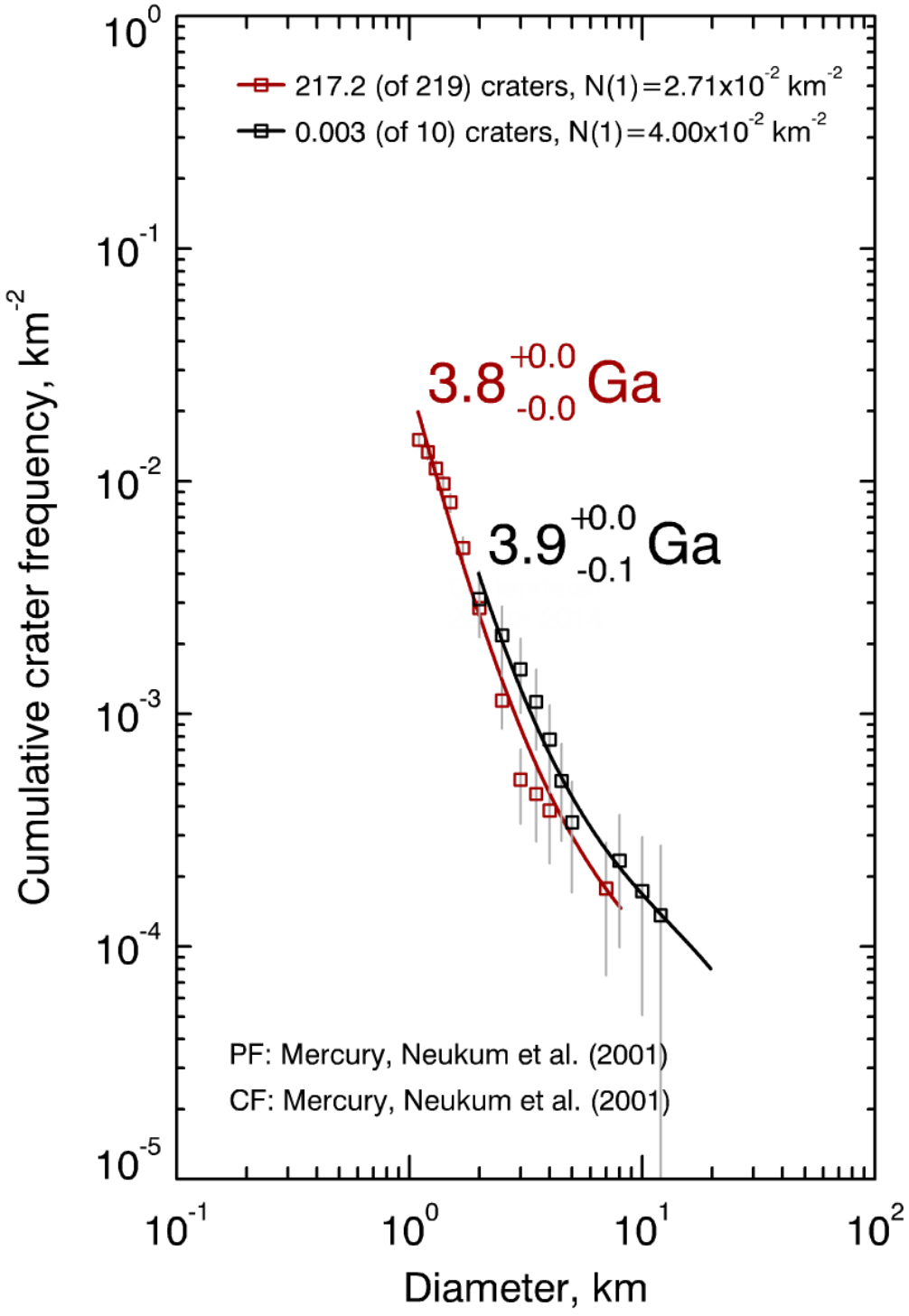

## Appendix 3

Le Feuvre & Wieczorek (2011) (LeF&W) Model production function (MPF) plots for the model ages presented in Chapter 3 Table 3.2 – using porous scaling.

**A3a**: LeF&W MPF porous scaling results for Beethoven, black indicates the smooth plains, red indicates the basin-edge scarp.

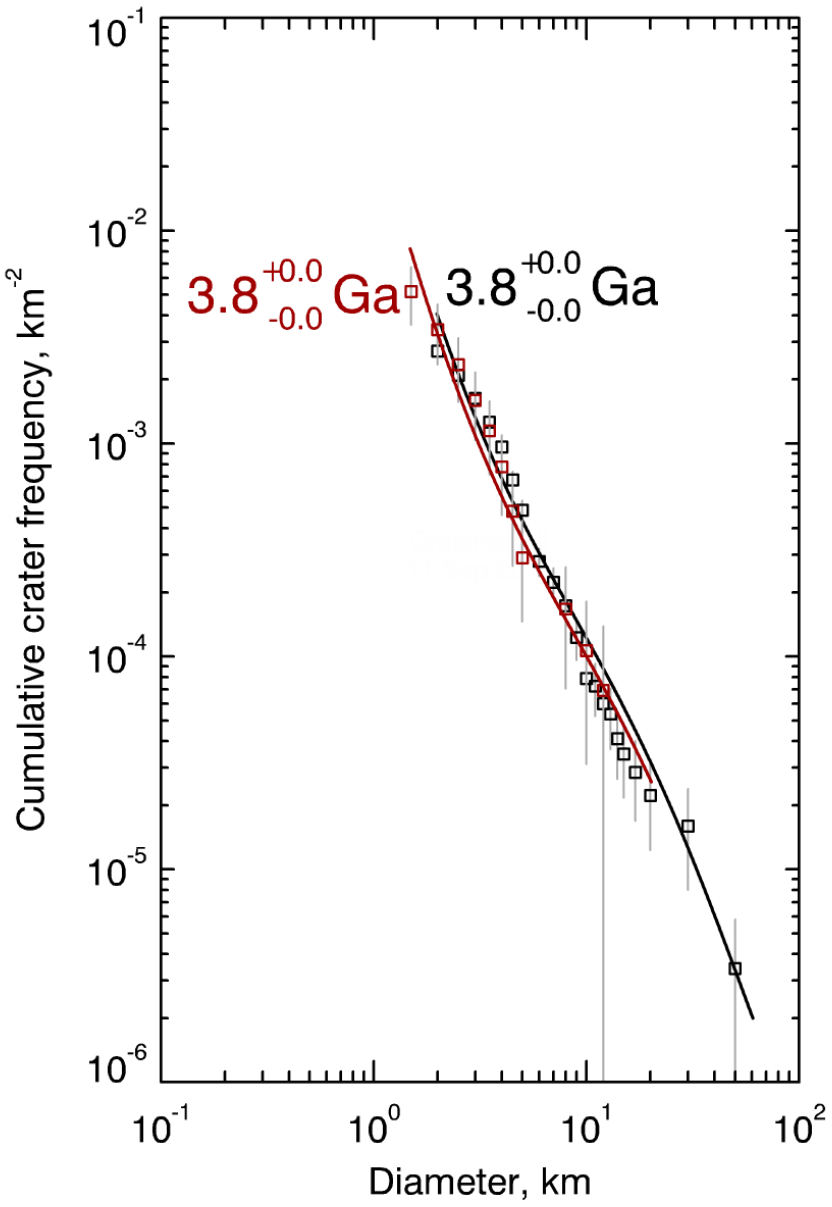

**A3b**: LeF&W MPF porous scaling results for Hafiz, black indicates the smooth plains, red indicates the basin-edge scarp.

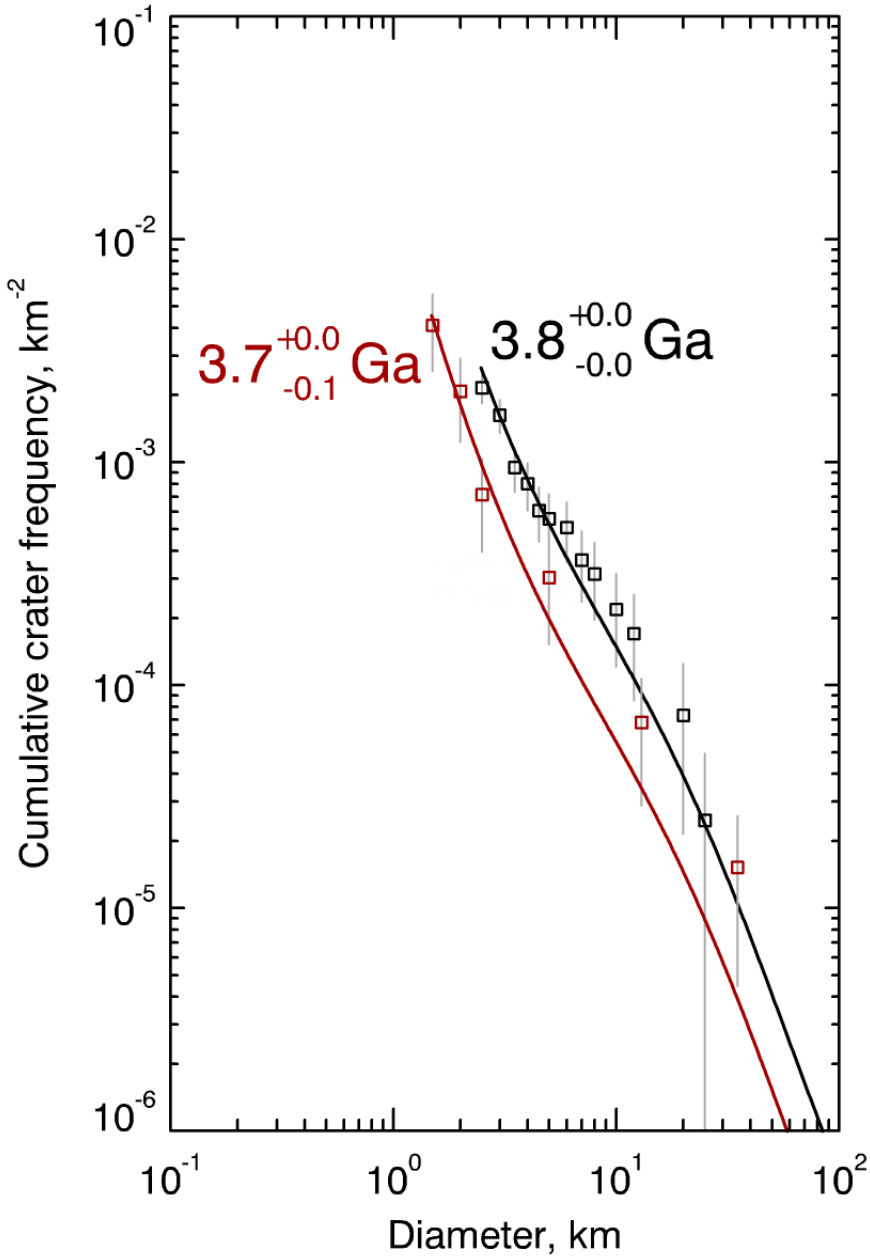

**A3c**: LeF&W MPF porous scaling results for Shakespeare, black indicates the smooth plains, red indicates the basin-edge scarp.

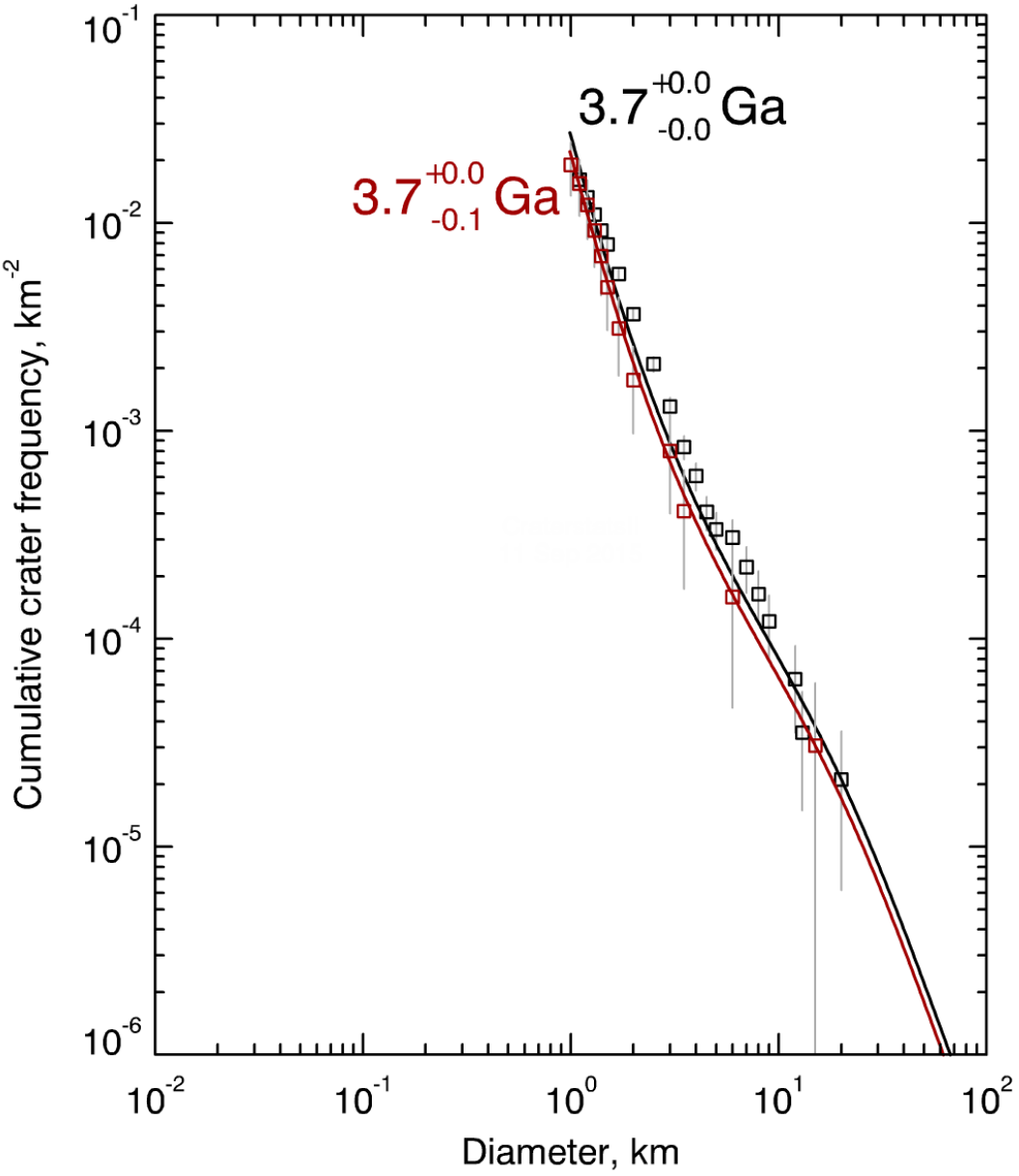

**A3d**: LeF&W MPF porous scaling results for Shevchenko, black indicates the smooth plains, red indicates the basin-edge scarp.

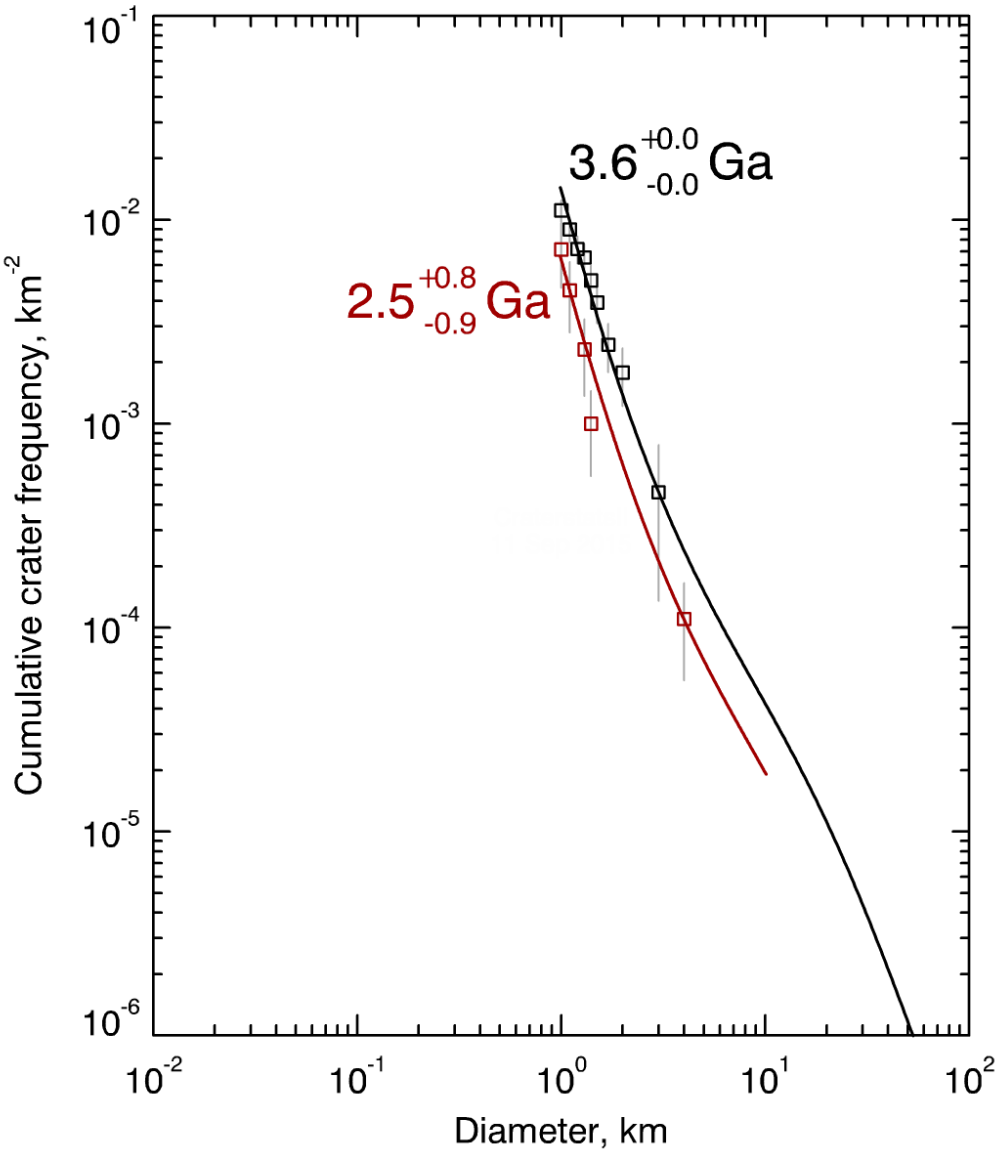

**A3e**: LeF&W MPF porous scaling results for Unnamed [-40,-70], black indicates the smooth plains, red indicates the basin-edge scarp.

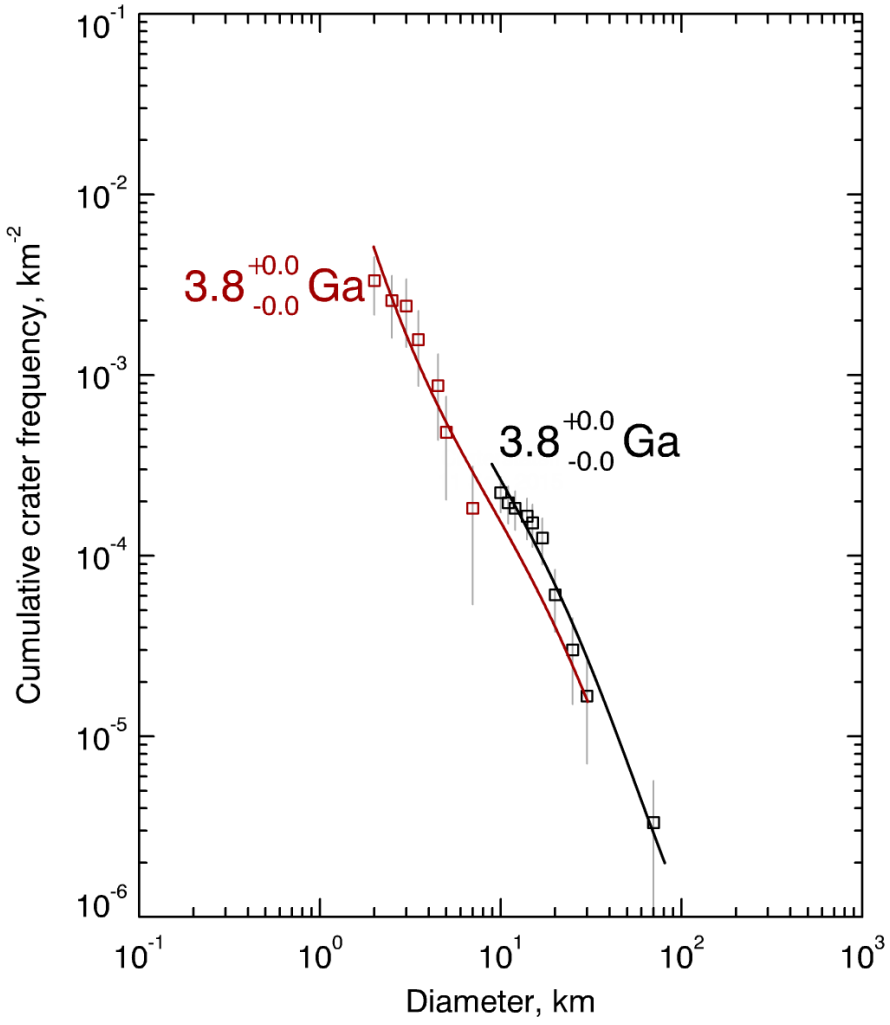

**A3f**: LeF&W MPF porous scaling results for Unnamed [91,38], black indicates the smooth plains, red indicates the basin-edge scarp.

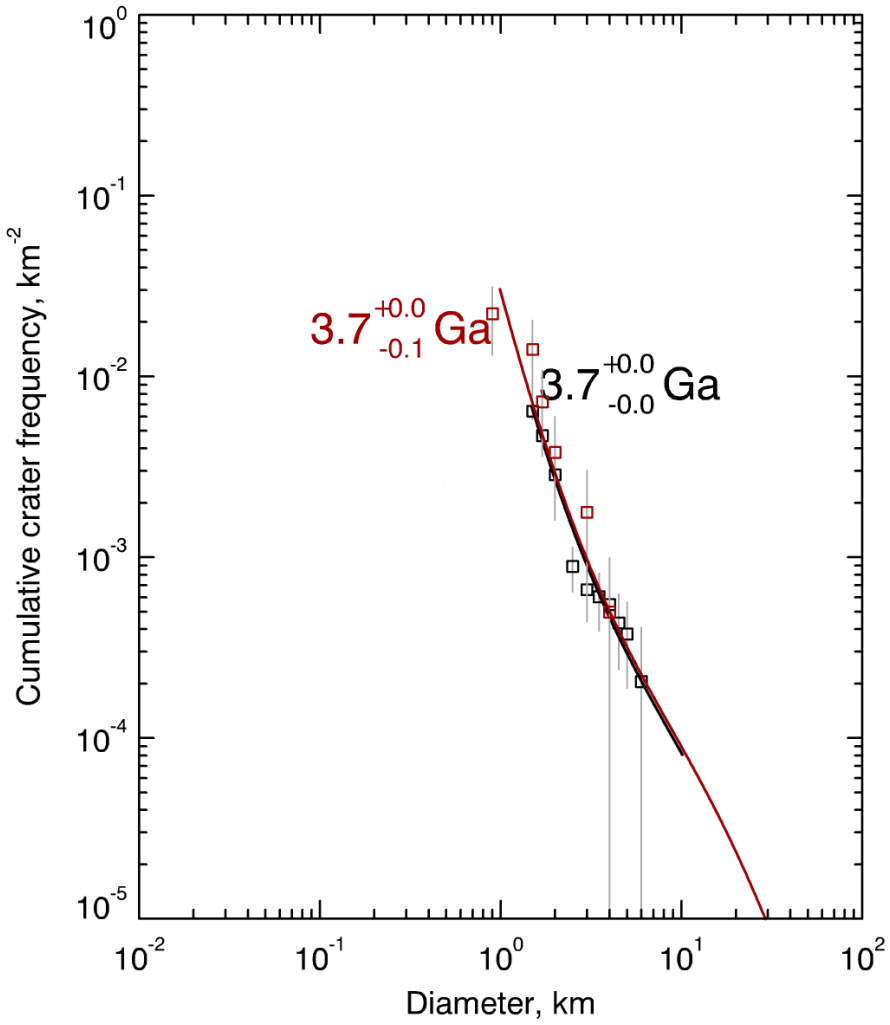

**A3g**: LeF&W MPF porous scaling results for Unnamed [150,-10], black indicates the smooth plains, red indicates the basin-edge scarp.

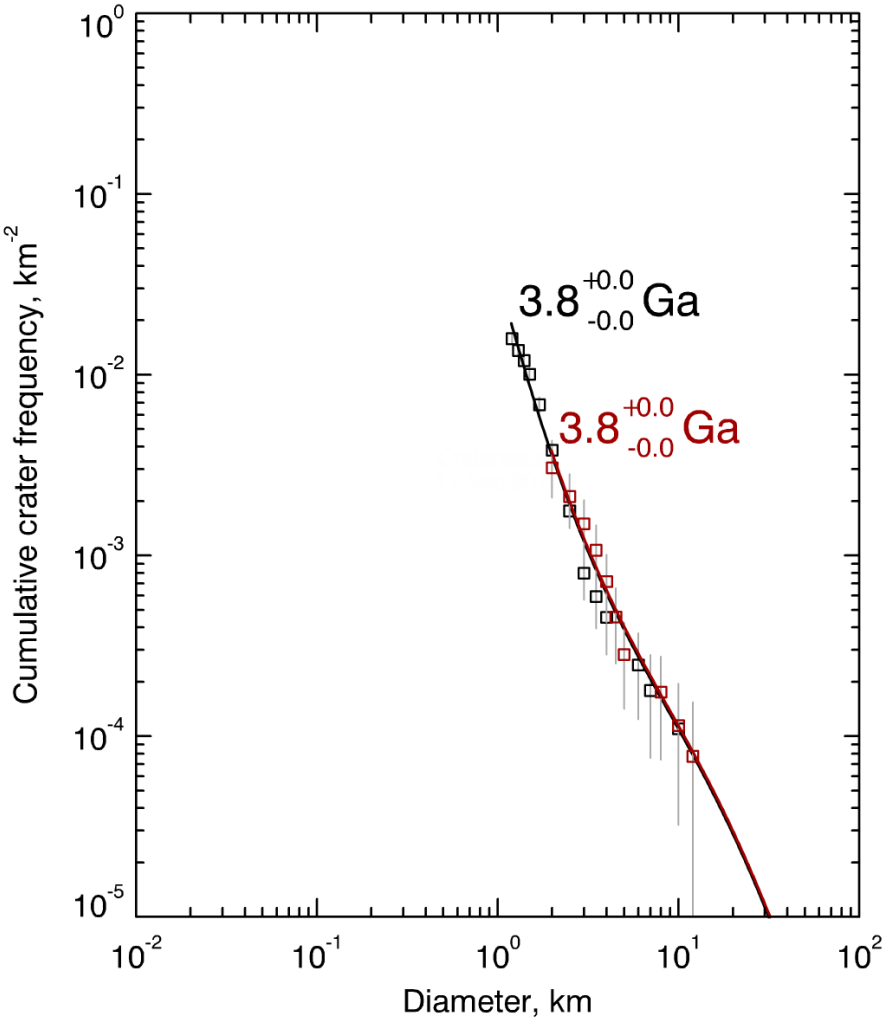

## Appendix 4

Le Feuvre & Wieczorek (2011) (LeF&W) Model production function (MPF) plots for the model ages presented in Chapter 3 Table 3.2 – using non-porous scaling.

**A4a**: LeF&W MPF non-porous scaling results for Beethoven, black indicates the smooth plains, red indicates the basin-edge scarp.

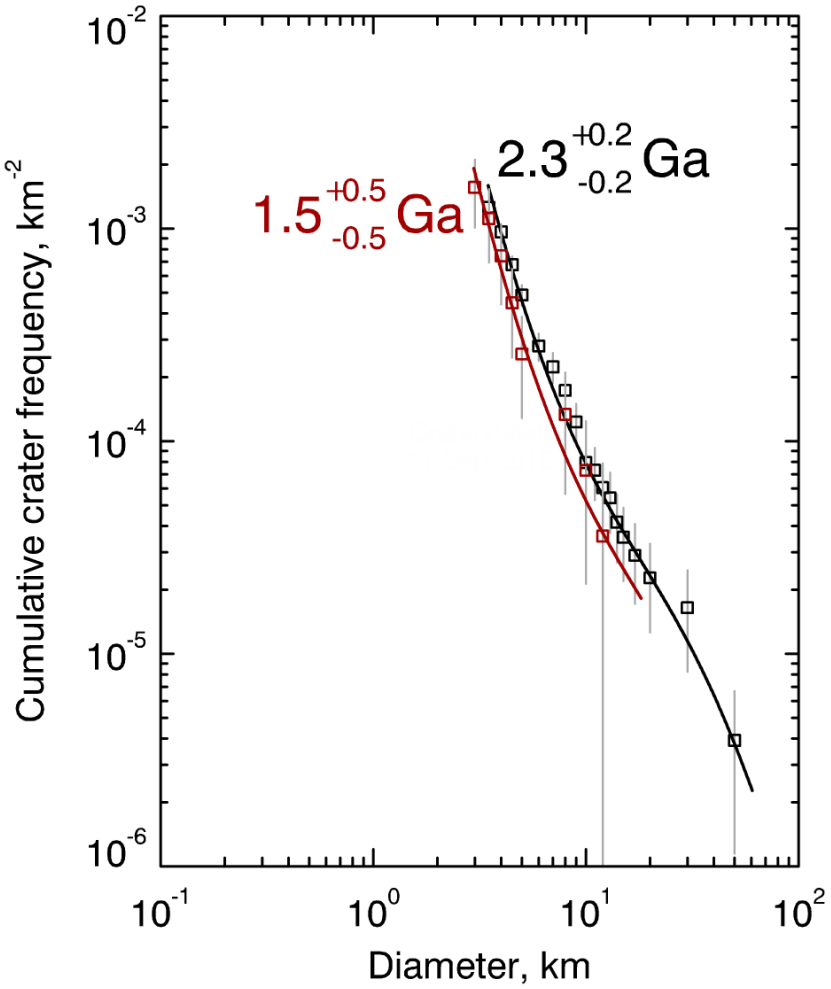

**A4b**: LeF&W MPF non-porous scaling results for Hafiz, black indicates the smooth plains, red indicates the basin-edge scarp.

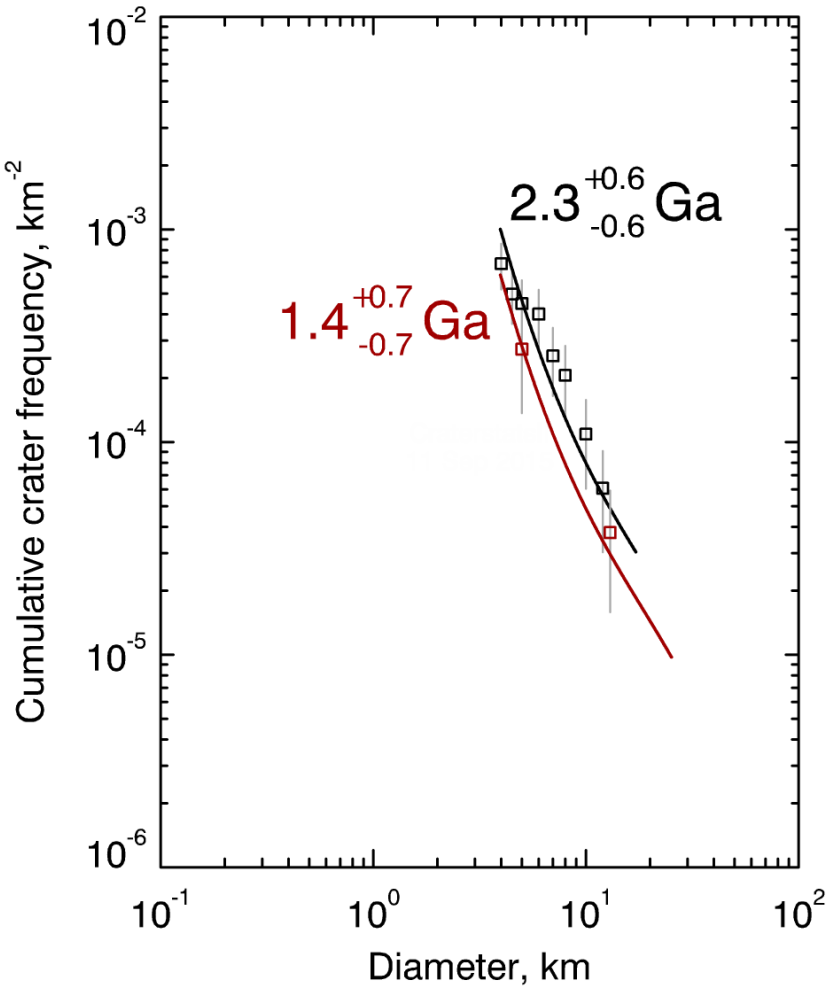

**A4c**: LeF&W MPF non-porous scaling results for Shakespeare, black indicates the smooth plains, red indicates the basin-edge scarp.

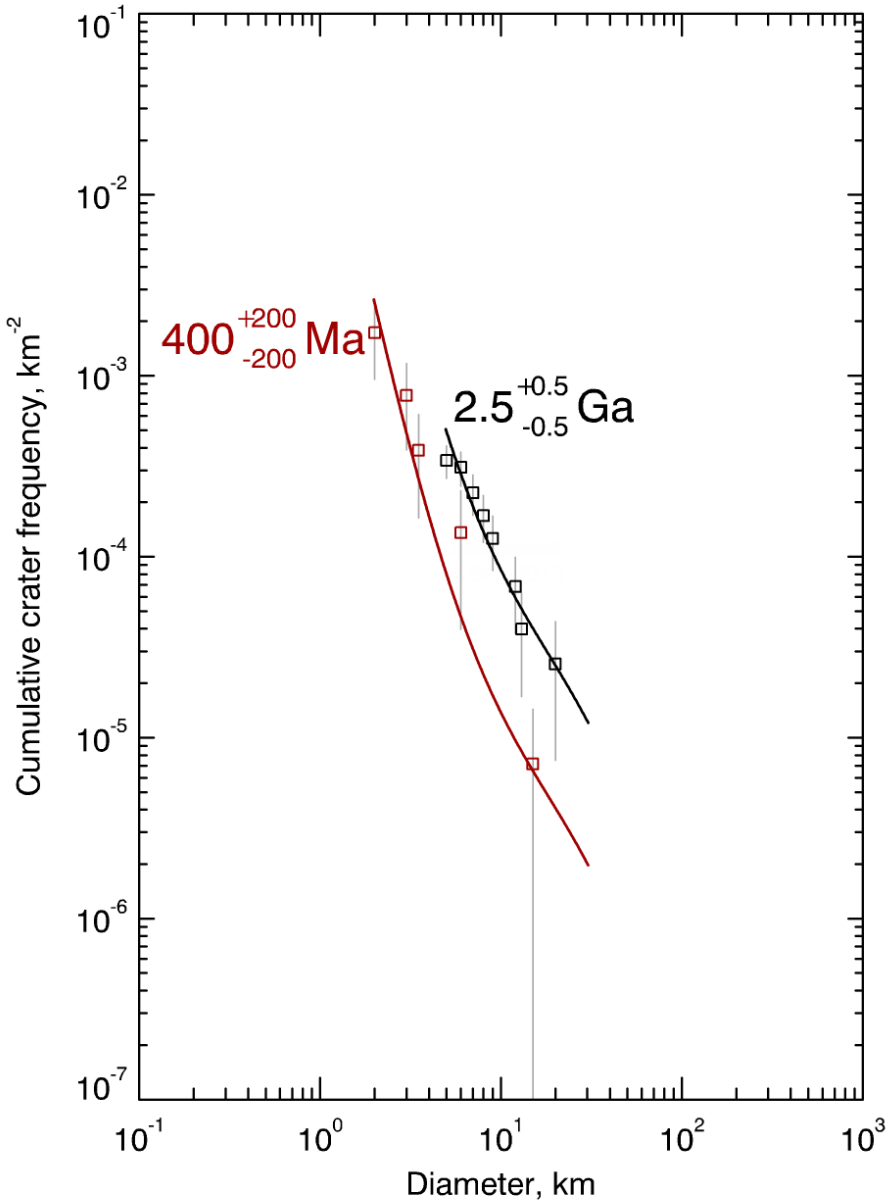

**A4d**: LeF&W MPF non-porous scaling results for Shevchenko, black indicates the smooth plains, red indicates the basin-edge scarp.

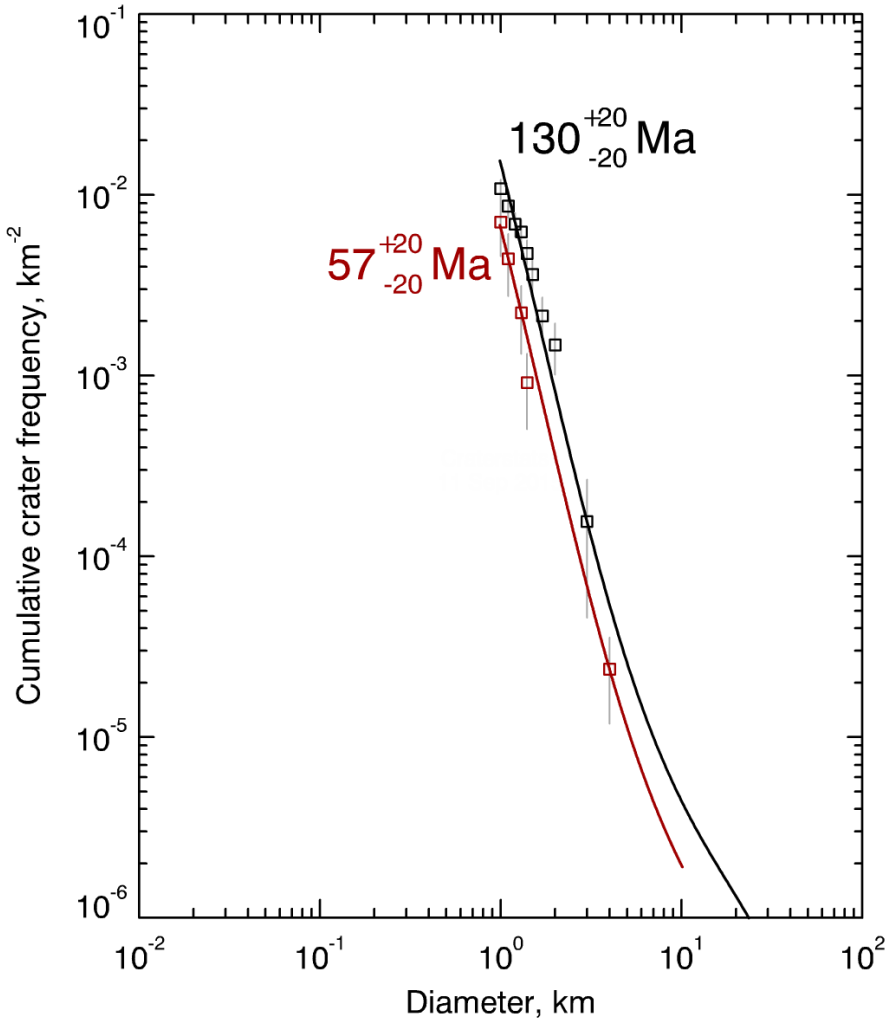

**A4e**: LeF&W MPF non-porous scaling results for Unnamed [-40,-70], black indicates the smooth plains, red indicates the basin-edge scarp.

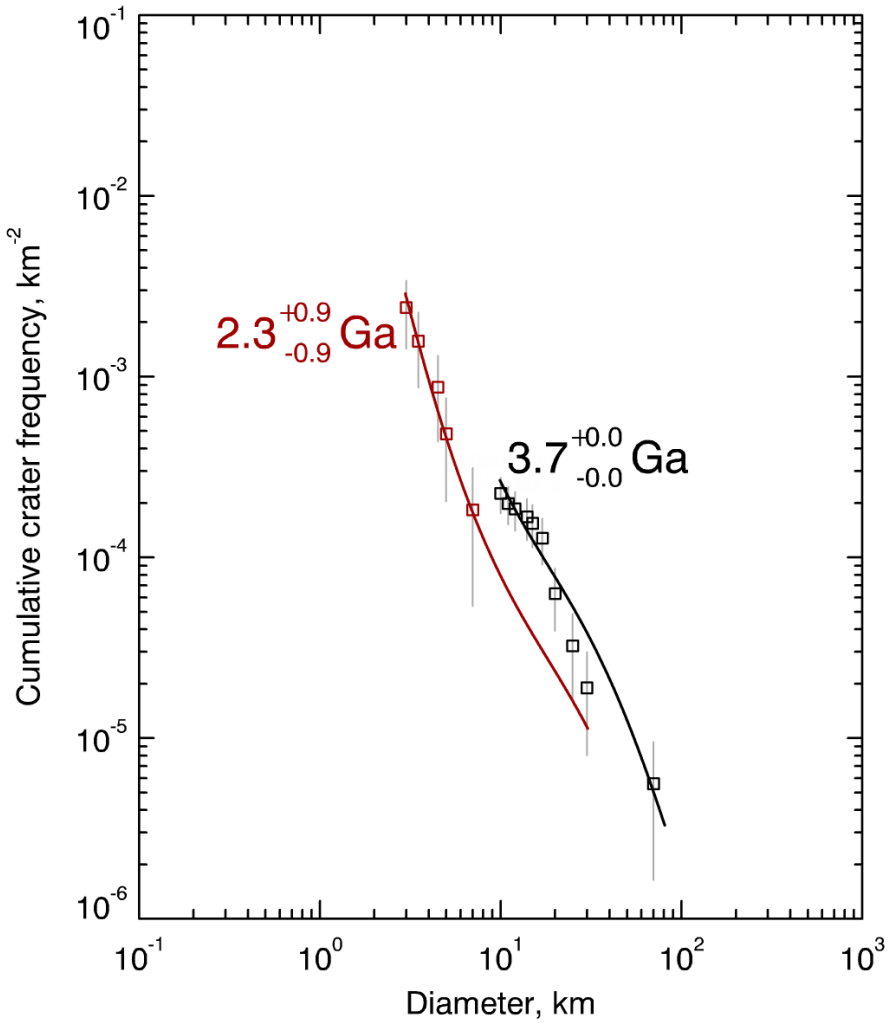

**A4f**: LeF&W MPF non-porous scaling results for Unnamed [91,38], black indicates the smooth plains, red indicates the basin-edge scarp.

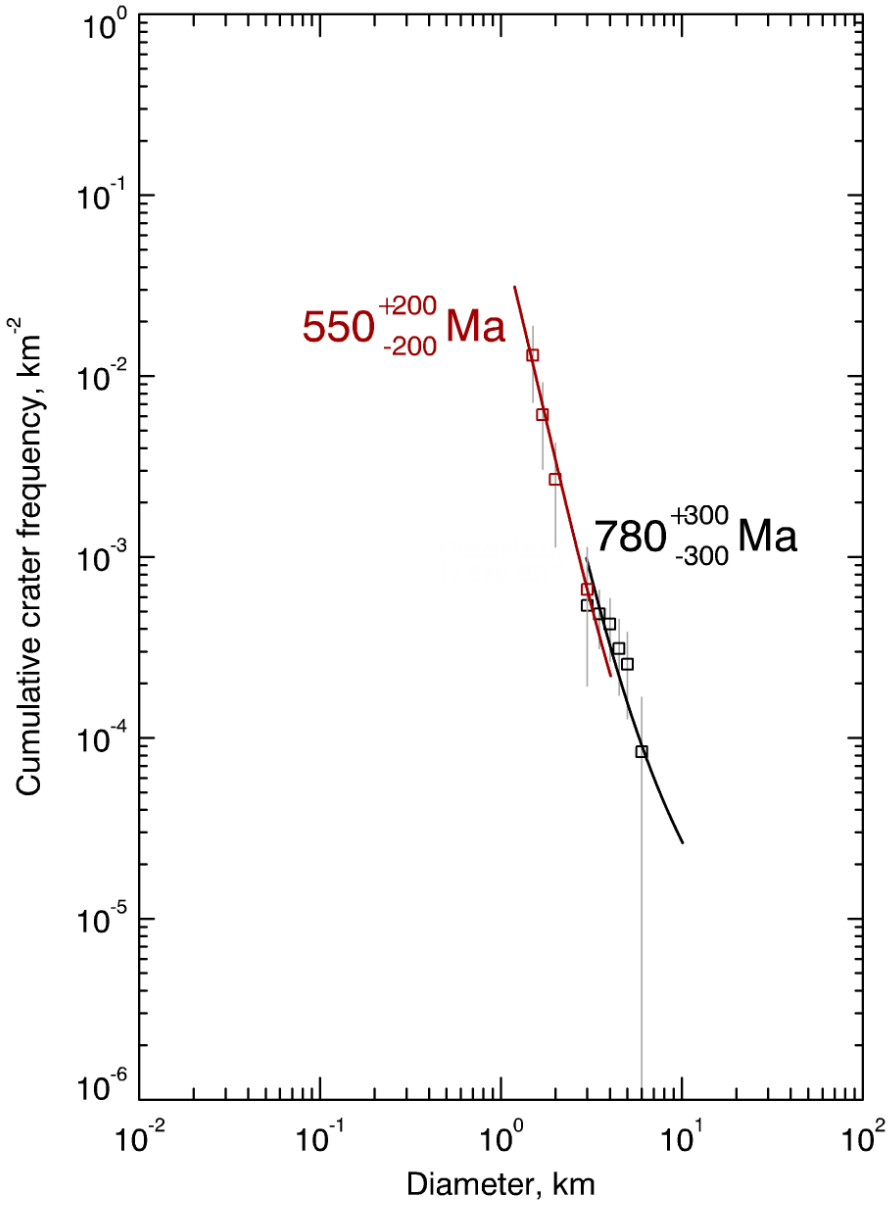

**A4g**: LeF&W MPF non-porous scaling results for Unnamed [150,-10], black indicates the smooth plains, red indicates the basin-edge scarp.

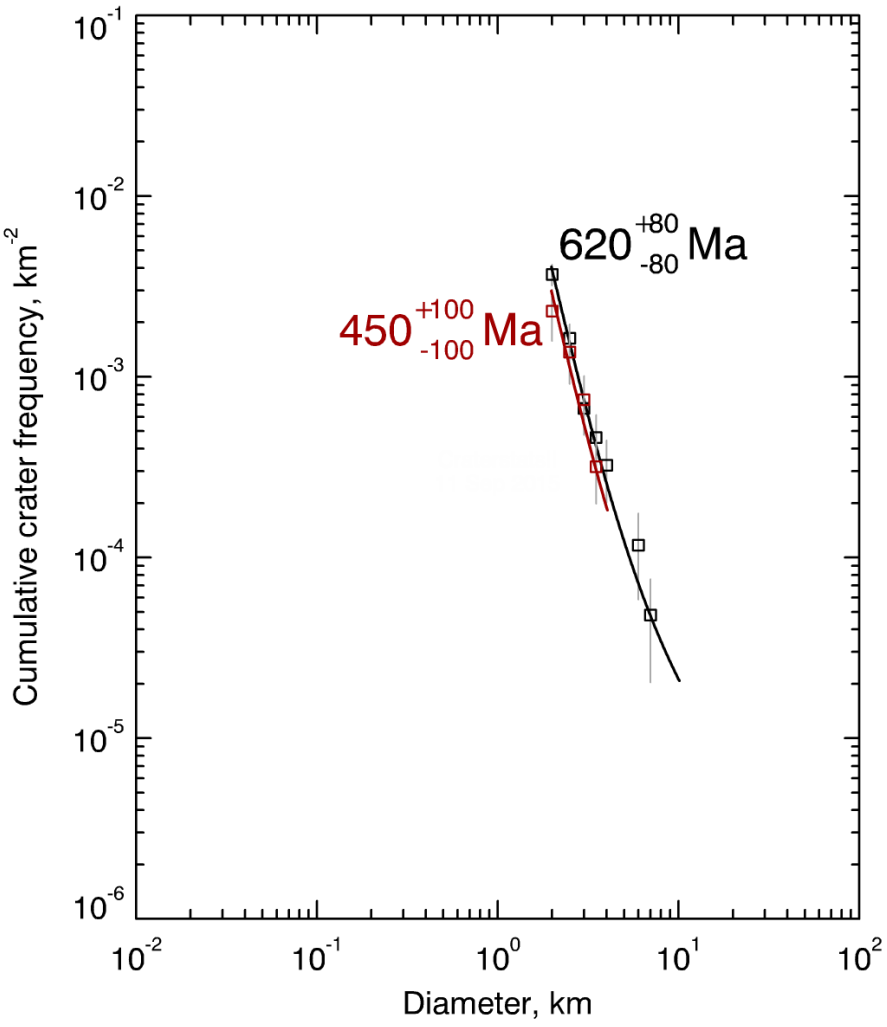

## Appendix 5

The shapefile I created during my global survey of catenae (the red lines seen on the image below) can be found on ORDO open access system: https://ou.figshare.com/. The contents of the attribute table of the shapefile are printed in this Appendix, detailing the categorisation of catenae depending on the following:

"Clear secondary": whether they are clear secondary impact crater chains (0 if not, 1 if so, and 2 if it is not possible to determine)

"Crater at end": whether the last crater in the catenae (at either end) is more than double the width of the rest of the craters in the chain (0 if not, 1 if so).

"Kink/bend": whether the catena shows a noticeable bend or kink along its length (0 if not, 1 if so).

FID_ is the identifier for each catena, and mid-point latitude is the latitude (decimal degrees) for the middle of each catena.

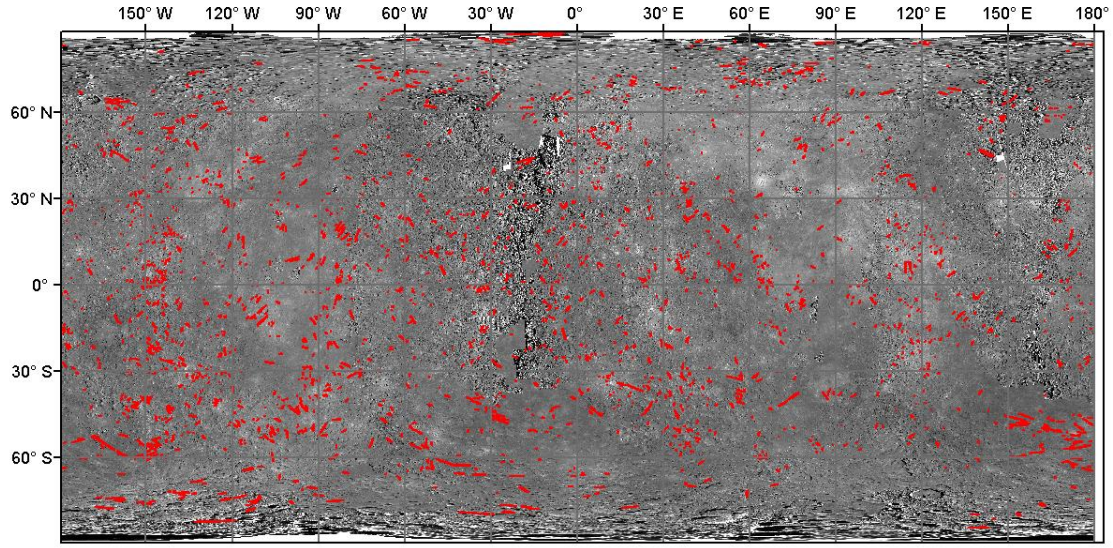


| FID_ | Clear secondary | crater at end | kink/bend | mid-point latitude |
|---|---|---|---|---|
| 0 | 1 | 1 | 0 | -11.47795392 |
| 1 | 1 | 0 | 0 | -51.31984609 |
| 2 | 1 | 0 | 0 | -51.55804388 |
| 3 | 2 | 1 | 0 | -6.154560799 |
| 4 | 2 | 0 | 0 | -40.00932173 |
| 5 | 2 | 0 | 0 | -52.75042369 |
| 6 | 1 | 0 | 0 | -5.040389662 |
| 7 | 1 | 0 | 1 | -77.94180235 |

| | | | | |
|---|---|---|---|---|
| 8 | 1 | 1 | 0 | -79.20391094 |
| 9 | 1 | 1 | 0 | -76.5608503 |
| 10 | 1 | 1 | 0 | -66.06927139 |
| 11 | 1 | 1 | 0 | -64.12233145 |
| 12 | 1 | 1 | 0 | -66.58930749 |
| 13 | 2 | 0 | 0 | 24.84167497 |
| 14 | 1 | 0 | 0 | -0.561119601 |
| 15 | 0 | 0 | 0 | 1.411680714 |
| 16 | 2 | 0 | 1 | -33.06756439 |
| 17 | 2 | 0 | 1 | -32.1893663 |
| 18 | 2 | 0 | 1 | -41.04275725 |
| 19 | 1 | 1 | 0 | 47.36202769 |
| 20 | 1 | 0 | 0 | -18.74258434 |
| 21 | 1 | 0 | 0 | 0.063132507 |
| 22 | 1 | 1 | 0 | 0.928768876 |
| 23 | 1 | 1 | 0 | 1.344106523 |
| 24 | 1 | 0 | 0 | -20.44110038 |
| 25 | 1 | 1 | 1 | -20.75527033 |
| 26 | 1 | 0 | 0 | -17.93386507 |
| 27 | 1 | 0 | 0 | -10.83220677 |
| 28 | 1 | 0 | 0 | 8.650877182 |
| 29 | 1 | 0 | 0 | 10.55615119 |
| 30 | 1 | 0 | 0 | 37.20499712 |
| 31 | 0 | 0 | 1 | 29.63604824 |
| 32 | 1 | 0 | 1 | 25.95456204 |
| 33 | 0 | 1 | 0 | 20.88535968 |
| 34 | 1 | 1 | 0 | -60.76607847 |
| 35 | 0 | 0 | 1 | 7.429123189 |
| 36 | 1 | 0 | 0 | 57.94692122 |
| 37 | 1 | 0 | 1 | 39.31924452 |
| 38 | 1 | 0 | 1 | 23.0894625 |
| 39 | 2 | 0 | 0 | 12.17246862 |
| 40 | 0 | 0 | 1 | 7.143952847 |
| 41 | 2 | 1 | 1 | 23.04153219 |
| 42 | 2 | 1 | 0 | -5.834170024 |
| 43 | 1 | 0 | 0 | -38.06102668 |
| 44 | 0 | 1 | 1 | -14.96217676 |
| 45 | 1 | 0 | 0 | -16.84963188 |
| 46 | 1 | 0 | 1 | -3.321934305 |
| 47 | 0 | 0 | 1 | -2.686812756 |
| 48 | 1 | 0 | 0 | -0.706535667 |
| 49 | 1 | 0 | 0 | 0.585334222 |
| 50 | 1 | 0 | 0 | -0.161347197 |
| 51 | 0 | 0 | 1 | -1.338564181 |
| 52 | 1 | 0 | 0 | 3.272451344 |
| 53 | 1 | 1 | 1 | 16.78602562 |
| 54 | 1 | 0 | 0 | 35.30857461 |
| 55 | 1 | 0 | 0 | -17.46790144 |

| | | | | |
|---|---|---|---|---|
| 56 | 1 | 0 | 0 | -29.38856471 |
| 57 | 1 | 0 | 0 | -43.25306779 |
| 58 | 0 | 0 | 1 | -42.72625311 |
| 59 | 1 | 0 | 1 | -43.73203118 |
| 60 | 1 | 0 | 0 | -60.79103706 |
| 61 | 1 | 0 | 1 | -51.77495835 |
| 62 | 0 | 0 | 0 | -28.73373527 |
| 63 | 0 | 0 | 1 | 7.95086766 |
| 64 | 1 | 0 | 0 | 9.718886249 |
| 65 | 1 | 0 | 0 | 9.091676632 |
| 66 | 2 | 0 | 0 | 24.07738075 |
| 67 | 1 | 0 | 0 | -9.778669094 |
| 68 | 1 | 0 | 0 | -26.87569533 |
| 69 | 1 | 1 | 0 | -56.77755791 |
| 70 | 1 | 0 | 1 | -55.73219051 |
| 71 | 0 | 0 | 0 | -20.41810098 |
| 72 | 0 | 0 | 0 | 28.83173123 |
| 73 | 0 | 1 | 1 | 11.35486579 |
| 74 | 0 | 0 | 1 | 4.511145864 |
| 75 | 0 | 0 | 1 | 5.654016566 |
| 76 | 0 | 0 | 1 | 6.281612475 |
| 77 | 1 | 0 | 0 | 8.188877314 |
| 78 | 1 | 0 | 0 | 9.982088677 |
| 79 | 1 | 0 | 1 | 9.746415862 |
| 80 | 2 | 0 | 0 | 3.827426256 |
| 81 | 2 | 0 | 0 | 5.782202714 |
| 82 | 1 | 0 | 1 | 1.849336786 |
| 83 | 2 | 0 | 0 | 4.741292562 |
| 84 | 0 | 0 | 0 | -3.908528456 |
| 85 | 2 | 1 | 1 | 44.60043086 |
| 86 | 1 | 0 | 0 | 37.85892518 |
| 87 | 1 | 0 | 1 | 34.13441425 |
| 88 | 1 | 0 | 1 | 35.18681625 |
| 89 | 1 | 0 | 0 | 19.93891786 |
| 90 | 0 | 1 | 1 | 22.04663245 |
| 91 | 0 | 0 | 1 | 20.8712464 |
| 92 | 2 | 1 | 1 | 10.43038767 |
| 93 | 0 | 0 | 0 | 30.46911527 |
| 94 | 1 | 1 | 1 | 33.79223855 |
| 95 | 1 | 0 | 1 | 32.87980132 |
| 96 | 1 | 0 | 0 | -5.15907614 |
| 97 | 2 | 1 | 0 | -6.0418094 |
| 98 | 1 | 1 | 0 | -5.172434249 |
| 99 | 1 | 0 | 0 | -5.386940129 |
| 100 | 1 | 0 | 1 | -14.6992116 |
| 101 | 2 | 1 | 1 | -10.70597577 |
| 102 | 2 | 0 | 1 | -11.88974782 |
| 103 | 2 | 0 | 1 | -9.658386993 |

| | | | | |
|---|---|---|---|---|
| 104 | 2 | 1 | 1 | -3.950340099 |
| 105 | 0 | 0 | 0 | -4.226548527 |
| 106 | 0 | 0 | 1 | -8.325050419 |
| 107 | 0 | 0 | 1 | -20.99275075 |
| 108 | 1 | 0 | 1 | -21.2430257 |
| 109 | 0 | 0 | 0 | -54.41374636 |
| 110 | 1 | 0 | 1 | -53.52637591 |
| 111 | 0 | 0 | 1 | -53.66693917 |
| 112 | 0 | 0 | 1 | 47.18229037 |
| 113 | 0 | 1 | 1 | 46.99267287 |
| 114 | 1 | 0 | 0 | 48.70439957 |
| 115 | 1 | 0 | 0 | 48.47032176 |
| 116 | 1 | 0 | 1 | 45.28893107 |
| 117 | 0 | 1 | 0 | 52.63242478 |
| 118 | 1 | 0 | 0 | -27.62429556 |
| 119 | 1 | 0 | 1 | -28.79108366 |
| 120 | 0 | 0 | 1 | -57.16771942 |
| 121 | 1 | 1 | 1 | -54.01331508 |
| 122 | 0 | 0 | 0 | -52.53584581 |
| 123 | 1 | 1 | 0 | -59.51608921 |
| 124 | 0 | 0 | 0 | -58.93622596 |
| 125 | 2 | 1 | 0 | -14.24986559 |
| 126 | 1 | 0 | 0 | -10.12782403 |
| 127 | 2 | 0 | 1 | 1.412341938 |
| 128 | 1 | 0 | 1 | 0.466394688 |
| 129 | 2 | 0 | 1 | -40.30777607 |
| 130 | 2 | 1 | 1 | 42.70403094 |
| 131 | 0 | 0 | 0 | 8.45775558 |
| 132 | 1 | 0 | 0 | 9.436655645 |
| 133 | 0 | 1 | 0 | 8.94075697 |
| 134 | 0 | 0 | 0 | 8.476670106 |
| 135 | 1 | 0 | 1 | 6.165724009 |
| 136 | 1 | 0 | 0 | 19.61643805 |
| 137 | 1 | 1 | 1 | 18.01947233 |
| 138 | 1 | 1 | 0 | 19.41214822 |
| 139 | 1 | 0 | 0 | 19.97882449 |
| 140 | 1 | 0 | 1 | 16.46288614 |
| 141 | 1 | 0 | 1 | 17.90644699 |
| 142 | 1 | 0 | 1 | 8.193910689 |
| 143 | 1 | 0 | 0 | 44.98465379 |
| 144 | 2 | 0 | 1 | 25.17774896 |
| 145 | 1 | 0 | 1 | 27.46649242 |
| 146 | 2 | 0 | 1 | 28.12500769 |
| 147 | 1 | 0 | 0 | 27.55392003 |
| 148 | 1 | 1 | 0 | 1.206141469 |
| 149 | 0 | 0 | 0 | -0.723144168 |
| 150 | 2 | 1 | 1 | 1.643349482 |
| 151 | 1 | 0 | 0 | -2.412599772 |

| | | | | |
|---|---|---|---|---|
| 152 | 1 | 1 | 0 | -7.363899831 |
| 153 | 1 | 0 | 0 | -17.15061972 |
| 154 | 1 | 1 | 0 | -16.75921969 |
| 155 | 0 | 1 | 1 | -12.62422325 |
| 156 | 1 | 1 | 0 | -8.189061786 |
| 157 | 1 | 0 | 1 | -6.999674478 |
| 158 | 1 | 0 | 1 | -29.20864178 |
| 159 | 0 | 0 | 0 | -31.59021201 |
| 160 | 1 | 0 | 0 | -35.9915433 |
| 161 | 1 | 0 | 1 | -35.83994599 |
| 162 | 2 | 0 | 0 | -42.30051863 |
| 163 | 1 | 0 | 0 | -60.87381678 |
| 164 | 1 | 0 | 1 | -61.56181423 |
| 165 | 2 | 0 | 1 | -62.68133379 |
| 166 | 1 | 0 | 0 | -61.33485028 |
| 167 | 2 | 0 | 1 | -55.45651184 |
| 168 | 1 | 0 | 0 | -54.0999498 |
| 169 | 1 | 0 | 1 | -55.16916092 |
| 170 | 0 | 0 | 1 | -50.83275236 |
| 171 | 1 | 0 | 1 | -44.20261283 |
| 172 | 1 | 0 | 1 | -42.26314041 |
| 173 | 1 | 0 | 0 | -49.76243982 |
| 174 | 0 | 0 | 0 | -50.37441263 |
| 175 | 0 | 1 | 1 | -47.13605008 |
| 176 | 1 | 0 | 0 | -45.18615949 |
| 177 | 0 | 1 | 1 | -35.12562327 |
| 178 | 1 | 1 | 0 | -29.9794792 |
| 179 | 1 | 0 | 1 | -30.91083571 |
| 180 | 0 | 0 | 0 | -28.64735407 |
| 181 | 2 | 1 | 1 | -27.81087293 |
| 182 | 1 | 1 | 0 | -28.57797214 |
| 183 | 1 | 0 | 1 | -30.47380853 |
| 184 | 1 | 1 | 1 | -21.86830667 |
| 185 | 1 | 0 | 0 | -11.16524813 |
| 186 | 0 | 0 | 0 | -11.3750896 |
| 187 | 1 | 0 | 0 | -8.557695277 |
| 188 | 1 | 0 | 1 | -5.152837976 |
| 189 | 1 | 1 | 1 | -5.218237702 |
| 190 | 1 | 1 | 0 | -4.165450652 |
| 191 | 2 | 0 | 1 | 1.276554922 |
| 192 | 2 | 0 | 1 | -5.795541832 |
| 193 | 1 | 0 | 0 | -7.448616678 |
| 194 | 2 | 0 | 1 | -6.112629055 |
| 195 | 1 | 0 | 1 | -7.017976802 |
| 196 | 2 | 0 | 1 | -21.2942291 |
| 197 | 2 | 0 | 0 | -45.52123567 |
| 198 | 2 | 1 | 0 | -45.7435074 |
| 199 | 2 | 1 | 0 | -46.600794 |

| | | | | |
|---|---|---|---|---|
| 200 | 2 | 0 | 0 | -46.94083999 |
| 201 | 2 | 0 | 0 | -46.80136453 |
| 202 | 2 | 0 | 0 | -46.86744586 |
| 203 | 2 | 1 | 0 | -47.38510485 |
| 204 | 2 | 1 | 0 | -47.76229285 |
| 205 | 1 | 0 | 0 | -22.12400337 |
| 206 | 1 | 0 | 0 | -21.03431788 |
| 207 | 1 | 0 | 0 | -19.44903804 |
| 208 | 1 | 0 | 0 | -15.60898752 |
| 209 | 2 | 0 | 1 | -15.13302154 |
| 210 | 2 | 0 | 1 | -15.61534002 |
| 211 | 1 | 0 | 1 | -9.463425807 |
| 212 | 1 | 0 | 0 | 4.947089772 |
| 213 | 1 | 0 | 0 | 10.10372689 |
| 214 | 1 | 0 | 0 | 53.28530352 |
| 215 | 1 | 0 | 0 | 64.81789732 |
| 216 | 1 | 0 | 0 | 55.34244531 |
| 217 | 2 | 0 | 1 | -26.88833092 |
| 218 | 2 | 0 | 1 | -46.393355 |
| 219 | 2 | 0 | 1 | -47.74221627 |
| 220 | 0 | 0 | 0 | -45.43128697 |
| 221 | 0 | 0 | 1 | -50.0046479 |
| 222 | 1 | 0 | 0 | -48.55280252 |
| 223 | 1 | 0 | 1 | -56.86087548 |
| 224 | 1 | 1 | 1 | -58.51790316 |
| 225 | 1 | 0 | 1 | -50.08339401 |
| 226 | 1 | 0 | 0 | -50.28506386 |
| 227 | 1 | 0 | 0 | -49.66814118 |
| 228 | 1 | 0 | 0 | -48.93959482 |
| 229 | 1 | 0 | 1 | -45.93808952 |
| 230 | 1 | 0 | 0 | -46.81067272 |
| 231 | 1 | 1 | 1 | -48.26572202 |
| 232 | 1 | 1 | 0 | -47.59750081 |
| 233 | 1 | 0 | 1 | -46.40727369 |
| 234 | 2 | 0 | 1 | -45.82944548 |
| 235 | 1 | 0 | 1 | -49.85843032 |
| 236 | 1 | 1 | 0 | -43.20929395 |
| 237 | 2 | 0 | 1 | -61.95760373 |
| 238 | 2 | 0 | 0 | -63.2492798 |
| 239 | 0 | 0 | 0 | 17.15838917 |
| 240 | 2 | 1 | 0 | 19.80541583 |
| 241 | 1 | 0 | 0 | 20.02720146 |
| 242 | 1 | 0 | 1 | 28.71024092 |
| 243 | 1 | 0 | 0 | 25.19053632 |
| 244 | 1 | 0 | 0 | -15.50029273 |
| 245 | 1 | 0 | 1 | -14.02040409 |
| 246 | 1 | 0 | 0 | -23.24850124 |
| 247 | 1 | 0 | 1 | 13.87276746 |

| | | | | |
|---|---|---|---|---|
| 248 | 1 | 0 | 0 | 16.75597884 |
| 249 | 0 | 0 | 1 | 25.98360272 |
| 250 | 0 | 0 | 1 | 25.94705667 |
| 251 | 0 | 0 | 1 | 25.95189295 |
| 252 | 0 | 0 | 1 | 26.05751482 |
| 253 | 0 | 0 | 1 | 25.54265418 |
| 254 | 1 | 0 | 1 | -15.91467178 |
| 255 | 1 | 0 | 0 | -43.59254343 |
| 256 | 1 | 0 | 0 | -39.66580719 |
| 257 | 2 | 0 | 0 | -29.40102063 |
| 258 | 1 | 0 | 0 | 22.75104892 |
| 259 | 1 | 0 | 0 | 22.10594887 |
| 260 | 1 | 0 | 0 | 83.56597836 |
| 261 | 1 | 0 | 0 | 83.33703489 |
| 262 | 2 | 0 | 1 | 68.90866856 |
| 263 | 2 | 0 | 0 | 67.93170884 |
| 264 | 1 | 0 | 0 | 66.53442996 |
| 265 | 1 | 1 | 0 | 67.13981552 |
| 266 | 1 | 1 | 0 | 66.46790568 |
| 267 | 1 | 1 | 0 | 67.02566352 |
| 268 | 1 | 0 | 0 | 61.99363275 |
| 269 | 1 | 0 | 0 | 58.65963803 |
| 270 | 1 | 0 | 0 | 57.06206718 |
| 271 | 1 | 1 | 0 | 45.37033338 |
| 272 | 2 | 0 | 0 | 46.9958081 |
| 273 | 1 | 0 | 1 | -62.8832976 |
| 274 | 1 | 0 | 1 | -63.91024828 |
| 275 | 1 | 1 | 0 | -65.74827559 |
| 276 | 1 | 0 | 1 | -72.63311869 |
| 277 | 1 | 1 | 1 | -61.81509197 |
| 278 | 2 | 0 | 0 | -77.40047434 |
| 279 | 1 | 0 | 0 | -76.81205763 |
| 280 | 1 | 0 | 0 | -77.33338969 |
| 281 | 1 | 0 | 1 | -79.63713628 |
| 282 | 0 | 0 | 0 | -82.35294363 |
| 283 | 0 | 0 | 1 | -70.56012733 |
| 284 | 1 | 0 | 0 | -69.6933994 |
| 285 | 1 | 0 | 0 | -58.03081369 |
| 286 | 2 | 1 | 1 | -59.01005568 |
| 287 | 1 | 1 | 0 | -38.64078288 |
| 288 | 1 | 0 | 0 | -41.31290371 |
| 289 | 1 | 0 | 0 | -16.85507922 |
| 290 | 2 | 0 | 0 | -36.19515645 |
| 291 | 2 | 1 | 0 | -37.45313999 |
| 292 | 2 | 0 | 0 | -42.18356091 |
| 293 | 2 | 0 | 0 | -43.247514 |
| 294 | 1 | 0 | 1 | -71.14785852 |
| 295 | 1 | 0 | 0 | -66.59953265 |

| | | | | |
|---|---|---|---|---|
| 296 | 1 | 0 | 0 | -32.83275283 |
| 297 | 2 | 0 | 0 | -32.17259506 |
| 298 | 1 | 0 | 1 | -31.76946713 |
| 299 | 1 | 0 | 0 | -31.58117751 |
| 300 | 1 | 0 | 0 | -29.92674944 |
| 301 | 1 | 0 | 1 | -26.40968954 |
| 302 | 1 | 0 | 0 | -38.58673601 |
| 303 | 1 | 0 | 1 | -49.21864251 |
| 304 | 1 | 0 | 0 | -59.35248445 |
| 305 | 1 | 1 | 1 | -52.95363784 |
| 306 | 1 | 0 | 0 | -44.59511271 |
| 307 | 1 | 0 | 1 | -60.09949923 |
| 308 | 0 | 0 | 1 | -53.07080126 |
| 309 | 2 | 0 | 1 | -54.47120614 |
| 310 | 1 | 0 | 1 | -51.753824 |
| 311 | 1 | 0 | 1 | -50.01967312 |
| 312 | 2 | 0 | 1 | -51.91521105 |
| 313 | 2 | 0 | 0 | -13.4424046 |
| 314 | 2 | 1 | 0 | -11.95668151 |
| 315 | 2 | 0 | 0 | 16.14768329 |
| 316 | 1 | 1 | 1 | 19.06328718 |
| 317 | 1 | 0 | 0 | -43.56143831 |
| 318 | 1 | 0 | 0 | 48.44570613 |
| 319 | 1 | 0 | 0 | 49.31010239 |
| 320 | 2 | 0 | 1 | -11.91606207 |
| 321 | 1 | 0 | 0 | -27.75721504 |
| 322 | 1 | 0 | 0 | -39.92736111 |
| 323 | 1 | 0 | 1 | -39.42532394 |
| 324 | 1 | 0 | 1 | -39.2613919 |
| 325 | 1 | 0 | 0 | -40.85474494 |
| 326 | 1 | 0 | 0 | -41.24717185 |
| 327 | 1 | 0 | 0 | -42.50789729 |
| 328 | 1 | 1 | 0 | -38.52499819 |
| 329 | 2 | 0 | 0 | -19.59128463 |
| 330 | 1 | 0 | 0 | -25.79763226 |
| 331 | 1 | 0 | 1 | -12.25193203 |
| 332 | 2 | 1 | 0 | -5.773471347 |
| 333 | 2 | 0 | 0 | 1.196623066 |
| 334 | 1 | 0 | 0 | 5.093605766 |
| 335 | 1 | 0 | 0 | 6.98608495 |
| 336 | 1 | 1 | 0 | 12.82134625 |
| 337 | 1 | 0 | 0 | 11.7822597 |
| 338 | 1 | 0 | 1 | 17.97282784 |
| 339 | 1 | 0 | 0 | 30.26388892 |
| 340 | 1 | 1 | 1 | 43.07309745 |
| 341 | 1 | 1 | 0 | 44.24418172 |
| 342 | 2 | 1 | 1 | 38.56691665 |
| 343 | 2 | 1 | 0 | 37.27647149 |

| | | | | |
|---|---|---|---|---|
| 344 | 1 | 1 | 0 | 27.96470692 |
| 345 | 2 | 0 | 0 | 27.10805973 |
| 346 | 1 | 0 | 0 | 8.858662823 |
| 347 | 1 | 1 | 0 | -10.21933895 |
| 348 | 1 | 0 | 0 | -20.3262391 |
| 349 | 1 | 0 | 0 | -20.68145989 |
| 350 | 1 | 1 | 0 | -37.1691407 |
| 351 | 1 | 0 | 0 | -36.5976828 |
| 352 | 1 | 0 | 0 | -39.53145732 |
| 353 | 1 | 0 | 0 | -44.51858369 |
| 354 | 2 | 1 | 1 | -50.74930274 |
| 355 | 1 | 0 | 0 | -31.3730373 |
| 356 | 1 | 0 | 1 | -30.59852417 |
| 357 | 1 | 0 | 0 | -27.79287975 |
| 358 | 1 | 0 | 0 | -25.83352403 |
| 359 | 1 | 1 | 0 | -36.10466612 |
| 360 | 0 | 0 | 0 | -21.7382687 |
| 361 | 0 | 0 | 1 | -18.89003867 |
| 362 | 0 | 0 | 1 | -16.79458139 |
| 363 | 0 | 0 | 0 | -1.415753302 |
| 364 | 1 | 0 | 0 | 0.413722069 |
| 365 | 1 | 0 | 0 | 1.75404067 |
| 366 | 1 | 1 | 0 | 2.82932961 |
| 367 | 1 | 0 | 0 | -4.159123025 |
| 368 | 2 | 0 | 0 | -4.72240121 |
| 369 | 1 | 0 | 0 | -7.908651974 |
| 370 | 2 | 0 | 1 | -12.77666618 |
| 371 | 2 | 1 | 0 | 7.799841548 |
| 372 | 1 | 1 | 1 | 17.89978867 |
| 373 | 0 | 0 | 0 | -30.65550219 |
| 374 | 2 | 0 | 0 | -58.44895004 |
| 375 | 1 | 1 | 0 | -63.85494654 |
| 376 | 1 | 0 | 0 | -66.03834209 |
| 377 | 1 | 0 | 0 | -48.05990257 |
| 378 | 1 | 0 | 0 | -41.07824715 |
| 379 | 2 | 0 | 0 | -18.69402253 |
| 380 | 1 | 0 | 0 | -19.73206078 |
| 381 | 0 | 1 | 1 | -27.30366058 |
| 382 | 1 | 0 | 0 | -34.53628733 |
| 383 | 2 | 0 | 0 | -34.99528877 |
| 384 | 1 | 0 | 0 | -37.44831018 |
| 385 | 1 | 0 | 0 | -26.29505004 |
| 386 | 0 | 0 | 0 | -20.73543507 |
| 387 | 0 | 1 | 1 | -21.51357943 |
| 388 | 2 | 1 | 0 | -30.58207874 |
| 389 | 1 | 0 | 1 | -41.91944141 |
| 390 | 0 | 0 | 1 | -27.78406046 |
| 391 | 2 | 0 | 0 | 52.53840938 |

| | | | | |
|---|---|---|---|---|
| 392 | 1 | 0 | 1 | 45.93885215 |
| 393 | 1 | 0 | 0 | 33.2359602 |
| 394 | 2 | 0 | 1 | 32.85447105 |
| 395 | 2 | 0 | 0 | 4.573675862 |
| 396 | 2 | 1 | 0 | 28.74673226 |
| 397 | 1 | 1 | 0 | 5.83313939 |
| 398 | 1 | 0 | 0 | 73.46814349 |
| 399 | 1 | 0 | 0 | 66.44297699 |
| 400 | 2 | 1 | 1 | 47.70314403 |
| 401 | 1 | 0 | 1 | 48.12275134 |
| 402 | 1 | 0 | 0 | 84.78710552 |
| 403 | 1 | 0 | 0 | 67.28764654 |
| 404 | 2 | 1 | 1 | 45.48357114 |
| 405 | 1 | 0 | 0 | 63.12151361 |
| 406 | 1 | 0 | 0 | 64.50936707 |
| 407 | 1 | 1 | 0 | 66.86964501 |
| 408 | 1 | 1 | 0 | 18.80175494 |
| 409 | 0 | 1 | 1 | 28.71275097 |
| 410 | 0 | 0 | 1 | 28.81603597 |
| 411 | 2 | 1 | 0 | 27.39163047 |
| 412 | 0 | 0 | 0 | 29.77552555 |
| 413 | 2 | 0 | 0 | 33.67126422 |
| 414 | 1 | 0 | 1 | 16.85106053 |
| 415 | 1 | 0 | 1 | 14.41159699 |
| 416 | 1 | 0 | 0 | 12.57151585 |
| 417 | 0 | 1 | 1 | 29.88887053 |
| 418 | 2 | 0 | 1 | 26.52309281 |
| 419 | 1 | 1 | 0 | 26.28700313 |
| 420 | 1 | 0 | 0 | 14.46839011 |
| 421 | 1 | 0 | 0 | 53.83360855 |
| 422 | 1 | 0 | 0 | 1.701817871 |
| 423 | 1 | 0 | 0 | 6.086171607 |
| 424 | 1 | 0 | 1 | 6.747936114 |
| 425 | 1 | 0 | 1 | 6.540678443 |
| 426 | 1 | 0 | 0 | 5.280383037 |
| 427 | 1 | 0 | 0 | -5.269317103 |
| 428 | 1 | 0 | 0 | -0.04790666 |
| 429 | 2 | 0 | 1 | -8.100698532 |
| 430 | 1 | 0 | 1 | -7.58840958 |
| 431 | 1 | 0 | 0 | -31.55566985 |
| 432 | 1 | 0 | 0 | -35.76611226 |
| 433 | 1 | 1 | 0 | -50.46639299 |
| 434 | 1 | 0 | 1 | -44.83126198 |
| 435 | 0 | 0 | 0 | -41.6346123 |
| 436 | 1 | 0 | 0 | -53.51208191 |
| 437 | 0 | 1 | 0 | -43.24879065 |
| 438 | 0 | 0 | 0 | 16.70377711 |
| 439 | 0 | 0 | 1 | 23.51222831 |

| | | | | |
|---|---|---|---|---|
| 440 | 1 | 0 | 0 | 7.179627434 |
| 441 | 0 | 0 | 0 | 3.474717678 |
| 442 | 2 | 0 | 1 | -12.69507442 |
| 443 | 0 | 1 | 0 | -11.37551723 |
| 444 | 2 | 0 | 1 | -4.506010962 |
| 445 | 1 | 0 | 0 | -10.43894363 |
| 446 | 1 | 0 | 0 | -65.41873307 |
| 447 | 1 | 1 | 0 | -21.44560837 |
| 448 | 2 | 0 | 0 | -23.56223976 |
| 449 | 1 | 0 | 0 | 7.460451382 |
| 450 | 1 | 0 | 0 | 1.738557679 |
| 451 | 1 | 0 | 1 | -2.243184315 |
| 452 | 1 | 0 | 1 | 6.039500895 |
| 453 | 2 | 0 | 1 | 10.37385064 |
| 454 | 1 | 0 | 1 | -38.00892874 |
| 455 | 1 | 0 | 0 | -55.39084134 |
| 456 | 1 | 0 | 1 | -14.95632211 |
| 457 | 2 | 0 | 1 | -14.36284439 |
| 458 | 1 | 0 | 0 | -5.943245088 |
| 459 | 2 | 1 | 1 | -3.342707102 |
| 460 | 2 | 0 | 1 | -47.67915249 |
| 461 | 1 | 0 | 0 | -47.18299142 |
| 462 | 0 | 0 | 1 | -37.50661469 |
| 463 | 1 | 1 | 0 | -20.07225107 |
| 464 | 1 | 0 | 0 | -38.66340655 |
| 465 | 1 | 0 | 0 | -52.5223551 |
| 466 | 1 | 0 | 1 | -64.37360467 |
| 467 | 1 | 1 | 0 | -63.31207371 |
| 468 | 1 | 0 | 1 | -60.46564539 |
| 469 | 2 | 0 | 1 | -55.32934121 |
| 470 | 1 | 0 | 0 | -54.07608922 |
| 471 | 1 | 0 | 0 | -53.61324262 |
| 472 | 2 | 0 | 1 | -51.50166874 |
| 473 | 1 | 0 | 0 | -51.61715711 |
| 474 | 1 | 0 | 1 | -52.27230331 |
| 475 | 1 | 1 | 1 | -54.71823398 |
| 476 | 1 | 0 | 0 | -46.28197119 |
| 477 | 0 | 0 | 0 | -47.69865852 |
| 478 | 2 | 1 | 0 | -50.11347523 |
| 479 | 1 | 0 | 0 | -50.80040011 |
| 480 | 1 | 0 | 1 | -43.23312927 |
| 481 | 1 | 0 | 0 | -44.57492562 |
| 482 | 1 | 0 | 0 | -11.64885349 |
| 483 | 1 | 0 | 1 | -20.76993221 |
| 484 | 2 | 0 | 0 | -20.3429342 |
| 485 | 2 | 0 | 1 | 45.55033188 |
| 486 | 1 | 0 | 0 | 20.72815543 |
| 487 | 0 | 0 | 1 | 20.48698341 |

| | | | | |
|---|---|---|---|---|
| 488 | 1 | 0 | 1 | 19.69570479 |
| 489 | 1 | 0 | 0 | 11.08588359 |
| 490 | 1 | 1 | 0 | 28.95060139 |
| 491 | 1 | 0 | 0 | 28.47858792 |
| 492 | 1 | 0 | 0 | 27.89414182 |
| 493 | 2 | 0 | 0 | 31.63334308 |
| 494 | 1 | 0 | 0 | 28.37260052 |
| 495 | 1 | 0 | 0 | 29.41204087 |
| 496 | 0 | 0 | 0 | 8.702266172 |
| 497 | 0 | 0 | 0 | 8.593578783 |
| 498 | 2 | 1 | 0 | 8.342140109 |
| 499 | 1 | 0 | 0 | 7.888074408 |
| 500 | 0 | 0 | 0 | 2.400726622 |
| 501 | 0 | 0 | 1 | -2.504097303 |
| 502 | 0 | 0 | 0 | -2.578840977 |
| 503 | 0 | 0 | 0 | -2.323408704 |
| 504 | 0 | 0 | 1 | -3.151947398 |
| 505 | 2 | 0 | 0 | -3.746160188 |
| 506 | 0 | 0 | 0 | -3.171692521 |
| 507 | 0 | 0 | 0 | -4.607746642 |
| 508 | 0 | 0 | 0 | -4.856274265 |
| 509 | 1 | 0 | 0 | -5.917677861 |
| 510 | 1 | 0 | 1 | -25.78163048 |
| 511 | 1 | 0 | 1 | -26.15832917 |
| 512 | 1 | 0 | 1 | -25.97600903 |
| 513 | 2 | 1 | 0 | -25.89851193 |
| 514 | 1 | 0 | 1 | -21.73836013 |
| 515 | 1 | 0 | 0 | -22.0527065 |
| 516 | 1 | 0 | 0 | -23.56122614 |
| 517 | 1 | 1 | 1 | -21.54560628 |
| 518 | 1 | 0 | 1 | -16.11919842 |
| 519 | 0 | 0 | 0 | -17.9898912 |
| 520 | 1 | 1 | 1 | -32.19116149 |
| 521 | 0 | 1 | 1 | -35.00639178 |
| 522 | 0 | 0 | 1 | -35.34288673 |
| 523 | 1 | 0 | 1 | -42.13031729 |
| 524 | 0 | 0 | 0 | -34.25788671 |
| 525 | 1 | 1 | 0 | -33.93563555 |
| 526 | 1 | 0 | 0 | -41.28180622 |
| 527 | 1 | 0 | 1 | -40.6585644 |
| 528 | 1 | 0 | 1 | -40.38140218 |
| 529 | 2 | 0 | 0 | -39.97773745 |
| 530 | 1 | 0 | 0 | -42.39858016 |
| 531 | 1 | 0 | 1 | -48.74682623 |
| 532 | 1 | 0 | 1 | -48.81047931 |
| 533 | 0 | 0 | 1 | -47.45696879 |
| 534 | 1 | 0 | 0 | -40.49101838 |
| 535 | 1 | 0 | 0 | -46.94721395 |

| | | | | |
|---|---|---|---|---|
| 536 | 1 | 0 | 1 | 4.921707726 |
| 537 | 1 | 0 | 1 | 0.615229251 |
| 538 | 1 | 0 | 0 | -0.466609415 |
| 539 | 2 | 1 | 1 | -11.76540195 |
| 540 | 0 | 1 | 0 | -21.00927253 |
| 541 | 1 | 1 | 0 | -20.80278656 |
| 542 | 1 | 0 | 0 | -21.13487186 |
| 543 | 1 | 0 | 1 | -34.2650636 |
| 544 | 1 | 0 | 1 | -34.58927751 |
| 545 | 1 | 0 | 1 | -34.94490686 |
| 546 | 1 | 0 | 0 | -46.0670179 |
| 547 | 1 | 1 | 0 | -36.50015336 |
| 548 | 1 | 1 | 0 | -37.70905628 |
| 549 | 2 | 0 | 0 | -38.0323879 |
| 550 | 1 | 0 | 1 | -37.53790265 |
| 551 | 1 | 1 | 0 | -6.652795662 |
| 552 | 0 | 0 | 0 | 1.294908301 |
| 553 | 0 | 0 | 0 | 0.946987845 |
| 554 | 1 | 0 | 1 | 12.43704029 |
| 555 | 1 | 0 | 0 | 15.69062358 |
| 556 | 1 | 0 | 0 | 16.33368026 |
| 557 | 1 | 0 | 0 | 11.06773626 |
| 558 | 1 | 0 | 1 | 6.516131892 |
| 559 | 1 | 0 | 0 | 7.486596138 |
| 560 | 1 | 1 | 0 | 7.693807378 |
| 561 | 1 | 0 | 0 | 7.319235793 |
| 562 | 2 | 0 | 0 | 3.81011674 |
| 563 | 1 | 0 | 0 | -3.744406846 |
| 564 | 2 | 0 | 1 | 2.980865235 |
| 565 | 1 | 0 | 1 | 17.52273084 |
| 566 | 1 | 0 | 0 | 12.6942776 |
| 567 | 1 | 0 | 1 | 36.3781503 |
| 568 | 1 | 0 | 1 | 50.5375465 |
| 569 | 1 | 0 | 0 | 46.81849363 |
| 570 | 1 | 0 | 1 | 33.65198126 |
| 571 | 1 | 0 | 0 | 33.63070361 |
| 572 | 0 | 0 | 1 | 33.33580859 |
| 573 | 2 | 0 | 1 | 33.18833969 |
| 574 | 1 | 0 | 1 | 33.72454295 |
| 575 | 1 | 0 | 0 | 35.51352158 |
| 576 | 2 | 0 | 1 | 35.87029247 |
| 577 | 0 | 0 | 0 | 35.57483776 |
| 578 | 0 | 0 | 0 | 35.58532669 |
| 579 | 1 | 0 | 1 | 33.61775273 |
| 580 | 1 | 0 | 0 | 34.81421772 |
| 581 | 1 | 0 | 0 | 26.90737544 |
| 582 | 1 | 0 | 0 | 27.87384242 |
| 583 | 1 | 0 | 0 | 24.58282445 |

| | | | | |
|---|---|---|---|---|
| 584 | 2 | 0 | 1 | 25.2849499 |
| 585 | 2 | 0 | 1 | 25.0069077 |
| 586 | 2 | 0 | 0 | 24.72904117 |
| 587 | 1 | 0 | 0 | 24.30834199 |
| 588 | 1 | 0 | 0 | 24.34729717 |
| 589 | 2 | 0 | 1 | 24.79700544 |
| 590 | 0 | 0 | 0 | 22.99029633 |
| 591 | 1 | 0 | 0 | 23.0478796 |
| 592 | 0 | 1 | 0 | 23.43776679 |
| 593 | 0 | 0 | 0 | 21.94663903 |
| 594 | 1 | 1 | 0 | 21.98252273 |
| 595 | 1 | 0 | 1 | 21.9974237 |
| 596 | 1 | 1 | 0 | 19.7570613 |
| 597 | 1 | 0 | 0 | 12.07757392 |
| 598 | 1 | 0 | 0 | 11.2959718 |
| 599 | 1 | 1 | 0 | 10.90464242 |
| 600 | 0 | 0 | 1 | 5.107840657 |
| 601 | 0 | 0 | 0 | 5.087581326 |
| 602 | 0 | 1 | 0 | -2.757304831 |
| 603 | 0 | 0 | 0 | -2.595198329 |
| 604 | 1 | 0 | 1 | -2.541059749 |
| 605 | 1 | 0 | 0 | -3.791605387 |
| 606 | 1 | 1 | 0 | -4.743255209 |
| 607 | 1 | 0 | 0 | -5.154616359 |
| 608 | 1 | 0 | 0 | -6.324756312 |
| 609 | 1 | 0 | 0 | -7.011960181 |
| 610 | 1 | 0 | 0 | -6.704931399 |
| 611 | 1 | 0 | 1 | -10.80435467 |
| 612 | 1 | 0 | 0 | -10.66681545 |
| 613 | 1 | 0 | 0 | -11.06166955 |
| 614 | 1 | 0 | 0 | -11.11395147 |
| 615 | 1 | 1 | 0 | -12.24627263 |
| 616 | 0 | 0 | 0 | -13.73651566 |
| 617 | 2 | 0 | 1 | -14.44672565 |
| 618 | 1 | 0 | 1 | -30.03716546 |
| 619 | 1 | 0 | 0 | -29.98568323 |
| 620 | 0 | 0 | 1 | -30.44399111 |
| 621 | 0 | 0 | 0 | -31.33006531 |
| 622 | 1 | 0 | 1 | -56.2649891 |
| 623 | 1 | 0 | 0 | -60.0370291 |
| 624 | 1 | 1 | 0 | -60.40677232 |
| 625 | 1 | 0 | 0 | -60.79165279 |
| 626 | 2 | 0 | 0 | -59.40120686 |
| 627 | 2 | 0 | 0 | -59.31882741 |
| 628 | 2 | 1 | 1 | -54.3697404 |
| 629 | 1 | 0 | 1 | -55.5074485 |
| 630 | 1 | 1 | 1 | -56.28641459 |
| 631 | 1 | 1 | 0 | -56.38969066 |

| | | | | |
|---|---|---|---|---|
| 632 | 1 | 0 | 0 | -55.69542817 |
| 633 | 1 | 0 | 0 | -58.76213128 |
| 634 | 1 | 0 | 0 | -59.41989587 |
| 635 | 1 | 0 | 0 | -54.28201637 |
| 636 | 1 | 1 | 1 | -55.90738095 |
| 637 | 1 | 0 | 0 | -56.08775383 |
| 638 | 1 | 0 | 1 | -52.49005107 |
| 639 | 1 | 0 | 0 | -53.78520118 |
| 640 | 1 | 0 | 0 | -46.69154168 |
| 641 | 1 | 0 | 0 | -45.87964256 |
| 642 | 1 | 0 | 0 | -45.94068366 |
| 643 | 1 | 0 | 0 | -47.68647756 |
| 644 | 0 | 0 | 1 | -46.53999043 |
| 645 | 1 | 0 | 0 | -46.57834087 |
| 646 | 1 | 0 | 1 | -46.80502946 |
| 647 | 2 | 0 | 0 | -38.95612657 |
| 648 | 2 | 0 | 0 | -42.07175993 |
| 649 | 2 | 0 | 0 | -42.74480846 |
| 650 | 1 | 0 | 0 | -43.44760933 |
| 651 | 1 | 0 | 0 | -44.15580835 |
| 652 | 2 | 0 | 0 | -44.60994967 |
| 653 | 2 | 1 | 0 | -45.71925045 |
| 654 | 1 | 0 | 0 | -28.61828384 |
| 655 | 1 | 0 | 0 | -31.99600455 |
| 656 | 1 | 0 | 0 | -31.60266939 |
| 657 | 2 | 0 | 0 | -33.54550811 |
| 658 | 0 | 0 | 0 | -26.45592944 |
| 659 | 1 | 0 | 1 | -26.31589217 |
| 660 | 1 | 0 | 0 | -27.29673934 |
| 661 | 1 | 0 | 0 | -28.09886294 |
| 662 | 1 | 0 | 0 | -19.57069971 |
| 663 | 1 | 0 | 0 | -28.02172029 |
| 664 | 1 | 0 | 0 | -26.99341872 |
| 665 | 2 | 0 | 1 | -28.94773446 |
| 666 | 1 | 0 | 0 | -15.52925161 |
| 667 | 1 | 0 | 0 | -15.7503601 |
| 668 | 1 | 0 | 1 | -13.67082408 |
| 669 | 2 | 1 | 1 | -15.87173878 |
| 670 | 1 | 1 | 0 | -16.84166171 |
| 671 | 1 | 1 | 0 | 47.53256118 |
| 672 | 1 | 0 | 0 | 48.32161169 |
| 673 | 1 | 0 | 0 | 51.56341722 |
| 674 | 1 | 0 | 0 | 56.75424462 |
| 675 | 1 | 0 | 0 | 54.37330681 |
| 676 | 0 | 1 | 0 | 55.46184552 |
| 677 | 1 | 0 | 0 | 41.25704462 |
| 678 | 2 | 0 | 1 | 37.3838817 |
| 679 | 1 | 0 | 0 | 37.25720432 |

| | | | | |
|---|---|---|---|---|
| 680 | 2 | 0 | 1 | 31.59799612 |
| 681 | 2 | 1 | 0 | 29.84717147 |
| 682 | 1 | 0 | 0 | 28.38609624 |
| 683 | 1 | 0 | 0 | 27.9182495 |
| 684 | 1 | 1 | 0 | 29.24457172 |
| 685 | 1 | 0 | 0 | 58.42146922 |
| 686 | 1 | 0 | 0 | 58.25770563 |
| 687 | 2 | 0 | 0 | 57.99402973 |
| 688 | 1 | 0 | 0 | 57.85885419 |
| 689 | 1 | 1 | 0 | 56.4324533 |
| 690 | 1 | 0 | 0 | 58.37770956 |
| 691 | 1 | 0 | 0 | 57.45627869 |
| 692 | 0 | 0 | 0 | 55.83809925 |
| 693 | 1 | 0 | 0 | 49.89884538 |
| 694 | 0 | 0 | 1 | 49.95092835 |
| 695 | 1 | 1 | 0 | 47.09940082 |
| 696 | 1 | 0 | 1 | 54.96323571 |
| 697 | 0 | 0 | 1 | 39.9319331 |
| 698 | 2 | 0 | 1 | 40.14613318 |
| 699 | 2 | 0 | 1 | 41.99717827 |
| 700 | 2 | 0 | 0 | 39.34495706 |
| 701 | 1 | 0 | 1 | 37.52149336 |
| 702 | 1 | 0 | 0 | 42.73196183 |
| 703 | 1 | 0 | 0 | 37.02843108 |
| 704 | 2 | 1 | 1 | 37.30236616 |
| 705 | 0 | 0 | 1 | 40.56637851 |
| 706 | 1 | 0 | 0 | 25.02373498 |
| 707 | 2 | 0 | 0 | 20.17738012 |
| 708 | 1 | 0 | 0 | 19.54267108 |
| 709 | 1 | 0 | 0 | 20.10582106 |
| 710 | 1 | 0 | 0 | 28.07011329 |
| 711 | 1 | 0 | 0 | 27.84448739 |
| 712 | 2 | 0 | 1 | -3.37062884 |
| 713 | 1 | 0 | 0 | -2.462375924 |
| 714 | 1 | 0 | 0 | -1.722791491 |
| 715 | 1 | 0 | 0 | -10.03125562 |
| 716 | 0 | 0 | 0 | 16.28106433 |
| 717 | 0 | 0 | 0 | 40.49324294 |
| 718 | 0 | 0 | 0 | 40.88679476 |
| 719 | 0 | 0 | 0 | 39.37102119 |
| 720 | 1 | 0 | 0 | 53.70519755 |
| 721 | 1 | 0 | 0 | 56.11582478 |
| 722 | 1 | 0 | 0 | 53.02083355 |
| 723 | 1 | 0 | 0 | 31.33874554 |
| 724 | 2 | 0 | 1 | 29.22570873 |
| 725 | 0 | 1 | 0 | 30.96712376 |
| 726 | 0 | 0 | 1 | 27.45980665 |
| 727 | 0 | 0 | 1 | 26.79947112 |

| | | | | |
|---|---|---|---|---|
| 728 | 1 | 0 | 0 | 18.59238081 |
| 729 | 1 | 1 | 0 | 13.01627668 |
| 730 | 1 | 0 | 1 | 15.01140508 |
| 731 | 2 | 0 | 0 | 14.67381313 |
| 732 | 1 | 0 | 0 | 15.00427151 |
| 733 | 1 | 0 | 0 | 13.83951679 |
| 734 | 0 | 0 | 0 | 12.61202059 |
| 735 | 0 | 0 | 0 | 13.13778462 |
| 736 | 0 | 0 | 0 | -1.57451436 |
| 737 | 1 | 0 | 0 | -8.72144954 |
| 738 | 1 | 0 | 0 | -9.366632553 |
| 739 | 1 | 0 | 0 | -7.693009564 |
| 740 | 2 | 0 | 0 | -7.034074481 |
| 741 | 2 | 1 | 0 | -4.842357524 |
| 742 | 1 | 0 | 0 | -3.383722189 |
| 743 | 1 | 0 | 1 | -3.010430038 |
| 744 | 2 | 0 | 1 | 2.331833465 |
| 745 | 2 | 0 | 0 | -12.52783829 |
| 746 | 2 | 0 | 1 | -12.2285454 |
| 747 | 2 | 0 | 0 | -11.65782371 |
| 748 | 2 | 0 | 0 | -7.032920661 |
| 749 | 0 | 0 | 0 | -16.1858548 |
| 750 | 2 | 1 | 0 | -12.9499078 |
| 751 | 0 | 0 | 0 | -13.28748798 |
| 752 | 1 | 0 | 1 | -34.91552175 |
| 753 | 0 | 0 | 0 | -42.25976096 |
| 754 | 2 | 0 | 1 | -48.01017517 |
| 755 | 2 | 0 | 1 | -44.38506811 |
| 756 | 2 | 0 | 0 | -44.87890695 |
| 757 | 2 | 0 | 1 | -44.88287052 |
| 758 | 2 | 0 | 1 | -45.13648067 |
| 759 | 2 | 0 | 1 | -42.99392478 |
| 760 | 2 | 0 | 0 | -43.82241913 |
| 761 | 2 | 0 | 1 | -43.33801984 |
| 762 | 0 | 0 | 1 | -41.17060473 |
| 763 | 1 | 0 | 0 | -40.16006409 |
| 764 | 0 | 0 | 0 | -42.00682583 |
| 765 | 1 | 0 | 0 | -42.9708561 |
| 766 | 0 | 1 | 1 | -45.42543786 |
| 767 | 1 | 1 | 0 | -45.17865331 |
| 768 | 1 | 0 | 1 | -45.82918011 |
| 769 | 1 | 0 | 0 | -49.72004998 |
| 770 | 1 | 0 | 0 | -46.28541729 |
| 771 | 1 | 1 | 1 | -26.65789862 |
| 772 | 0 | 0 | 1 | -25.25265846 |
| 773 | 1 | 0 | 0 | -21.13528213 |
| 774 | 1 | 0 | 0 | 0.101740072 |
| 775 | 0 | 0 | 0 | 1.004351207 |

| | | | | |
|---|---|---|---|---|
| 776 | 1 | 0 | 1 | 5.833535376 |
| 777 | 1 | 1 | 1 | 7.063752924 |
| 778 | 1 | 0 | 0 | 3.214829518 |
| 779 | 0 | 1 | 1 | 14.77147343 |
| 780 | 1 | 0 | 0 | 19.82964399 |
| 781 | 1 | 0 | 1 | 21.00248531 |
| 782 | 1 | 0 | 1 | 19.31550903 |
| 783 | 1 | 1 | 0 | 7.684762132 |
| 784 | 0 | 0 | 0 | 4.766325099 |
| 785 | 2 | 0 | 1 | 10.79056949 |
| 786 | 0 | 0 | 0 | 8.824508156 |
| 787 | 1 | 1 | 1 | 12.68973322 |
| 788 | 1 | 0 | 0 | 11.088034 |
| 789 | 1 | 0 | 0 | 13.42901514 |
| 790 | 2 | 1 | 0 | 15.30315445 |
| 791 | 1 | 0 | 1 | 15.40115471 |
| 792 | 1 | 0 | 1 | 15.53537208 |
| 793 | 1 | 0 | 0 | 11.97887962 |
| 794 | 0 | 0 | 0 | 13.35574043 |
| 795 | 1 | 0 | 0 | 17.01510535 |
| 796 | 0 | 0 | 0 | 17.55977636 |
| 797 | 1 | 0 | 0 | 20.09090167 |
| 798 | 1 | 1 | 0 | 25.5403085 |
| 799 | 1 | 1 | 0 | 27.29486731 |
| 800 | 1 | 0 | 0 | 29.91491494 |
| 801 | 2 | 1 | 1 | 31.3567098 |
| 802 | 1 | 1 | 0 | 24.73660087 |
| 803 | 2 | 0 | 0 | 24.71348725 |
| 804 | 0 | 0 | 0 | 21.34176405 |
| 805 | 0 | 0 | 0 | 23.78619274 |
| 806 | 1 | 0 | 1 | 19.04237614 |
| 807 | 1 | 1 | 0 | 33.7766874 |
| 808 | 0 | 0 | 1 | 34.933094 |
| 809 | 0 | 0 | 0 | 34.89970415 |
| 810 | 0 | 0 | 0 | 34.85896203 |
| 811 | 1 | 0 | 0 | 33.95420711 |
| 812 | 0 | 0 | 1 | 34.71031902 |
| 813 | 1 | 0 | 1 | 34.05102796 |
| 814 | 1 | 0 | 0 | 34.66156495 |
| 815 | 1 | 0 | 0 | 34.87415077 |
| 816 | 2 | 0 | 1 | 35.89277686 |
| 817 | 0 | 0 | 0 | 35.65696857 |
| 818 | 1 | 0 | 1 | 37.47451357 |
| 819 | 1 | 0 | 0 | 36.70688232 |
| 820 | 1 | 0 | 0 | 36.87202622 |
| 821 | 1 | 0 | 1 | 36.29724235 |
| 822 | 1 | 0 | 0 | 36.31788445 |
| 823 | 0 | 0 | 0 | 36.97145096 |

| | | | | |
|---|---|---|---|---|
| 824 | 1 | 0 | 0 | 46.03845673 |
| 825 | 1 | 0 | 0 | 56.92193575 |
| 826 | 1 | 1 | 1 | 56.12656564 |
| 827 | 0 | 1 | 1 | 52.49944083 |
| 828 | 1 | 0 | 0 | 52.58445047 |
| 829 | 2 | 0 | 0 | 48.64554362 |
| 830 | 1 | 0 | 0 | 84.45649772 |
| 831 | 0 | 0 | 0 | 82.12442433 |
| 832 | 1 | 0 | 0 | 83.01266432 |
| 833 | 1 | 0 | 0 | 83.29439253 |
| 834 | 1 | 0 | 0 | 84.61480275 |
| 835 | 1 | 0 | 0 | 83.87823575 |
| 836 | 1 | 0 | 0 | 83.64817337 |
| 837 | 1 | 0 | 0 | 84.17926016 |
| 838 | 1 | 0 | 0 | 84.4430681 |
| 839 | 1 | 0 | 0 | 81.07290116 |
| 840 | 1 | 0 | 0 | 70.90837323 |
| 841 | 1 | 0 | 0 | 73.47693023 |
| 842 | 1 | 0 | 0 | 73.32551114 |
| 843 | 0 | 0 | 0 | 74.08457283 |
| 844 | 1 | 0 | 1 | 68.72006089 |
| 845 | 1 | 0 | 0 | 67.18870994 |
| 846 | 2 | 1 | 0 | 67.30794451 |
| 847 | 1 | 0 | 0 | 66.98108048 |
| 848 | 2 | 0 | 0 | 67.4377119 |
| 849 | 2 | 0 | 0 | 68.01473205 |
| 850 | 2 | 1 | 0 | 63.65358746 |
| 851 | 1 | 0 | 0 | 63.93647932 |
| 852 | 2 | 0 | 0 | 51.24637428 |
| 853 | 1 | 0 | 0 | 50.9394418 |
| 854 | 1 | 0 | 1 | 52.97924939 |
| 855 | 1 | 0 | 0 | 55.74845925 |
| 856 | 1 | 1 | 0 | 61.18123333 |
| 857 | 1 | 0 | 0 | 59.44124811 |
| 858 | 2 | 1 | 1 | 47.07178388 |
| 859 | 2 | 1 | 0 | 45.49881517 |
| 860 | 1 | 0 | 0 | 66.94761635 |
| 861 | 1 | 0 | 0 | 64.80903481 |
| 862 | 1 | 0 | 1 | 64.71246405 |
| 863 | 1 | 1 | 1 | 64.94470589 |
| 864 | 1 | 0 | 0 | 64.55377733 |
| 865 | 1 | 1 | 0 | 63.98634923 |
| 866 | 1 | 0 | 1 | 61.56940261 |
| 867 | 1 | 0 | 0 | 61.66560116 |
| 868 | 1 | 0 | 0 | 61.93272393 |
| 869 | 1 | 1 | 0 | 61.11200503 |
| 870 | 1 | 0 | 0 | 39.89659987 |
| 871 | 1 | 0 | 0 | 38.53386856 |

| | | | | |
|---|---|---|---|---|
| 872 | 2 | 0 | 0 | 51.09185446 |
| 873 | 1 | 0 | 1 | 62.20242943 |
| 874 | 1 | 0 | 0 | 62.98845008 |
| 875 | 1 | 0 | 0 | 68.17986572 |
| 876 | 1 | 1 | 1 | 64.79517979 |
| 877 | 2 | 0 | 0 | 56.47294223 |
| 878 | 1 | 1 | 0 | 55.78585788 |
| 879 | 2 | 1 | 1 | 57.69234689 |
| 880 | 2 | 0 | 1 | 57.1608344 |
| 881 | 1 | 0 | 0 | 56.17131647 |
| 882 | 1 | 0 | 1 | 59.40851615 |
| 883 | 1 | 1 | 0 | 58.43648506 |
| 884 | 2 | 1 | 0 | 60.71403759 |
| 885 | 1 | 0 | 0 | 57.04506031 |
| 886 | 1 | 0 | 0 | 50.32634789 |
| 887 | 2 | 1 | 0 | 52.99754971 |
| 888 | 1 | 0 | 0 | 58.20699134 |
| 889 | 2 | 0 | 0 | 46.19506469 |
| 890 | 1 | 0 | 0 | 68.13913934 |
| 891 | 1 | 0 | 0 | 67.26568974 |
| 892 | 1 | 0 | 1 | 67.25662308 |
| 893 | 1 | 1 | 1 | 67.03211918 |
| 894 | 1 | 0 | 0 | 67.4403836 |
| 895 | 0 | 0 | 1 | 67.31524541 |
| 896 | 1 | 0 | 0 | 67.70662893 |
| 897 | 1 | 0 | 0 | 70.28698557 |
| 898 | 1 | 0 | 0 | 69.51416988 |
| 899 | 1 | 0 | 1 | 71.90080831 |
| 900 | 2 | 0 | 1 | 71.92895343 |
| 901 | 1 | 0 | 1 | 73.85013006 |
| 902 | 1 | 0 | 0 | 75.71905562 |
| 903 | 1 | 0 | 0 | 76.00665594 |
| 904 | 2 | 0 | 1 | 77.95804028 |
| 905 | 1 | 0 | 0 | 76.99588958 |
| 906 | 1 | 0 | 0 | 76.78946951 |
| 907 | 1 | 0 | 0 | 76.96596492 |
| 908 | 1 | 0 | 1 | 74.72749241 |
| 909 | 1 | 0 | 0 | 74.34756316 |
| 910 | 1 | 0 | 1 | 76.07052676 |
| 911 | 2 | 0 | 0 | 76.97240165 |
| 912 | 2 | 0 | 0 | 78.2769968 |
| 913 | 1 | 1 | 0 | 68.83288326 |
| 914 | 2 | 0 | 0 | 71.79483887 |
| 915 | 1 | 0 | 0 | 70.77319484 |
| 916 | 1 | 0 | 0 | 69.84813295 |
| 917 | 1 | 0 | 0 | 70.28270979 |
| 918 | 1 | 1 | 0 | 69.50920162 |
| 919 | 1 | 0 | 0 | 73.3854367 |

| | | | | |
|---|---|---|---|---|
| 920 | 1 | 1 | 1 | 75.24099253 |
| 921 | 1 | 0 | 0 | 73.5341602 |
| 922 | 1 | 0 | 0 | 76.1891025 |
| 923 | 1 | 0 | 1 | 73.50410193 |
| 924 | 1 | 0 | 1 | 74.42471345 |
| 925 | 1 | 0 | 0 | 76.88097742 |
| 926 | 1 | 0 | 0 | 66.90945779 |
| 927 | 2 | 1 | 0 | 20.88926194 |
| 928 | 0 | 1 | 0 | 76.07030177 |
| 929 | 2 | 0 | 0 | 63.56220645 |
| 930 | 0 | 0 | 1 | 61.25815991 |
| 931 | 2 | 0 | 0 | 61.39239076 |
| 932 | 0 | 0 | 1 | 58.69712013 |
| 933 | 1 | 0 | 0 | 56.97497897 |
| 934 | 1 | 0 | 0 | 56.85568973 |
| 935 | 1 | 0 | 0 | 57.34474882 |
| 936 | 0 | 0 | 0 | 58.23459288 |
| 937 | 0 | 1 | 1 | 58.9471528 |
| 938 | 0 | 0 | 0 | 58.57284572 |
| 939 | 0 | 1 | 0 | 42.30296112 |
| 940 | 0 | 0 | 0 | 41.79578163 |
| 941 | 0 | 0 | 0 | 41.29692633 |
| 942 | 0 | 1 | 0 | 14.47215635 |
| 943 | 1 | 0 | 1 | 15.28419408 |
| 944 | 0 | 1 | 0 | 22.94125537 |
| 945 | 0 | 0 | 0 | 24.35708318 |
| 946 | 1 | 0 | 1 | 25.44223447 |
| 947 | 1 | 0 | 0 | 24.51495343 |
| 948 | 0 | 0 | 0 | 30.36895966 |
| 949 | 0 | 1 | 1 | 32.68093175 |
| 950 | 0 | 0 | 0 | 22.92259811 |
| 951 | 0 | 0 | 0 | 42.71689602 |
| 952 | 1 | 0 | 0 | 41.62696 |
| 953 | 1 | 0 | 0 | 41.91654809 |
| 954 | 1 | 1 | 0 | 42.45409087 |
| 955 | 2 | 1 | 0 | 49.07500957 |
| 956 | 1 | 1 | 0 | 49.96236286 |
| 957 | 0 | 0 | 1 | 52.25717136 |
| 958 | 1 | 0 | 1 | 53.40736203 |
| 959 | 0 | 1 | 0 | 54.84812953 |
| 960 | 0 | 0 | 1 | 53.61064599 |
| 961 | 1 | 1 | 0 | 53.50195718 |
| 962 | 1 | 0 | 0 | 54.559131 |
| 963 | 0 | 0 | 0 | 53.32123908 |
| 964 | 1 | 1 | 0 | 48.93742271 |
| 965 | 2 | 0 | 1 | 52.58621529 |
| 966 | 1 | 1 | 0 | 40.65948132 |
| 967 | 0 | 1 | 0 | 39.05906933 |

| | | | | |
|---|---|---|---|---|
| 968 | 1 | 1 | 1 | 39.23320718 |
| 969 | 0 | 0 | 0 | 39.19212204 |
| 970 | 0 | 0 | 1 | 48.07071062 |
| 971 | 0 | 0 | 1 | 48.87388102 |
| 972 | 1 | 0 | 0 | 48.2810866 |
| 973 | 0 | 0 | 0 | 49.02057828 |
| 974 | 0 | 0 | 0 | 48.85369723 |
| 975 | 0 | 0 | 1 | 48.55678518 |
| 976 | 1 | 0 | 1 | 47.65195417 |
| 977 | 1 | 0 | 0 | 47.41655534 |
| 978 | 2 | 0 | 0 | 49.10637464 |
| 979 | 1 | 0 | 1 | 47.52672078 |
| 980 | 1 | 0 | 0 | 47.71920028 |
| 981 | 1 | 0 | 0 | 46.61764985 |
| 982 | 1 | 0 | 0 | 43.37205142 |
| 983 | 2 | 0 | 1 | 40.47980181 |
| 984 | 1 | 0 | 0 | 43.82254439 |
| 985 | 0 | 1 | 1 | 53.83647723 |
| 986 | 0 | 1 | 0 | 55.58315632 |
| 987 | 0 | 1 | 0 | 54.87202798 |
| 988 | 0 | 1 | 0 | 57.26189156 |
| 989 | 1 | 0 | 0 | 59.75478403 |
| 990 | 1 | 0 | 0 | 60.36513775 |
| 991 | 2 | 1 | 1 | 65.36918364 |
| 992 | 1 | 1 | 0 | 68.77654994 |
| 993 | 2 | 0 | 0 | 68.78224643 |
| 994 | 1 | 0 | 0 | 69.24099128 |
| 995 | 1 | 1 | 0 | 74.25498417 |
| 996 | 1 | 0 | 0 | 75.67162891 |
| 997 | 1 | 1 | 1 | 74.53568183 |
| 998 | 1 | 0 | 0 | 73.77453499 |
| 999 | 1 | 0 | 0 | 74.03261677 |
| 1000 | 1 | 0 | 0 | 72.45225151 |
| 1001 | 1 | 0 | 0 | 74.08969818 |
| 1002 | 1 | 0 | 0 | 71.11589788 |
| 1003 | 1 | 0 | 0 | 69.64985781 |
| 1004 | 1 | 0 | 0 | 69.27444725 |
| 1005 | 1 | 0 | 0 | 69.45710661 |
| 1006 | 1 | 0 | 0 | 71.18840076 |
| 1007 | 1 | 0 | 1 | 75.09669291 |
| 1008 | 1 | 1 | 0 | 70.61523723 |
| 1009 | 2 | 0 | 1 | 70.2286569 |
| 1010 | 1 | 0 | 0 | 67.12992172 |
| 1011 | 1 | 1 | 0 | 67.53815404 |
| 1012 | 0 | 0 | 0 | 68.26531657 |
| 1013 | 1 | 0 | 0 | 69.41866773 |
| 1014 | 1 | 0 | 1 | 70.86622841 |
| 1015 | 1 | 0 | 0 | 71.00558257 |

| | | | | |
|---|---|---|---|---|
| 1016 | 0 | 0 | 0 | 71.75985217 |
| 1017 | 1 | 0 | 0 | 71.57806963 |
| 1018 | 1 | 0 | 1 | 71.11906256 |
| 1019 | 1 | 1 | 0 | 70.96086797 |
| 1020 | 1 | 1 | 0 | 73.01904401 |
| 1021 | 1 | 0 | 1 | 71.32645322 |
| 1022 | 1 | 1 | 0 | 47.73197371 |
| 1023 | 1 | 0 | 0 | 47.03884931 |
| 1024 | 2 | 0 | 0 | 48.50319608 |
| 1025 | 1 | 0 | 0 | -52.47693743 |
| 1026 | 1 | 0 | 0 | -52.4690442 |
| 1027 | 1 | 0 | 0 | -50.12171088 |
| 1028 | 1 | 0 | 0 | -50.68778334 |
| 1029 | 1 | 0 | 0 | -51.21446366 |
| 1030 | 0 | 1 | 0 | -35.2607329 |
| 1031 | 1 | 0 | 0 | -33.04818361 |
| 1032 | 1 | 0 | 0 | -32.98506514 |
| 1033 | 0 | 1 | 1 | -31.59071351 |
| 1034 | 2 | 0 | 0 | -39.58609709 |
| 1035 | 2 | 0 | 0 | -38.76282731 |
| 1036 | 2 | 1 | 0 | -54.70585061 |
| 1037 | 2 | 0 | 0 | -54.93268805 |
| 1038 | 1 | 0 | 0 | -53.97388755 |
| 1039 | 1 | 1 | 0 | -73.19162841 |
| 1040 | 1 | 0 | 0 | -68.3391595 |
| 1041 | 1 | 0 | 1 | -64.30760369 |
| 1042 | 1 | 0 | 1 | -64.55357218 |
| 1043 | 1 | 0 | 1 | -63.79445546 |
| 1044 | 1 | 0 | 0 | -73.76662572 |
| 1045 | 1 | 0 | 0 | 33.38092947 |
| 1046 | 1 | 0 | 0 | 35.30832757 |
| 1047 | 1 | 0 | 0 | 75.48273161 |
| 1048 | 2 | 0 | 0 | 72.95653105 |
| 1049 | 1 | 0 | 0 | 73.812174 |
| 1050 | 1 | 0 | 0 | 58.90149636 |
| 1051 | 1 | 0 | 0 | 51.6809847 |
| 1052 | 0 | 0 | 0 | 43.93003347 |
| 1053 | 0 | 0 | 0 | 47.40789414 |
| 1054 | 1 | 0 | 0 | 47.37085945 |
| 1055 | 0 | 0 | 0 | 46.36892464 |
| 1056 | 1 | 0 | 0 | 48.16760322 |
| 1057 | 1 | 0 | 1 | 37.61825558 |
| 1058 | 1 | 0 | 0 | 27.95369626 |
| 1059 | 0 | 1 | 1 | 49.00749312 |
| 1060 | 2 | 0 | 0 | 42.69282162 |
| 1061 | 1 | 0 | 0 | 52.44075563 |
| 1062 | 0 | 1 | 0 | 53.10527879 |
| 1063 | 0 | 1 | 1 | 45.77520803 |

| | | | | |
|---|---|---|---|---|
| 1064 | 1 | 0 | 0 | 56.03702415 |
| 1065 | 1 | 0 | 0 | 56.35239116 |
| 1066 | 1 | 0 | 0 | 55.38791875 |
| 1067 | 0 | 0 | 0 | 54.76152702 |
| 1068 | 0 | 0 | 1 | 54.50321877 |
| 1069 | 1 | 0 | 0 | 59.95437395 |
| 1070 | 1 | 0 | 1 | 59.89300086 |
| 1071 | 1 | 1 | 0 | 50.36897472 |
| 1072 | 2 | 1 | 0 | 50.26606265 |
| 1073 | 2 | 0 | 0 | 31.86714662 |
| 1074 | 1 | 0 | 1 | 22.83138674 |
| 1075 | 1 | 0 | 1 | 38.75397075 |
| 1076 | 1 | 0 | 1 | 39.60358936 |
| 1077 | 0 | 0 | 0 | 43.44368474 |
| 1078 | 1 | 0 | 0 | 42.65047781 |
| 1079 | 1 | 1 | 1 | 43.46184846 |
| 1080 | 2 | 0 | 0 | 32.65242371 |
| 1081 | 0 | 1 | 1 | 39.09196154 |
| 1082 | 2 | 0 | 0 | 29.08576714 |
| 1083 | 1 | 0 | 0 | 28.841233 |
| 1084 | 1 | 0 | 0 | 33.87609295 |
| 1085 | 1 | 0 | 1 | 34.26376356 |
| 1086 | 1 | 1 | 0 | 42.24270984 |
| 1087 | 1 | 1 | 0 | 51.38005865 |
| 1088 | 1 | 0 | 0 | 56.04670828 |
| 1089 | 1 | 0 | 1 | 63.54616169 |
| 1090 | 1 | 0 | 1 | 63.74237128 |
| 1091 | 2 | 0 | 0 | 64.60291921 |
| 1092 | 2 | 0 | 0 | 64.9395359 |
| 1093 | 1 | 0 | 1 | 66.91445623 |
| 1094 | 0 | 0 | 0 | 68.63022062 |
| 1095 | 1 | 0 | 0 | 69.33312627 |
| 1096 | 1 | 0 | 1 | 69.18723774 |
| 1097 | 1 | 0 | 0 | 72.20085392 |
| 1098 | 1 | 0 | 0 | 71.31514951 |
| 1099 | 1 | 0 | 0 | 72.69792601 |
| 1100 | 1 | 1 | 0 | 74.43154587 |
| 1101 | 1 | 0 | 1 | 74.16305925 |
| 1102 | 1 | 0 | 0 | 74.10219197 |
| 1103 | 0 | 0 | 0 | 68.38086918 |
| 1104 | 0 | 0 | 0 | 69.66419563 |
| 1105 | 1 | 0 | 0 | 66.30663243 |
| 1106 | 0 | 0 | 0 | 66.50379929 |
| 1107 | 1 | 0 | 1 | 64.52462461 |
| 1108 | 1 | 0 | 0 | 56.42622415 |
| 1109 | 1 | 1 | 0 | 70.84518357 |
| 1110 | 1 | 0 | 0 | 71.60475234 |
| 1111 | 1 | 0 | 0 | 72.52520442 |

| | | | | |
|---|---|---|---|---|
| 1112 | 2 | 0 | 0 | 74.14512238 |
| 1113 | 1 | 0 | 0 | 72.66094672 |
| 1114 | 1 | 0 | 1 | 74.63995072 |
| 1115 | 1 | 0 | 0 | 73.79731708 |
| 1116 | 1 | 0 | 0 | 76.25142829 |
| 1117 | 1 | 0 | 1 | 73.68107389 |
| 1118 | 1 | 0 | 0 | 70.98781872 |
| 1119 | 1 | 0 | 0 | 70.83389361 |
| 1120 | 0 | 0 | 1 | 71.02334636 |
| 1121 | 1 | 0 | 0 | 63.77546554 |
| 1122 | 1 | 0 | 0 | 35.67018871 |
| 1123 | 0 | 0 | 1 | 33.9894901 |
| 1124 | 1 | 0 | 0 | 30.76244183 |
| 1125 | 1 | 0 | 0 | 32.25335391 |
| 1126 | 1 | 0 | 0 | 12.1582156 |
| 1127 | 0 | 0 | 0 | 11.94788202 |
| 1128 | 0 | 0 | 1 | 17.64496901 |
| 1129 | 2 | 1 | 0 | 17.85508078 |
| 1130 | 2 | 0 | 1 | 48.63787298 |
| 1131 | 1 | 1 | 0 | 38.65881985 |
| 1132 | 1 | 1 | 0 | 35.58160501 |
| 1133 | 1 | 0 | 0 | 35.29451142 |
| 1134 | 2 | 0 | 0 | 36.75947919 |
| 1135 | 1 | 0 | 0 | 29.97424197 |
| 1136 | 1 | 0 | 0 | 24.92877918 |
| 1137 | 1 | 0 | 0 | 26.53330232 |
| 1138 | 1 | 1 | 1 | 20.56895021 |
| 1139 | 1 | 0 | 0 | 17.40431893 |
| 1140 | 0 | 0 | 0 | 18.37747055 |
| 1141 | 1 | 0 | 0 | 16.68936366 |
| 1142 | 1 | 0 | 1 | 8.99476786 |
| 1143 | 2 | 0 | 1 | 8.7308418 |
| 1144 | 1 | 0 | 1 | 1.920477372 |
| 1145 | 1 | 0 | 0 | 1.69288884 |
| 1146 | 0 | 0 | 1 | 4.687823605 |
| 1147 | 0 | 0 | 0 | 0.329147221 |
| 1148 | 1 | 0 | 1 | 0.568981657 |
| 1149 | 1 | 0 | 1 | -0.191678866 |
| 1150 | 1 | 0 | 0 | -0.051824711 |
| 1151 | 1 | 0 | 0 | -6.520168968 |
| 1152 | 1 | 0 | 0 | -6.485141245 |
| 1153 | 1 | 0 | 0 | -5.132756561 |
| 1154 | 1 | 1 | 0 | 0.181621167 |
| 1155 | 1 | 0 | 1 | 2.038430842 |
| 1156 | 1 | 0 | 1 | 4.431163645 |
| 1157 | 1 | 0 | 0 | 2.081581749 |
| 1158 | 1 | 0 | 0 | 2.802352025 |
| 1159 | 1 | 0 | 1 | 2.033148384 |

| | | | | |
|---|---|---|---|---|
| 1160 | 2 | 0 | 1 | 7.145636325 |
| 1161 | 1 | 0 | 1 | 6.69048286 |
| 1162 | 1 | 0 | 0 | 8.374582327 |
| 1163 | 2 | 0 | 0 | 10.17733044 |
| 1164 | 2 | 0 | 0 | 10.39956525 |
| 1165 | 1 | 1 | 0 | 11.94078408 |
| 1166 | 1 | 0 | 0 | 30.73378128 |
| 1167 | 1 | 0 | 0 | 30.98365875 |
| 1168 | 2 | 0 | 0 | 24.02446262 |
| 1169 | 2 | 0 | 0 | 20.70128736 |
| 1170 | 2 | 0 | 1 | 17.47406227 |
| 1171 | 0 | 0 | 0 | 15.05418984 |
| 1172 | 0 | 0 | 0 | 16.66799604 |
| 1173 | 0 | 0 | 0 | 20.19860397 |
| 1174 | 2 | 0 | 1 | 20.49443561 |
| 1175 | 0 | 0 | 0 | 21.89092904 |
| 1176 | 2 | 0 | 0 | 18.27769719 |
| 1177 | 1 | 0 | 0 | 17.49167 |
| 1178 | 1 | 0 | 0 | 21.18325111 |
| 1179 | 0 | 0 | 1 | 22.09874844 |
| 1180 | 0 | 1 | 0 | 27.57875974 |
| 1181 | 1 | 0 | 0 | 28.95543944 |
| 1182 | 2 | 0 | 0 | 37.75932277 |
| 1183 | 1 | 0 | 0 | 32.09167132 |
| 1184 | 1 | 0 | 0 | 26.93086455 |
| 1185 | 2 | 0 | 0 | 27.25621808 |
| 1186 | 1 | 1 | 1 | 25.31120758 |
| 1187 | 0 | 0 | 0 | 25.77857248 |
| 1188 | 0 | 0 | 1 | 25.74732197 |
| 1189 | 0 | 0 | 0 | 33.64801183 |
| 1190 | 1 | 0 | 0 | 32.49667425 |
| 1191 | 2 | 0 | 0 | 34.16887512 |
| 1192 | 2 | 0 | 1 | 32.00535436 |
| 1193 | 2 | 0 | 0 | 23.09796246 |
| 1194 | 2 | 0 | 0 | 19.45366692 |
| 1195 | 1 | 0 | 0 | 17.98881767 |
| 1196 | 1 | 0 | 1 | 17.89874171 |
| 1197 | 1 | 0 | 0 | 18.31372367 |
| 1198 | 2 | 0 | 0 | 18.16029445 |
| 1199 | 1 | 0 | 0 | 17.9181609 |
| 1200 | 1 | 0 | 0 | 17.57998834 |
| 1201 | 1 | 0 | 0 | 17.77313859 |
| 1202 | 1 | 0 | 0 | 17.67278267 |
| 1203 | 1 | 0 | 0 | 18.89815986 |
| 1204 | 1 | 1 | 0 | 15.7733516 |
| 1205 | 1 | 0 | 0 | 19.45301041 |
| 1206 | 1 | 0 | 0 | 19.7681512 |
| 1207 | 1 | 0 | 0 | 20.28352899 |

| | | | | |
|---|---|---|---|---|
| 1208 | 1 | 1 | 0 | 17.16456379 |
| 1209 | 1 | 0 | 0 | 15.0076744 |
| 1210 | 0 | 0 | 0 | 14.83197777 |
| 1211 | 0 | 0 | 0 | 14.57353383 |
| 1212 | 0 | 0 | 0 | 14.56147575 |
| 1213 | 0 | 0 | 0 | 14.50642157 |
| 1214 | 1 | 0 | 0 | 15.14035634 |
| 1215 | 1 | 0 | 0 | 14.51817513 |
| 1216 | 1 | 0 | 0 | 15.89932777 |
| 1217 | 1 | 0 | 0 | 13.86984611 |
| 1218 | 1 | 0 | 0 | 12.28754162 |
| 1219 | 1 | 0 | 0 | 12.33512494 |
| 1220 | 1 | 0 | 0 | 12.2857984 |
| 1221 | 0 | 1 | 1 | 16.61439402 |
| 1222 | 0 | 0 | 0 | 23.43657112 |
| 1223 | 0 | 0 | 0 | 22.20222408 |
| 1224 | 1 | 0 | 0 | 24.28574984 |
| 1225 | 2 | 1 | 1 | 24.16580447 |
| 1226 | 2 | 0 | 0 | 23.15752957 |
| 1227 | 1 | 0 | 1 | 20.81756771 |
| 1228 | 2 | 0 | 1 | 27.27912034 |
| 1229 | 2 | 0 | 1 | 27.59855812 |
| 1230 | 0 | 0 | 1 | 26.70994837 |
| 1231 | 1 | 0 | 0 | 31.2526243 |
| 1232 | 0 | 0 | 0 | 25.82519272 |
| 1233 | 1 | 1 | 0 | 8.269883683 |
| 1234 | 2 | 0 | 1 | 4.187957075 |
| 1235 | 1 | 1 | 0 | 3.810278168 |
| 1236 | 1 | 0 | 1 | 1.659548927 |
| 1237 | 2 | 0 | 1 | 0.837240076 |
| 1238 | 1 | 0 | 0 | 0.968506048 |
| 1239 | 1 | 0 | 0 | -0.664594776 |
| 1240 | 1 | 0 | 0 | 0.267055079 |
| 1241 | 1 | 0 | 0 | 1.494740334 |
| 1242 | 1 | 1 | 0 | -0.73947833 |
| 1243 | 1 | 0 | 0 | -0.572362581 |
| 1244 | 1 | 1 | 0 | 0.974793858 |
| 1245 | 1 | 1 | 0 | 1.704724954 |
| 1246 | 1 | 0 | 0 | 0.981298844 |
| 1247 | 1 | 0 | 1 | 2.381144536 |
| 1248 | 1 | 0 | 0 | 0.575381727 |
| 1249 | 1 | 0 | 0 | 5.683900515 |
| 1250 | 0 | 0 | 1 | 21.87793184 |
| 1251 | 1 | 1 | 0 | 12.67307392 |
| 1252 | 1 | 0 | 0 | 8.326475046 |
| 1253 | 1 | 0 | 0 | 8.361818248 |
| 1254 | 1 | 0 | 1 | 8.312263168 |
| 1255 | 0 | 0 | 1 | 5.833555286 |

| | | | | |
|---|---|---|---|---|
| 1256 | 1 | 0 | 0 | 6.835110093 |
| 1257 | 1 | 0 | 1 | 7.076709819 |
| 1258 | 1 | 0 | 1 | 4.822919525 |
| 1259 | 1 | 0 | 1 | 2.886663886 |
| 1260 | 2 | 0 | 0 | 3.040624925 |
| 1261 | 1 | 0 | 1 | -0.02411978 |
| 1262 | 1 | 0 | 0 | 4.64265733 |
| 1263 | 1 | 0 | 0 | 4.111789703 |
| 1264 | 1 | 0 | 1 | -0.212032491 |
| 1265 | 1 | 1 | 0 | 0.041134433 |
| 1266 | 0 | 0 | 1 | -0.027363216 |
| 1267 | 1 | 0 | 0 | -1.485412876 |
| 1268 | 1 | 0 | 0 | -3.803125814 |
| 1269 | 1 | 1 | 0 | -6.572597613 |
| 1270 | 1 | 1 | 0 | -7.912651948 |
| 1271 | 1 | 0 | 0 | -7.06236408 |
| 1272 | 1 | 0 | 0 | -3.768746191 |
| 1273 | 1 | 1 | 1 | -4.716322707 |
| 1274 | 1 | 0 | 0 | -21.09102538 |
| 1275 | 1 | 0 | 1 | -38.94288474 |
| 1276 | 1 | 0 | 0 | -42.79059959 |
| 1277 | 1 | 0 | 0 | -42.04132658 |
| 1278 | 1 | 1 | 0 | -42.17974292 |
| 1279 | 2 | 0 | 0 | -45.59451272 |
| 1280 | 2 | 1 | 1 | -53.2459994 |
| 1281 | 1 | 1 | 0 | -53.80126085 |
| 1282 | 1 | 1 | 0 | -55.44258523 |
| 1283 | 1 | 0 | 0 | -56.93797377 |
| 1284 | 1 | 0 | 1 | -51.55287669 |
| 1285 | 1 | 0 | 0 | -46.0343628 |
| 1286 | 1 | 1 | 0 | -39.49685452 |
| 1287 | 1 | 1 | 0 | -39.99744159 |
| 1288 | 1 | 0 | 0 | -40.30168803 |
| 1289 | 1 | 0 | 1 | -40.82267316 |
| 1290 | 1 | 0 | 0 | -40.85178586 |
| 1291 | 1 | 0 | 0 | -40.79883587 |
| 1292 | 0 | 0 | 0 | -41.28258843 |
| 1293 | 1 | 0 | 1 | -41.15507527 |
| 1294 | 2 | 0 | 1 | -40.76212181 |
| 1295 | 1 | 1 | 0 | -40.32150091 |
| 1296 | 2 | 0 | 1 | -44.81948774 |
| 1297 | 1 | 0 | 0 | -46.74160188 |
| 1298 | 1 | 0 | 0 | -59.99419362 |
| 1299 | 1 | 0 | 1 | -50.01738369 |
| 1300 | 0 | 0 | 0 | -44.05668899 |
| 1301 | 1 | 0 | 0 | -38.37442672 |
| 1302 | 1 | 0 | 0 | -38.49368104 |
| 1303 | 1 | 0 | 0 | -39.45485093 |

| | | | | |
|---|---|---|---|---|
| 1304 | 1 | 0 | 0 | -40.07465751 |
| 1305 | 0 | 0 | 0 | -40.42821333 |
| 1306 | 1 | 1 | 1 | -44.16632995 |
| 1307 | 0 | 0 | 0 | -43.0516902 |
| 1308 | 0 | 0 | 0 | -43.20440122 |
| 1309 | 0 | 0 | 1 | -42.19048399 |
| 1310 | 2 | 1 | 1 | -39.73729396 |
| 1311 | 0 | 0 | 0 | -42.58910746 |
| 1312 | 1 | 0 | 0 | -49.01688467 |
| 1313 | 1 | 1 | 1 | -59.4428882 |
| 1314 | 1 | 0 | 1 | -60.15986143 |
| 1315 | 1 | 0 | 0 | -51.32149073 |
| 1316 | 1 | 1 | 0 | -52.35171943 |
| 1317 | 1 | 0 | 0 | -57.11088279 |
| 1318 | 1 | 1 | 0 | -57.95846113 |
| 1319 | 1 | 0 | 0 | -57.93960722 |
| 1320 | 1 | 0 | 0 | -57.35897841 |
| 1321 | 1 | 0 | 0 | -58.87301262 |
| 1322 | 1 | 0 | 0 | -57.40067288 |
| 1323 | 1 | 0 | 0 | -54.3840559 |
| 1324 | 1 | 0 | 0 | -53.58329488 |
| 1325 | 1 | 0 | 1 | -54.98700583 |
| 1326 | 1 | 0 | 0 | -51.6041358 |
| 1327 | 1 | 0 | 0 | -51.06882424 |
| 1328 | 1 | 1 | 0 | -49.13050108 |
| 1329 | 1 | 0 | 0 | -50.22057529 |
| 1330 | 1 | 0 | 1 | -49.15475124 |
| 1331 | 1 | 0 | 0 | -42.60883046 |
| 1332 | 1 | 0 | 0 | -45.62853314 |
| 1333 | 1 | 0 | 0 | -45.66300814 |
| 1334 | 1 | 0 | 1 | -49.15052532 |
| 1335 | 1 | 0 | 0 | -47.13281555 |
| 1336 | 0 | 0 | 1 | -30.40405289 |
| 1337 | 1 | 0 | 1 | -32.34544752 |
| 1338 | 1 | 1 | 0 | -33.85568663 |
| 1339 | 0 | 0 | 0 | -30.35029142 |
| 1340 | 0 | 0 | 0 | -30.88608768 |
| 1341 | 0 | 0 | 0 | -31.04754668 |
| 1342 | 1 | 0 | 0 | -32.06366651 |
| 1343 | 1 | 0 | 1 | -31.53421139 |
| 1344 | 0 | 0 | 0 | -33.98362886 |
| 1345 | 0 | 0 | 0 | -37.23928318 |
| 1346 | 1 | 0 | 0 | -38.67716859 |
| 1347 | 1 | 0 | 0 | -36.74402436 |
| 1348 | 0 | 1 | 1 | -37.402818 |
| 1349 | 1 | 0 | 0 | -35.89250483 |
| 1350 | 1 | 0 | 0 | -34.69088979 |
| 1351 | 0 | 0 | 0 | -36.16630968 |

| | | | | |
|---|---|---|---|---|
| 1352 | 1 | 1 | 1 | -30.79137587 |
| 1353 | 1 | 1 | 0 | -30.52425539 |
| 1354 | 1 | 0 | 0 | -29.63884995 |
| 1355 | 0 | 0 | 0 | -36.49529159 |
| 1356 | 2 | 0 | 0 | -36.47937089 |
| 1357 | 1 | 0 | 0 | -15.33692415 |
| 1358 | 0 | 0 | 0 | -2.418859976 |
| 1359 | 1 | 0 | 1 | 7.048473057 |
| 1360 | 1 | 0 | 0 | 8.040000594 |
| 1361 | 1 | 0 | 1 | 14.2602615 |
| 1362 | 1 | 0 | 0 | 4.455439012 |
| 1363 | 1 | 1 | 0 | 5.286465906 |
| 1364 | 1 | 1 | 1 | -0.700854458 |
| 1365 | 1 | 0 | 0 | -0.316391694 |
| 1366 | 0 | 0 | 0 | -2.278574887 |
| 1367 | 1 | 1 | 0 | 0.597661181 |
| 1368 | 0 | 0 | 0 | 25.86665641 |
| 1369 | 1 | 0 | 0 | 32.82763113 |
| 1370 | 1 | 1 | 1 | 32.71949116 |
| 1371 | 1 | 0 | 0 | 32.42860475 |
| 1372 | 1 | 0 | 0 | 17.45644454 |
| 1373 | 1 | 1 | 0 | 10.74984913 |
| 1374 | 1 | 0 | 0 | 9.083377784 |
| 1375 | 1 | 0 | 0 | 8.405653373 |
| 1376 | 0 | 0 | 0 | -18.36605059 |
| 1377 | 1 | 1 | 0 | -23.9294552 |
| 1378 | 1 | 0 | 0 | -24.7497223 |
| 1379 | 1 | 0 | 0 | -22.60217685 |
| 1380 | 2 | 0 | 0 | -23.45835764 |
| 1381 | 1 | 0 | 0 | -21.23482907 |
| 1382 | 1 | 0 | 0 | -24.93611189 |
| 1383 | 1 | 0 | 0 | -24.31772421 |
| 1384 | 1 | 0 | 0 | -23.99289091 |
| 1385 | 1 | 0 | 0 | 27.07490619 |
| 1386 | 2 | 0 | 1 | -51.09814567 |
| 1387 | 2 | 0 | 1 | -50.4881908 |
| 1388 | 0 | 0 | 0 | -39.07379103 |
| 1389 | 1 | 0 | 1 | -29.55193086 |
| 1390 | 1 | 0 | 0 | -31.26300328 |
| 1391 | 1 | 0 | 0 | -27.17864228 |
| 1392 | 1 | 0 | 0 | -27.73175758 |
| 1393 | 1 | 0 | 1 | 6.967651355 |
| 1394 | 1 | 0 | 1 | 7.41292104 |
| 1395 | 1 | 0 | 0 | 10.28688427 |
| 1396 | 1 | 0 | 0 | 27.2081141 |
| 1397 | 0 | 1 | 1 | 31.61920986 |
| 1398 | 1 | 1 | 0 | 21.63303784 |
| 1399 | 1 | 0 | 1 | 16.94370009 |

| | | | | |
|---|---|---|---|---|
| 1400 | 1 | 1 | 0 | 18.34680349 |
| 1401 | 1 | 0 | 0 | 23.72338079 |
| 1402 | 1 | 0 | 0 | 23.29271523 |
| 1403 | 1 | 0 | 0 | 22.84900324 |
| 1404 | 1 | 0 | 1 | 9.858151164 |
| 1405 | 1 | 0 | 1 | 7.795345332 |
| 1406 | 1 | 0 | 0 | 7.515687191 |
| 1407 | 1 | 0 | 0 | -1.710846661 |
| 1408 | 1 | 0 | 1 | -1.124823459 |
| 1409 | 1 | 0 | 1 | 0.052933644 |
| 1410 | 1 | 0 | 1 | -2.103991302 |
| 1411 | 1 | 1 | 0 | -9.395280073 |
| 1412 | 1 | 0 | 0 | -26.67448131 |
| 1413 | 0 | 0 | 0 | -40.09038768 |
| 1414 | 0 | 0 | 0 | -46.95598397 |
| 1415 | 2 | 0 | 1 | -30.39739394 |
| 1416 | 1 | 1 | 0 | -31.2578171 |
| 1417 | 1 | 0 | 0 | -23.719648 |
| 1418 | 2 | 1 | 1 | -25.39954772 |
| 1419 | 1 | 0 | 1 | -21.92691022 |
| 1420 | 1 | 1 | 0 | -13.16416707 |
| 1421 | 1 | 0 | 0 | -20.30521218 |
| 1422 | 1 | 0 | 1 | -17.26844223 |
| 1423 | 1 | 0 | 1 | -57.02736091 |
| 1424 | 1 | 0 | 0 | -33.3707221 |
| 1425 | 1 | 1 | 0 | -2.471945948 |
| 1426 | 2 | 0 | 1 | 7.489394602 |
| 1427 | 1 | 1 | 0 | 9.30856443 |
| 1428 | 0 | 0 | 0 | 9.933821443 |
| 1429 | 1 | 0 | 0 | 11.2731641 |
| 1430 | 1 | 0 | 1 | 12.96520401 |
| 1431 | 1 | 0 | 1 | 16.46658839 |
| 1432 | 1 | 0 | 1 | 38.04569339 |
| 1433 | 0 | 0 | 0 | 25.11856789 |
| 1434 | 1 | 0 | 0 | 23.28241066 |
| 1435 | 0 | 0 | 1 | 16.11160661 |
| 1436 | 1 | 0 | 1 | 13.40571979 |
| 1437 | 2 | 0 | 0 | 10.88378492 |
| 1438 | 1 | 0 | 0 | 6.380488704 |
| 1439 | 1 | 0 | 0 | 6.172056835 |
| 1440 | 1 | 0 | 0 | 7.531743543 |
| 1441 | 1 | 0 | 0 | 6.669886557 |
| 1442 | 1 | 0 | 0 | 5.445758337 |
| 1443 | 1 | 0 | 0 | 4.810239181 |
| 1444 | 0 | 0 | 0 | 6.420114837 |
| 1445 | 1 | 0 | 0 | 3.460554734 |
| 1446 | 2 | 0 | 0 | 2.460426854 |
| 1447 | 1 | 0 | 0 | 1.559517947 |

| | | | | |
|---|---|---|---|---|
| 1448 | 1 | 0 | 0 | 1.137626024 |
| 1449 | 1 | 0 | 0 | -2.049665468 |
| 1450 | 0 | 0 | 0 | -1.920990003 |
| 1451 | 1 | 0 | 0 | -15.74999723 |
| 1452 | 1 | 1 | 0 | 6.190180065 |
| 1453 | 1 | 0 | 0 | 1.727771507 |
| 1454 | 1 | 0 | 0 | 1.565993942 |
| 1455 | 1 | 0 | 0 | 1.66230763 |
| 1456 | 1 | 0 | 0 | -0.581261873 |
| 1457 | 1 | 0 | 0 | 1.187409889 |
| 1458 | 1 | 0 | 0 | 1.236428749 |
| 1459 | 0 | 1 | 1 | 0.133376922 |
| 1460 | 1 | 1 | 0 | -0.669060826 |
| 1461 | 1 | 1 | 0 | 0.568787237 |
| 1462 | 1 | 1 | 1 | 0.181286003 |
| 1463 | 1 | 0 | 1 | -0.16320183 |
| 1464 | 1 | 0 | 0 | 0.259583877 |
| 1465 | 1 | 0 | 1 | 0.794414776 |
| 1466 | 1 | 0 | 0 | -1.617637 |
| 1467 | 1 | 1 | 1 | -2.752758662 |
| 1468 | 1 | 0 | 0 | 6.839332422 |
| 1469 | 1 | 0 | 0 | 5.96085607 |
| 1470 | 1 | 0 | 0 | 7.510975173 |
| 1471 | 1 | 0 | 1 | 7.437331221 |
| 1472 | 2 | 0 | 1 | 9.533360498 |
| 1473 | 0 | 1 | 0 | 8.175332229 |
| 1474 | 2 | 0 | 0 | 10.08005192 |
| 1475 | 2 | 1 | 0 | 10.00067071 |
| 1476 | 2 | 0 | 1 | 0.137465329 |
| 1477 | 1 | 0 | 1 | 2.41780658 |
| 1478 | 2 | 1 | 1 | 6.568192819 |
| 1479 | 1 | 0 | 0 | 3.831073788 |
| 1480 | 1 | 0 | 0 | 2.12451502 |
| 1481 | 2 | 0 | 1 | 1.001274303 |
| 1482 | 2 | 0 | 1 | -0.827873205 |
| 1483 | 1 | 0 | 0 | -1.545509251 |
| 1484 | 1 | 1 | 0 | -1.1525227 |
| 1485 | 1 | 0 | 0 | -3.470120172 |
| 1486 | 1 | 0 | 1 | 3.171002808 |
| 1487 | 1 | 0 | 0 | -4.94290524 |
| 1488 | 1 | 0 | 0 | -5.459815266 |
| 1489 | 1 | 0 | 0 | -6.033843311 |
| 1490 | 2 | 0 | 1 | -6.57657945 |
| 1491 | 1 | 0 | 1 | -5.459171365 |
| 1492 | 2 | 0 | 0 | -1.617538861 |
| 1493 | 2 | 0 | 0 | -4.730402142 |
| 1494 | 0 | 0 | 1 | -7.087332886 |
| 1495 | 1 | 0 | 0 | -7.235569909 |

| | | | | |
|---|---|---|---|---|
| 1496 | 1 | 0 | 1 | -14.87690105 |
| 1497 | 0 | 0 | 0 | -14.62498275 |
| 1498 | 2 | 0 | 0 | -13.9339068 |
| 1499 | 1 | 1 | 1 | -7.246227036 |
| 1500 | 1 | 0 | 1 | 19.77039299 |
| 1501 | 1 | 0 | 0 | 23.61309395 |
| 1502 | 1 | 0 | 0 | -13.57899582 |
| 1503 | 1 | 0 | 1 | -14.90016266 |
| 1504 | 1 | 0 | 0 | -13.90559692 |
| 1505 | 1 | 0 | 0 | -24.90289079 |
| 1506 | 1 | 1 | 0 | -23.59294017 |
| 1507 | 1 | 1 | 0 | -29.84074797 |
| 1508 | 1 | 0 | 1 | -29.45698113 |
| 1509 | 2 | 0 | 1 | -29.59291921 |
| 1510 | 1 | 0 | 0 | -31.86144156 |
| 1511 | 1 | 1 | 0 | -31.06613012 |
| 1512 | 1 | 1 | 0 | -25.07697881 |
| 1513 | 1 | 0 | 1 | -23.13440167 |
| 1514 | 1 | 0 | 0 | -23.89638098 |
| 1515 | 1 | 1 | 0 | -31.64730005 |
| 1516 | 1 | 0 | 0 | -33.54865255 |
| 1517 | 0 | 0 | 1 | -38.7269815 |
| 1518 | 0 | 0 | 0 | -41.42511777 |
| 1519 | 1 | 0 | 0 | -43.59487176 |
| 1520 | 2 | 0 | 0 | -28.36264757 |
| 1521 | 1 | 0 | 0 | -27.54958217 |
| 1522 | 1 | 1 | 0 | -49.63198432 |
| 1523 | 1 | 0 | 0 | -55.77402428 |
| 1524 | 1 | 0 | 0 | -54.83034634 |
| 1525 | 1 | 0 | 0 | -15.77710024 |
| 1526 | 1 | 0 | 1 | -15.72993154 |
| 1527 | 1 | 1 | 0 | -17.95226423 |
| 1528 | 1 | 0 | 0 | -11.54593196 |
| 1529 | 1 | 0 | 0 | -14.16435193 |
| 1530 | 2 | 0 | 1 | -9.761935435 |
| 1531 | 1 | 0 | 0 | -9.815564152 |
| 1532 | 1 | 0 | 1 | -4.540758651 |
| 1533 | 1 | 1 | 1 | -4.512268782 |
| 1534 | 2 | 0 | 1 | -3.706132673 |
| 1535 | 0 | 1 | 1 | -15.55743922 |
| 1536 | 2 | 1 | 0 | -17.19665506 |
| 1537 | 2 | 0 | 0 | -19.99410453 |
| 1538 | 2 | 0 | 0 | -19.56617541 |
| 1539 | 2 | 0 | 1 | -19.75157366 |
| 1540 | 1 | 0 | 0 | -19.86823058 |
| 1541 | 1 | 0 | 0 | -13.70967915 |
| 1542 | 1 | 0 | 1 | -14.30458125 |
| 1543 | 2 | 0 | 0 | -14.34224041 |

| | | | | |
|---|---|---|---|---|
| 1544 | 1 | 0 | 0 | -14.58170793 |
| 1545 | 2 | 1 | 1 | -20.42699954 |
| 1546 | 2 | 1 | 0 | -20.8925344 |
| 1547 | 1 | 0 | 1 | -48.8465511 |
| 1548 | 1 | 0 | 0 | -48.91913201 |
| 1549 | 2 | 0 | 0 | -49.13365602 |
| 1550 | 1 | 0 | 0 | -51.23617433 |
| 1551 | 1 | 0 | 0 | -54.53676916 |
| 1552 | 1 | 0 | 0 | -45.22656167 |
| 1553 | 2 | 1 | 1 | -51.36376013 |
| 1554 | 2 | 0 | 1 | -52.58761462 |
| 1555 | 2 | 0 | 0 | -52.24714045 |
| 1556 | 1 | 0 | 0 | -53.81100151 |
| 1557 | 2 | 0 | 0 | -53.55234247 |
| 1558 | 1 | 0 | 0 | -51.35172505 |
| 1559 | 0 | 0 | 1 | -52.56120469 |
| 1560 | 1 | 0 | 1 | -50.86429802 |
| 1561 | 1 | 0 | 0 | -51.27120887 |
| 1562 | 1 | 0 | 0 | -55.5741171 |
| 1563 | 1 | 0 | 1 | -56.3579377 |
| 1564 | 1 | 0 | 0 | -56.94122994 |
| 1565 | 0 | 0 | 0 | -58.11953106 |
| 1566 | 1 | 0 | 0 | -52.39543484 |
| 1567 | 1 | 0 | 1 | -59.85319444 |
| 1568 | 1 | 0 | 1 | -59.72367261 |
| 1569 | 2 | 1 | 1 | -59.41667233 |
| 1570 | 1 | 0 | 1 | -63.16751326 |
| 1571 | 1 | 1 | 1 | -61.03613617 |
| 1572 | 1 | 1 | 0 | -60.36740737 |
| 1573 | 0 | 0 | 0 | -43.86570759 |
| 1574 | 1 | 0 | 1 | -48.1432561 |
| 1575 | 1 | 0 | 0 | -60.15755408 |
| 1576 | 1 | 0 | 1 | -60.22566684 |
| 1577 | 0 | 0 | 0 | -49.24979415 |
| 1578 | 1 | 0 | 0 | -46.07127884 |
| 1579 | 1 | 0 | 0 | -51.7399275 |
| 1580 | 2 | 0 | 1 | -50.42950183 |
| 1581 | 1 | 1 | 1 | -36.87510975 |
| 1582 | 1 | 0 | 1 | -39.30921502 |
| 1583 | 1 | 0 | 1 | -38.63076567 |
| 1584 | 1 | 1 | 0 | -27.19889332 |
| 1585 | 1 | 0 | 0 | -17.55793472 |
| 1586 | 1 | 1 | 0 | -8.407437153 |
| 1587 | 1 | 1 | 0 | -7.002796195 |
| 1588 | 1 | 0 | 0 | 5.121379321 |
| 1589 | 0 | 1 | 1 | 6.387891429 |
| 1590 | 1 | 0 | 0 | 7.605507554 |
| 1591 | 0 | 0 | 0 | 32.13209978 |

| | | | | |
|---|---|---|---|---|
| 1592 | 1 | 0 | 0 | 35.01952674 |
| 1593 | 2 | 1 | 1 | 54.51693295 |
| 1594 | 1 | 0 | 1 | 39.377523 |
| 1595 | 1 | 0 | 0 | 38.50658572 |
| 1596 | 1 | 0 | 0 | 39.25703324 |
| 1597 | 1 | 0 | 0 | 39.82504197 |
| 1598 | 1 | 1 | 0 | 39.15720623 |
| 1599 | 1 | 1 | 0 | 37.58122758 |
| 1600 | 1 | 0 | 1 | 38.12755773 |
| 1601 | 1 | 0 | 0 | 34.97366565 |
| 1602 | 1 | 0 | 0 | 34.42228728 |
| 1603 | 1 | 1 | 0 | 32.96010601 |
| 1604 | 0 | 0 | 1 | 32.19657977 |
| 1605 | 0 | 0 | 0 | 26.89229759 |
| 1606 | 2 | 1 | 1 | 50.22753993 |
| 1607 | 2 | 0 | 1 | 61.52113041 |
| 1608 | 1 | 1 | 0 | 63.22405362 |
| 1609 | 1 | 0 | 0 | 57.35156382 |
| 1610 | 1 | 0 | 1 | 58.08910558 |
| 1611 | 2 | 0 | 0 | 57.66732331 |
| 1612 | 1 | 0 | 1 | 57.53520591 |
| 1613 | 2 | 0 | 1 | 28.76195326 |
| 1614 | 1 | 0 | 0 | 28.906908 |
| 1615 | 1 | 0 | 0 | 30.09196893 |
| 1616 | 1 | 1 | 0 | 13.79275883 |
| 1617 | 1 | 0 | 0 | 15.55476314 |
| 1618 | 1 | 0 | 0 | 8.153287625 |
| 1619 | 1 | 1 | 0 | -9.872031828 |
| 1620 | 2 | 0 | 1 | -13.3025619 |
| 1621 | 1 | 1 | 0 | -14.2076691 |
| 1622 | 1 | 0 | 0 | -12.99656589 |
| 1623 | 1 | 0 | 0 | -12.50108857 |
| 1624 | 0 | 1 | 0 | -20.15298982 |
| 1625 | 1 | 0 | 1 | -22.79095534 |
| 1626 | 1 | 0 | 0 | -22.14642158 |
| 1627 | 0 | 0 | 0 | -16.03670101 |
| 1628 | 1 | 0 | 0 | -6.15838529 |
| 1629 | 1 | 0 | 1 | -6.70285349 |
| 1630 | 1 | 0 | 0 | -6.661004768 |
| 1631 | 1 | 0 | 0 | -5.423244959 |
| 1632 | 2 | 0 | 1 | -1.560919423 |
| 1633 | 1 | 0 | 0 | 1.702387076 |
| 1634 | 1 | 0 | 0 | 1.130221939 |
| 1635 | 1 | 0 | 0 | -3.781579538 |
| 1636 | 1 | 0 | 0 | 13.20515526 |
| 1637 | 2 | 1 | 1 | 15.07329895 |
| 1638 | 1 | 0 | 1 | -35.08167618 |
| 1639 | 1 | 0 | 1 | -13.1681118 |

| | | | | |
|---|---|---|---|---|
| 1640 | 2 | 1 | 0 | 10.9063266 |
| 1641 | 0 | 1 | 0 | 24.50002877 |
| 1642 | 0 | 0 | 0 | 24.45560319 |
| 1643 | 2 | 0 | 0 | 24.74337311 |
| 1644 | 1 | 0 | 0 | 24.46741529 |
| 1645 | 1 | 0 | 0 | 24.2881934 |
| 1646 | 2 | 0 | 1 | 15.39491162 |
| 1647 | 0 | 0 | 1 | 6.054258721 |
| 1648 | 1 | 0 | 1 | 0.228252387 |
| 1649 | 0 | 0 | 0 | 9.519589455 |
| 1650 | 2 | 0 | 1 | 10.11027124 |
| 1651 | 2 | 1 | 0 | 8.661814381 |
| 1652 | 1 | 1 | 0 | 7.113419806 |
| 1653 | 2 | 0 | 1 | 8.841981622 |
| 1654 | 1 | 1 | 0 | 9.808856575 |
| 1655 | 1 | 0 | 0 | 10.00858123 |
| 1656 | 1 | 0 | 0 | 9.314081774 |
| 1657 | 1 | 0 | 0 | 1.400655174 |
| 1658 | 1 | 0 | 0 | 0.08292188 |
| 1659 | 1 | 0 | 1 | 10.63222883 |
| 1660 | 1 | 0 | 0 | 27.27955599 |
| 1661 | 1 | 0 | 0 | 25.88962812 |
| 1662 | 1 | 0 | 1 | 30.87011643 |
| 1663 | 1 | 0 | 0 | 24.56355249 |
| 1664 | 1 | 1 | 0 | 16.59381382 |
| 1665 | 1 | 0 | 0 | 14.34955347 |
| 1666 | 1 | 1 | 1 | 12.89234975 |
| 1667 | 0 | 0 | 0 | 11.76885262 |
| 1668 | 1 | 0 | 1 | 19.85064538 |
| 1669 | 2 | 0 | 0 | 11.01668875 |
| 1670 | 1 | 0 | 1 | 9.407374758 |
| 1671 | 2 | 1 | 1 | -2.066318166 |
| 1672 | 1 | 0 | 1 | -1.535650237 |
| 1673 | 1 | 0 | 1 | -0.608912166 |
| 1674 | 1 | 0 | 0 | -0.61131732 |
| 1675 | 0 | 0 | 1 | -1.278358314 |
| 1676 | 0 | 0 | 1 | -2.205527352 |
| 1677 | 2 | 0 | 1 | -2.263191069 |
| 1678 | 1 | 0 | 0 | -5.462089069 |
| 1679 | 2 | 0 | 1 | -5.497761773 |
| 1680 | 1 | 0 | 0 | -6.481317345 |
| 1681 | 1 | 0 | 0 | -6.826612294 |
| 1682 | 1 | 0 | 0 | -7.563374224 |
| 1683 | 1 | 0 | 0 | -7.579265076 |
| 1684 | 1 | 0 | 0 | -8.592250825 |
| 1685 | 1 | 0 | 1 | -11.50306862 |
| 1686 | 0 | 0 | 1 | -16.70178527 |
| 1687 | 1 | 0 | 1 | -16.7294756 |

| | | | | |
|---|---|---|---|---|
| 1688 | 2 | 0 | 1 | -16.10570327 |
| 1689 | 1 | 0 | 0 | -19.45084194 |
| 1690 | 1 | 1 | 0 | -19.3968907 |
| 1691 | 0 | 0 | 0 | -17.80728422 |
| 1692 | 1 | 0 | 0 | -16.40662728 |
| 1693 | 1 | 0 | 0 | -31.53060274 |
| 1694 | 1 | 0 | 0 | -30.74548102 |
| 1695 | 1 | 0 | 0 | -31.18354833 |
| 1696 | 1 | 0 | 0 | -32.16181701 |
| 1697 | 1 | 0 | 0 | -32.45826241 |
| 1698 | 1 | 0 | 0 | -32.51792958 |
| 1699 | 1 | 0 | 0 | -30.34730162 |
| 1700 | 1 | 0 | 0 | -17.94853453 |
| 1701 | 1 | 0 | 0 | -12.40613103 |
| 1702 | 0 | 0 | 0 | -13.46102356 |
| 1703 | 1 | 0 | 0 | -33.03885281 |
| 1704 | 1 | 0 | 1 | -43.01331714 |
| 1705 | 1 | 0 | 0 | -43.84290992 |
| 1706 | 0 | 0 | 0 | -56.22482538 |
| 1707 | 1 | 0 | 1 | -52.51278659 |
| 1708 | 2 | 0 | 0 | -52.18226291 |
| 1709 | 1 | 0 | 1 | -50.34978335 |
| 1710 | 0 | 0 | 0 | -45.89781272 |
| 1711 | 1 | 0 | 0 | -48.01813292 |
| 1712 | 1 | 0 | 0 | -48.14036636 |
| 1713 | 1 | 0 | 0 | -48.00603616 |
| 1714 | 1 | 0 | 0 | -41.96032359 |
| 1715 | 0 | 0 | 0 | -32.16001992 |
| 1716 | 1 | 0 | 1 | -38.08560374 |
| 1717 | 1 | 0 | 0 | -39.17780718 |
| 1718 | 1 | 1 | 0 | -39.60147344 |
| 1719 | 1 | 0 | 1 | -40.69834037 |
| 1720 | 0 | 0 | 1 | -41.34700208 |
| 1721 | 1 | 0 | 1 | -43.06358418 |
| 1722 | 1 | 0 | 1 | -43.0220165 |
| 1723 | 1 | 0 | 0 | -44.03688055 |
| 1724 | 0 | 0 | 0 | -43.43847105 |
| 1725 | 1 | 0 | 0 | -44.26486004 |
| 1726 | 2 | 1 | 0 | -38.97591216 |
| 1727 | 2 | 0 | 0 | -42.25941397 |
| 1728 | 1 | 1 | 1 | -44.05773486 |
| 1729 | 1 | 0 | 0 | -38.83868319 |
| 1730 | 1 | 0 | 0 | -38.95452305 |
| 1731 | 1 | 0 | 0 | -38.90424695 |
| 1732 | 1 | 0 | 1 | -25.89204022 |
| 1733 | 1 | 0 | 0 | -20.9259375 |
| 1734 | 1 | 0 | 0 | -37.57777545 |
| 1735 | 2 | 0 | 0 | -40.42955478 |

| | | | | |
|---|---|---|---|---|
| 1736 | 1 | 0 | 1 | -32.36774329 |
| 1737 | 0 | 0 | 1 | -25.53534758 |
| 1738 | 1 | 1 | 0 | -26.52740336 |
| 1739 | 0 | 0 | 1 | -24.43474329 |
| 1740 | 1 | 0 | 0 | -24.09001399 |
| 1741 | 1 | 0 | 1 | -24.06291689 |
| 1742 | 0 | 0 | 0 | -24.26014378 |
| 1743 | 0 | 0 | 1 | -24.71478065 |
| 1744 | 0 | 0 | 1 | -25.37921926 |
| 1745 | 1 | 0 | 0 | -25.20183707 |
| 1746 | 1 | 0 | 0 | -13.57916992 |
| 1747 | 1 | 0 | 0 | -12.78015644 |
| 1748 | 1 | 0 | 0 | -13.27197927 |
| 1749 | 1 | 0 | 1 | -13.24277751 |
| 1750 | 1 | 1 | 0 | -17.1881461 |
| 1751 | 1 | 0 | 1 | -22.23293467 |
| 1752 | 1 | 0 | 0 | -21.87097856 |
| 1753 | 1 | 0 | 1 | -21.5208521 |
| 1754 | 0 | 0 | 0 | -20.12723583 |
| 1755 | 1 | 1 | 0 | -22.28773048 |
| 1756 | 1 | 1 | 0 | -21.36857578 |
| 1757 | 1 | 1 | 0 | -22.75016879 |
| 1758 | 1 | 0 | 0 | -22.07323283 |
| 1759 | 0 | 0 | 0 | -25.1333814 |
| 1760 | 0 | 0 | 0 | -33.31083898 |
| 1761 | 1 | 0 | 1 | -22.67107108 |
| 1762 | 0 | 1 | 0 | -35.38713074 |
| 1763 | 0 | 0 | 0 | -45.26885506 |
| 1764 | 1 | 0 | 0 | -50.94273863 |
| 1765 | 1 | 0 | 0 | -51.38423187 |
| 1766 | 1 | 0 | 1 | -55.19236269 |
| 1767 | 2 | 1 | 1 | -56.2823238 |
| 1768 | 0 | 1 | 1 | -41.82114623 |
| 1769 | 1 | 0 | 0 | -31.12714888 |
| 1770 | 1 | 0 | 0 | -31.07590091 |
| 1771 | 1 | 0 | 0 | -32.03101628 |
| 1772 | 1 | 0 | 0 | -32.51152701 |
| 1773 | 1 | 0 | 0 | -33.62770203 |
| 1774 | 1 | 0 | 1 | -34.35535642 |
| 1775 | 1 | 0 | 0 | -33.81673964 |
| 1776 | 1 | 0 | 0 | -32.75574084 |
| 1777 | 1 | 0 | 0 | -31.16343109 |
| 1778 | 1 | 0 | 0 | -32.58050417 |
| 1779 | 1 | 0 | 1 | -36.40523774 |
| 1780 | 1 | 0 | 1 | -40.24397817 |
| 1781 | 1 | 0 | 0 | -41.55779435 |
| 1782 | 1 | 0 | 1 | -37.76837918 |
| 1783 | 0 | 0 | 0 | -47.94446926 |

| | | | | |
|---|---|---|---|---|
| 1784 | 1 | 0 | 0 | -47.40551692 |
| 1785 | 1 | 0 | 0 | -30.48130695 |
| 1786 | 1 | 0 | 1 | -30.16813257 |
| 1787 | 0 | 0 | 0 | -28.21516755 |
| 1788 | 1 | 0 | 0 | -29.39436771 |
| 1789 | 1 | 0 | 0 | -11.70056449 |
| 1790 | 2 | 0 | 0 | 8.217545602 |
| 1791 | 1 | 0 | 0 | 10.41544207 |
| 1792 | 0 | 0 | 1 | -7.734217003 |
| 1793 | 1 | 0 | 1 | -8.025092077 |
| 1794 | 1 | 0 | 1 | -11.59519748 |
| 1795 | 2 | 0 | 0 | -11.3254282 |
| 1796 | 1 | 1 | 1 | -10.47144321 |
| 1797 | 1 | 0 | 1 | -19.09922195 |
| 1798 | 1 | 0 | 0 | -20.51081307 |
| 1799 | 1 | 0 | 0 | -19.23704345 |
| 1800 | 1 | 1 | 1 | -26.08417107 |
| 1801 | 0 | 0 | 0 | -40.49374309 |
| 1802 | 1 | 1 | 0 | -41.88717956 |
| 1803 | 1 | 0 | 1 | -42.99731949 |
| 1804 | 0 | 0 | 0 | -38.66193667 |
| 1805 | 0 | 0 | 0 | -39.10694998 |
| 1806 | 1 | 0 | 0 | -35.99094422 |
| 1807 | 1 | 0 | 0 | -50.81473166 |
| 1808 | 1 | 1 | 0 | -50.49210684 |
| 1809 | 1 | 0 | 1 | -43.47864642 |
| 1810 | 1 | 0 | 0 | -12.32014649 |
| 1811 | 1 | 0 | 0 | -12.05218443 |
| 1812 | 1 | 0 | 0 | -8.420033116 |
| 1813 | 1 | 1 | 0 | -11.18487992 |
| 1814 | 1 | 1 | 0 | -5.899301663 |
| 1815 | 1 | 0 | 0 | -43.91529869 |
| 1816 | 2 | 0 | 1 | -42.71782387 |
| 1817 | 1 | 1 | 0 | -60.72412916 |
| 1818 | 1 | 0 | 0 | -60.75666061 |
| 1819 | 1 | 0 | 0 | -59.03914463 |
| 1820 | 2 | 0 | 0 | -59.92792909 |
| 1821 | 2 | 1 | 0 | -63.25251645 |
| 1822 | 1 | 0 | 1 | -59.48646946 |
| 1823 | 1 | 0 | 1 | -61.56335595 |
| 1824 | 1 | 0 | 0 | -51.18560099 |
| 1825 | 1 | 0 | 0 | -38.99051488 |
| 1826 | 0 | 0 | 0 | -33.85261081 |
| 1827 | 1 | 0 | 0 | -35.31868621 |
| 1828 | 1 | 0 | 1 | -32.98360834 |
| 1829 | 1 | 1 | 1 | -2.992167025 |
| 1830 | 1 | 0 | 0 | -8.976697892 |
| 1831 | 1 | 0 | 0 | -8.301839332 |

| | | | | |
|---|---|---|---|---|
| 1832 | 1 | 0 | 0 | -16.01058258 |
| 1833 | 1 | 1 | 0 | -31.86615984 |
| 1834 | 1 | 0 | 0 | -32.69112056 |
| 1835 | 0 | 0 | 0 | -30.20628351 |
| 1836 | 1 | 0 | 0 | -55.66524981 |
| 1837 | 0 | 0 | 0 | -57.26087463 |
| 1838 | 1 | 0 | 0 | -55.75834618 |
| 1839 | 1 | 0 | 0 | -48.89035655 |
| 1840 | 1 | 0 | 0 | -55.30789733 |
| 1841 | 1 | 0 | 0 | -49.48345737 |
| 1842 | 2 | 0 | 1 | -49.72372909 |
| 1843 | 2 | 0 | 0 | -30.86598495 |
| 1844 | 0 | 0 | 0 | -30.66449959 |
| 1845 | 1 | 0 | 0 | -18.7983434 |
| 1846 | 0 | 0 | 0 | -19.30160924 |
| 1847 | 2 | 0 | 0 | -18.854402 |
| 1848 | 2 | 1 | 0 | -9.186972576 |
| 1849 | 1 | 1 | 0 | -10.48962209 |
| 1850 | 1 | 0 | 0 | -9.280092663 |
| 1851 | 1 | 0 | 1 | -27.47489225 |
| 1852 | 0 | 0 | 0 | -28.55711273 |
| 1853 | 1 | 0 | 0 | -25.39109397 |
| 1854 | 1 | 0 | 0 | -27.76697222 |
| 1855 | 1 | 0 | 1 | -29.19512409 |
| 1856 | 1 | 0 | 1 | -6.963069754 |
| 1857 | 1 | 0 | 0 | -6.37069221 |
| 1858 | 1 | 0 | 1 | -6.421478163 |
| 1859 | 1 | 0 | 0 | -2.983715704 |
| 1860 | 1 | 0 | 0 | 22.17881039 |
| 1861 | 1 | 0 | 0 | 57.28399629 |
| 1862 | 1 | 0 | 0 | 58.02526547 |
| 1863 | 1 | 0 | 0 | 58.68957432 |
| 1864 | 1 | 0 | 1 | 54.59650498 |
| 1865 | 1 | 0 | 0 | 27.93747158 |
| 1866 | 1 | 0 | 1 | 29.27146758 |
| 1867 | 1 | 0 | 0 | 28.8496232 |
| 1868 | 1 | 0 | 0 | 29.42575343 |
| 1869 | 1 | 0 | 0 | 26.81218422 |
| 1870 | 1 | 0 | 0 | 26.02173012 |
| 1871 | 1 | 1 | 0 | 27.86406098 |
| 1872 | 1 | 0 | 1 | 22.43914428 |
| 1873 | 1 | 0 | 0 | 11.33998877 |
| 1874 | 1 | 0 | 0 | 9.868004258 |
| 1875 | 1 | 0 | 0 | 3.635375263 |
| 1876 | 1 | 1 | 1 | 13.02957168 |
| 1877 | 1 | 1 | 0 | 13.38183309 |
| 1878 | 1 | 0 | 0 | 12.42241244 |
| 1879 | 1 | 0 | 1 | 14.10806595 |

| | | | | |
|---|---|---|---|---|
| 1880 | 1 | 0 | 0 | 13.20726374 |
| 1881 | 2 | 0 | 0 | -19.12741927 |
| 1882 | 2 | 1 | 0 | -39.56336121 |
| 1883 | 0 | 0 | 1 | -41.74643806 |
| 1884 | 1 | 1 | 0 | -38.49555847 |
| 1885 | 1 | 0 | 0 | -38.1230143 |
| 1886 | 1 | 0 | 0 | -39.75172822 |
| 1887 | 2 | 0 | 1 | -34.34458141 |
| 1888 | 1 | 0 | 0 | -33.40107804 |
| 1889 | 2 | 0 | 1 | -31.81683012 |
| 1890 | 1 | 0 | 1 | -32.41979024 |
| 1891 | 1 | 0 | 0 | -32.33844973 |
| 1892 | 1 | 1 | 1 | -30.89705354 |
| 1893 | 1 | 1 | 1 | -32.01259912 |
| 1894 | 1 | 0 | 0 | -31.86336097 |
| 1895 | 1 | 0 | 1 | -32.1749338 |
| 1896 | 1 | 1 | 0 | -33.56950377 |
| 1897 | 2 | 0 | 0 | -34.83102154 |
| 1898 | 1 | 0 | 1 | -31.65323369 |
| 1899 | 1 | 0 | 0 | -37.35619956 |
| 1900 | 1 | 0 | 0 | -38.16897794 |
| 1901 | 1 | 0 | 0 | -38.40070386 |
| 1902 | 0 | 0 | 0 | -36.33959961 |
| 1903 | 1 | 0 | 0 | -35.28015658 |
| 1904 | 1 | 0 | 0 | -41.0883154 |
| 1905 | 1 | 0 | 0 | -49.61576438 |
| 1906 | 2 | 0 | 1 | -55.58309671 |
| 1907 | 1 | 0 | 0 | -55.56226705 |
| 1908 | 2 | 0 | 1 | -55.19618125 |
| 1909 | 1 | 0 | 1 | -57.45407482 |
| 1910 | 1 | 0 | 0 | -56.72645797 |
| 1911 | 1 | 0 | 0 | -55.04655038 |
| 1912 | 1 | 0 | 1 | -56.05381854 |
| 1913 | 1 | 0 | 0 | -50.65505993 |
| 1914 | 1 | 0 | 0 | -50.59916215 |
| 1915 | 1 | 0 | 0 | -50.53989177 |
| 1916 | 1 | 0 | 0 | -52.73921495 |
| 1917 | 1 | 0 | 0 | -51.42378808 |
| 1918 | 1 | 0 | 0 | -50.57025538 |
| 1919 | 1 | 0 | 1 | -51.61508402 |
| 1920 | 1 | 1 | 0 | -39.08094894 |
| 1921 | 1 | 1 | 0 | -39.97727435 |
| 1922 | 1 | 0 | 0 | -39.3426806 |
| 1923 | 1 | 0 | 0 | -39.61106158 |
| 1924 | 1 | 0 | 1 | -36.83670462 |
| 1925 | 0 | 0 | 1 | -36.79317508 |
| 1926 | 1 | 0 | 0 | -33.18393798 |
| 1927 | 0 | 1 | 0 | -30.13882301 |

| | | | | |
|---|---|---|---|---|
| 1928 | 1 | 0 | 0 | -31.87634955 |
| 1929 | 1 | 0 | 0 | -0.061689276 |
| 1930 | 1 | 0 | 1 | 1.350813217 |
| 1931 | 2 | 1 | 0 | -33.68265755 |
| 1932 | 1 | 0 | 0 | -58.23553018 |
| 1933 | 2 | 0 | 1 | -58.7162323 |
| 1934 | 2 | 0 | 0 | -59.40112683 |
| 1935 | 1 | 0 | 0 | -56.13761971 |
| 1936 | 1 | 0 | 0 | -50.20593506 |
| 1937 | 0 | 0 | 0 | -52.69576509 |
| 1938 | 1 | 0 | 0 | -49.67792378 |
| 1939 | 0 | 0 | 0 | -52.84881902 |
| 1940 | 0 | 0 | 1 | -54.35914135 |
| 1941 | 1 | 0 | 1 | -57.35129298 |
| 1942 | 2 | 0 | 0 | -58.21094878 |
| 1943 | 1 | 0 | 0 | -55.60179924 |
| 1944 | 1 | 0 | 0 | -56.00784886 |
| 1945 | 0 | 0 | 0 | -55.04022079 |
| 1946 | 1 | 0 | 0 | -49.49553178 |
| 1947 | 1 | 0 | 0 | -49.61605254 |
| 1948 | 2 | 1 | 0 | -53.4505031 |
| 1949 | 1 | 0 | 1 | -46.92614359 |
| 1950 | 1 | 0 | 0 | -43.33948796 |
| 1951 | 2 | 0 | 1 | -41.13150145 |
| 1952 | 1 | 1 | 0 | -37.13915727 |
| 1953 | 1 | 0 | 1 | -36.80812724 |
| 1954 | 1 | 0 | 0 | -25.47738174 |
| 1955 | 1 | 1 | 0 | -23.6451567 |
| 1956 | 1 | 0 | 0 | -21.66723897 |
| 1957 | 1 | 0 | 0 | -21.40843734 |
| 1958 | 0 | 0 | 0 | -17.27238649 |
| 1959 | 0 | 0 | 0 | -16.67372505 |
| 1960 | 1 | 0 | 0 | -16.16276195 |
| 1961 | 0 | 0 | 0 | -16.50478535 |
| 1962 | 0 | 0 | 0 | -10.77371451 |
| 1963 | 1 | 0 | 0 | -5.220857342 |
| 1964 | 1 | 0 | 1 | 3.977655948 |
| 1965 | 0 | 0 | 0 | 6.769596862 |
| 1966 | 1 | 0 | 0 | 13.06189897 |
| 1967 | 1 | 0 | 0 | 15.3937421 |
| 1968 | 1 | 0 | 0 | 18.72666611 |
| 1969 | 1 | 0 | 0 | 21.03249635 |
| 1970 | 1 | 0 | 0 | 19.33468325 |
| 1971 | 1 | 1 | 1 | 20.1407073 |
| 1972 | 1 | 0 | 0 | 13.67453532 |
| 1973 | 1 | 0 | 0 | 12.32446045 |
| 1974 | 1 | 0 | 0 | 3.611517999 |
| 1975 | 0 | 0 | 0 | 3.377359604 |

| | | | | |
|---|---|---|---|---|
| 1976 | 1 | 0 | 0 | 2.28749706 |
| 1977 | 1 | 0 | 0 | 1.550889694 |
| 1978 | 1 | 0 | 0 | -37.59716878 |
| 1979 | 1 | 0 | 1 | -51.04692262 |
| 1980 | 1 | 0 | 0 | -64.53728512 |
| 1981 | 1 | 1 | 0 | -54.57601426 |
| 1982 | 2 | 0 | 1 | -38.75252308 |
| 1983 | 1 | 0 | 0 | -38.27641237 |
| 1984 | 0 | 0 | 0 | -32.21091989 |
| 1985 | 2 | 0 | 1 | -26.70559544 |
| 1986 | 1 | 0 | 1 | -39.55367617 |
| 1987 | 1 | 1 | 0 | -21.07341924 |
| 1988 | 1 | 0 | 0 | -22.38501779 |
| 1989 | 1 | 1 | 0 | -6.987049648 |
| 1990 | 1 | 0 | 1 | -37.61256005 |
| 1991 | 1 | 0 | 0 | -61.4477654 |
| 1992 | 1 | 0 | 0 | -61.8494608 |
| 1993 | 1 | 0 | 0 | -48.48667568 |
| 1994 | 1 | 0 | 0 | -48.37456709 |
| 1995 | 1 | 0 | 0 | -52.65030556 |
| 1996 | 0 | 0 | 0 | -63.1812383 |
| 1997 | 1 | 0 | 0 | -63.8312798 |
| 1998 | 1 | 0 | 0 | -64.83085811 |
| 1999 | 1 | 0 | 0 | -67.01442194 |
| 2000 | 0 | 0 | 0 | -72.65378133 |
| 2001 | 1 | 0 | 0 | -66.93228477 |
| 2002 | 1 | 0 | 0 | -71.43804033 |
| 2003 | 1 | 0 | 0 | -70.73636469 |
| 2004 | 1 | 0 | 0 | -65.78567525 |
| 2005 | 1 | 1 | 0 | -62.64647501 |
| 2006 | 1 | 0 | 0 | -67.04280438 |
| 2007 | 1 | 0 | 1 | -72.60005256 |
| 2008 | 1 | 0 | 0 | -70.4762377 |
| 2009 | 1 | 0 | 0 | -70.32996665 |
| 2010 | 1 | 0 | 1 | -65.87310921 |
| 2011 | 1 | 0 | 0 | -66.27642427 |
| 2012 | 1 | 0 | 0 | -65.55992136 |
| 2013 | 1 | 0 | 0 | -73.71561667 |
| 2014 | 1 | 0 | 0 | -72.37281786 |
| 2015 | 1 | 1 | 0 | -70.53057488 |
| 2016 | 1 | 0 | 0 | -64.6780767 |
| 2017 | 1 | 0 | 0 | -38.85126849 |
| 2018 | 1 | 0 | 1 | -47.8917824 |
| 2019 | 1 | 1 | 0 | -12.35993992 |
| 2020 | 1 | 0 | 1 | -68.15652524 |
| 2021 | 0 | 1 | 0 | -69.13362071 |
| 2022 | 1 | 0 | 0 | -70.08656302 |
| 2023 | 1 | 0 | 1 | -64.66341016 |

| | | | | |
|---|---|---|---|---|
| 2024 | 1 | 0 | 1 | -63.43891138 |
| 2025 | 1 | 0 | 0 | -79.95308598 |
| 2026 | 2 | 1 | 1 | -74.38593706 |
| 2027 | 1 | 0 | 0 | -74.06369467 |
| 2028 | 1 | 0 | 0 | -72.51022121 |
| 2029 | 1 | 0 | 1 | -72.67483598 |
| 2030 | 1 | 0 | 1 | -68.40431336 |
| 2031 | 0 | 0 | 0 | -69.22487601 |
| 2032 | 1 | 0 | 0 | -57.29745423 |
| 2033 | 1 | 0 | 0 | -25.98256491 |
| 2034 | 0 | 0 | 0 | 33.4232377 |
| 2035 | 1 | 0 | 0 | 32.07494762 |
| 2036 | 1 | 1 | 0 | 33.30307964 |
| 2037 | 1 | 0 | 0 | 24.17073265 |
| 2038 | 1 | 0 | 0 | 2.497358223 |
| 2039 | 1 | 0 | 0 | 2.334183193 |
| 2040 | 1 | 0 | 0 | -19.36547592 |
| 2041 | 1 | 1 | 0 | -38.50019905 |
| 2042 | 1 | 0 | 0 | -39.24149527 |
| 2043 | 1 | 0 | 1 | -41.79267088 |
| 2044 | 1 | 1 | 0 | -45.75015028 |
| 2045 | 0 | 0 | 0 | -63.70877853 |
| 2046 | 0 | 0 | 0 | -50.66843301 |
| 2047 | 2 | 0 | 0 | -44.07184456 |
| 2048 | 0 | 0 | 0 | -38.42611342 |
| 2049 | 1 | 0 | 0 | -27.04311793 |
| 2050 | 1 | 0 | 0 | -27.40444777 |
| 2051 | 1 | 0 | 0 | -23.19387274 |
| 2052 | 2 | 0 | 0 | -8.436152068 |
| 2053 | 2 | 0 | 0 | -8.736344378 |
| 2054 | 2 | 0 | 0 | -9.548839183 |
| 2055 | 2 | 0 | 0 | -3.781919759 |
| 2056 | 2 | 1 | 0 | -1.833247008 |
| 2057 | 2 | 0 | 0 | -0.954648715 |
| 2058 | 1 | 0 | 0 | 1.437862734 |
| 2059 | 1 | 1 | 0 | 1.357310994 |
| 2060 | 0 | 0 | 0 | 31.48699712 |
| 2061 | 0 | 0 | 0 | 37.26517401 |
| 2062 | 1 | 0 | 0 | 45.41071794 |
| 2063 | 2 | 0 | 0 | 47.31485905 |
| 2064 | 1 | 0 | 0 | 54.70131448 |
| 2065 | 1 | 0 | 0 | 40.42569409 |
| 2066 | 1 | 0 | 1 | 38.78222903 |
| 2067 | 1 | 0 | 0 | 6.245125666 |
| 2068 | 2 | 0 | 1 | 14.08780965 |
| 2069 | 1 | 0 | 0 | 17.481794 |
| 2070 | 1 | 1 | 0 | 16.22686015 |
| 2071 | 0 | 0 | 0 | 16.33415466 |

| | | | | |
|---|---|---|---|---|
| 2072 | 0 | 0 | 0 | 18.02970166 |
| 2073 | 1 | 0 | 0 | 16.63082065 |
| 2074 | 0 | 0 | 0 | 15.69390595 |
| 2075 | 1 | 0 | 0 | 18.2261029 |
| 2076 | 1 | 0 | 0 | 17.34103744 |
| 2077 | 1 | 0 | 0 | 17.50173239 |
| 2078 | 2 | 0 | 0 | 13.44798968 |
| 2079 | 2 | 0 | 0 | 13.91280423 |
| 2080 | 2 | 0 | 0 | 13.13170485 |
| 2081 | 1 | 0 | 0 | 11.56208633 |
| 2082 | 0 | 0 | 0 | 12.7991781 |
| 2083 | 0 | 0 | 0 | 12.10419934 |
| 2084 | 0 | 0 | 0 | 13.49187947 |
| 2085 | 1 | 0 | 0 | 11.39929577 |
| 2086 | 1 | 0 | 0 | 8.152383266 |
| 2087 | 1 | 0 | 0 | 7.562489289 |
| 2088 | 1 | 1 | 0 | 12.74480504 |
| 2089 | 1 | 0 | 0 | 2.286787701 |
| 2090 | 1 | 1 | 0 | 4.064209005 |
| 2091 | 1 | 0 | 0 | 11.35058986 |
| 2092 | 1 | 1 | 0 | 24.31355178 |
| 2093 | 1 | 0 | 0 | 29.83483908 |
| 2094 | 1 | 0 | 0 | 36.92200794 |
| 2095 | 1 | 1 | 0 | 37.08805962 |
| 2096 | 1 | 1 | 1 | 36.36782038 |
| 2097 | 1 | 0 | 0 | 38.58368505 |
| 2098 | 1 | 0 | 1 | 41.03629174 |
| 2099 | 2 | 1 | 0 | 41.93295853 |
| 2100 | 1 | 0 | 0 | 40.5786731 |
| 2101 | 1 | 0 | 0 | 42.74249772 |
| 2102 | 1 | 0 | 1 | 32.72118436 |
| 2103 | 1 | 0 | 0 | 31.91120214 |
| 2104 | 1 | 0 | 1 | 29.3877801 |
| 2105 | 1 | 0 | 0 | 29.67993992 |
| 2106 | 1 | 0 | 0 | 35.14955173 |
| 2107 | 1 | 1 | 1 | 37.28042589 |
| 2108 | 1 | 0 | 0 | 38.32109908 |
| 2109 | 0 | 1 | 0 | 50.70743456 |
| 2110 | 1 | 0 | 0 | 41.95266633 |
| 2111 | 1 | 0 | 0 | 35.33658996 |
| 2112 | 1 | 0 | 0 | 33.62857288 |
| 2113 | 1 | 0 | 0 | 18.81871077 |
| 2114 | 1 | 0 | 0 | 18.24885627 |
| 2115 | 2 | 1 | 0 | 11.19581237 |
| 2116 | 1 | 0 | 0 | 9.641305924 |
| 2117 | 1 | 1 | 0 | 10.36417871 |
| 2118 | 1 | 0 | 1 | 8.796502521 |
| 2119 | 0 | 0 | 0 | 5.77300642 |

| | | | | |
|---|---|---|---|---|
| 2120 | 1 | 0 | 1 | 2.817850815 |
| 2121 | 1 | 0 | 1 | -0.676008419 |
| 2122 | 0 | 0 | 0 | -13.23480296 |
| 2123 | 0 | 0 | 1 | -25.43640665 |
| 2124 | 1 | 0 | 0 | 20.38344265 |
| 2125 | 1 | 0 | 0 | 20.17609332 |
| 2126 | 1 | 0 | 0 | 20.86978764 |
| 2127 | 1 | 0 | 0 | 24.27494283 |
| 2128 | 1 | 0 | 0 | 45.78858886 |
| 2129 | 1 | 0 | 1 | 49.18038076 |
| 2130 | 1 | 0 | 1 | 58.79006546 |
| 2131 | 1 | 0 | 0 | 45.72374273 |
| 2132 | 1 | 0 | 0 | 6.169174193 |
| 2133 | 2 | 0 | 1 | 2.496939154 |
| 2134 | 1 | 1 | 0 | 59.72427178 |
| 2135 | 1 | 1 | 0 | 58.79817201 |
| 2136 | 1 | 0 | 0 | 56.73301107 |
| 2137 | 1 | 0 | 0 | 59.20009653 |
| 2138 | 1 | 0 | 0 | 57.45799925 |
| 2139 | 1 | 0 | 1 | 69.54202789 |
| 2140 | 1 | 0 | 0 | 67.94421596 |
| 2141 | 1 | 0 | 0 | 23.47433596 |
| 2142 | 0 | 0 | 0 | 24.38267169 |
| 2143 | 1 | 1 | 1 | 15.51921473 |
| 2144 | 1 | 0 | 0 | 16.49274026 |
| 2145 | 1 | 1 | 1 | 6.072735393 |
| 2146 | 2 | 0 | 1 | 16.07650293 |
| 2147 | 1 | 0 | 0 | 18.09461738 |
| 2148 | 1 | 0 | 0 | 18.51700024 |
| 2149 | 1 | 0 | 0 | 17.08512248 |
| 2150 | 0 | 0 | 0 | 17.85041906 |
| 2151 | 0 | 1 | 0 | 20.68445393 |
| 2152 | 1 | 0 | 0 | 20.66111188 |
| 2153 | 1 | 0 | 0 | 22.4120281 |
| 2154 | 0 | 0 | 0 | 21.46595176 |
| 2155 | 1 | 0 | 0 | 61.37357484 |
| 2156 | 1 | 0 | 1 | 57.33116393 |
| 2157 | 1 | 0 | 1 | 56.60932438 |
| 2158 | 1 | 0 | 0 | 58.6869071 |
| 2159 | 2 | 0 | 1 | 61.71721945 |
| 2160 | 1 | 1 | 0 | 66.94657057 |
| 2161 | 2 | 0 | 0 | 63.77790637 |
| 2162 | 1 | 0 | 0 | 64.65770332 |
| 2163 | 1 | 0 | 1 | 64.19653221 |
| 2164 | 1 | 0 | 0 | 63.74119449 |
| 2165 | 1 | 0 | 0 | 62.16492341 |
| 2166 | 1 | 0 | 0 | 61.26489557 |
| 2167 | 1 | 1 | 0 | 61.29664417 |

| | | | | |
|---|---|---|---|---|
| 2168 | 1 | 0 | 1 | 32.0835437 |
| 2169 | 1 | 0 | 0 | 16.32664086 |
| 2170 | 0 | 1 | 0 | 5.609108396 |
| 2171 | 1 | 0 | 0 | -2.551819442 |
| 2172 | 1 | 0 | 0 | 4.08124653 |
| 2173 | 1 | 0 | 1 | 11.07253045 |
| 2174 | 1 | 0 | 0 | 11.8492664 |
| 2175 | 1 | 0 | 0 | 7.423888226 |
| 2176 | 1 | 0 | 0 | 7.645122233 |
| 2177 | 2 | 1 | 0 | 5.548833971 |
| 2178 | 1 | 0 | 0 | 1.124586271 |
| 2179 | 1 | 0 | 0 | 1.113667626 |
| 2180 | 1 | 0 | 1 | -4.302925358 |
| 2181 | 1 | 0 | 0 | -4.605895006 |
| 2182 | 1 | 0 | 0 | 6.799722093 |
| 2183 | 1 | 0 | 1 | 24.24790612 |
| 2184 | 1 | 0 | 0 | 23.4620818 |
| 2185 | 0 | 0 | 0 | 12.54728955 |
| 2186 | 1 | 0 | 0 | 6.829762813 |
| 2187 | 1 | 0 | 0 | -24.07016989 |
| 2188 | 1 | 0 | 1 | -34.75379672 |
| 2189 | 1 | 0 | 1 | -6.630315904 |
| 2190 | 0 | 0 | 1 | 6.543921761 |
| 2191 | 1 | 0 | 0 | -21.15291771 |
| 2192 | 1 | 0 | 0 | -21.04961254 |
| 2193 | 1 | 0 | 0 | 1.296711994 |
| 2194 | 1 | 1 | 0 | -74.55437567 |
| 2195 | 2 | 0 | 1 | -74.57682853 |
| 2196 | 2 | 0 | 0 | -76.21368746 |
| 2197 | 1 | 0 | 0 | -78.27036331 |
| 2198 | 1 | 0 | 0 | -75.23257643 |
| 2199 | 1 | 0 | 0 | -75.69735369 |
| 2200 | 1 | 0 | 1 | -63.32133735 |
| 2201 | 1 | 0 | 0 | -42.54542036 |
| 2202 | 1 | 1 | 0 | -15.27245267 |
| 2203 | 2 | 0 | 1 | -38.80161033 |
| 2204 | 1 | 0 | 0 | -53.16579743 |
| 2205 | 1 | 0 | 1 | -59.59484403 |
| 2206 | 1 | 1 | 0 | -63.96034837 |
| 2207 | 1 | 0 | 0 | -75.81533939 |
| 2208 | 1 | 0 | 1 | -75.47478439 |
| 2209 | 1 | 0 | 0 | -76.32654376 |
| 2210 | 1 | 0 | 0 | -74.8341648 |
| 2211 | 1 | 1 | 0 | -74.74250192 |
| 2212 | 1 | 1 | 0 | -74.25101061 |
| 2213 | 1 | 1 | 0 | -74.0741048 |
| 2214 | 2 | 0 | 0 | -74.70943213 |
| 2215 | 1 | 0 | 0 | -79.88879262 |

| | | | | |
|---|---|---|---|---|
| 2216 | 1 | 0 | 0 | -81.53135716 |
| 2217 | 1 | 0 | 1 | -84.46455262 |
| 2218 | 1 | 0 | 0 | -72.30721618 |
| 2219 | 1 | 0 | 1 | -55.02333273 |
| 2220 | 1 | 0 | 1 | -54.64906794 |
| 2221 | 1 | 0 | 0 | -56.48725796 |
| 2222 | 1 | 0 | 0 | -55.82365618 |
| 2223 | 1 | 0 | 0 | -55.87364062 |
| 2224 | 0 | 0 | 1 | -42.67728543 |
| 2225 | 1 | 0 | 1 | -20.30272803 |
| 2226 | 1 | 0 | 0 | -77.69814251 |
| 2227 | 0 | 0 | 0 | -6.175783352 |
| 2228 | 1 | 0 | 0 | -28.73448776 |
| 2229 | 2 | 0 | 0 | -29.36998514 |
| 2230 | 2 | 0 | 0 | -28.70849649 |
| 2231 | 1 | 0 | 0 | -32.48990153 |
| 2232 | 1 | 0 | 0 | -30.09047755 |
| 2233 | 1 | 0 | 0 | -24.45184656 |
| 2234 | 1 | 0 | 0 | -35.78511599 |
| 2235 | 1 | 0 | 0 | -34.98803323 |
| 2236 | 1 | 0 | 1 | -36.40828553 |
| 2237 | 1 | 0 | 1 | -33.53553165 |
| 2238 | 1 | 0 | 0 | -4.73850049 |
| 2239 | 1 | 0 | 0 | 29.39897599 |
| 2240 | 2 | 0 | 1 | 32.27513351 |
| 2241 | 0 | 0 | 1 | 29.63318415 |
| 2242 | 1 | 0 | 0 | 29.72610399 |
| 2243 | 1 | 0 | 0 | 29.73686899 |
| 2244 | 2 | 0 | 0 | 35.12511824 |
| 2245 | 1 | 0 | 1 | 6.91936044 |
| 2246 | 1 | 1 | 0 | 20.91573425 |
| 2247 | 0 | 0 | 1 | 30.89181096 |
| 2248 | 1 | 1 | 0 | 36.7744511 |
| 2249 | 1 | 0 | 0 | 30.13626704 |
| 2250 | 1 | 0 | 0 | -8.137833896 |
| 2251 | 1 | 0 | 0 | 25.86650823 |
| 2252 | 1 | 1 | 1 | -12.18612196 |
| 2253 | 1 | 0 | 0 | -0.421076452 |
| 2254 | 1 | 0 | 0 | 70.0334569 |
| 2255 | 1 | 0 | 0 | 69.43612481 |
| 2256 | 1 | 0 | 0 | 67.39664896 |
| 2257 | 0 | 1 | 0 | 67.14615378 |
| 2258 | 2 | 0 | 1 | 68.05886627 |
| 2259 | 1 | 0 | 0 | 68.20253212 |
| 2260 | 0 | 1 | 0 | 75.27898142 |
| 2261 | 0 | 0 | 0 | 65.97975261 |
| 2262 | 2 | 0 | 0 | 65.41264244 |
| 2263 | 0 | 0 | 0 | 65.60332579 |

| | | | | |
|---|---|---|---|---|
| 2264 | 1 | 0 | 0 | 85.10227598 |
| 2265 | 1 | 0 | 1 | 85.1489956 |
| 2266 | 1 | 0 | 1 | 49.95457463 |
| 2267 | 1 | 0 | 1 | 53.46920494 |
| 2268 | 2 | 0 | 0 | 3.434795549 |
| 2269 | 1 | 0 | 0 | -4.918246495 |
| 2270 | 1 | 0 | 0 | -3.714273078 |
| 2271 | 1 | 0 | 0 | -6.308552719 |
| 2272 | 1 | 0 | 0 | -13.72326545 |
| 2273 | 1 | 0 | 0 | -5.229338298 |
| 2274 | 1 | 0 | 0 | 8.680634374 |
| 2275 | 1 | 0 | 1 | 8.146090997 |
| 2276 | 2 | 0 | 0 | 20.92641487 |
| 2277 | 1 | 0 | 1 | 41.74429186 |
| 2278 | 1 | 0 | 1 | 23.5008567 |
| 2279 | 1 | 1 | 1 | -25.62215172 |
| 2280 | 1 | 1 | 0 | -26.02914598 |
| 2281 | 0 | 0 | 1 | -28.00690524 |
| 2282 | 1 | 0 | 0 | -1.29504656 |
| 2283 | 1 | 0 | 0 | 51.4102397 |
| 2284 | 1 | 0 | 0 | 57.51889022 |
| 2285 | 1 | 0 | 1 | 58.99441186 |
| 2286 | 1 | 0 | 0 | 7.557122805 |
| 2287 | 2 | 0 | 1 | -17.82642508 |
| 2288 | 0 | 0 | 0 | 3.296318035 |
| 2289 | 1 | 0 | 0 | 37.13641354 |
| 2290 | 1 | 0 | 0 | 18.67899616 |
| 2291 | 0 | 1 | 0 | 19.4143279 |
| 2292 | 1 | 0 | 0 | 3.290162365 |
| 2293 | 1 | 0 | 0 | 2.438858365 |
| 2294 | 0 | 0 | 0 | 6.556290497 |
| 2295 | 0 | 0 | 0 | 8.435013683 |
| 2296 | 0 | 0 | 1 | 8.310622961 |
| 2297 | 1 | 0 | 0 | 2.753030361 |
| 2298 | 1 | 0 | 0 | 3.664854771 |
| 2299 | 1 | 0 | 1 | -0.891888725 |
| 2300 | 1 | 1 | 0 | -2.532332355 |
| 2301 | 0 | 1 | 0 | 63.67902337 |
| 2302 | 1 | 0 | 0 | 62.81396214 |
| 2303 | 1 | 0 | 0 | 59.44327925 |
| 2304 | 1 | 0 | 0 | 70.46401118 |
| 2305 | 1 | 1 | 0 | 75.8185983 |
| 2306 | 0 | 0 | 0 | 78.55228949 |
| 2307 | 0 | 0 | 0 | 84.0522828 |
| 2308 | 1 | 0 | 1 | 81.10110803 |
| 2309 | 1 | 0 | 1 | 65.24649698 |
| 2310 | 1 | 1 | 0 | 69.42111348 |
| 2311 | 1 | 0 | 0 | 52.34375708 |

| | | | | |
|---|---|---|---|---|
| 2312 | 1 | 0 | 0 | 36.35612757 |
| 2313 | 0 | 0 | 0 | 33.714268 |
| 2314 | 0 | 0 | 0 | 33.74061839 |
| 2315 | 1 | 0 | 0 | 37.11865826 |
| 2316 | 1 | 0 | 0 | 57.05097585 |
| 2317 | 1 | 0 | 1 | 60.28593665 |
| 2318 | 1 | 0 | 1 | 59.21094385 |
| 2319 | 1 | 0 | 0 | 60.33748048 |
| 2320 | 1 | 0 | 0 | 74.03975847 |
| 2321 | 1 | 0 | 0 | 16.44260508 |
| 2322 | 1 | 0 | 0 | 12.19857571 |
| 2323 | 1 | 0 | 0 | -11.7580281 |
| 2324 | 1 | 0 | 1 | -2.153930946 |
| 2325 | 0 | 0 | 0 | -59.73295957 |
| 2326 | 1 | 0 | 0 | -60.61900744 |
| 2327 | 1 | 0 | 0 | -60.16575769 |
| 2328 | 0 | 0 | 0 | 52.26231089 |
| 2329 | 1 | 0 | 0 | 70.7276102 |
| 2330 | 1 | 0 | 1 | 57.73905946 |
| 2331 | 0 | 0 | 0 | -3.309765611 |
| 2332 | 1 | 0 | 0 | -59.88475436 |
| 2333 | 1 | 0 | 0 | -59.69969947 |
| 2334 | 1 | 0 | 0 | -59.80726533 |
| 2335 | 1 | 0 | 0 | -36.67013458 |
| 2336 | 2 | 0 | 0 | 14.47203031 |
| 2337 | 1 | 0 | 0 | 14.65744273 |
| 2338 | 2 | 1 | 0 | -74.76436505 |
| 2339 | 1 | 0 | 0 | -72.55139858 |
| 2340 | 1 | 0 | 0 | -72.22879608 |
| 2341 | 1 | 0 | 0 | -73.10659189 |
| 2342 | 1 | 0 | 1 | -28.54277571 |
| 2343 | 1 | 0 | 0 | 29.48685694 |
| 2344 | 1 | 0 | 1 | -8.134328838 |
| 2345 | 1 | 0 | 0 | 68.50625561 |
| 2346 | 1 | 0 | 1 | 68.46603856 |
| 2347 | 0 | 0 | 1 | 68.3914475 |
| 2348 | 1 | 0 | 1 | 84.89583633 |
| 2349 | 1 | 0 | 0 | 85.55331766 |
| 2350 | 1 | 0 | 0 | 86.64912021 |
| 2351 | 1 | 0 | 1 | 87.22902099 |
| 2352 | 1 | 0 | 0 | -6.855848429 |
| 2353 | 1 | 0 | 0 | 43.7531047 |
| 2354 | 1 | 0 | 1 | -1.970170276 |
| 2355 | 1 | 0 | 0 | -1.856664839 |
| 2356 | 2 | 1 | 0 | 65.40609628 |
| 2357 | 1 | 0 | 0 | 65.6642294 |
| 2358 | 1 | 0 | 0 | -60.16497436 |
| 2359 | 1 | 0 | 1 | -71.98447802 |

| | | | | |
|---|---|---|---|---|
| 2360 | 1 | 0 | 0 | -71.94125546 |
| 2361 | 1 | 1 | 0 | -0.274441061 |
| 2362 | 0 | 0 | 0 | -19.12380359 |
| 2363 | 1 | 1 | 0 | 43.99506679 |
| 2364 | 1 | 0 | 0 | 31.11595609 |